Mathematical and Computational Modelling of Arterial Mechanobiology: Application to Cerebral Vasospasm

The University Of Sheffield.

Giulia Pederzani

Supervisor - Dr. Paul Watton

Co-Supervisor - Prof. Anne Robertson

A thesis submitted in partial fulfilment of the degree of Doctor of Philosophy in Computer Science

April 6, 2021

Abstract

Cerebral vasospasm is a prolonged acute constriction of a cerebral artery and an aftermath of subarachnoid haemorrhage. It is the leading cause of death in patients who survive hospitalisation due to the decrease in blood, and therefore oxygen, supply to the brain. Despite its prevalence, its complex multifactorial pathophysiology make it a still poorly understood disease. Recent results concerning the treatment strategy, i.e. the success of stent retrievers in some cases, has challenged the current understanding of the disease. Stents represent a safer option compared to the traditional treatment via balloon angioplasty and thus there is motivation to further understand the disease with the aim of personalising the treatment strategy for individual patients.

A novel hypothesis is formulated on the pathophysiology of cerebral vasospasm and tested in a mathematical model. The artery is represented as a non-linearly elastic cylindrical membrane and a constrained mixture approach is adopted which includes elastin, collagen and vascular smooth muscle cells. The key interest is in the study of how the pressure-diameter curve changes from health to vasospasm and predict the magnitude of pressure that an interventional device should apply in order to resolve the disease. The success criterion for a device is a strain-based damage criterion for the smooth muscle cells. The predictions of the model are consistent with published clinical observations.

The membrane model assumes a uniform strain-field across the arterial wall thickness: this is reasonable for a healthy vessel but likely to no longer be true in moderate to severe cases of vasospasm. The model is therefore integrated into a finite element framework which has been successfully used to model aneurysm growth and remodelling with anisotropic volumetric growth. The framework is extended to accommodate a more realistic material model of collagen to include a fibre waviness distribution and remodeling, a material model for vascular smooth muscle cells with contractile active response and remodelling, and a damage model. Analogously to the mathematical

model, the evolution of the pressure-diameter curves is studied and predictions of the magnitude of pressure required for effective treatment are obtained and compared to the mathematical model.

A sophistication is finally included to account for the effect of the growth and remodelling of collagen on the development of vasospasm and its treatment, which had initially be assumed negligible. The results suggest that collagen growth and remodelling can play a significant role and should be included in models that aim at providing clinical support in the treatment decision.

The work presented in this thesis is an illustration of how mathematical and computational modelling can be a useful tool for hypothesis testing in problems of clinical relevance. There is still however a lack of experimental data to inform the model: this holds not only for cerebral vasospasm in particular, but also for general knowledge of cell mechanobiology, i.e. the interaction between the mechanical environment of the cell and its biological function. The hope is that computational modelling motivates further research into these topics and offers suggestions regarding which research questions to address.

Statement of Originality

I, Giulia Pederzani, declare that this thesis titled “Mathematical and Computational Modelling of Arterial Mechanobiology: Application to Cerebral Vasospasm" and the work presented in it are my own. I confirm that:

- This work was done only or mainly while in candidature for a degree at the University of Sheffield;
- Where any part of this thesis has been submitted for a degree or any other qualification at this University or any other institution, this has been clearly stated;
- Where I have consulted the published work of others, this is always clearly attributed;
- Where I have quoted from the work of others, the source is always given. With the exception of such quotations, this thesis is entirely my own work;
- I have ackowledged all main sources of help;
- Where the thesis is based on work done by myself jointly with others, I have made clear exactly what was done by others and what I have contributed myself.

Giulia Pederzani,

September 24, 2020.

This page has been intentionally left blank.

Acknowledgments

I would like to express my gratitude to my supervisor, Dr. Paul Watton, for his valuable support and guidance throughout these past four years. I will forever be grateful for the opportunities he has given me to connect with other researchers in the field and to grow as a researcher and academic. Thank you also for your guidance in finding a good work-life balance.

I'm sincerely grateful to Prof. Anne Robertson who has welcomed me for a visit to her research laboratory in Pittsburgh and provided extremely valuable feedback on my work and research process. Thank you also to Prof. Namrata Gundiah who allowed me to visit her Biomechanics laboratory in Bangalore at the beginning of my Ph.D. providing a valuable different perspective.

I'm deeply grateful to Dr. Andrii Grytsan who helped me wade into the field of finite element analysis and helped me learn the software package FEAP. Thank you also for the illumnating discussions on both a professional and personal level.

Thank you to Shakti, Hamna, I-Tung, Yuqian and all the colleagues at Insigneo for the atmosphere of mutual support and friendship I found in the office.

Thank you to all my friends outside of the office for your continued support and treasured friendship.

Immeasurable gratitude goes out my parents for their unwavering support, love and guidance. None of this would have been possible without you.

And thank you Alex for bringing new light and inspiration to my life, and for supporting me in the quiet and the trying times.

This page has been intentionally left blank.

Dissemination

Peer-Reviewed Journal Papers

1. Bhogal P., **Pederzani G.** , Grytsan A., Loh Y., Brouwer P.A., Andersson T., Gundiah N., Robertson, A.M., Watton P.N., Söderman M. (2019) *The Unexplained Success of Stentplasty Vasospasm Treatment: Insights using Mechanistic Mathematical Modeling*, Clinical Neuroradiology, 29, 763-774

Peer-Reviewed Conference Proceedings

1. **Pederzani G.** , Grytsan A., Bhogal P., Robertson, A.M., Watton P.N. (2019) *Application of theories of arterial growth, remodelling and damage to understand cerebral vasospasm and its response to treatment*, Biomedical Engineering Conference (BioMedEng), September 5-6, London, UK

2. **Pederzani G.** , Grytsan A., Bhogal P., Robertson, A.M., Watton P.N. (2019) *Application of theories of arterial growth, remodelling and damage to understand cerebral vasospasm and its response to treatment*, SoftMech 4th Workshop, June 5-7, 2019, Glasgowk, UK 1st prize for "Best Ph.D. student presentation"

3. **Pederzani G.**, Bhogal P., Robertson A.M., Watton P.N. (2018) *A mathematical model of cerebral vasospasm and comparison between treatment strategies*, Virtual Physiological Human Conference (VPH), Sep 5-7, Zaragoza, Spain

4. **Pederzani G.**, Bhogal P., Robertson A.M., Watton P.N. (2018) *A mathematical model of cerebral vasospasm and comparison between treatment strategies*, British Applied Mathematics Colloquium (BAMC), Mar 26-29, St Andrews, UK

5. Bhogal P., **Pederzani G.** , Grytsan A., Loh Y., Brouwer P.A., Andersson T., Söderman M., Gundiah N., Robertson, A.M., Watton P.N. (2018) *A mathematical model of cerebral vasospasm and comparison between treatment strategies*, Interventional Neurovascular Exploratory Workshop (iNEW), February 7-9,

Zürich, Switzerland

6. Bhogal P., **Pederzani G.** , Grytsan A., Loh Y., Brouwer P.A., Andersson T., Söderman M., Gundiah N., Robertson, A.M., Watton P.N. (2018) *A new hypothesis on the pathophysiology of cerebral vasospasm and its consequences on potential treatment strategies*, ABC WIN (Anatomy-Biology-Clinical correlations - Working group in Interventional Neuroradiology), January 14-20, Val d'Isére, France

Public Engagement

1. **Pederzani G.** , Grytsan A., Bhogal P., Robertson, A.M., Watton P.N. (2019), *A novel mathematical model of cerebral vasospasm: a revolution of treatment strategies* (poster presentation), STEM for Britain, March 13, London, UK

Contents

This page has been intentionally left blank.

List of Figures

This page has been intentionally left blank.

List of Tables

This page has been intentionally left blank.

Chapter 1

Introduction

The relationship between form and function is crucial for the understanding of the behaviour of soft tissue in development, health and disease. Arteries play the essential role of containing and directing the flow of blood throughout the body and their correct functioning is fundamental for the health of the entire body. The structure of the arterial wall (Section 1.1) must therefore balance rigidity and compliance in order to not only contain blood and maintain pressure but also allow the blood to flow at the appropriate speed and adapt to states of low to high exertion. The main translational application presented in this dissertation concerns cerebral vasospasm, a prolonged acute constriction of a cerebral artery that in severe cases impairs the blood supply to the brain and resulting in high morbidity and mortality (1.2). The modelling framework adopted is characterised by the inclusion of both biomechanical and mechanobiological aspects, where the former refers to the study of the mechanical properties of living tissue while the latter is concerned with the relationship between the mechanical environment and the activity of the cell. Key aspects of mechanobiology are overviewed in Section 1.3. Finally, fundamental concepts of mathematical and computational modelling of soft tissue that underpin the work presented here are discussed in Section 1.4.

1.1 Structure of the Arterial Wall

Most of the content in this Section comes diffusely from three main sources and therefore they are listed here for convenience: Alberts et al. (2015), Holzapfel et al. (2000), Robertson & Watton (2013). In-text citations remain for specific claims when appropriate.

The arterial wall can be divided into **three concentric layers**, each comprised of a number of **vascular cells** (such as *endothelial cells*, *smooth muscle cells*, and *fibroblasts*) embedded in a network of macromolecules called the **extracellular matrix** (ECM). The macromolecules in the ECM are mostly proteins (*elastin*, *collagen*, *fibronectin* and *laminin*) and *glycosaminoglycans* (GAGs), i.e. unbranched polysaccharide chains. Among serving other functions, GAGs draw water into the ECM giving it a gel-like consistency which accounts for its compressive resistance and enables diffusion of molecules within the wall.

Vascular cells play a crucial role in the production, degradation and repair of the ECM, which is crucial for the good functioning of the arterial wall. The mechanisms of ECM maintenance are dictated by the interpretation of chemical and mechanical signals in the extracellular environment: examples of chemical signals are acidity, oxygenation, concentration of growth factors or other relevant molecules, while examples of mechanical signals are changes in cyclic deformations, wall shear stress and wall shear stress gradient among others. These signals are communicated to the cell nucleus, where they regulate DNA transcription and thus influence the cell morphology, proliferation, migration, alignment, etc.

The three concentric layers comprising the arterial wall are structured as follows (see Fig. 1.1):

- **Endothelium**: this is the innermost layer and is mainly comprised of endothelial cells in direct contact with the blood flow within the lumen on one side and attached to a collagen network called the basement membrane on the other.
- **Tunica media**: this is the middle layer and is mostly occupied by smooth muscle cells in a network of elastin and collagen fibres.
- **Tunica adventitia**: this is the outermost layer and it mostly consists of collagen fibres maintained by a population of fibroblasts.

The layers are divided by the so called **elastic laminae**, which consist of concentric sheets of elastin fibres punctuated by *fenestrae* (windows) which allow transport of substances between the layers:

- the **internal elastic lamina** separates the endothelial from the medial layer, and
- the **external elastic lamina** separates the medial from the adventitial layer.

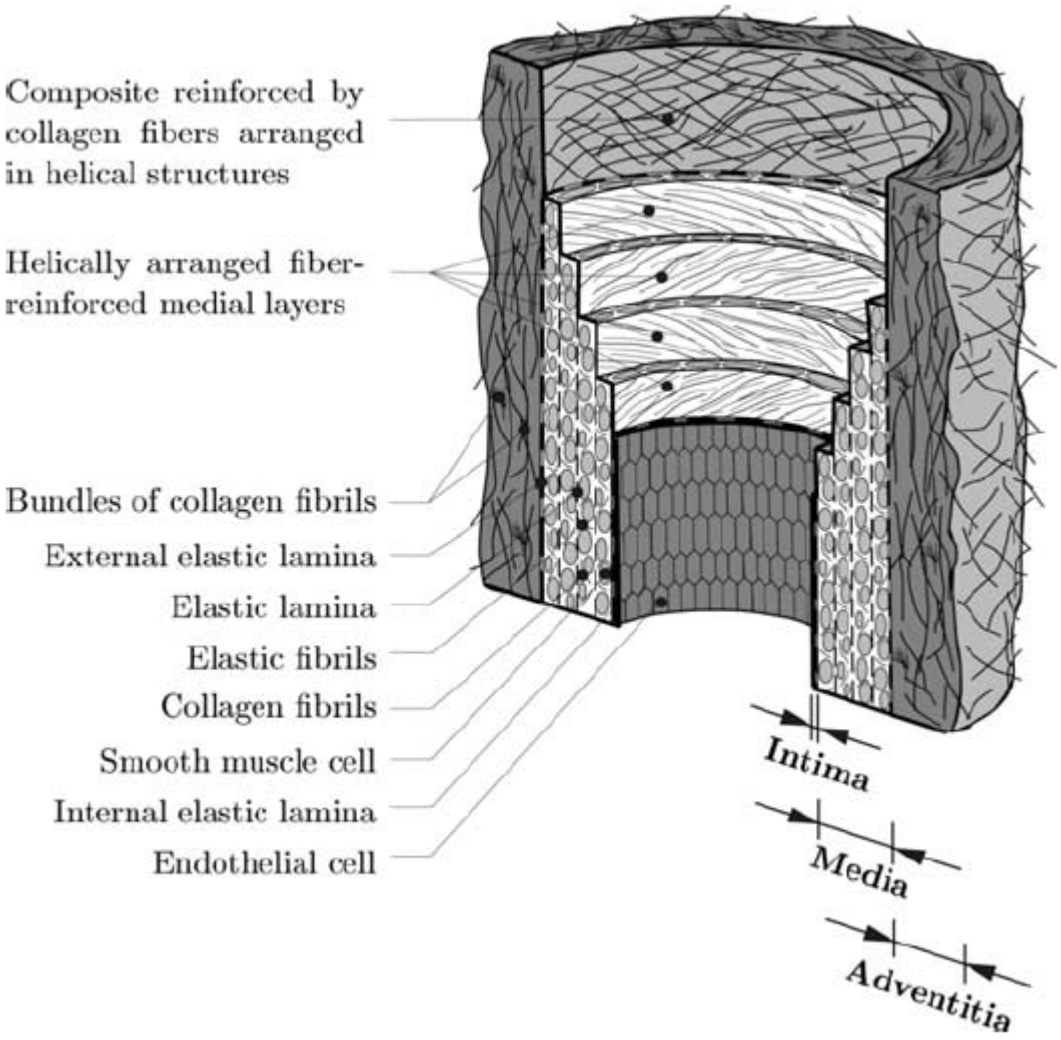

Figure 1.1: Structure of arterial wall. The innermost layer (intima) is mostly comprised of endothelial cells; the middle layer (media) contains mostly smooth muscle cells and elastin; the outermost layer (adventitia) is mostly formed by collagen fibres and fibroblast cells. Each layer is separated from the next by an elastic lamina. Source: Holzapfel et al. (2000)

The components of the arterial wall that are more often incorporated in computational models will now be described in more detail: collagen, elastin, endothelial cells, smooth muscle cells and fibroblasts.

Collagen is not understood as a single molecule, but as a heterogeneous family of molecules sharing the same structure: each collagen molecule comprises three polypeptide right-handed α-chains, where each strand is a left-handed helix with three amino acids per turn. There are 28 different types of collagen that have been discovered to date, each identified by a Roman numeral. Collagen molecules can organize into *fibrils*, *microfibrils*, *filaments* and *network-like* structures, according to

the function they serve. These can in turn be arranged into more complex structures, for example fibrils can arrange into *fibres* and *lamellae*, while network-like structures can assemble into *basement membrane*, among others. The structural integrity of collagen is crucial to its mechanical function. *Hydrogen bonds* and *lysine* are two elements that play a key role in the robustness of the structures: the first binds the α-chains thus stabilizing the helical structure, while the second is an amino acid responsible for the cross-linking between α-chains and between collagen molecules.
More than 90% of vascular collagen is of type I, III or V, which are of the fibril-forming kind and play the most important role in mechanical load-bearing. Fibrils can be $10-500$nm in diameter in mammals and can combine to form larger fibres ($0.5-3\mu$m), which in turn assemble into *fibre bundles*. The morphology of the fibres changes across the wall and throughout the vasculature and displays different fibre diameters, orientation and tortuosity. In unloaded arterial tissue, all collagen fibres appear crimped with different levels of waviness. They are responsible for the strong non-linearity of the arterial response at higher stretches, since the fibres are progressively recruited to load-bearing. Collagen types I and III represent roughly 60% and 30% of the total arterial collagen respectively, with the remaining 10% being mostly Collagen V and others.
Another relevant type of Collagen is number IV, which is exclusively found in *basal laminae*. It is a key component of the basement membrane but is also found in the basal lamina surrounding VSMCs, where it is believed to influence their migration, proliferation and phenotype (Steucke et al. (2015)).

Elastin is an extremely hydrophobic protein formed of loose, unstructured polypeptide chains, in contrast with the highly organized collagen molecule. It is responsible for storing the majority of the elastic energy of the arterial wall, making it highly flexible at low loads and very resilient. The elastin molecules are arranged in *fibrils* about 10nm in diameter, which are in turn assembled into fibres and *lamellae*.
The majority of arterial elastin is formed during the perinatal period and the wall's capacity to maintain it drops significantly after puberty (Hill et al. (2012)). The absence of elastin turnover means that any damage to the constituent will be hard, if not impossible, to repair, but it could also play a stabilizing role for growth and remodelling processes within the wall, since the unloaded configuration of elastin can be of reference for the entire wall.

Endothelial cells (ECs) play a crucial role in *mechanotransduction* and *transport* of molecules through the arterial wall.

Due to their being in direct contact with the blood flow, ECs can sense changes in mechanical stimuli, such as cyclic deformations, wall shear stress, wall shear stress gradient, etc., and translate them into chemical signals. Although this process, called mechanotransduction, is not completely understood, a few elements have been identified as playing an important role, namely the intracellular cytoskeletal structure, cell-to-matrix binding molecules (e.g. integrins) and cell-to-cell binding molecules. When these elements sense a perturbation, they communicate it to the nucleus which changes its regulatory activity and the cell further relays the signals throughout the remainder of the wall.
Furthermore, the direct contact with blood makes the endothelial layer the key regulator of wall *permeability*, i.e. the rate of absorption of molecules from the blood stream, such as oxygen, nutrients, leukocytes, etc. This is a crucial process for vascular homeostasis and wound healing. A central factor in determining the permeability of the wall is the level of overlap of the edges of ECs.

Smooth Muscle Cells (SMCs) have a spindle-like shape and are mostly found in the medial layer, aligned in the circumferential direction (Rothermel et al. (2020), Ushiwata & Ushiki (1990)). They are about 100μm long and 5μm wide. Contrary to the other cells and constituents in the arterial wall, SMCs can not only undergo passive elastic stretch, but also provide an *active* contraction which allows them to regulate the arterial diameter, blood pressure and blood flow distribution.
In a healthy artery, they mostly appeared in a *contractile* state, but can adopt a range of phenotypes between the contractile and the *synthetic*. The latter is characterized by a more cobblestone-like shape and higher rates of proliferation, migration and synthesis of ECM, especially collagen. The switching between phenotypes can be remarkably fast, allowing them to enact quick changes in vessel caliber as well as a prompt response when tissue repair is necessary.

Fibroblasts are mostly found in the adventitial layer where they are responsible for the regulation of the ECM. This is a very important task since the adventitia becomes the main load bearer at higher stretches, when the risk of tissue rupture increases. Fibroblasts are known to be able to secrete ~ 3.5 million procollagen molecules per day, where procollagen is a precursory molecule to collagen. They also secrete a number of other ECM components, as well as molecules that balance the production and degradation of collagen, such as matrix metalloproteinases (MMPs) and their inhibitors (TIMPs). They also play a key role in wound healing and in the initiation, modulation and maintenance of the inflammatory response.

Fibroblasts display a range of phenotypes characterized by different levels of activity such as proliferation, differentiation and ECM regulation. Phenotypes with high activity levels are called *myofibroblasts* and are activated in, for example, inflammation or wound healing.
Fibroblasts are connected to the adventitial ECM through protein aggregates called *focal adhesions*, e.g. integrins. These adhesions are mechanosensitive and can transmit mechanical signals to the inside of the cell, where they are translated into chemical signals that regulate cell activity (Beningo et al. (2001), Webster et al. (2014)).

The functionality of the arterial wall obviously depends not only on the single constituents but on their interaction and relative spatial distribution. Understanding cell signalling and cell activity regulation is a crucial component of understanding the growth and remodelling processes occurring within the wall in both health and disease.

1.2 Cerebral Vasospasm

Cerebral vasospasm (CV) is a prolonged constriction of a cerebral artery which diminishes blood flow to the brain and in severe cases can lead to cerebral ischemia or infarction. It is likely to occur in patients presenting with subarachnoid hemorrhage (SAH), which is in turn most often caused by either rupture of an intracranial aneurysm (IA) or by traumatic head injury (Humphrey et al. (2007 September *a*)). In the former case, it will occur in about 70% of patients, manifesting between three and five days post IA rupture; $30 - 50\%$ of patients will show neurological deficits (Bhogal et al. (2016), Wicker et al. (2008)). For patients who survive hospitalization after IA rupture, it is the leading cause of morbidity and mortality. The peak of constriction occurs about 7 to 10 days after the initial bleed, thus a prompt and effective clinical response is critical. However cases have been observed in which vasospasm self-resolves and the affected vessel returns to its nominal diameter in an average time of four weeks (Humphrey et al. (2007 September *a*), Reilly et al. (2004)), therefore it is also important to correctly determine whether treatment is necessary. The etiology and pathogenesis of the disease are complex, multifactorial and not yet completely understood.

The current understanding of the disease is summarized as follows. The location of the constriction is observed to coincide with the area of blood accumulation and the severity appears to be proportional to the size of the blood clot, therefore there is little doubt that the hemorrhage is the initial causal factor of disease inception. This is in

fact thought to cause an increase in the production of vasoconstricting substances, in particular oxyhemoglobin and endothelin-1, which drive the contraction of smooth muscle cells (SMCs) in the medial layer (Macdonald & Weir (1991), Provencio & Vora (2005)). This first immediate (up to 3 days) phase can be reversed by administration of vasodilators, but the fact that this is no longer effective in later stages suggests that other processes begin to occur (Macdonald et al. (1995), Matsui et al. (1994), Nakagomi et al. (1990), Vorkapic et al. (1991*a*, 1990, 1991*b*)). It is believed that these changes in the arterial wall cause an increase in stiffness and thus a leftward shift in the active force-diameter curve (Bevan et al. (1987), Humphrey et al. (2007 September*a*), Macdonald et al. (1995), Matsui et al. (1994), Nagasawa et al. (1982), Vorkapic et al. (1991*a*, 1990), Yamaguchi-Okada et al. (2005)). Secondarily, the increasing vasoconstriction can severely corrugate and damage the endothelial layer (Kapp et al. (1985), Mizukami et al. (1976), Nakagomi et al. (1990), Smith et al. (1985), Zubkov et al. (2002)), with some cells detaching from the arterial wall and leaving exposed subintimal connective tissue that platelets and other blood elements can attach to, possibly forming mural thrombi (Kapp et al. (1982)). Endothelial damage can also alter mechanotransduction of hemodynamic signals into cellular activity in the medial and adventitial layer, together with exacerbating the chemical imbalance responsible for SMCs contraction: for example endothelial cells (ECs) are, among other things, capable of releasing vasodilating nitric oxide (Kassell et al. (1985)).

Finally, inflammation has been observed in vasospastic arteries (Hughes & Schianchi (1978), Mayberg et al. (1990)). This could be caused by the extravascular blood clot and exacerbated by damage to the endothelium and could be the cause of other observed changes in wall structure. The pathophysiology of vasospasm indeed appears to be a highly complex and multifactorial process and the morphological changes occurring in the arterial wall appear to depend not only on the severity of the disease but also on the time since SAH. Analysis of the literature on human and animal models of vasospasm is complicated by the highly time-dependent evolution of the disease and the fact that this time scale is not always reported in the studies or, especially in older ones, not even considered. The most relevant morphological changes reported in the literature are the following:

- **Intimal thickening**: in human models it is reported by Mizukami et al. (1976) as " intimal thickening consisting of loosely arranged eellulofibrous tissue confined to one side of the arterial wall" and by Hughes & Schianchi (1978) who observe one case in which "the subendothelial thickening consist-ed of collagen fibers,

fibroblasts, and foamy macrophages"; the monkey model presented by Findlay et al. (1989) reported presence of collagen which is confirmed by Macdonald et al. (1992) who stained for specific types of collagen proteins and identified types I and III.

- **Myointimal cells**, i.e. muscle-like cells in the intimal layer of the wall. This is reported in several studies such as Findlay et al. (1989), Kapp et al. (1985), Mayberg et al. (1990), Smith et al. (1985) and Sacher & Tenner (1978). In particular Macdonald et al. (1992) and Hughes & Schianchi (1978) report it as a feature of vasospasm that only appears at a late stage, specifically at day 28 and after three weeks respectively, where Macdonald et al. (1992) made observations every 7 days.

- **Corrugation of the internal elastic lamina** is easily observed and has thus been reported in several studies such as Findlay et al. (1989), Hughes & Schianchi (1978), Kapp et al. (1985), Macdonald et al. (1992), Mayberg et al. (1990), Nakagomi et al. (1990), Sacher & Tenner (1978), Zubkov et al. (2002) and Mizukami et al. (1976). This results in the elastic lamina bending and looking “wavy" at the microscope.

- **Myonecrosis**, i.e. necrosis of smooth muscle cells, has been observed in some cases in Kapp et al. (1985), Mayberg et al. (1990) and Findlay et al. (1989), more consistently in Sacher & Tenner (1978), Smith et al. (1985) and Mizukami et al. (1976), and finally Hughes & Schianchi (1978) reports it as very significant after three weeks.

- **VSMC differentiation** into a synthetic and migratory phenotype is observed in Yamaguchi-Okada et al. (2005) and Mayberg et al. (1990). Chen et al. (2009) report an increase of molecules p-ERK1/2 where ERK1/2 are hinges of the MAPK signalling pathway, which is the main pathway regulating vascular proliferation; this can therefore be considered as indirect evidence of VSMC proliferation.

- **Medial fibrosis** has been analysed in several studies with varying and sometimes conflicting results. It is observed in Hughes & Schianchi (1978), Kapp et al. (1985), Macdonald et al. (1992), Mayberg et al. (1990), Smith et al. (1985), Yamaguchi-Okada et al. (2005) and Sacher & Tenner (1978) but the identity of the proteins responsible for this fibrosis have not been clearly identified: Kasuya et al. (1993) reports an increase in the gene expression of procollagen I and III

as well as TGF-β, an up-regulating molecule of collagen synthesis; Yamaguchi-Okada et al. (2005) has quantified collagen content in vasospasm over time and but a statistically significant increase was only observed at day 14, while it was not significant at days 7 and 28; they therefore submit that the increased connective tissue might consist of a different molecule. Finally Macdonald et al. (1992) observes no increase in collagen via both qualitative and quantitative methods, but does report increased immunoreactivity to fibronectin. It is therefore suggested that medial fibrosis could consist of molecules of fibronectin, which additionally participate in the cross-inking of collagen molecules, and could therefore contribute to the increased stiffness of the arterial wall.

When the studies consider the time course of the disease, it is evident that there is a high dependence on time from SAH of the remodelling processes occurring within the arterial wall during the disease. This of course has a significant impact on the choice of a suitable treatment method.

If vasospasm is detected in its first phase, it is possible to resolve it by sole administration of vasodilating substances, for example nimodipine or other calcium-channel antagonists (Vorkapic et al. (1990)). If the constriction is too severe or detected at a later stage, a different treatment strategy must be adopted. One option is through hypertension, hypervolemia and hemodilution (HHH), which has been shown to be effective in some cases. However, it is not clear which of the three mechanisms is actually effective and why, and comes with serious risks, such as cardiac failure, electrolyte abnormalities, cerebral edema, bleeding abnormalities, and rupture of an unsecured aneurysm (Mayberg et al. (1994)). The most often adopted treatment strategy for severe cases of vasospasm is balloon angioplasty. This consists in the insertion of a balloon in the area of the vessel affected by vasospasm, inflation of the balloon until a desired diameter or pressure is achieved, and finally deflation and retrieval of the balloon (Fig. 1.2). A review of reported cases shows that angioplasty achieves reduction of neurological damage in 31% to 81% of cases and vasospasm does not recur following treatment (Li et al. (2019)). The main drawback of this interventional method is that complications occur in 5% of cases and can be severe, such as rupture of the arterial wall, which is almost inevitably fatal, and stroke due to interruption of blood flow during the procedure (Macdonald (2006)). Moreover, balloon angioplasty has been shown to damage the extracellular matrix and cause a decrease in arterial response to vasoconstricting substances.

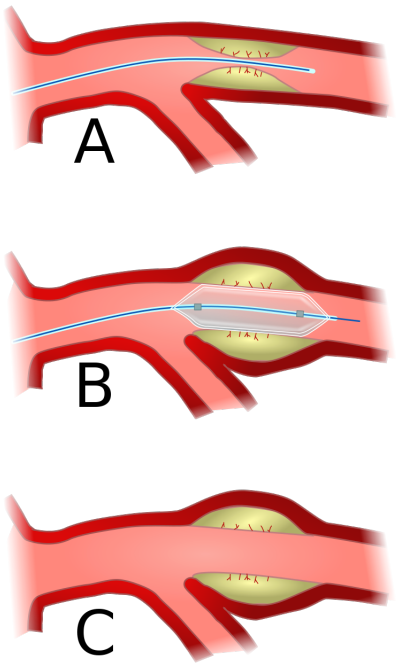

Figure 1.2: Schematic of balloon angioplasty. First the balloon catheter is inserted into the area of interest (A), then the balloon is inflated to a desired diameter (B), finally it is deflated and retrieved (C). (Courtesy of Wikimedia, licence CC BY-SA 3.0, https://commons.wikimedia.org/w/index.php?curid=19334307)

Recently, a new treatment strategy has been proposed by Bhogal et al. (Bhogal et al. (2016), Bhogal et al. (2017)), which advocates the use of self-expanding stent-retrievers for the mechanical dilation of the artery (Figure 1.3). Stent-retrievers were originally designed to retrieve blood clots that could be occluding an artery. These stents are enveloped in a sheath, the sheath is inserted into the artery then pulled back to release the stent in a desired location. The stent slowly “springs" open trying to return to its stress-free diameter until it touches the vessel wall and an equilibrium is reached between the expanding force of the stent and the resistance of the wall to this dilation which depends on its stiffness.

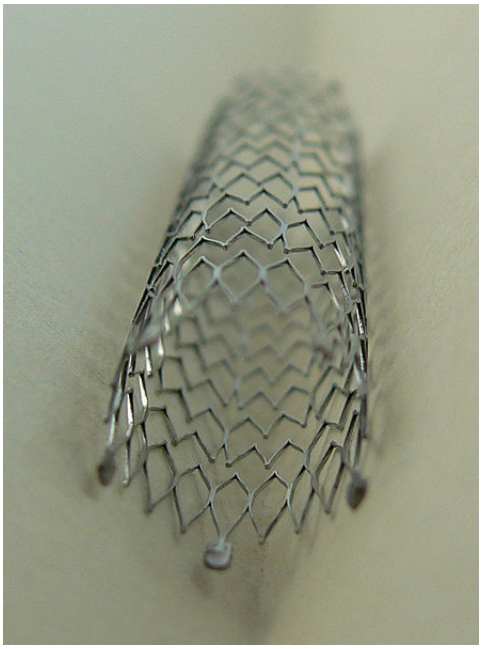

Figure 1.3: Photograph of a stent. (Courtesy of Frank C. Müller, licence CC BY-SA 4.0, https://creativecommons.org/licenses/by-sa/4.0/deed.en)

The advantages of this treatment are related to the significantly lower forces exerted by the stents compared to balloon catheter. These would in fact cause little to no damage to the extracellular matrix and there would be no risk of arterial wall rupture. This treatment strategy has been observed to be successful in arteries of up to about 3mm diameter, while they have had no effect in larger arteries (Bhogal et al. (2016), Bhogal et al. (2017)). An ideal mechanical treatment would exceed the minimum sufficient pressure to resolve the disease by the smallest amount possible so as to avoid exerting unnecessary pressures that could damage the arterial wall. Because of the dramatically lower forces exerted by stent-retrievers compared to balloon angioplasty, it is relevant to answer the following questions:

- what magnitude of internal pressure should an interventional device provide to mechanically resolve cerebral vasospasm?
- is it sufficient to “disrupt" the smooth muscle cells or should other constituents such as the ECM be “damaged" too?

At the moment it is not specified what is meant by “disruption" or “damage" and the issue is discussed in more detail in later Chapters. Since the precise mechanism of action of either balloon angioplasty or stent treatment is unknown, in this work no assumption is made on the precise nature of the damage but as a mathematical idealisation it is

meant that a constituent is no longer contributing to load bearing. These questions have constituted the motivation behind the model I discuss in Chapter 2. The focus of the model has been on hypotheses regarding the microstructural remodelling of the arterial wall, in particular of smooth muscle cells, and the model predictions have been consistent with documented cases of treatment via self-expandable stents. If further validated, this could lead to a revolution in the treatment strategy of the disease, decreasing its risk factors and its negative side effects post-intervention.

Mathematical modelling can be a useful method to test competing hypotheses on the pathogenesis of the disease and help in discerning which interventional strategy is better suited to a specific case of cerebral vasospasm. In order to do this, the model presented in Chapter 2 will need to be sophisticated and possible directions for further research are discussed in Chapter 6.

1.3 Cell structure and mechanobiology

Observations that the mechanical environment of a cell has an influence on its biological function go back to at least a century ago and in the last fifty years interest in the study of this relationship has been rising. Indeed it is thought that a deeper understanding in this field, termed *mechanobiology*, is crucial to gain insight into the development processes of various diseases and thus improve the ability to predict disease progression and eventually treatment strategy.

There are two main pathways by which a cell might receive mechanical signals: either via cell-to-cell interaction or via cell-to-matrix. In both cases proteins on the cell membrane connect to either another cell or a protein of the extracellular matrix and transmit the mechanical signal to the cytoskeleton of the cell, which might communicate with either the cell nucleus or another mechano-sensing protein in a different location on the cell membrane.

On the inside of the cell wall, mechanical signals are transmitted by the cell's cytoskeleton, a complex network of several types of proteins that give the cell its structure, mechanical as well as motor function. There are three main families of filaments: *actin*, *microtubules* and *intermediate filaments*. Actin filaments shape the cell surface and are the key actors in cell locomotion; microtubules connect to cytoplasmic organelles and direct intracellular transport, while intermediate filaments provide mechanical strength. The structure of the cytoskeleton is not fixed in time, but is highly adaptable and responds to chemical and mechanical cues. This adaption is realised by the

assembly and disassembly of specific filaments depending on the circumstances.

At the cell membrane, the mechano-sensing proteins regulating cell-to-cell communication involving the cytoskeleton are of two types: *adherens junctions* anchor to actin filaments within the cell, while *hemidesmosomes* anchor to intermediate filaments. Other types of connections exist that do not connect to the cytoskeleton: *tight junctions* connect adjacent cells tightly having one of their ends in one cell and the other in the adjacent cell, while *gap junctions* function as "channels" connecting the cytoplasm (Alberts et al. (2015)). For cell-to-matrix junctions, the most important type is called *focal adhesion*. Each of these junctions consists of a number of proteins but the main role is played by the transmembrane protein connecting the interior of the cell to the outside. This can belong to one of two families: *cadherins* regulate cell-to-cell communication, while *integrins* connect the cell to the matrix. A particularly interesting feature of integrins is their ability to adopt a range of states from *active* to *passive* which affect its conformation and the relative positions of the two subunits that comprise them, denominated α and β. This range of activity allows the cell to rapidly assemble or disassemble connections to the cytoskeleton and thus have more refined communication with the matrix surrounding it.

Cell-to-matrix interaction is particularly important since the ECM is maintained by residing cells which regulate its production, degradation and organisation. For example newly secreted collagen is attached to the matrix by a "crawling"-like movement of the cell along existing fibres (Robertson & Watton (2013)). Moreover, it has been shown that cells, in particular fibroblasts, apply tension to the extracellular matrix, tugging on it, and organise the structure of the matrix. Depending on the mechanical environment, they are capable of identifying the "correct" orientation at which collagen must be deposited (Alberts et al. (2015)). Tension plays a key role in the assembly of fibronectin as well: indeed fibres of this type assemble at the cell surface where the tension applied by the cell reveals otherwise concealed binding sites that allow the fibrils to bind to each other and form complete fibres.

The insight that the mechano-sensitivity of cells might play a key role in the development of various soft tissue diseases has led mathematical and computational modellers to formulate mechanobiologically motivated hypotheses that have found many useful applications. Humphrey (2008) advanced the hypothesis of "tensional homeostasis", namely the existence of an optimal level of stress that a cell aims to maintain. This can differ among cell types and indirectly apply to non-living tissue components, such as collagen. Indeed, although collagen is maintained by an external entity which is

the cell, it is possible for the cell to “know" the optimal level of stress at which to maintain the collagen fabric. This simple hypothesis has found good success and proved powerful in several modelling scenarios (Cyron (2019), Humphrey & Holzapfel (2012)) and has also been adapted to a “homeostatic stretch" version compared to the original “homeostatic stress" formulation (Eriksson et al. (2014), Grytsan et al. (2017), Watton et al. (2004), Watton, Ventikos & Holzapfel (2009)). From the perspective of numerical implementation, the stress formulation is more natural since stress is a convenient variable that is solved for and explicitly computed in biomechanical problems and thus is easier to work with in a computational model. On the other hand, the stretch formulation is directly measurable in experiments and therefore easier to validated experimentally.

Recently it has been proposed that the hypothesis of the homeostatic level of stress/stretch being constant could be refined to an “adaptive homeostasis" hypothesis that allows the definition of homeostasis to vary according to the chemo-mechanical environment of the cell (Ambrosi et al. (2019), Aparìcio et al. (2016), Ateshian & Humphrey (2012), Watton, Ventikos & Holzapfel (2009)). This has proved to yield more realistic results in some cases (Chen (2014)) and warrants further exploration.

In general the study of mechanobiology is attracting growing interest and will play a crucial role for the successful modelling of various soft tissue diseases especially leading to better predictions of disease development thus affecting clinical decision-making. A challenge in the modelling of mechanobiological phenomena is the current paucity of experimental data and therefore deeper collaborations are warranted in this field. Moreover recommended future directions include the incorporation of chemical signalling pathways, since there is continuous translation of mechanical stimuli into chemical ones and viceversa, and thus the aim of a realistic model of soft tissue evolution warrants coupling of the two mechanisms (Ambrosi et al. (2019), Ateshian & Humphrey (2012), Irons & Humphrey (2020)).

1.4 Overview of previous modelling

The models presented in this dissertation are based upon the framework originally proposed by Holzapfel, Gasser and Ogden (Holzapfel et al. (2000)) and later expanded by Watton et al. (Watton et al. (2004), Watton, Ventikos & Holzapfel (2009)). The framework proposed in Holzapfel et al. (2000) was the first to include histological information about the arterial tissue differentiating between the layers that comprise

the structure of the arterial wall and the microstructural constituents within each layer. In particular, the strain energy density function was additively split into the contribution of the isotropic components, like elastin and ground matrix, and that of the anisotropic components like collagen:

$$\Psi = \sum_{L=M,A} \frac{c_L}{2}(\overline{I}_1 - 3) + \frac{k_{1L}}{2\ k_{2L}} \sum_{i=1}^{n} (\exp\left(k_{2L}(\overline{I}_{iL} - 1)^2\right) - 1), \tag{1.1}$$

where $L = M, A$ indicates the medial and adventitial layer, c_L, k_{1L} and k_{2L} are material parameters, and $\overline{I_1}, \overline{I_i L}$, $i = 1, \ldots, n$ are invariants of the modified Cauchy-Green tensor $\overline{C}$ defined as $\overline{I_1} = \overline{C} : I$, $I_{iL} = \overline{C} : A_{iL}$ where A_{iL} is the structure tensor associated with the directions of the collagen fibres in family i (n being the number of fibre families).

For clinical purposes it was important to not only have a biomechanical model of arterial tissue that would allow the study of the tissue properties at a fixed moment in time, but also to model how the structure of the tissue, and therefore its mechanical function, evolved over time. The initial models were therefore extended to include “growth and remodelling": “growth" describes the changes in mass of a tissue constituent, while “remodelling" refers to structural changes that may alter the constituent properties, such as reorientation, increased or decreased cross-linking, etc. In Humphrey & Rajagopal (2002) the first *constrained mixture* model of growth and remodelling is proposed, in which individual constituents could undergo changes in mass and structure while consistency of deformation was maintained for the whole tissue. The SEDF was then changed to the following

$$\Psi = \sum_{i,L} v_L\ \phi_L^k\ \Psi_L^k, \tag{1.2}$$

where v_L is the volume fraction of layer L, ϕ_L^k is the mass fraction of constituent k in layer L and Ψ_L^k is the SEDF of constituent k in layer L.

This framework became widely popular as it allows the definition of different mechanical behaviours for different constituents as well as the possibility to consider changes in mass and/or volume whenever v_L, ϕ_L^k and Ψ are time dependent. This opened up the possibility of defining evolution laws for these variables, or other variables they would depend on, and thus *growth and remodelling* models were created.

A particular subset of this type of model is that focused on mechanobiologically-informed growth and remodelling laws. As discussed in Section 1.3, the mechanical environment of living cells affects their activity in various ways and the interplay between the two can play a critical role in the stabilisation or lack thereof of eventual pathologies (Humphrey (2008)). There has therefore been significant interest in developing G&R laws that related mechanical variables (pressure, stretch, stress, wall shear stress, etc.) to cell activity, which can influence the mass and/or configuration of tissue constituents.

Two different approaches have been developed for the problem: an *integral* and a *differential* formulation. The former was first proposed by Baek et al. (2005) and expresses the current mass fraction of a constituent as the integral up to time t of the production rate $m_L^k(\tau)$ times the survival function $q(t-\tau)$. It is a natural and intuitive formulation, but has a drawback in the need to store a large quantity of information (i.e. the history in time interval $[\tau, t]$) which limits its numerical application. The differential formulation was first proposed by Watton et al. (2004) where differential equations are used and mass growth/atrophy as well as other variable changes are *rate*-dependent. This avoids the need for numerical integration entirely, making it more feasible for numerical implementation, although some information is lost as only the result of the production and degradation of a constituent is explicitly saved, not the two separate processes.

The constrained mixture differential formulation proposed by Watton et al. (2004) was integrated into a thick-walled finite element framework and coupled with haemodynamics in Watton, Ventikos & Holzapfel (2009). The framework allowed the study of the effect that transmurally heterogeneous material properties within the arterial wall have on the stress distribution in the evolution of abdominal aortic aneurysms. Finally Eriksson et al. (2014) extended the finite element framework to include volumetric growth and Grytsan et al. (2017) implemented a model of *anisotropic* volumetric growth. The most recent extension of the framework has been proposed by Aparìcio et al. (2016) who introduced a bio-chemo-mechanical feedback cycle which relates changes in the concentrations of relevant signalling molecules to growth and remodelling process which are finally coupled to the haemodynamics. As a first iteration this has been implemented with a membrane assumption but it would be straight-forward to integrate it into the finite element framework.

This modelling framework has been used to model aneurysms, both cerebral and abdominal aortic, but its general nature allow for a wider scope of application and

it can therefore be applied to model other soft tissue diseases. In the case of this dissertation, the interest is in modelling cerebral vasospasm.

To the author's knowledge only one mathematical model of the development and progression of cerebral vasospasm has been proposed. Humphrey et al. (2007 September*b*) and Baek et al. (2007) have proposed a constrained mixture growth and remodelling model of non-severe cases which hypothesizes that the development of vasospasm is initially driven by a chemically-induced increased vasoconstriction accompanied by cell and matrix turnover that increase the wall stiffness, while a later phase is dominated by mechanical and haemodynamical signals that alter the growth and remodelling process in a way that returns the vessel to its original healthy state. The model is two-dimensional in the geometry, one-dimensional in the haemodynamics and zero-dimensional in the chemical insult to the tissue. The model indeed captures salient features of the pathophysiology of vasospasm such as the decreased contractility and compliance of the vessel wall in the chronic phase of vasospasm and the potential of the disease to "self-reverse" in some cases once the extravascular blood clot has been cleared and the haemodynamical stimuli gradually restore the vessel to its physiological geometry.

1.5 Contributions to the state of the art

The work presented in this dissertation consists of a mathematical and a finite element model of cerebral vasospasm based on a novel hypothesis that the disease is primarily driven by contraction and remodelling of vascular smooth muscle cells. Moreover it aims to estimate the amount of pressure that an interventional device, such as a balloon or a stent, needs to apply in order to mechanically resolve the disease. The model is built on the framework developed by Watton et al. (2004), which is selected as it allows to more easily neglect the haemodynamics as a first step and focus on the growth and remodelling processes occurring in the arterial wall. Since the model has mostly been applied to aneurysms, where vascular smooth muscle cells are often considered necrosed and negligible, it needs to be extended to include a material model for VSMCS: this is adapted from Baek et al. (2007). The resulting model is presented in Chapter 2. The mathematical model is then integrated into a finite element framework to study whether the non-uniformity of the strain field across the wall thickness has an effect on the pressure predictions related to the treatment of the disease. The adopted finite element framework is the one developed by Watton,

Eriksson and Grytsan (Eriksson et al. (2014), Grytsan et al. (2017), Watton, Ventikos & Holzapfel (2009)) and applied to aneurysms. Analogously to the mathematical model, the framework needs to be extended to accommodate the role of VSMCs in the model as well as damage mechanisms to the constituents. These extensions are described in Chapter 3. The finite element model resulting from the integration of the mathematical model into the extended finite element framework is described in Chapter 4. Chapter 5 describes an extension to the mathematical model that includes collagen growth and remodelling. Indeed an assumption of the mathematical model presented in Chapter 2 is that the role of collagen growth and remodelling is negligible for the purpose of modelling cerebral vasospasm at the time at which it most often requires treatment, i.e. 1-2 weeks after subarachnoid hemorrhage. However is it possible that even small changes have an effect on the pressure predictions for treatment and thus a study is conducted for this purpose. Finally the main achievements and limitations of these models are discussed in Chapter 6.

Chapter 2

1D Model of Cerebral Vasospasm

2.1 Introduction

This Chapter presents a model of cerebral vasospasm which focuses on the microstructural adaptations occurring in the arterial wall and how these affect its mechanical response. This choice was made in view of the specific translational motivation, which is to determine the magnitude of pressure that an interventional device (such as a stent-retriever or balloon catheter) should provide in order to mechanically resolve the disease. The model is based on the framework developed by Watton et al. (2004), Watton, Ventikos & Holzapfel (2009), i.e. a constrained mixture of the relevant constituents of the vessel wall (in this case elastin, collagen and vascular smooth muscle cells) where the mass and reference configuration of the constituents can change over time according to custom evolution equations. Our main hypothesis is that vasospasm is driven by VSMC remodelling: following an initially chemically-driven contraction, the cells remodel their cytoskeleton and attachments to the extracellular matrix in order to maintain a preferred state of stretch. Based on a strain-based damage model for VSMCs, predictions are obtained of success or lack thereof for commonly available stents and compared to reported clinical observations.

2.2 Methods

The artery is modelled as a nonlinear elastic incompressible cylindrical membrane, subject to internal pressure and a constant axial stretch. By modelling the artery as a membrane it is assumed that the variations in the stress field across the wall thickness

are negligible and thus only the value of the stress at the mid-plane is used. It is also assumed that bending moments and transverse shears are negligible. The configuration corresponding to the absence of forces acting on the artery, in which therefore the stress within the wall is null, is referred to as the *unloaded configuration*. In this state, the artery has wall thickness H, radius R and length L. The mechanical stretch of the tissue is defined in relation to this configuration and thus it is denominated the *reference configuration*. After applying an internal pressure p equal to systolic blood pressure and an axial pre-stretch λ_z, the cylinder is in its *loaded configuration*. In this state the circumference has been stretched by a factor λ and the new wall thickness h, radius r and length l are equal to

$$h = \frac{H}{\lambda_z \, \lambda}, \tag{2.1}$$

$$r = \lambda \, R, \tag{2.2}$$

$$l = \lambda_z \, L. \tag{2.3}$$

See Fig. 2.1 for reference.

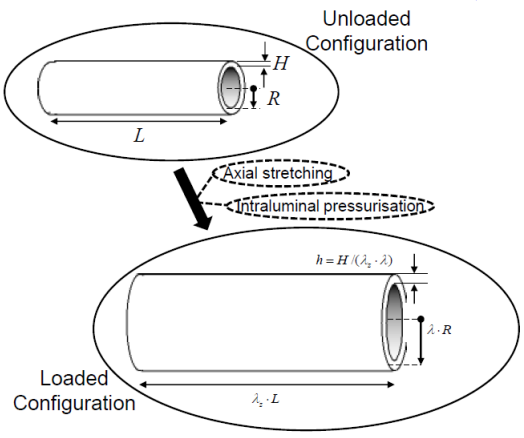

Figure 2.1: Effect of axial stretching and intraluminal pressurization on elastic cylinder. Source: Aparìcio et al. (2016).

The force balance equation for a pressurised and axially stretched cylinder can be expressed as

$$p = \frac{h}{r} \frac{1}{\lambda_z \lambda} \sigma, \tag{2.4}$$

where σ is the Cauchy stress through the entire wall.

A constrained mixture approach is adopted where the overall stress response of the tissue is the sum of the contributions of its microstructural load-bearing constituents. Each constituent has its own independent reference configuration but deforms consistently with the rest of the tissue. The differences in mechanical properties and reference configurations among the constituents allow us to capture the different mechanical roles they play. The most mechanically relevant constituents are considered: elastin (E), collagen (C) and vascular smooth muscle cells (M).

For each constituent it is postulated that there exists a preferred state of stretch, which optimizes its mechanical function in some sense. This state of stretch is called the *attachment stretch* or *homeostatic stretch*. In healthy, physiological conditions the constituents aim to maintain this optimal level of stretch and thus it is assumed that in these conditions all constituent stretches equal their respective attachment stretches. Mathematically,

$$\lambda_E = \lambda_E^{ATT} \qquad \text{in health,} \tag{2.5}$$

$$\lambda_M = \lambda_M^{ATT} \qquad \text{in health.} \tag{2.6}$$

where $\lambda_{(\cdot)}$ is the current stretch of a constituent defined with respect to its reference configuration, which may differ from one constituent to another. For collagen, it is assumed that there isn't a single value of stretch for all fibres comprising the constituent, but instead a continuous distribution of collagen fibre stretches: more details are given later. In this case the distribution of fibre stretches Λ_C in the healthy artery equals the attachment distribution Λ_C^{ATT}:

$$\Lambda_C = \Lambda_C^{ATT} \qquad \text{in health.} \tag{2.7}$$

All stretches in this model are to be interpreted as occurring *at systole*. In the particular case of elastin, which has a very long halflife, it is assumed that its stretch equals the tissue stretch:

$$\lambda_E = \lambda \qquad \text{always.} \tag{2.8}$$

The above holds in all conditions. The attachment stretch for elastin therefore equals

the physiological circumferential stretch of the vessel, which is assumed equal to 1.3 (see Table 2.1):

$$\lambda_E^{ATT} = \lambda^{ATT}. \tag{2.9}$$

It is now possible to define the *recruitment* stretch of a constituent as the level of tissue stretch at which it is recruited to load bearing, i.e. at which the constituent stretch equals 1. The assumption that constituent stretches equal their attachment stretches in health, i.e. when $\lambda = \lambda^{ATT}$, allows us to determine the recruitment stretch of a constituent by a simple proportion:

$$\lambda_{(\cdot)}^R = \frac{\lambda^{ATT}}{\lambda_{(\cdot)}^{ATT}}, \tag{2.10}$$

where $(\cdot) = E, M$.

In Fig. 2.2 a schematic is shown of how the constituent stretches change as the tissue is stretched from its reference configuration Ω_0 to its current "healthy" configuration Ω_t. In the stress-free configuration Ω_0 elastin has unitary stretch, since this is equal to the tissue stretch, while the other constituents have stretches lower than 1, i.e. are wavy or crimped. In the figure an individual collagen fibre is considered and thus a single value of attachment and recruitment stretch: this is for illustrative purposes only since in the real model there is a distribution of stretches. As the tissue is stretched, the configuration in which the stretch of VSMCs is unitary ($\lambda_M = 1$) is achieved and the level of tissue stretch at this configuration is the recruitment stretch of VSMCs λ_M^R. Analogously the recruitment stretch for collagen is defined, λ_C^R. Finally, the current "healthy" configuration is obtained in which all constituent stretches equal their attachment stretches.

In the case of collagen, the model assumes that there is not a single value for the recruitment variable but a distribution of them. Following Chen (2014) and Aparìcio et al. (2016), a triangular distribution is assumed (see Figure 2.3):

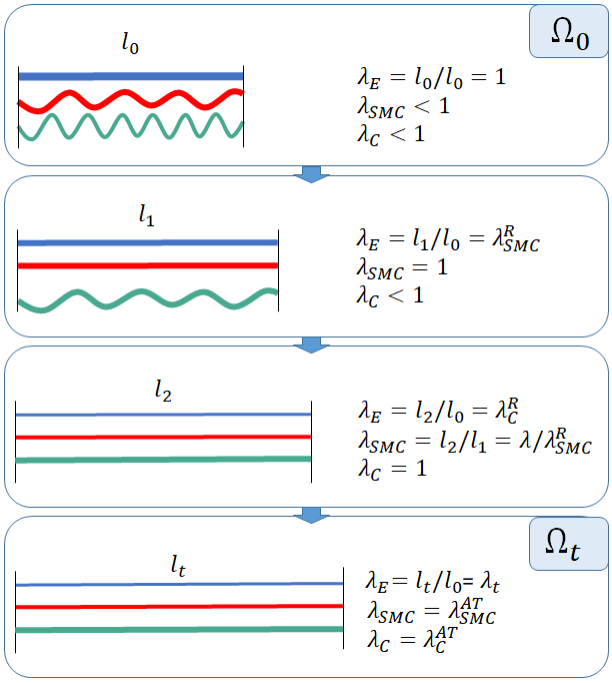

Figure 2.2: Definition of recruitment stretch for a constrained mixture of elastin (blue), smooth muscle cells (red) and collagen (green).

$$\rho(\lambda^R_C) = \begin{cases} 0 & \text{if } \lambda^R_C < a, \\ \frac{2(\lambda^R_C - a)}{(b-a)(c-a)} & \text{if } a \leq \lambda^R_C < c, \\ \frac{2(b-\lambda^R_C)}{(b-a)(b-c)} & \text{if } c \leq \lambda^R_C < b, \\ 0 & \text{if } b \leq \lambda^R_C, \end{cases} \tag{2.11}$$

where the following abbreviations are used: $\lambda^{min}_R, \lambda^{max}_R$ and λ^{mod}_R by a, b and c respectively (see Fig. 2.2). Two separate distributions of recruitment stretches are assumed for medial and adventital collagen: this allows us to capture the fact that medial collagen is load-bearing in health, while adventitial collagen plays a protective role and is only recruited to load bearing at higher, supraphysiological stretches. The distribution for medial collagen ρ^{me}_C is determined by the triplet of values $(\lambda^{min}_{R_{me}}, \lambda^{mod}_{R_{me}}, \lambda^{max}_{R_{me}}) = (1.215, 1.287, 1.3)$, which correspond to actual fibre stretches between 1 and 1.07, while the distribution for adventitial collagen ρ^{ad}_C is determined by the triplet $(\lambda^{min}_{R_{ad}}, \lambda^{mod}_{R_{ad}}, \lambda^{max}_{R_{ad}}) = (1.3, 1.444, 1.625)$, which correspond to actual fibre stretches between 0.8 and 1. (see Table 2.1). Given that the physiological tissue stretch is $\lambda = 1.3$, it holds that at that level of tissue stretch medial collagen has been fully recruited to load bearing (actual fibre stretches are ≥ 1), while no part of the

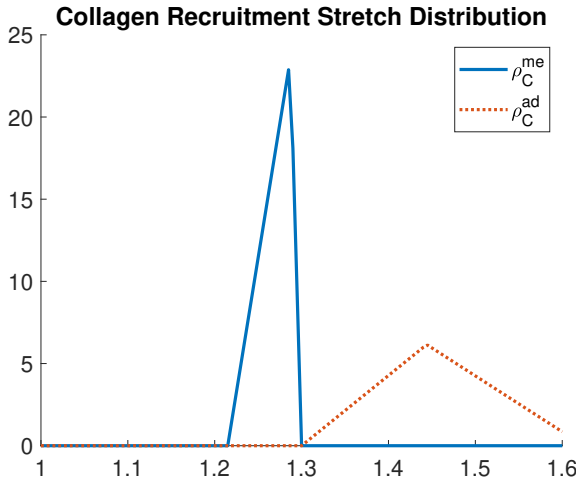

Figure 2.3: Distribution of recruitment stretches of medial and adventitial collagen.

adventitial collagen population has (all fibre stretches are ≤ 1) (see Fig. 2.3).

It is assumed that the stress of the entire tissue equals the sum of the stress contributions of its microstructural constituents. Mathematically:

$$\sigma = \sigma_E + \sigma_C^{me} + \sigma_C^{ad} + \sigma_M^{pass} + \sigma_M^{act}, \tag{2.12}$$

where σ is the stress of the entire tissue, σ_E the contribution from elastin, σ_C^{me} and σ_C^{ad} the contributions from medial and adventitial collagen respectively, σ_{VSMC}^{pass} and σ_{VSMC}^{act} the passive and active contributions of smooth muscle cells respectively. The active response of VSMCs is added to represent their ability to relax and contract in order to control the vessel diameter, ability which is unique to this constituent in arterial tissue.

Constitutive models are now assigned to the constituents to describe how their stress contributions depend on the stretch they experience.

For elastin an isotropic neo-Hookean model is chosen, which is standard from the literature (Gundiah et al. (2007), Holzapfel et al. (2000)). For a cylindrical geometry, the stress function for a neo-Hookean material is given by

$$\sigma_E(\lambda) = k_E\ \lambda^2\ \left(1 - \frac{1}{{\lambda_z}^2\ \lambda^4}\right), \tag{2.13}$$

where k_E is the material parameter for elastin, λ_z is the fixed axial stretch. Recall that elastin stretch equals the tissue stretch $\lambda = \lambda_E$.

For collagen, it is assumed that individual fibres display a linear stress response, i.e.

$$\tilde{\Psi}_{C_J}(\lambda_{C_J}) = \frac{k_{C_J}}{2}\left(\lambda_{C_J} - 1\right)^2, \tag{2.14}$$

where $J \in \{me, ad\}$ denotes medial or adventitial collagen and k_{C_J} is the material parameter for either fibre population (see Table 2.1). To obtain the stress contribution of the whole fibre population, it is necessary to integrate over the recruitment stretch distribution:

$$\Psi_{C_J}(\lambda) = \int_1^{\lambda} \tilde{\Psi}_{C_J}(\lambda_{C_J})\ \rho_{C_J}(\lambda^R_{C_J})\ d\lambda^R_{C_J}, \tag{2.15}$$

where $\lambda_{C_J} = \lambda/\lambda^R_{C_J}$. Derivation of the Cauchy stress is as follows:

$$\sigma_{C_J}(\lambda) = \lambda\ \frac{\partial}{\partial\lambda}\Psi_{C_J}(\lambda). \tag{2.16}$$

For the passive response of VSMCs a neo-Hookean model is adopted, following Humphrey et al. (2007 September*b*):

$$\sigma^{pass}_M(\lambda_M) = f_p k^{pass}_M\ \lambda^2\ \left(1 - \frac{1}{{\lambda_z}^2\ {\lambda_M}^4}\right), \tag{2.17}$$

where k^{pass}_M is the material parameter modulating the passive response and f_p is a parameter that is set as unitary in health: $f_p = 1$ in health. It may increase in vasospasm to represent a possible stiffening of the cell (see Section 2.3.3).

For the active response the model proposed by Humphrey et al. (2007 September*a*) is used with a slight simplification. The material model proposed follows in turn the experimental measurements of Rachev & Hayashi (1999). Therefore the active stress response takes the following form:

$$\sigma^{act}_M = f_a\ c_v\ k^{act}_M\ \lambda_M\ \left[1 - \left(\frac{\lambda^{mean}_M - \lambda_M}{\lambda^{mean}_M - \lambda^{min}_M}\right)\right], \tag{2.18}$$

where k^{act}_M is the material parameter modulating the active response, c_v is the baseline ratio of concentrations of vasoconstrictors to vasodilators equal to $c_v = 0.68$ (Humphrey et al. (2007 September*a*)), λ^{min}_M is the minimum cell stretch at which the active response is non-zero, λ^{mean}_M regulates the cell stretch at which the active response is maximal,

and f_a is a parameter that is set as unitary in health: $f_a = 1$ in health. It may increase in vasospasm to represent the increase in vasoactive tone caused by the increased concentration of vasoconstrictors (see Section 2.3.3). The stress-stretch relationship σ_M^{act} as a function of λ_M is displayed in Figure 2.4.

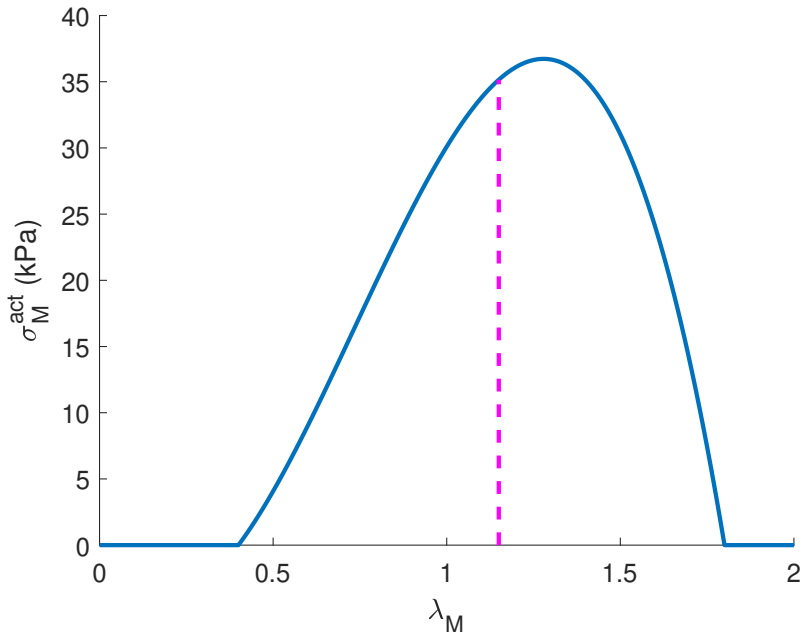

Figure 2.4: Active component of the stress response of vascular smooth muscle cells as a function of their stretch (continuous curve). The dashed line corresponds to the stress response when VSMC stretch equals its attachment value $\lambda_M = \lambda_M^{ATT} = 1.15$.

Finally the material parameters must be determined. In the case of elastin this has been estimated experimentally at around $100kPa$ Grytsan et al. (2017), Holzapfel et al. (2000). For the other constituents, the parameters are computed by imposing two conditions:

- the load-bearing proportions are such that elastin bears about 60% of the load, passive VSMCs 20%, active VSMCs 10% and collagen 10% (Robertson & Watton (2013), Watton, Ventikos & Holzapfel (2009));
- if the VSMC active response is null, the diameter of the healthy artery is 15% larger than if the active stress was present (Robertson & Watton (2013)).

At this point the mechanical behaviour of the arterial tissue in relation to that of its microstructural constituents has been fully described. The pressure-diameter curve for a healthy artery is plotted in Figure 2.5, where a nominal diameter of 2.9mm is assumed which is the average value for a middle cerebral artery. The solid curve is the

pressure-diameter curve for the whole wall: if the reader imagines gradually "inflating" an unloaded arterial wall, i.e. applying an internal pressure, this curve describes which diameter corresponds to which internal pressure. Physiological systolic blood pressure, i.e. 16kPa corresponds to the nominal diameter of 2.9mm. The non-solid curves represent the contributions to load-bearing of each individual constituents. The distance between the x-axis and the point at which a constituent curve cuts the red vertical dashed line at $x = 2.9$ gives the proportion of the pressure load borne by each constituent: elastin is the main load bearer by a rather wide margin, followed by passive VSMC, active VSMC and finally collagen. It is also worth noting how, despite the linear stress response of individual collagen fibres, the implementation of a stretch distribution still allows us to capture the exponential-like behaviour that has been experimentally observed and traditionally represented by an explicitly exponential function.

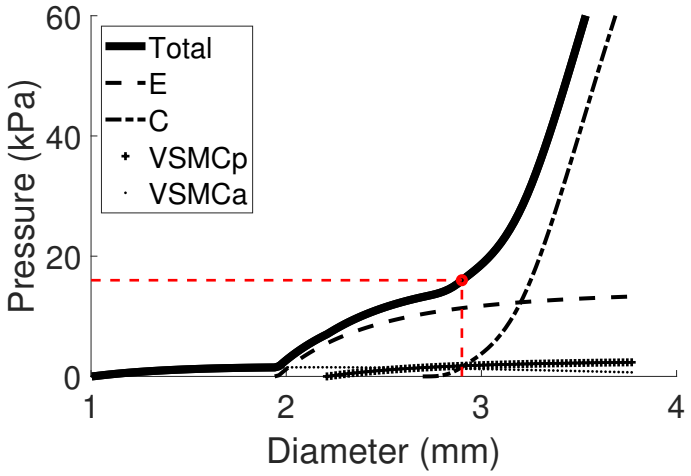

Figure 2.5: Pressure-diameter curve for a middle cerebral artery with profiles of stress contributions of mechanically relevant constituents.

The main equation describing mechanical equilibrium that is solved by the simulation is obtained by combining Eq. 2.4 and 2.12:

$$p = \frac{h}{r}\frac{1}{\lambda_z \lambda}\left(\sigma_E + \sigma_C^{me} + \sigma_C^{ad} + \sigma_M^{pass} + \sigma_M^{act}\right), \tag{2.19}$$

and finally by plugging into each stress component $\sigma_{(\cdot)}$ its corresponding function, which is given respectively by Eq. 2.13 for σ_E, Eq. 2.16 for σ_C (where σ_C^{me} and σ_C^{ad} are differentiated by the respective stretch distributions), Eq. 2.17 for σ_M^{pass} and Eq. 2.18 for σ_M^{act}. Each stress contribution is a function of the related constituent stretch and the constituent stretch is related to the tissue stretch via

$$\lambda_l = \frac{\lambda}{\lambda_l^R}, \tag{2.20}$$

where λ_l is the stretch of constituent l, λ is the tissue stretch and $\frac{R}{L}$ is the recruitment stretch of constituent l. Therefore Equation (2.19) describes the pressure-stretch relationship for the arterial tissue. This is the key equation that is solved by the model.

Now that the model of the healthy artery has been set up, it is necessary to formulate hypotheses on how the microstructure of the wall changes in vasospasm.

Based on reports in the literature, vasospasm is modelled as follows. The extravascular blood clot that formed following SAH causes an increase in oxyhaemoglobin, which causes a signalling cascade resulting in an increased ratio of vasoconstrictor to vasodilator concentration. This causes the VSMCs to contract which results in an initial diameter reduction. Following this initial constriction, it is assumed that the following occurs on a time scale of the order of days to weeks (much larger than the cardiac cycle):

- VSMCs remodel to return their actual stretch to their preferred value (VSMC attachment stretch) via remodelling (Watton et al. (2004), Watton, Ventikos & Holzapfel (2009)): this is achieved through reconfiguration of their internal cytoskeleton and/or attachments to the ECM;
- as VSMCs remodel and become the primary load bearer at the smaller diameter, in order to maintain force-balance, they increase their stiffness and/or their active tone; this is captured mathematically by increasing the parameters f_p and/or f_a respectively;
- elastin and collagen do not remodel; elastin production ceases after puberty and the collagen halflife is assumed to be large compared to the considered time course.

Following these changes, it is now possible to study how the pressure-diameter curve changes for an artery from healthy conditions to vasospasm.

Finally, since the aim of the model is to evaluate the effectiveness of mechanical treatment via stents, a success criterion is needed for mechanical intervention. The precise mechanism behind the resolution of vasospasm via stents is currently unknown. Damage to the vascular smooth muscle cells could take many forms, such as rupture

of cytoskeletal components, detachment from other VSMCs and/or the extracellular matrix, or inhibition of their contractility. As a mathematical idealisation, in this model it is assumed that an interventional device is successful if it causes sufficient damage to the smooth muscle cells to nullify their stress contributions. A strain-based damage criterion is selected: if the VSMCs are stretched beyond a threshold, denominated dilatation threshold, then they are so damaged that their contribution to the stress response of the tissue becomes null. The dilatation threshold is assumed to be a cell stretch of 1.8, as a conservative choice based on the experimental data reported in Fischell et al. (1990).

Parameter	Value	Reference
h/r	1/5	Watton et al. (2004)
λ_z	1.3	Wicker et al. (2008)
λ_M^{ATT}	1.15	-
λ_E^{ATT}	1.3	Watton, Ventikos & Holzapfel (2009)
$\lambda_{R,me}^{min}$	1.215	
$\lambda_{R,me}^{mod}$	1.287	stretch distributions selected
$\lambda_{R,me}^{max}$	1.300	as reasonable estimates with media
$\lambda_{R,ad}^{min}$	1.300	load bearing in health, not adventitia
$\lambda_{R,ad}^{mod}$	1.444	Robertson & Watton (2013)
$\lambda_{R,ad}^{max}$	1.625	
k_E	$93.14kPa$	material parameters determined via
k_M^{pass}	$22.09kPa$	load-bearing proportions from
k_M^{act}	$18.07kPa$	Watton, Ventikos & Holzapfel (2009)
$k_{C,me}$	$639.5kPa$	Robertson & Watton (2013)
$k_{C,ad}$	$5115.6kPa$	
c_v	0.68	Humphrey et al. (2007 September*a*)
f_p (healthy)	1	-
f_a (healthy)	1	-
λ_M^{min}	0.4	Humphrey et al. (2007 September*a*)
λ_M^{mean}	1.1	Humphrey et al. (2007 September*a*)

Table 2.1: Table of relevant model parameters.

The time-continuous evolution of the arterial tissue from health to vasospasm is not captured in this model. First the system is parametrised for the healthy state so that either the relevant parameters come directly from experimental measurements or they replicate features of the tissue that have been experimentally observed, such as the load-bearing proportions of the different constituents or the increased compliance of the tissue in absence of the active response of VSMCs. The vasospastic state is obtained by prescribing that the new vessel diameter is half the healthy value, thus

capturing a 50% level of stenosis, and that in this state the VSMCs have returned to their attachment stretch. By Eq. 2.2, in order for the vessel diameter to be half its healthy value, the same must hold for the tissue stretch, i.e. in vasospasm $\lambda = \frac{\lambda^{ATT}}{2}$. Assuming that the VSMCs have returned to their attachment stretch in vasospasm, implies that their recruitment stretch has changed and is now $\lambda_M^R = \frac{\frac{\lambda^{ATT}}{2}}{\lambda_M^{ATT}} = \frac{\lambda^{ATT}}{2\,\lambda_M^{ATT}}$. These two prescriptions, together with the choice of parameter pair (f_a, f_p) which is explored in the Parameter Study (see Section 2.3.3), allows the study of the new pressure-stretch relationship for a vasospastic artery and therefore the estimation of the effectiveness of stents as treatment strategy.

The code for the implementation of this model in MATLAB is reported in Appendix A.

2.3 Results

2.3.1 Pressure-diameter curves for healthy and vasospastic artery

As a result of the remodelling process prescribed to occur in vasospasm, the structure of the wall adapts to the evolving geometry and thus the pressure-diameter curve changes accordingly. In Figure 2.6 the pressure-diameter curve for a middle cerebral artery at 50% stenosis (reduction in diameter) is shown, together with the contributions to load bearing of its individual constituents, namely the pressure-diameter curve of the arterial tissue if only one constituent was present. A comparison between the pressure-diameter curves in health and vasospasm (those relating to the whole tissue) is shown in Fig. 2.7. These are the solid curves shown in Figure 2.5 for the healthy tissue and in Figure 2.6 for the vasospastic tissue, shown in the same Figure for ease of comparison. For illustrative purposes, parameters f_p and f_a, which regulate the load-bearing potential for passive and active VSMCs respectively, are increased by 20% and 47.5% respectively; the reader is referred to Section 2.3.3 for a more detailed parameter study.

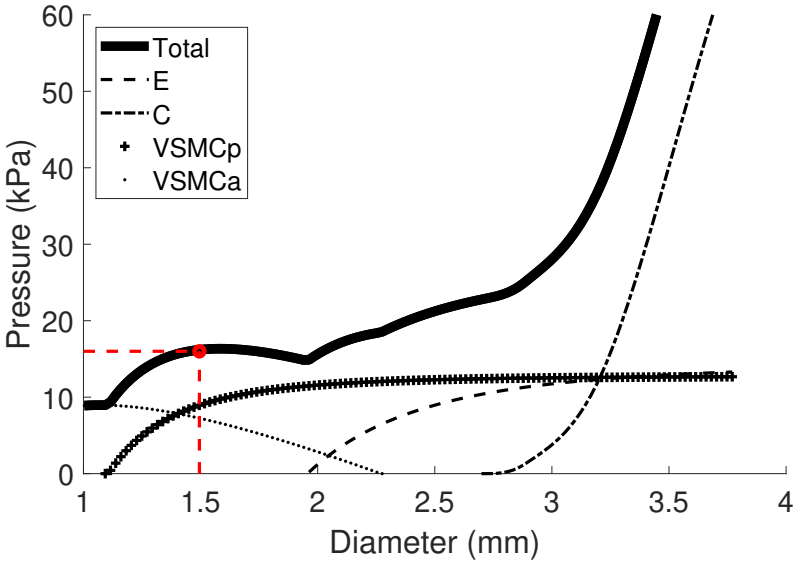

Figure 2.6: Pressure-diameter curve for a middle cerebral artery in vasospasm at 50% stenosis with profiles of stress contributions of mechanically relevant constituents.

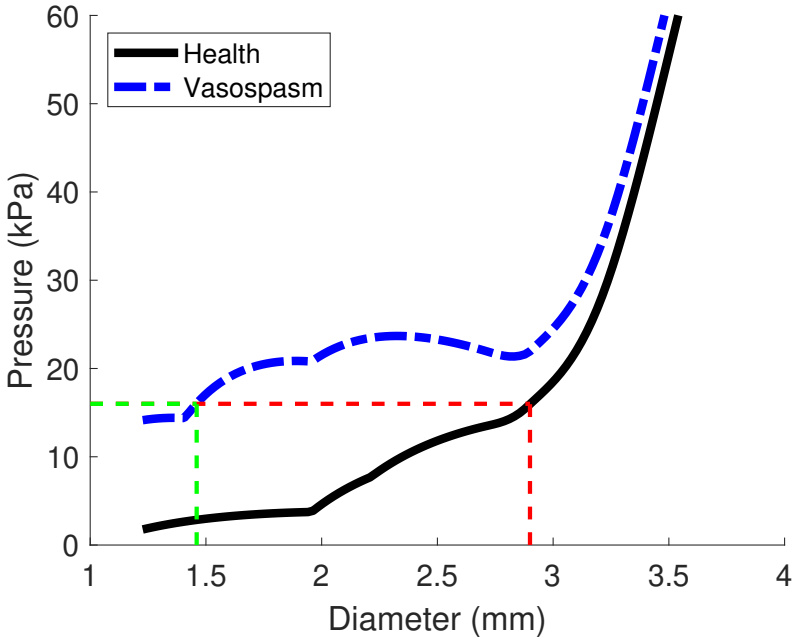

Figure 2.7: Comparison between mechanical equilibrium curve for an artery of nominal diameter 2.9mm in health and in vasospasm at 50% stenosis. The dashed lines highlight what diameter corresponds at physiological systolic pressure thus showing the nominal diameter of 2.9mm and the diameter in disease at about 1.45mm.

It is immediate to notice that the value of physiological systolic blood pressure 16kPa now corresponds to a diameter of about 1.49mm, which is an approximate level of stenosis of 50%. The curves for elastin and collagen are unaltered, while the passive

and active stress contributions from VSMCs have shifted to the left and increased in intensity: the leftward-shift and part of the increase in intensity is the consequence of the remodelling of the cells to return their level of stretch to the attachment value, while a further increase in intensity is modulated by the two factors f_p and f_a.

In Figure 2.8 the concept of the dilatation threshold is illustrated. The thicker solid curve is the pressure-diameter curve for the vasospastic artery, the same as in Figure 2.6. In vasospasm, namely at a diameter of 1.49mm, the level of VSMC stretch equals the attachment stretch, as per the assumption of remodelling in vasospasm. If an increasing internal pressure was applied to the vessel, a configuration would be reached at which VSMC stretch equals the dilatation threshold, i.e. a cell stretch of 1.8. In this example, this corresponds to an arterial diameter of about 2.75mm. At this threshold, the stress contributions from VSMCs become null and pressure load is now borne by elastin and collagen only: this is illustrated by the blue arrow "jumping" from the thicker to the thinner solid curve. Mathematically, the pressure-diameter relationship for the arterial tissue goes from

$$p = \frac{h}{r}\frac{1}{\lambda_z\,\lambda}\left(\sigma_E + \sigma_C + \sigma_M^{pass} + \sigma_M^{act}\right) \tag{2.21}$$

before damage, to

$$p = \frac{h}{r}\frac{1}{\lambda_z\,\lambda}\left(\sigma_E + \sigma_C\right) \tag{2.22}$$

after the smooth muscle cells cease to contribute to load bearing.

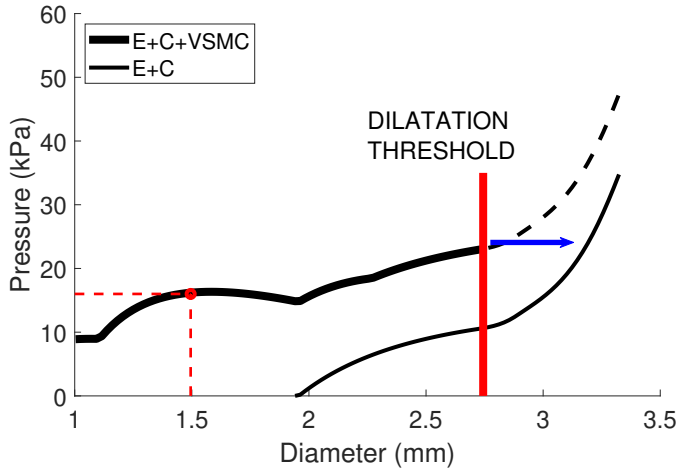

Figure 2.8: Illustration of the concept of dilatation threshold for a middle cerebral artery at 50% stenosis: the threshold corresponds to a VSMC stretch of 1.8, at which it is assumed that the cells can no longer contribute to load bearing.

2.3.2 Treatment Simulation

Now that the pressure-diameter curve for the vasospastic artery is known as well as how to identify the dilatation threshold, it is possible to determine what magnitude of pressure is necessary to overstretch the smooth muscle cells until damage and mechanically resolve the disease. In order to do this, the effect of applying an additional intraluminal pressure is simulated as would be provided by four commonly available stent-retrievers: Solitaire 6, Solitaire 4, Capture 3 and Trevo 4x20. At first their deployment in a middle cerebral artery at 50% stenosis will be simulated, as wwas modelled in Section 2.3.1, and subsequently in cerebral arteries of $1.5, 2$ and 4mm respectively, at the same level of stenosis.

In order to do this, the *chronic outward force* data provided by the stent manufacturers needs to be transformed into the corresponding pressure they would exert on the arterial wall. According to Cabrera et al. (2017), the following derivation is carried out:

1. The *chronic outward force* (CO_F) data provided by the manufacturer has dimension N/mm and is defined as

$$CO_F = \frac{H_F}{l}, \tag{2.23}$$

   where l is the length of the stent and H_F is the *hoop force* the stent applies in the circumferential direction.

2. By definition of stress, it holds that

$$H_F = \sigma \, l \, h, \tag{2.24}$$

   and by the law of Laplace

$$\sigma = P \, \frac{r}{h}, \tag{2.25}$$

   where r is the arterial radius and h the wall thickness.

3. Putting the above together, one obtains

$$P = \frac{H_F}{r \, l} = \frac{CO_F}{r}. \tag{2.26}$$

The plots for the Chronic Outward Force of the four considered stents are reported in Figure 2.9 and the derived curves for the pressure exerted are in Figure 2.10. It

is worth noting how the curves decrease as the stents expand: this is the opposite of what happens in balloon angioplasty, where pressure inside the balloon must be increased to increase dilation, and one of the key reasons why stent retrievers would be a safer treatment strategy.

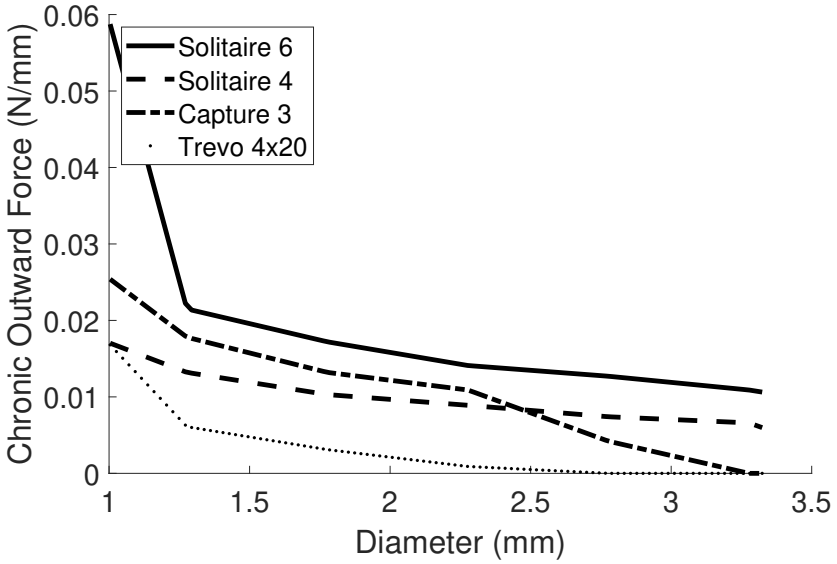

Figure 2.9: Chronic Outward Force exerted by four commonly available stent retrievers as a function of their diameter following deployment.

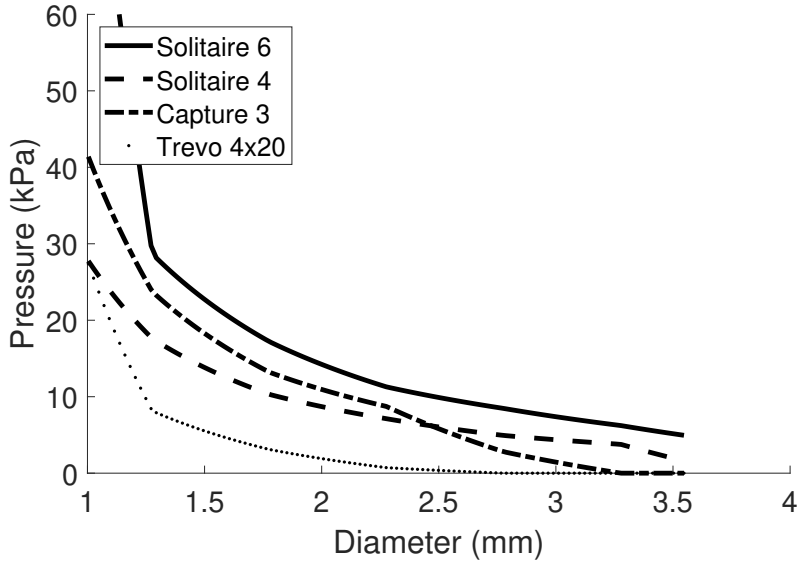

Figure 2.10: Pressure exerted by four commonly available stent retrievers as a function of their diameter following deployment.

Now that the internal pressure that a stent would provide has been identified, the *effective pressure* is defined as the sum of systolic blood pressure and the stent pressure.

This is the total pressure that would be acting on the arterial wall following stent deployment.

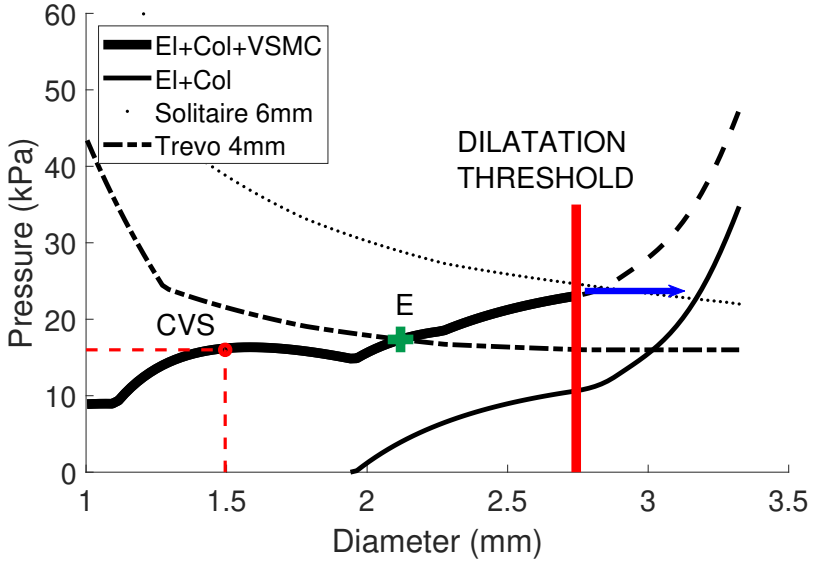

Figure 2.11: Evaluation of the effectiveness or lack thereof of a stent retriever in the mechanical resolution of vasospasm. A stent is effective if its related *effective pressure* curve remains above the mechanical equilibrium curve (solid, thick) up until the dilatation threshold.

Using the pressure-diameter relationships identified in Section 2.3.1, it is now possible to determine the effectiveness of stent-retrievers in the mechanical resolution of vasospasm. This is possible by modelling the stent deployment as quasi-static. This is illustrated in Figure 2.11, where the solid lines describe mechanical equilibrium within the arterial wall when all constituents are bearing load (thicker curve) and when load is borne by elastin and collagen only (thinner curve). The dotted and dashed lines instead represent the *effective pressures* associated to each stent-retriever, of which only two are considered for illustration. A stent is effective if its related effective pressure curve remains above the mechanical equilibrium curve from the point corresponding to the initial vasospastic diameter up until the dilatation threshold. This signifies that the stent is applying more pressure to the wall than the wall can balance out and thus the artery keeps expanding up until the VSMCs are damaged. If instead the two curves intersect before the threshold, that corresponds to the system reaching a new mechanical equilibrium in which the stent has stretched the artery but has not damaged any of the constituents; upon retrieval of the stent, the artery would return to its vasospastic diameter. Thus in Figure 2.11 the stent Solitaire 6 would be successful in resolving vasospasm, while Trevo 4mm would be ineffective.

Finally, the effectiveness of the four considered stent retrievers is tested in arteries of different original diameters, all at a 50% level of stenosis. These are shown in Figure 2.12: case A corresponds to an original diameter of 1.5mm, case B of 2mm, case C of 2.9mm and case D of 4mm.

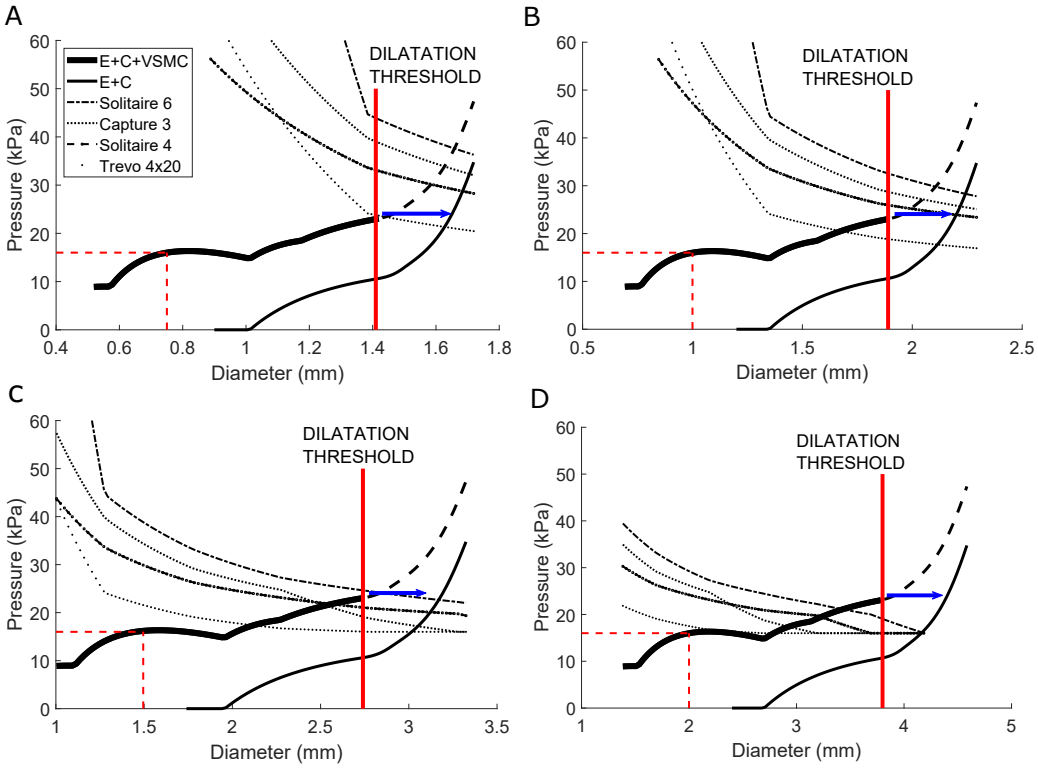

Figure 2.12: Evaluation of the effectiveness or lack thereof of four stent retrievers in the treatment of vasospasm in four arteries of different physiological diameter at 50% stenosis. Most stents are successful in the smaller arteries but their effectiveness decreases with increasing vessel diameter.

It is worth noticing that the effectiveness of the stent retrievers decreases as the value of the physiological arterial diameter increases. Most stents are effective up to 2mm, none are successful at 4mm and one could infer that the threshold of effectiveness is around 3mm. This is consistent with published clinical observations: reported cases of success involve arteries like the M2 section of the middle cerebral artery (mean 2.2mm) or the A2 section of the anterior cerebral artery (mean 2.5mm), while failure is consistently reported for larger arteries like the internal carotid arteries ($>$ 4mm) and there are mixed results for the M1 segment of the middle cerebral artery ($>$ 3mm) (Bhogal et al. (2016, 2017, 2019), Li et al. (2019)).

2.3.3 Parameter study

As a result of the increased smooth muscle contraction, the vessel cross-section is reduced. Without remodelling, this decreases the stretch of the elastin and collagen components thus decreasing the proportion of pressure load that they bear. With progressive remodelling of the VSMCs, the vessel diameter is further decreased until in severe cases of vasospasm the stretches of elastin and collagen drop below one. As a result, VSMCs become the sole load bearer of the transmural pressure load. Since VSMCs are modelled as providing both a passive and an active stress contribution, the increased pressure load must be distributed between the two. Given the absence of experimental data on this process and the possibility that his may be dependent on patient-specific characteristics, a parameter study is run to explore the possible impact that the variations in relative load bearing proportions would have on treatment requirements.

The relative roles of active and passive VSMCs are modulated by parameters f_p and f_a (see Section 2.4 for a biological interpretation of these changes). The parameters are unitary in health and need to increase in this model to capture the increased load borne by the stress response. The two variables are coupled so that the mechanical equilibrium of the arterial wall is maintained. In the previous Section 2.3 a specific case ($f_p = 1.2$, $f_a = 1.475$) was considered. Here the entire parameter space is explored.

First the solutions for the two extreme cases are obtained, i.e. when only one of the two parameters is changed and the other remains unitary. If the passive response is not affected ($f_p = 1$), then f_a must increase by 75%; conversely, if $f_a = 1$, then f_p increases by 55% (Fig. 2.13). Then f_p is gradually increased from 1 to 1.55 (with $f_p = 1.55$ corresponding to $f_a = 1$ by small constant increments and the equation of mechanical equilibrium (Eq. (2.27)) is solved: this gives us the relationship between f_a and f_p (see Fig. 2.13).

$$p = \frac{h}{r}\frac{1}{\lambda_z \lambda}\left(f_p\, \sigma_M^{pass} + f_a\, \sigma_M^{act}\right) \tag{2.27}$$

For each pair of values the critical pressure is computed, i.e. the amount of pressure that should be applied to the arterial wall in order to reach the dilatation threshold and thus damage the VSMCs (see Fig. 2.14). Systolic blood pressure (16kPa) is then subtracted from the critical pressure to obtain the additional pressure: this is the amount required from an interventional device in order to mechanically resolve

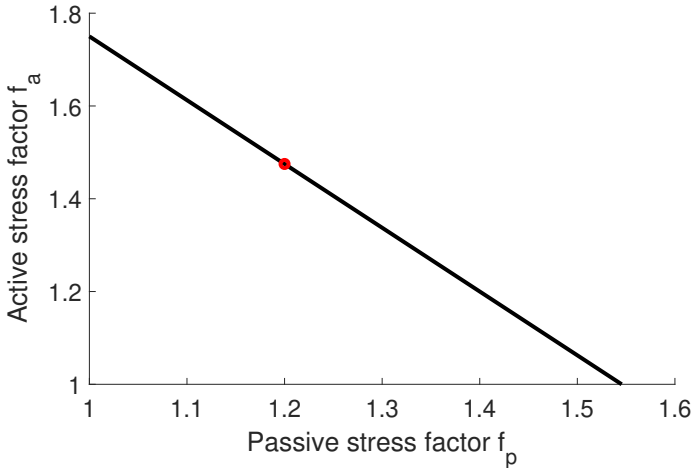

Figure 2.13: Relationship between active stress factor f_a and passive stress factor f_p in response to increased load bearing proportion for VSMCs in vasospasm.

vasospasm.

The results show that the minimum pressure required from a device is 5kPa while the maximum is around 11kPa. Although these values are relatively significant and can make a difference in the success or lack thereof of a specific stent in different patients, they are relatively low values which could be achieved by either currently available or specifically designed stents. The range of results remains an order of magnitude lower than what is required from balloon angioplasty.

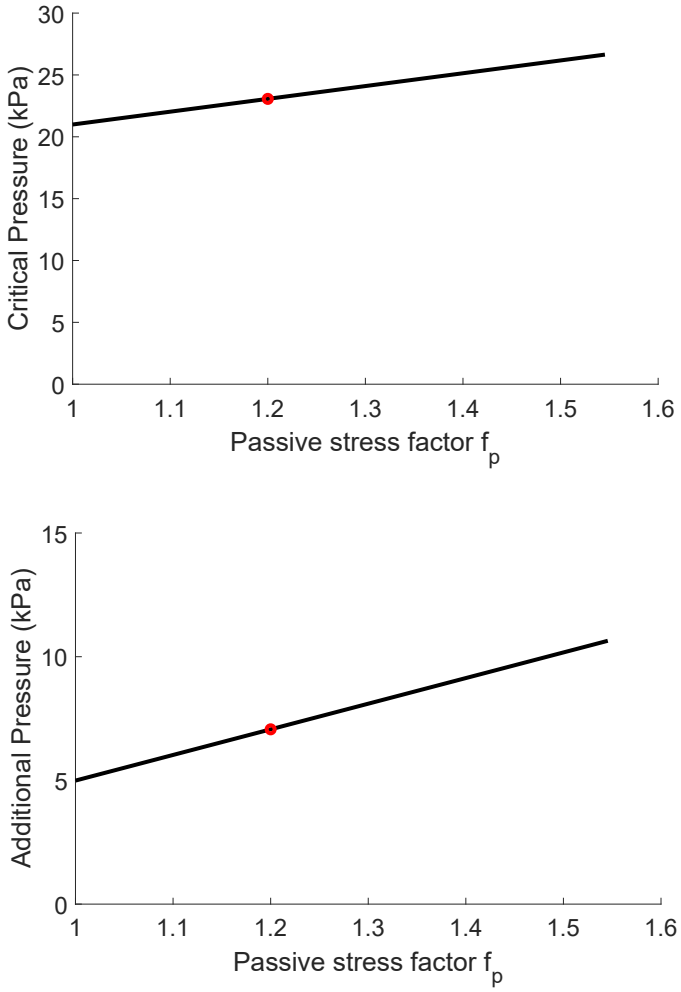

Figure 2.14: Critical and additional pressures required to mechanically resolve vasospasm over the parameter space spanned by the active and passive stress factors.

2.4 Discussion

In Chapter 2 a biomechanical model of pronounced cerebral vasospasm is proposed with a focus on the role of smooth muscle cells and the evolution of their stress response with the changing geometry. The model captures the essential mechanism of the disease by means of a simple assumption on the attempt by arterial constituents to maintain a preferred state of stretch. Its aim is to determine the magnitude of pressure that an interventional device should provide in order to mechanically resolve the disease. This can have important translational applications such as advising the use of stent-retrievers in place of balloon angioplasty in smaller arteries (diameter < 3mm), which is a less invasive and less risky procedure. It is important however to remember that the success of the stent depends not only on the original arterial diameter, but

also on the degree of spasm, the time elapsed since subarachnoid haemorrhage and possibly patient-specific characteristics. With regards to providing support in clinical decisions, the model is still at too early a stage to be reliable and more experimental data is needed to corroborate the assumptions that have been made. However, the results show that the magnitude of pressure necessary for the mechanical resolution of the disease is far lower than what is currently deemed necessary ($10-20$kPa compared to 300kPa for balloon angioplasty) and there is potential for the design of specific stents that could apply such pressures and become the primary treatment strategy for the disease bringing a significant decrease in the risk of tissue rupture during intervention.

The model presented in this Chapter was developed as a conceptual first step to test the formulated key assumptions. Some simplifications have therefore been made and priority was given to the representation of mechanical aspects of the problem without capturing the full biological complexity of the arterial wall or its temporal evolution.

The main limitation of the model is that it is based on a membrane, thin wall assumption. This is reasonable for a healthy artery where experimental measurements have shown the presence of a pre-stress which results in a uniform strain-field across the wall thickness. However, this is likely to no longer hold true in vasospasm due to the severe constriction. It is also likely to affect the resulting predictions of the model since the stent would apply higher stress on the cells or constituents closer to the lumen compared to those closer to the adventitial layer; thus damage to the VSMCs may not be uniform across the thickness of the vessel wall. This limitation is addressed by integrating this model into a finite element framework: the framework is extended for this purpose as described in Chapter 3 and applied to model vasospasm for comparison with this model as detailed in Chapter 4.

The time-course of vasospasm is such that the peak of the constriction usually occurs at 7-10 days following SAH. It is therefore within this time frame that evidence of vasospasm is likely to appear and treatment decisions are made. This time frame is much smaller than the halflife of arterial collagen, which is on average around 70 days, and therefore it has been assumed that the effect of collagen remodelling is negligible in the presented model. However it is possible that even partial remodelling could affect the results or that the cells' activities regarding ECM maintenance are altered or accelerated since collagen turnover rate has been shown to decrease down to about 10 days in pathological conditions. This limitation is addressed in Chapter 5 where this model is extended to include growth and remodelling of the collagen matrix.

The remodelling of VSMCs, which is assumed to be the key driver of vasospasm, is a complex and multifactorial process which involves both chemical signals (the interaction between vasoconstrictors, vasodilators and their inhibitors) and the mechanical environment that the cells perceive. It is also a time-dependent process where the early stage is dominated by the chemical signals while in the chronic stage it is the mechanical environment that plays the greater role. In the model these detailed processes are not explicitly captured but the return of the stretch of VSMCs to their homeostatic value is simply prescribed. The prediction on the pressure necessary for treatment thus assume that this remodelling is complete, while in reality this is a gradual change in the structure of the cells and may not be complete at the time of treatment. At the time of writing experimental data is lacking on the timescale of these remodelling mechanisms. An interesting model extension would therefore be an explicitly time-dependent one where the entire time course of the disease is described and the treatment prediction could be dependent on how mny days have been elapsed since subarachnoid haeomrrhage as well.

Finally, although the endothelial layer plays a negligible mechanical role, it is responsible for the mechanotransduction of intraluminal mechanical signals (pressure, wall shear stress, etc.) through the arterial wall (Kassell et al. (1985)). Due to the severe constriction, the endothelial layer is crimped: this can both damage it through desquamation (loss of endothelial cells, Kapp et al. (1985), Mizukami et al. (1976), Nakagomi et al. (1990), Smith et al. (1985), Zubkov et al. (2002)), possibly followed by inflammation, and impair the signalling process which is responsible for the regulation of cell function. This model did not consider the endothelial layer since the interest lied in the mechanical resolution of the disease; however, it would be an important sophistication to include this, especially for modelling the disease evolution.

The role of inflammation also appears to be prominent in vasospasm and would be worth including (Hughes & Schianchi (1978), Mayberg et al. (1990)). Indeed there is evidence that it is inflammatory processes that drive some of the growth and remodelling mechanisms occurring within the arterial wall during disease progress and relating these processes to inflammatory signalling would result in a more precise mode of the pathophysiology of vasospasm.

Despite its limitations, the model presented here captures some essential aspects of the disease and is a promising first step towards a clinical tool that can advise on viable treatment strategies. Although a parameter study is necessary, the results produced so far are consistent with reported clinical cases of use of stent-retrievers

for the treatment of the disease, which supports the validity of the model. It has been interestingly obtained that stent-retrievers are in some cases a better treatment strategy and thus the results help foster an improvement in the care of patients presenting with CVS, since this type of intervention involves significantly reduced damage to the extracellular matrix, eliminates the need to interrupt blood flow and greatly reduces the risk of arterial tissue rupture.

These positive initial results corroborate the validity of the hypothesis that vasospasm is primarily driven by vascular smooth muscle contraction and remodelling, and that therefore treatment should be calibrated accordingly. It would be extremely useful if this hypothesis could be supported by experimental results. A possible experiment involves the application of arterial blood to different samples excised *ex vivo* of the same section of a cerebral artery: this should cause vasospasm and each sample could then be observed at the microscope after different amounts of time, such as 7, 14 and 21 days, in order to study the morphology of the VSMCs at different phases of the disease.

2.5 Conclusion

The model of cerebral vasospasm presented in this Chapter is based on a novel hypothesis that the constriction is driven by the remodelling of vascular smooth muscle cells towards a homeostatic level of stretch and that the necessary and sufficient condition to treat the disease is to overstretch these cells to functional failure, i.e. a state in which they bear no pressure load. This hypothesis is consistent with observations of morphological changes observed in the arterial wall in both human and animal models as well as with clinical data on the time-course of the disease and its response to pharmacological treatment. This hypothesis also potentially reconciles conflicting reports on the increase or lack thereof of connective tissue mass in the medial layer, which was hypothesised to be the main reason for the increased stiffness of the wall.

Despite its significant morbidity and mortality, cerebral vasospasm has been a historically poorly understood disease, in part due do its complex and multifactorial aetiology. The success of stent retrievers in treating the constriction has challenged the commonly held assumption that it was necessary to damage the extracellular matrix in order to resolve the constriction. Further experimental validation is warranted in this regard, but this novel hypothesis could help shed light on the mechanism by which

this disease progresses and thus lead to improved and safer treatment strategies.

This page has been intentionally left blank.

Chapter 3

Finite Element Framework Extension

In the one-dimensional model of cerebral vasospasm presented in Chapter 2 the arterial wall was idealised as a non-linear elastic cylindrical membrane. The membrane assumption is reasonable when considering that arterial tissue is pre-stressed, as evidenced by the presence of an "opening angle" at which it springs open when cut longitudinally. This makes the stress field uniform across the wall thickness and allows us to assume that constituent stresses will be uniform along the radial direction.

However, in the presence of a rapid and significant deformation such as that occurring in vasospasm, this is likely to no longer be true when the constriction is sufficiently severe. Therefore the model defined in Chapter 2 is hereby integrated into a three-dimensional finite element framework to compare the results against the one-dimensional membrane case.

The framework developed by Eriksson and Grytsan has been selected as the most suitable. It has already been successfully applied to model the evolution of abdominal aortic aneurysms (Eriksson et al. (2014), Grytsan et al. (2017, 2015)). The framework is a constrained mixture of elastin, ground matrix and collagen, with the possibility to include anisotropic volumetric growth. The framework is developed in the software package FEAP (http://projects.ce.berkeley.edu/feap/), an academic open source software which allows full customisation of material models as well as evolution equations.

In order to integrate the membrane model of cerebral vasospasm into the framework, three extensions to the model by Grytsan et al. (2017) are necessary:

- incorporation of new constitutive model of collagen to represent stretch distribu-

tion, and remodelling;

- incorporation of new constitutive model for vascular smooth muscle cells with both passive and active response, and remodelling;
- damage model for each constituent.

In this Chapter only those sophistications are described which have been implemented and numerically verified. In Section 3.1the basic definitions and relations from Solid Mechanics are summarised that the modelling framework is founded upon. In Section 3.2 the formulation, implementation and verification of the material model for collagen with stretch distribution and remodelling is presented. In Section 3.3.2 the same is done for vascular smooth muscle cells regarding the addition of the active response and remodelling. Finally in Section 3.4 the model for constituent damage is described and verified.

3.1 Concepts of Solid Mechanics

In this Section the basic concepts of Solid Mechanics are introduced that are relevant to the work described in this Chapter and the next. For more in-depth information, the reader is referred to Holzapfel (2000).

3.1.1 Kinematics

Consider a body $\mathcal{B}$ and a particle $P \in \mathcal{B}$ in a three-dimensional Euclidean space at a given time t. In order to describe the deformation of this body, it is useful to introduce a *reference frame* consisting of three orthonormal coordinate axes ($\mathbf{e_1}$, $\mathbf{e_2}$, $\mathbf{e_3}$) and a point of origin O. As the body is deformed through space and time, it occupies a continuous sequence of geometrical regions denominated *configurations*. The region occupied at time $t = 0$ is called the *initial configuration*. The region occupied by the body in a stress-free state is called the **reference configuration** and denoted by Ω_0. Notice that the two may not coincide. For the applications of interest in my work, the latter plays a far more important role since strains will be defined against the reference configuration and, in general, the initial configuration will not be stress-free, thus not coincide with the reference configuration. However, in the following the body is considered to be in the reference configuration at $t = 0$.The *position vector* $\mathbf{X}$ is defined as the vector describing the position of particle $P \in \mathcal{B}$ in the reference configuration with respect to the chosen coordinate system. After

undergoing a deformation, the body will occupy a different geometric region called the **current configuration** and denote by Ω. The vector describing the position of particle P in the current configuration is denoted by $\mathbf{x}$. Since the sequence of occupied regions is continuous, there exist a continuous vector field χ such that

$$\mathbf{x} = \chi(\mathbf{X}, t), \qquad \forall \mathbf{X} \in \Omega_0, \ \forall t. \tag{3.1}$$

This vector field is called the *motion* of body $\mathcal{B}$.

Consider now $\mathbf{X}$ and $\mathbf{x}$ to be not points but curves inside body $\mathcal{B}$, namely:

$$\mathbf{X} = \mathbf{\Gamma}(\xi) \subset \Omega_0, \tag{3.2}$$

$$\mathbf{x} = \gamma(\xi, t) \subset \Omega. \tag{3.3}$$

By definition of the motion vector field, it holds that

$$\mathbf{x} = \gamma(\xi, t) = \chi(\mathbf{\Gamma}(\xi), t). \tag{3.4}$$

The tangent vectors, also referred to as *line elements*, to the two curves are denoted by $d\mathbf{X}$ and $d\mathbf{x}$ respectively. Therefore

$$\mathrm{d}\mathbf{X} = \mathbf{\Gamma}'(\xi)\mathrm{d}\xi, \tag{3.5}$$

$$\mathrm{d}\mathbf{x} = \gamma'(\xi, t)\mathrm{d}\xi, \tag{3.6}$$

where the abbreviations $(\cdot)' = \frac{\partial(\cdot)}{\partial \xi}$ are used. From (3.4), it follows that

$$\mathrm{d}\mathbf{x} = \frac{\partial \chi(\mathbf{X}, t)}{\partial \mathbf{X}} \mathrm{d}\mathbf{X} = \mathbf{F}(\mathbf{X}, t)\mathrm{d}\mathbf{X}, \tag{3.7}$$

where $\mathbf{F}(\mathbf{X}, t)$ is defined as the **deformation gradient**, which is a crucial quantity and a primary measure of deformation.

Another relevant quantity to define is the **right Cauchy-Green tensor** C, also referred to as the **Green deformation tensor**. This is given by

$$\mathbf{C} = \mathbf{F}^T\mathbf{F} \tag{3.8}$$

and has the important properties of being *symmetric* and *positive definite* at each $\mathbf{X} \in \Omega_0$, namely

$$\mathbf{C} = \mathbf{F}^T\mathbf{F} = (\mathbf{F}^T\mathbf{F})^T = \mathbf{C}^T, \qquad \textit{(symmetry)}, \tag{3.9}$$

$$\mathbf{u} \cdot \mathbf{C}\mathbf{u} > 0 \quad \forall \mathbf{u} \neq \mathbf{o}, \qquad \textit{(positive definite)}. \tag{3.10}$$

The above properties hold for the **left Cauchy-Green tensor b** too, which is defined as

$$\mathbf{b} = \mathbf{F}\mathbf{F}^T \tag{3.11}$$

and is another important strain measure with reference to the current configuration.

3.1.2 Stress Tensors

Consider a plane surface intersecting body $\mathcal{B}$ passing a given point $\mathbf{x} \in \Omega$ in the current configuration. Let $\mathrm{d}s \in \partial\Omega$ be an infinitesimal surface element and let $\mathbf{n}$ be a unit vector normal to this surface. The **resultant force** acting on the surface element is denoted by $\mathrm{d}\mathbf{f}$. Finally, while $\mathbf{x}$, $\mathrm{d}s$ and $\mathbf{n}$ are defined in the current configuration, let $\mathbf{X}$, $\mathrm{d}S$ and $\mathbf{N}$ be the respective elements in the reference configuration.

Then, for every surface elements, it holds that

$$\mathrm{d}\mathbf{f} = \mathbf{t}\mathrm{d}s = \mathbf{T}\mathrm{d}S, \tag{3.12}$$

where

$$\mathbf{t} = \mathbf{t}(\mathbf{x}, t, \mathbf{n}), \tag{3.13}$$

$$\mathbf{T} = \mathbf{T}(\mathbf{X}, t, \mathbf{N}). \tag{3.14}$$

The first vector $\mathbf{t}$ is called the **Cauchy** (or **true**) **traction vector** and represents the force measured per unit surface element in the current configuration. Vector $\mathbf{T}$ is called the **first Piola-Kirchhoff** (or **nominal**) **traction vector** and represents the force measured per unit surface area in the reference configuration.

Cauchy's stress theorem is a fundamental result in solid mechanics and introduces stress tensors. It claims that there exist unique second-order tensor fields σ and $\mathbf{P}$ such that

$$\mathbf{t}(\mathbf{x}, t, \mathbf{n}) = \sigma(\mathbf{x}, t)\mathbf{n}, \tag{3.15}$$

$$\mathbf{T}(\mathbf{X}, t, \mathbf{N}) = \mathbf{P}(\mathbf{X}, t)\mathbf{N}, \tag{3.16}$$

where σ is called the **Cauchy** (or **true**) **stress tensor** and is *symmetric*, while $\mathbf{P}$ is called the **first Piola-Kirchhoff** (or **nominal**) **stress tensor**. Cauchy's stress theorem is a fundamental result in continuum mechanics and states that, if either stress tensor depends on the outward unit normal, then it must be linear in it.

It is possible to pass from one stress tensor to the other through the *Piola transformations*:

$$\mathbf{P} = J\sigma\mathbf{F}^{-T}, \tag{3.17}$$

$$\sigma = J^{-1}\mathbf{P}\mathbf{F}^{T}, \tag{3.18}$$

where $J = \det \mathbf{F}$.

Consider traction vector $\mathbf{t}$ and let $\mathbf{m}$ be a unit vector embedded in the surface ds orthogonal to $\mathbf{n}$. Then t can be written as the vector sum of a component parallel to $\mathbf{n}$ and one parallel to $\mathbf{m}$, namely

$$\mathbf{t} = \mathbf{t_n} + \mathbf{t_m} = (\mathbf{n} \cdot \mathbf{t})\mathbf{n} + (\mathbf{m} \cdot \mathbf{t})\mathbf{m} = \sigma\mathbf{n} + \tau\mathbf{m}. \tag{3.19}$$

The length σ of component $\mathbf{t_n}$ is called the **normal stress**, while the length τ of component $\mathbf{t_m}$ is called the **shear stress**.

Next,it is of interest to find the maximum and minimum normal stresses and their respective directions. In order to do this, it is necessary to determine the *eigenvalues* and *eigenvectors* of the Cauchy stress tensor σ and thus the characteristic equation of σ must be solved, i.e.

$$\det(\sigma - \lambda\mathbf{I}) = 0, \tag{3.20}$$

which can be rewritten as

$$\lambda^3 - I_1\lambda^2 + I_2\lambda - I_3 = 0. \tag{3.21}$$

In (3.21) the expression on the left-hand side is called the *characteristic polynomial* of σ and the factors $I_1,\ I_2$ and I_3 are called the **principal stress invariants** of tensor σ. They are equal to

$$I_1(\sigma) = \mathrm{tr}(\sigma), \tag{3.22}$$

$$I_2(\sigma) = \frac{1}{2}\left[(\mathrm{tr}(\sigma))^2 - \mathrm{tr}(\sigma^2)\right], \tag{3.23}$$

$$I_3(\sigma) = \det(\sigma). \tag{3.24}$$

Equation (3.21) yields three solutions $\lambda_i,\ i = 1, 2, 3$, called the eigenvalues of σ, which can be substituted in

$$(\sigma - \lambda_i I)\mathbf{v} = 0 \tag{3.25}$$

to find their corresponding eigenvectors $\mathbf{v}_i,\ i = 1, 2, 3$. The three eigenvalues λ_i are called the **principal normal stresses** and the maximum and minimum among them correspond to the maximum and minimum normal stresses. The corresponding eigenvectors are called the **principal directions**, while their related normal planes are called the **principal planes**. These are characterized by the fact that shear stress vanishes on the principal planes. Moreover, because σ is symmetric, the eigenvectors form an orthogonal basis.

Finally, a third stress tensor $\mathbf{S}$ is introduced, the **second Piola Kirchhoff stress tensor**. Although it does not admit a physical interpretation in terms of surface tractions, it is symmetric and, since it sits completely in the reference configuration and is not affected by rigid body rotations, it is a very useful stress measure. It is related to the Cauchy stress tensor by

$$\mathbf{S} = J\mathbf{F}^{-1}\sigma\mathbf{F}^{-T}, \tag{3.26}$$

with inverse

$$\sigma = J^{-1}\mathbf{F}\mathbf{S}\mathbf{F}^{T}. \tag{3.27}$$

3.1.3 Constitutive Equations

The material of the body under consideration is assumed to be **hyperelastic**, namely such that there exists a *Helmholtz free-energy function* Ψ, defined per unit volume, which is sufficient to describe the material mechanical behaviour. Since Ψ is assumed to depend solely on the deformation gradient $\mathbf{F}$, it is called a **strain energy function**. Once Ψ is defined, the stress tensors can be derived according to

$$\mathbf{P} = \frac{\partial \Psi(\mathbf{F})}{\partial \mathbf{F}}, \tag{3.28}$$

$$\sigma = J^{-1} \frac{\partial \Psi(\mathbf{F})}{\partial \mathbf{F}} \mathbf{F}^T = J^{-1} \mathbf{F} \left(\frac{\partial \Psi(\mathbf{F})}{\partial \mathbf{F}} \right)^T. \tag{3.29}$$

Since $\mathbf{C} = \mathbf{F}^T \mathbf{F}$, the strain energy function can be expressed as a function of the right Cauchy-Green tensor, namely $\Psi(\mathbf{F}) = \Psi(\mathbf{C})$. Then all three stress tensors can be derived according to

$$\sigma = 2J^{-1} \mathbf{F} \frac{\partial \Psi(\mathbf{C})}{\partial \mathbf{C}} \mathbf{F}^T, \tag{3.30}$$

$$\mathbf{P} = 2\mathbf{F} \frac{\partial \Psi(\mathbf{C})}{\partial \mathbf{C}}, \tag{3.31}$$

$$\mathbf{S} = 2 \frac{\partial \Psi(\mathbf{C})}{\partial \mathbf{C}}. \tag{3.32}$$

The material is also assumed to be **incompressible**, i.e. such that its volume is not changed throughout a motion. In order to enforce numerical incompressibility a multiplicative split of the deformation gradient is adopted in which:

$$\mathbf{F} = J^{\frac{1}{3}} \, \overline{\mathbf{F}}, \tag{3.33}$$

where $J = \det \mathbf{F}$ is the volume ratio and $\det \overline{\mathbf{F}} = 1$ (Holzapfel et al. (2000)).

In order to implement this constraint, the strain energy function is postulated to be of the form

$$\Psi = \Psi(\overline{\mathbf{F}} - p(J-1), \tag{3.34}$$

where p is a *Lagrange multiplier* that can be identified as **hydrostatic pressure**. Its

value can only be determined by equilibrium equations and boundary conditions.

The modified right Cauchy-Green tensor is defined as

$$\overline{\mathbf{C}} = \overline{\mathbf{F}}^T \overline{\mathbf{F}} \tag{3.35}$$

and the invariants of $\overline{\mathbf{C}}$ are given by

$$\overline{I_1} = tr(\overline{\mathbf{C}}), \tag{3.36}$$
$$\overline{I_2} = tr(\overline{\mathbf{C}})^2 - tr(\overline{\mathbf{C}}^2), \tag{3.37}$$
$$\overline{I_3} = \det(\overline{\mathbf{C}}) = 1, \tag{3.38}$$

and similarly for other invariants that will be defined later.

Parameter p, which is controlled through the bulk modulus in the numerical implementation, is used as a penalty parameter selecting for deformations that minimise volume changes, thus realising near-incompressibility.

The derivation of the stress tensors therefore becomes

$$\mathbf{P} = -p\overline{\mathbf{F}}^{-T} + \frac{\partial \Psi(\overline{\mathbf{F}})}{\partial \overline{\mathbf{F}}}, \tag{3.39}$$
$$\mathbf{S} = -p\overline{\mathbf{C}}^{-1} + 2\frac{\partial \Psi(\overline{\mathbf{C}})}{\partial \overline{\mathbf{C}}}, \tag{3.40}$$
$$\sigma = -p\mathbf{I} + \overline{\mathbf{F}} \left(\frac{\partial \Psi(\overline{\mathbf{F}})}{\partial \overline{\mathbf{F}}} \right)^T. \tag{3.41}$$

According to the chosen material model, the next step will be to express one of the above stress tensors as a function of the *invariants* of $\overline{\mathbf{C}}$, which are computationally more tractable than the entire tensors. For the application of this model, it will in general be more convenient to derive the second Piola-Kirchhoff stress tensor and then use equation (3.27) to find σ and thus identify principal stresses and planes.

To improve readability the remainder will omit the symbol $\bar{\cdot}$ and thus denote $\overline{\mathbf{F}}$ by $\mathbf{F}$ and $\overline{\mathbf{C}}$ by $\mathbf{C}$ since the original tensors are not directly used in the framework.

3.1.4 Constrained Mixture Model

In order to implement a constrained mixture model of arterial tissue, it is necessary to define its constitutive equation. A constrained mixture approach is adopted, which assumes that each material constituent has its own independent reference configuration but deforms consistently with the rest of the tissue. It is assumed that the stress response of the tissue is the sum of the stress contributions of its mechanically relevant microstructural constituents. Mathematically, the strain energy function is additively split as

$$\Psi = \Psi_{\text{el}} + \Psi_{\text{gm}} + \Psi_{\text{col,a}_0} + \Psi_{\text{col,g}_0} + \Psi^{pass}_{VSMC} + \Psi^{act}_{VSMC}, \tag{3.42}$$

where "el" stands for elastin, gm for ground matrix, col for collagen and VSMC for vascular smooth muscle cells. The following assumptions are made for these constituents:

1. elastin, ground matrix and the passive response of VSMCs behave as *isotropic neo-Hookean* materials;

2. collagen is highly *anisotropic*, being able to stretch in only one preferred direction for each fibre;

3. the active response of VSMCs is anisotropic, acting only in the circumferential direction, and has a functional form similar to a downward-facing parabola, which is motivated by experimental measurements and described in Section 2.2.

The collagen constituent consists of **two families of collagen fibres** oriented at symmetric angles with respect to the circumferential direction, corresponding to the additive terms $\Psi_{\text{col,a}_0}$ and $\Psi_{\text{col,g}_0}$. Let $\mathbf{a_0}$ and $\mathbf{g_0}$ be the unit vectors representing the directions of the collagen fibres. The constitutive equation for a generic incompressible isotropic material surrounded by two families of fibres depends on *nine* invariants: the

first three are defined in (3.22), while the remaining are defined by

$$I_4(\mathbf{C}, \mathbf{a_0}) = \mathbf{a_0} \cdot \mathbf{C}\mathbf{a_0}, \tag{3.43}$$

$$I_5(\mathbf{C}, \mathbf{a_0}) = \mathbf{a_0} \cdot \mathbf{C}^2\mathbf{a_0}, \tag{3.44}$$

$$I_6(\mathbf{C}, \mathbf{g_0}) = \mathbf{g_0} \cdot \mathbf{C}\mathbf{g_0}, \tag{3.45}$$

$$I_7(\mathbf{C}, \mathbf{g_0}) = \mathbf{g_0} \cdot \mathbf{C}^2\mathbf{g_0}, \tag{3.46}$$

$$I_8(\mathbf{C}, \mathbf{a_0}, \mathbf{g_0}) = \mathbf{a_0} \cdot \mathbf{C}\mathbf{g_0}, \tag{3.47}$$

$$I_9(\mathbf{a_0}, \mathbf{g_0}) = (\mathbf{a_0} \cdot \mathbf{g_0})^2. \tag{3.48}$$

Since I_9 is a geometrical constant that does not depend on the deformation, it is no longer considered. The resulting general constitutive equation is therefore given by

$$\mathbf{S} = -p\mathbf{C}^{-1} + 2\Bigg[\left(\frac{\partial \Psi}{\partial I_1} + I_1\frac{\partial \Psi}{\partial I_2}\right)\mathbf{I} - \frac{\partial \Psi}{\partial I_2}\mathbf{C} + I_3\frac{\partial \Psi}{\partial I_3}\mathbf{C}^{-1} \tag{3.49}$$

$$+\frac{\partial \Psi}{\partial I_4}\mathbf{A_0} + \frac{\partial \Psi}{\partial I_5}(\mathbf{a_0} \otimes \mathbf{C}\mathbf{a_0} + \mathbf{a_0}\mathbf{C} \otimes \mathbf{a_0}) \tag{3.50}$$

$$+\frac{\partial \Psi}{\partial I_6}\mathbf{G_0} + \frac{\partial \Psi}{\partial I_7}(\mathbf{g_0} \otimes \mathbf{C}\mathbf{g_0} + \mathbf{g_0}\mathbf{C} \otimes \mathbf{g_0}) \tag{3.51}$$

$$+\frac{1}{2}\frac{\partial \Psi}{\partial I_8}(\mathbf{a_0} \otimes \mathbf{g_0} + \mathbf{g_0} \otimes \mathbf{a_0})\Bigg], \tag{3.52}$$

where

$$\mathbf{A_0} = \mathbf{a_0} \otimes \mathbf{a_0}, \tag{3.53}$$

$$\mathbf{G_0} = \mathbf{g_0} \otimes \mathbf{g_0}. \tag{3.54}$$

$\mathbf{A_0}$ and $\mathbf{G_0}$ are referred to as **structural tensors**.

Vascular smooth muscle cells typically appeared to be aligned in the circumferential direction in healthy arteries. It is therefore assumed that the active contractile response is also anisotropic and only non-negative in that direction. Vector $\mathbf{m_0}$ is defined as the unit vector in the circumferential direction and $\mathbf{M_0} = \mathbf{m_0} \otimes \mathbf{m_0}$ is the structural tensor for the active response of VSMCs. The invariant associated to structural tensor $\mathbf{M_0}$ is defined analogously to (3.43) as

$$I_M(\mathbf{C}, \mathbf{m_0}) = \mathbf{m_0} \cdot \mathbf{C}\mathbf{m_0}. \tag{3.55}$$

Finally the functional form of the strain energy functions of the constituents must be specified. For **elastin**, **ground matrix** and **passive VSMCs** a **neo-Hookean** material model is adopted, namely

$$\Psi_{(\cdot)} = \frac{\mu_{(\cdot)}}{2}(I_1 - 3), \tag{3.56}$$

where $(\cdot) = el, gm$ and $\mu_{(\cdot)}$ is a material parameter. For collagen, a *distribution of recruitment stretches* is implemented following Grytsan et al. (2017) and Eriksson et al. (2014), which is described in more detail in Section 3.2.1. It is however assumed that the strain energy density function for collagen depends only on the fourth resp. sixth invariant, depending on the fibre family.

The material model for vascular smooth muscle cells is described in Section 3.3.2. The passive response is modelled as neo-hookean while the active response is assumed to be dependent on I_M only.

These choices of strain energy function Ψ are such that the dependence on I_2, I_5, I_7 and I_8 has been eliminated, while the dependence on I_3 has been substituted by the incompressibility constraint. Thus in this case, (3.49) becomes

$$\mathbf{S} = -p\mathbf{C}^{-1} + 2\left[\frac{\partial\Psi}{\partial I_1}\mathbf{I} + \frac{\partial\Psi}{\partial I_4}\mathbf{A_0} + \frac{\partial\Psi}{\partial I_6}\mathbf{G_0} + \frac{\partial\Psi}{\partial I_M}\mathbf{M_0}\right], \tag{3.57}$$

where p is the hydrostatic pressure and works as a penalty parameter that enforces incompressibility.

For the following, the main parts of the code used in the finite element modelling are reported in Appendix B and the input file for each simulation can be found in Appendix C.

3.2 Collagen Stretch Distribution: Constitutive Model and Remodelling

3.2.1 Motivation

In constrained mixture models of fibre-reinforced soft tissues, the stress response of collagen is often described using the HGO model, which uses an exponential-like function (Holzapfel et al. (2000)). Although this model successfully captures the

rapid stiffening of the tissue as the load borne by collagen increases, there has been difficulty in relating the parameters of the stress response to their biological meaning. Microscopic imaging of collagen in arterial walls have shown that this appear with varying levels of waviness, in a continuous distribution (Schrauwen et al. (2012)). Hill et al. (2012) showed that including a distribution of levels of waviness into the constitutive model of the material, as well as initiating recruitment at a finite stretch, yields the best fit to experimental data.

The material model initially included in the framework is therefore sophisticated to one that would represent this distribution of levels of waviness. In order to simplify notation and denomination, in the following the term "stretch" will indicate any state of linear deformation compared to the stress-free configuration, whether this be larger or smaller than 1, even though it would be more intuitive to speak of "waviness" or "undulation" when the stretch is smaller than 1.

The constitutive model proposed by Chen (2014) and Aparìcio et al. (2016) is adopted. This is an adaption of the model described in 2.2 into a three-dimensional framework and is described in the next Section.

3.2.2 Constitutive Model

It is assumed that collagen appears with a continuous distribution of levels of stretch. This distribution is modelled as triangular: this seems to be a reasonable approximations when considering experimental data (Hill et al. (2012), Schrauwen et al. (2012)) and is desirable for computational complexity, since it allows derivation of the analytical form for the total stress contribution of collagen, thus avoiding numerical integration, which would be computationally expensive.

The distribution is uniquely determined by the triplet of values

$$\left(\lambda_C^{AT,min}, \lambda_C^{AT,mod}, \lambda_C^{AT,max}\right), \tag{3.58}$$

where AT stands for "attachment" (stretch), $\lambda_C^{AT,min}$ and $\lambda_C^{AT,max}$ are the minimum and maximum stretches of collagen fibres respectively, while $\lambda_C^{AT,mod}$ corresponds to the stretch with maximum probability density, i.e. the "peak" of the triangle.

The distribution $\rho(\lambda_C^R)$ is then given by

$$\rho(\lambda_C^R) = \begin{cases} 0 & \text{if } \lambda_C^R < \lambda_C^{R,min}, \\ \frac{2(\lambda_C^R - \lambda_C^{R,min})}{(\lambda_C^{R,max} - \lambda_C^{R,min})(\lambda_C^{R,mod} - \lambda_C^{R,min})} & \text{if } \lambda_C^{R,min} \leq \lambda_C^R < \lambda_C^{R,mod}, \\ \frac{2(\lambda_C^{R,max} - \lambda_C^R)}{(\lambda_C^{R,max} - \lambda_C^{R,min})(\lambda_C^{R,max} - \lambda_C^{R,mod})} & \text{if } \lambda_C^{R,mod} \leq \lambda_C^R < \lambda_C^{R,max}, \\ 0 & \text{if } \lambda_C^{R,max} \leq \lambda_C^R, \end{cases} \tag{3.59}$$

where all stretches are to be understood as along the fibre direction.

A function $\tilde{\Psi}_C(\lambda_C)$ will then be defined which represents the contribution to the strain energy function given by the fibres recruited at λ_C^R. An individual fibre is assumed to have a linear stress response:

$$\tilde{\Psi}_C(\lambda_C) = \frac{\mu_C}{2} (\lambda_C - 1)^2 , \tag{3.60}$$

where μ_C is a stiffness-like material constant.

The total stress contribution from the collagen material is then obtain by integrating over the distribution of recruitment stretches:

$$\Psi_C(\lambda) = \int_1^{\lambda} \tilde{\Psi}_C \left(\frac{\lambda}{\lambda_C^R} \right) \rho(\lambda_C^R) \, d\lambda_C^R. \tag{3.61}$$

The choice of a triangular distribution of recruitment stretch results in the Piola-Kirchhoff stress admitting an analytical form of type:

$$\frac{\partial \Psi_C}{\lambda}(\lambda) = \mu_C \; C_1 \left[(\lambda + C_2) \ln(\frac{\lambda}{C_3}) + C_4 \; \lambda + C_5 \right], \tag{3.62}$$

where $C_i = C_i(\lambda_C^{R,min}, \lambda_C^{R,mod}, \lambda_C^{R,max})$ are constants depending on $\lambda_C^{R,min}, \lambda_C^{R,mod}$ and $\lambda_C^{R,max}$.

3.2.3 Remodelling

Vascular cells continuously maintain the collagen fabric: they secrete collagen-degrading enzymes called *matrix metalloproteinases* and their inhibitors TIMPs (*tissue inhibitors of metalloproteinases*), as well as synthesize and secrete new fibres which they then attach to the existing matrix. It is assumed that cells aim to maintain collagen with a

stretch distribution that optimises its mechanical function. Therefore a fibre stretch distribution is defined that corresponds to physiological homeostatic conditions:

$$\left(\lambda_C^{min,h}, \lambda_C^{mod,h}, \lambda_C^{max,h}\right). \tag{3.63}$$

Collagen can remodel towards this target distribution according to the following equations, which are linear in the deviation from the corresponding target stretches:

$$\frac{\partial \lambda_C^{R,min}}{\partial t} = \alpha_C \frac{\lambda_C^{max} - \lambda_C^{max,h}}{\lambda_C^{max,h}}, \tag{3.64}$$

$$\frac{\partial \lambda_C^{R,mod}}{\partial t} = \alpha_C \frac{\lambda_C^{mod} - \lambda_C^{mod,h}}{\lambda_C^{mod,h}}, \tag{3.65}$$

$$\frac{\partial \lambda_C^{R,max}}{\partial t} = \alpha_C \frac{\lambda_C^{min} - \lambda_C^{min,h}}{\lambda_C^{min,h}}, \tag{3.66}$$

where $\lambda_C^{min}, \lambda_C^{mod}$ and λ_C^{max} are the *current* collagen stretches while $\lambda_C^{R,min}, \lambda_C^{R,mod}$ and $\lambda_C^{R,max}$ the *current* recruitment stretches. Thus, if for example $\lambda_C^{max} > \lambda_C^{max,h}$, then the partial derivative of $\lambda_C^{R,min}$ is positive, the system will evolve to increase $\lambda_C^{R,min}$ and this corresponds to the desired decrease in λ_C^{max}. Similarly for $\lambda_C^{R,mod}$ and $\lambda_C^{R,max}$. In the above, time is treated numerically and thus the computational implementation is

$$\lambda_C^{R,min} = \lambda_C^{R,min} + \alpha_C \frac{\lambda_C^{max} - \lambda_C^{max,h}}{\lambda_C^{max,h}} \cdot dt, \tag{3.67}$$

where dt is a numerical time step. The analogous holds for the other variables. The reader is also reminder that λ_C is a function of λ_C^R according to $\lambda_C = \lambda/\lambda_C^R$ with λ the tissue stretch.

3.2.4 Implementation

In a finite element setting the initial configuration of the material is **unloaded**. If the natural state of the material to be studied is subject to loads, these must be gradually applied in a number n of numerical steps set by the user. Therefore the stages corresponding to numerical times $t = 0, \ldots, n$ correspond to **loading** of the

material and, if the loads applied are static, the configuration at numerical time $t = n$ corresponds to the **loaded configuration**. In the simulations of arterial geometry presented in this thesis, loading of the material will consist of the application of an internal pressure of $16kPa$ and of an axial stretch of $\lambda_Z = 1.3$. However this does not yet correspond to the healthy state of arterial tissue.

Indeed the models presented in this work characterises the healthy arterial tissue as not only being in the loaded configuration but also having all its constituent stretches equal to the respective attachment stretches. It is not straight-forward to know what distribution of stretches at time $t = 0$ results in the desired distribution at the end of the loading phase. In order to obviate this problem, a second phase is implemented during which all constituents *remodel* towards their attachment stretches according to the equations described in Section 3.2.3. Therefore it is only at the end of this second phase that the tissue represents a healthy arterial wall, after both loading and remodelling towards homeostasis.

In order to complete the constitutive model and carry out the necessary calculations, the program must receive the following information from the input file with regards to the collagen material: the direction vectors of the fibre families, the material parameter, the target homeostatic distribution and an initial guess distribution.

The direction vectors are supplied as an $n \times m$ matrix, where n is the number of nodes and $m = 3k$, where k is the number of fibre families and for each family the triplet of (x, y, z) coordinates of each direction vector must be provided. The material parameter is a scalar value and represents a stiffness-like material property. The target homeostatic distribution is given by the triplet of values as in (3.63). In addition, an initial distribution must be specified, corresponding to the unloaded configuration at $t = 0$.

To implement the constitutive model that includes the stretch distribution, two subroutines are created: one computes the first and second derivative of the strain energy density function, while the second computes the stress tensor and the tangent stiffness matrix, which depend on the direction vectors of the fibre families, from the two derivatives. The choice of a triangular distribution allows the integral defined in (3.61) to be expressed in an analytical form, thus bypassing the need for numerical integration. Following Chen (2014) and Aparìcio et al. (2016), the explicit expressions for the first Piola-Kirchhoff stress are obtained through application of equation (3.39): these are given by Eq. (3.68) where the abbreviations $a = \lambda_C^{R,min}$, $b = \lambda_C^{R,max}$ and

$c = \lambda_C^{R,mod}$ are used.

$$P_C(\lambda) = \begin{cases} 0 & \text{if } \lambda < a, \\ \gamma((a+\lambda)\ \log(\frac{\lambda}{a} + 2(a-\lambda))) & \text{if } a \leq \lambda < c, \\ \gamma((a+\lambda)\ \log(\frac{c}{a}) + a - c + (\frac{a}{c} - 1)\lambda) + ... & \\ \quad -\delta((b+\lambda)\log(\frac{\lambda}{c}) + b + c - (\frac{b}{c} + 1)\lambda) & \text{if } c \leq \lambda < b, \\ \gamma((a+\lambda)\ \log(\frac{c}{a}) + a - c + (\frac{a}{c} - 1)\lambda) + ... & \\ \quad -\delta((b+\lambda)\log(\frac{b}{c}) - b + c - (\frac{b}{c} - 1)\lambda) & \text{if } b \leq \lambda, \end{cases} \tag{3.68}$$

where

$$\gamma = \frac{2\mu}{(b-a)(c-a)}, \tag{3.69}$$

$$\delta = \frac{2\mu}{(b-a)(b-c)}. \tag{3.70}$$

The evolution laws that govern the remodelling (Eq. (3.64)) are discretised by means of the explicit Euler method and implemented in a subroutine that collects "user macros" which can be custom called by the user from the input file. The equations prescribe remodelling of the recruitment stretch so that the current constituent stretch evolves towards its homeostatic (attachment) value. The remodelling rate is linear in the deviation of the current stretch from its attachment value (Eq. (3.71)):

$$\frac{\partial \lambda_C^{R,min}}{\partial t} = \alpha \frac{I_{4C}^{max} - I_{4C}^{ATT,max}}{I_{4C}^{ATT,max}}, \tag{3.71}$$

$$\frac{\partial \lambda_C^{R,mod}}{\partial t} = \alpha \frac{I_{4C}^{mod} - I_{4C}^{ATT,mod}}{I_{4C}^{ATT,mod}}, \tag{3.72}$$

$$\frac{\partial \lambda_C^{R,max}}{\partial t} = \alpha \frac{I_{4C}^{min} - I_{4C}^{ATT,min}}{I_{4C}^{ATT,min}}. \tag{3.73}$$

3.2.5 Verification of Constitutive Model

In this Section a model of biaxial extension for a cubic sample of arterial tissue is presented. The model has been implemented in FEAP and used to verify the correct

implementation of the new constitutive model for collagen and later vascular smooth muscle cells. This is possible because the analytical solution for this simple case is available and computed through the software MATLAB.

A cubic sample of arterial tissue is modelled as a constrained mixture of elastin, ground matrix, collagen and VSMCs. Biaxial extension is enforced by applying the following deformation gradient:

$$\mathbf{F} = \begin{pmatrix} \lambda & 0 & 0 \\ 0 & \lambda & 0 \\ 0 & 0 & \frac{1}{\lambda^2} \end{pmatrix}, \tag{3.74}$$

where λ grows linearly from 1 to 2 in a number n of uniform steps. The first two diagonal elements are due to the uniform stretching of the tissue in the $x-$ and $y-$ directions, while the third follows from the incompressibility constraint $J = \det \mathbf{F} = 1$.

In order to solve equation (3.57), it is necessary to determine the hydrostatic pressure p. This is done by prescribing $S_{33} = 0$ where S_{33} is the entry of $\mathbf{S}$ in the third row and third column. This corresponds to absence of stress in the z direction. Since $\mathbf{a_0}$ and $\mathbf{g_0}$ are of the form

$$\begin{pmatrix} \cos\phi, \\ \sin\phi, \\ 0 \end{pmatrix},$$

it follows that the third diagonal elements of $\mathbf{A_0}$ and $\mathbf{G_0}$ are equal to 0. From this it follows that it is possible to determine the value of p by setting $S_{33} = 0$ in (3.57), thus obtaining

$$p = 2\,\frac{\partial \Psi}{\partial I_1}\,\frac{1}{\lambda^4}. \tag{3.75}$$

Now that p is known, it can be substituted into (3.57) and solve for $\mathbf{S}$. Finally, the transformation defined by (3.27) can be applied to obtain σ and identify the principal stresses.

Due to the symmetry of the geometry and the loading, only one eighth of the tissue sample is modelled, represented by a unit cube lying in the first octant. The mesh consists of $4 \times 4 \times 1$ (number of elements in x, y and z directions respectively) Q1P0 elements of 8 nodes each, yielding a total of 16 elements and 50 nodes. The cube is

positioned to have one corner in $(0, 0, 0)$ and be fully contained in the first octant (Figure 3.1). The following symmetry boundary conditions (BCs) are applied:

- displacement $u_x(x = 0) = 0$,
- displacement $u_y(y = 0) = 0$,
- displacement $u_z(z = 0) = 0$.

Displacement-controlled biaxial extension is implemented by prescribing:

- displacement $u_x(x = 1) = 1$, and
- displacement $u_y(y = 1) = 1$.

At every step of the simulation, the principal stresses are extracted at a specified node and compared with the analytical model. Due to the homogeneity of the stress state, the choice of the node can be arbitrary.

The parameters chosen for the model are listed in Table 3.1.

Parameter	Value
k_E	0.0093 MPa
k_C	5.8 MPa
$\lambda_C^{AT,min}$	0.85
$\lambda_C^{AT,mod}$	0.95
$\lambda_C^{AT,max}$	1.05
ϕ in $(\mathbf{a_0})$	$\frac{\pi}{4}$
ϕ in $(\mathbf{g_0})$	$-\frac{\pi}{4}$

Table 3.1: List of model parameters for biaxial extension validation.

The principal stress from the numerical and analytical mode are plotted in Fig. 3.3.

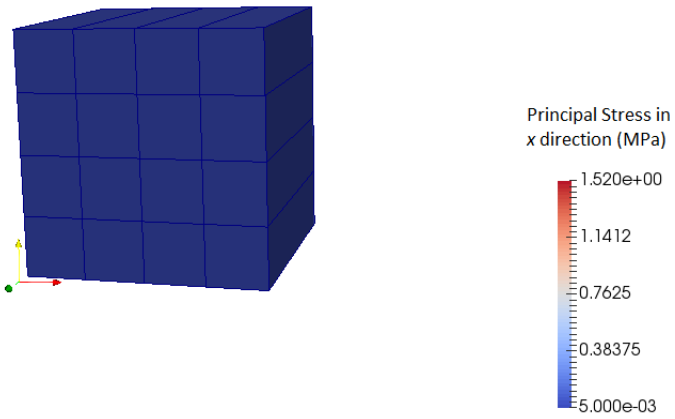

Figure 3.1: Biaxial extension verification case at $\lambda = 1$, corresponding to the beginning of the simulation.

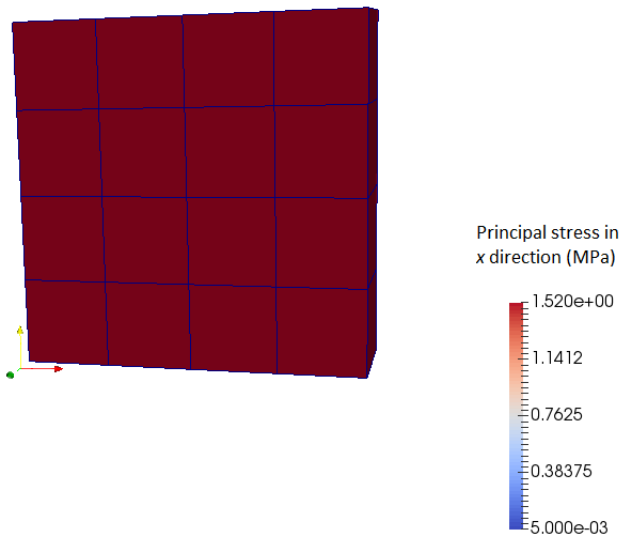

Figure 3.2: Biaxial extension verification case at $\lambda = 2$, corresponding to the end of the simulation.

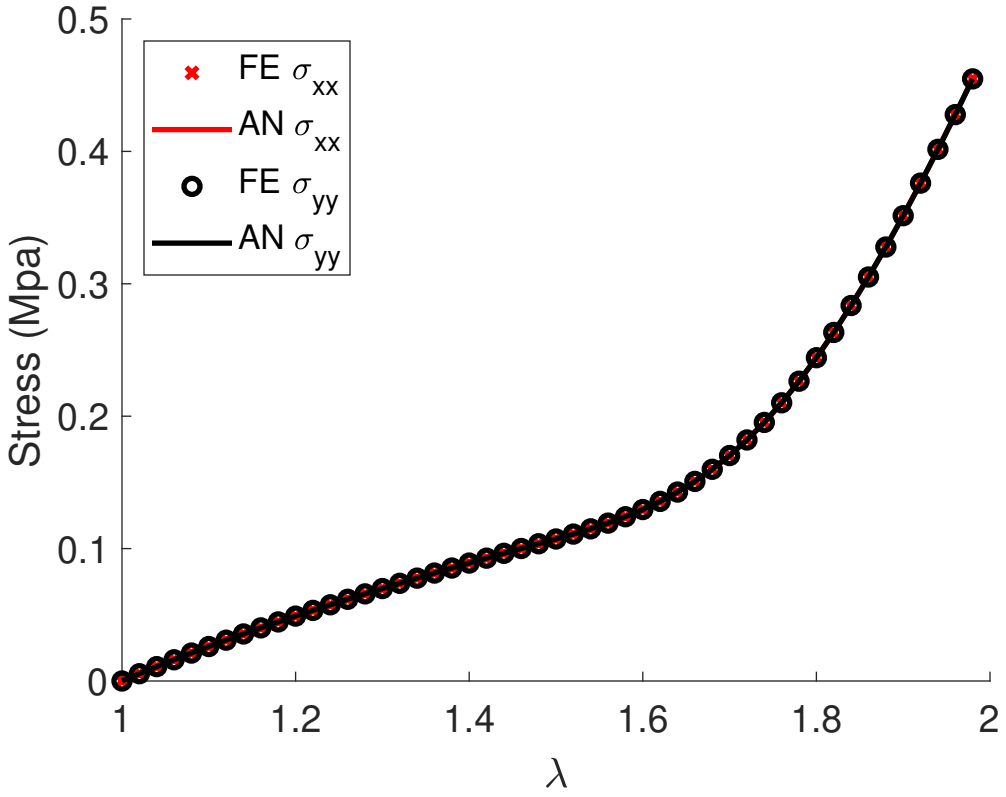

Figure 3.3: Comparison of principal stresses in the x-direction (σ_{xx}) and y-direction (σ_{yy}) from the analytical (AN) versus the numerical (FE) solutions in the case of symmetric biaxial stretching of a simple cube. The initial linear behaviour is due to the properties of elastin, which is the main load bearer at smaller stretches, while the visible stiffening of the tissue at higher stretches is due to the gradual recruitment to load-bearing of the collagen fibres.

3.2.6 Verification of Remodelling

In order to verify the correct implementation of the evolution laws governing remodelling of the collagen stretch distribution (3.64), the model of biaxial stretching presented in the previous Section is extended and tested for robustness against different initial conditions.

The first part of the model is equal to the one described in Section 3.2.5: a cubic sample of tissue is symmetrically stretched in the x- and y-directions, linearly over time until $\lambda = 2$. No remodelling occurs in this phase. When the final stretch $\lambda = 2$ is achieved, the tissue is held at this state of stretch and collagen remodelling begins, i.e. the user macro running the evolution equations is called at every time step. To ensure a small enough difference between the actual stretch distribution and the target distribution, the second part of the model is run for 450 time steps, until $t = 500$.

The target distribution is set at:

$$\lambda_{min}^{ATT} = 0.85, \tag{3.76}$$
$$\lambda_{mod}^{ATT} = 0.95, \tag{3.77}$$
$$\lambda_{max}^{ATT} = 1.05. \tag{3.78}$$

The remodelling equations are tested for robustness by varying the initial conditions. Four distinct cases are considered with different initial distributions corresponding to the following scenarios:

- Case 1 represents the case in which the initial distribution has the same width and same skew as the target one;
- Case 2 represents the case in which the initial distribution has the same width but different skew;
- Case 3 represents the case in which the initial distribution has different width compared to the target one but symmetric skew like the target one;
- Case 4 represents the case in which the initial distribution has different width and different (asymmetric) skew from the target one.

The corresponding initial distributions are given by the following values and plotted in Figure 3.4:

$$\text{Case 1}: \begin{cases} \lambda_C^{min} = & 0.75, \\ \lambda_C^{mod} = & 0.85, \\ \lambda_C^{max} = & 0.95; \end{cases} \tag{3.79}$$

$$\text{Case 2}: \begin{cases} \lambda_C^{min} = & 0.7, \\ \lambda_C^{mod} = & 0.85, \\ \lambda_C^{max} = & 0.9; \end{cases} \tag{3.80}$$

$$\text{Case 3}: \begin{cases} \lambda_C^{min} = & 0.6, \\ \lambda_C^{mod} = & 0.8, \\ \lambda_C^{max} = & 1.0; \end{cases} \tag{3.81}$$

$$\text{Case 4}: \begin{cases} \lambda_C^{min} = & 0.6, \\ \lambda_C^{mod} = & 0.8, \\ \lambda_C^{max} = & 0.9. \end{cases} \tag{3.82}$$

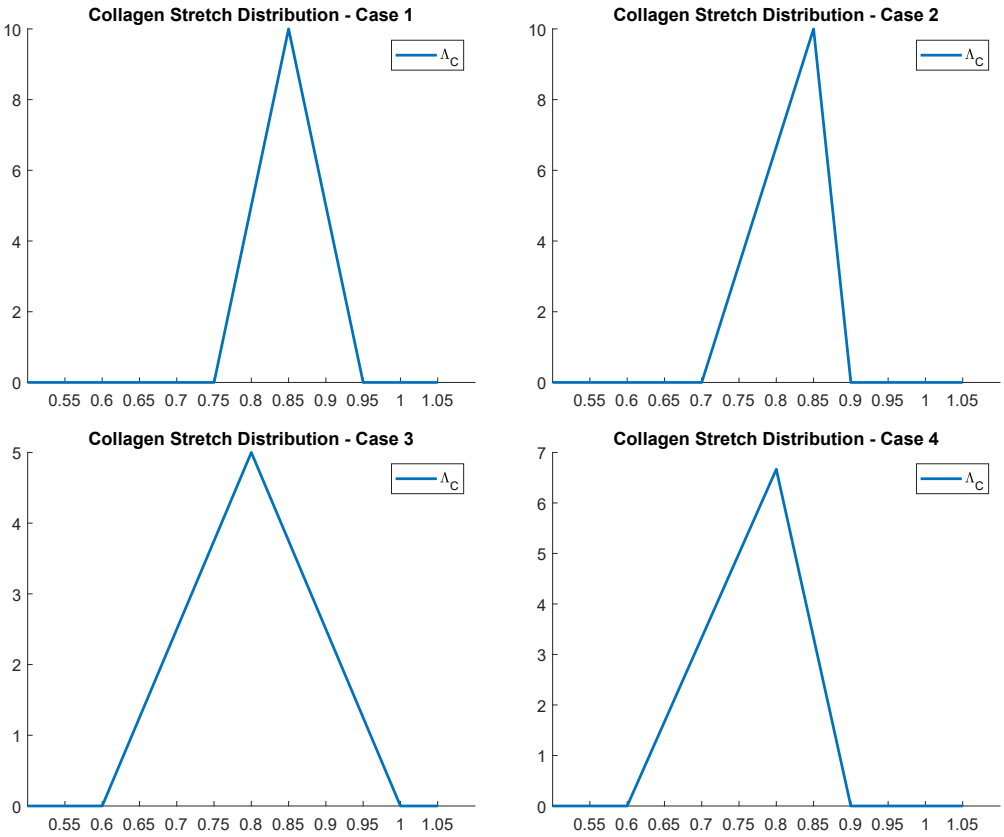

Figure 3.4: Collagen stretch distributions for the four representative cases selected for the verification of robustness of the remodelling equations for the collagen fibres.

Looking at Figures 3.5-3.8, it is easy to notice that all cases converge successfully towards the target distribution and that the evolution is robust in terms of the initial conditions: the values, width and skew of the initial distribution have no effect on the correct convergence of the stretch values. The implementation of the remodelling equations is thus considered verified.

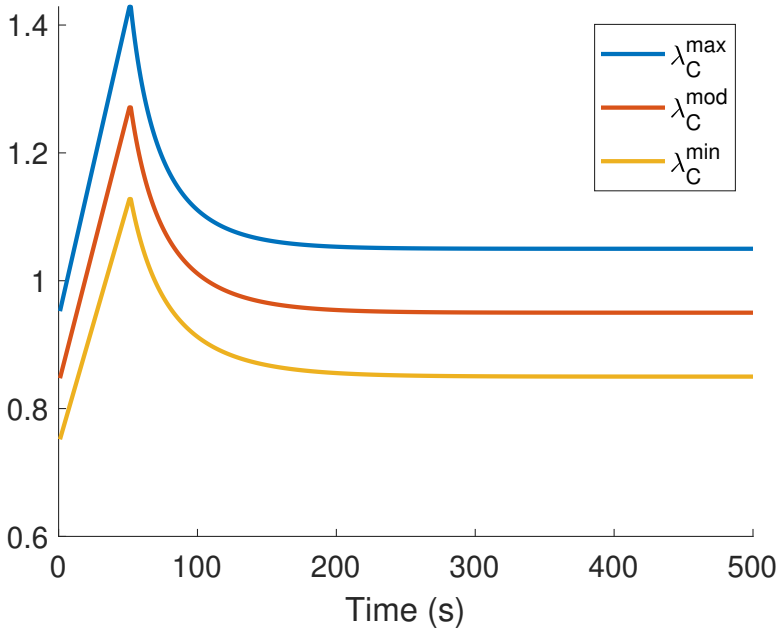

Figure 3.5: Evolution of collagen stretch distribution for Case 1 (initial distribution with same width and skew as target distribution). During the first 50 seconds the cubic sample is gradually stretched until $\lambda = 2$ and then it is held in position while collagen remodels towards its target distribution.

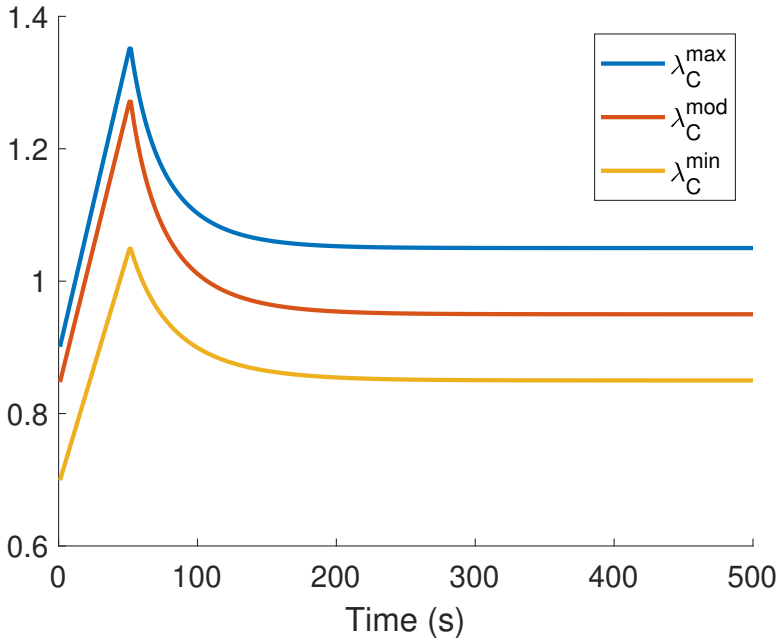

Figure 3.6: Evolution of collagen stretch distribution for Case 2 (initial distribution with same width but different skew compared to target distribution). During the first 50 seconds the cubic sample is gradually stretched until $\lambda = 2$ and then it is held in position while collagen remodels towards its target distribution.

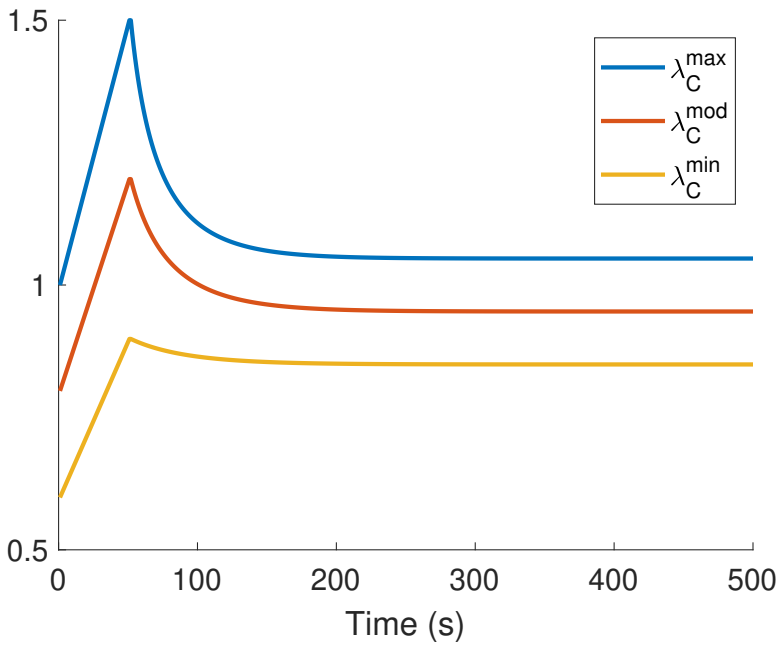

Figure 3.7: Evolution of collagen stretch distribution for Case 3 (initial distribution symmetric width like target distribution but different skew). During the first 50 seconds the cubic sample is gradually stretched until $\lambda = 2$ and then it is held in position while collagen remodels towards its target distribution.

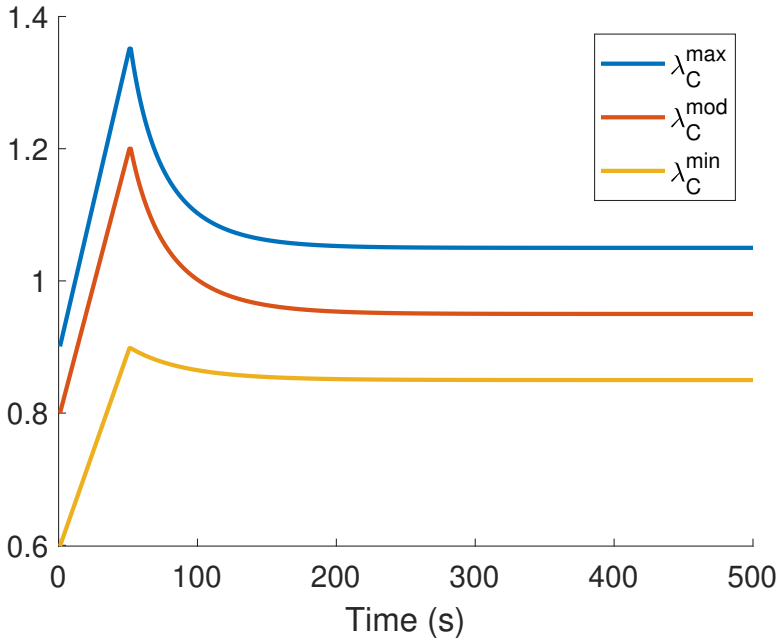

Figure 3.8: Evolution of collagen stretch distribution for Case 4 (initial distribution with different width and asymmetric skew compared to target distribution). During the first 50 seconds the cubic sample is gradually stretched until $\lambda = 2$ and then it is held in position while collagen remodels towards its target distribution.

3.3 Vascular Smooth Muscle Cells with Active Response: Constitutive Model and Remodelling

3.3.1 Motivation

One limitation to the finite element framework developed by Eriksson et al. (2014) and Grytsan et al. (2017) is the absence of a constitutive model for vascular smooth cells (VSMCs). Following Humphrey et al. (2007 September*a*) and Baek et al. (2007), a constitutive model is chosen that includes both a passive and active response, where the latter captures the ability of VSMCs to contract and dilate to regulate vessel diameter.

3.3.2 Constitutive Model

The passive response is modelled as neo-hookean with material parameter k_M^{pass}:

$$\Psi_M^{pass} = \frac{k_M^{pass}}{2} \left(\overline{I}_1 - 3\right)^2 \tag{3.83}$$

The active response follows Baek et al. (2007) who have chosen the simplest functional form that closely resembles the active response measured in animal experiments. This stress function is in principle the one that was implemented in Chapter 2 in Eq. (2.18): the only difference is that factors f_p and c_v are omitted. Vascular smooth muscle cells are assumed to be aligned in the circumferential direction and thus the active stress is assumed to act only in that direction (Rothermel et al. (2020), Ushiwata & Ushiki (1990)). In Baek et al. (2007) a general strain energy density function is not given, but since only its first and second derivative are needed for the implementation, it is only necessary to prescribe the former, which coincides with the first Piola-Kirchhoff stress. This is thus given by:

$$\frac{\partial \Psi_M^{act}}{\partial \lambda_M} = \begin{cases} 0 & \text{if } \lambda_M < \lambda_M^{min}, \\ k_M^{act}\ \lambda_M\ \left[1 - \left(\frac{\lambda_M^{mean} - \lambda_M}{\lambda_M^{mean} - \lambda_M^{min}}\right)\right], & \text{if } \lambda_M^{min} \leq \lambda_M \leq \lambda_M^{max}, \\ 0 & \text{if } \lambda_M^{max} < \lambda_M, \end{cases} \tag{3.84}$$

where

$$\lambda_M = \sqrt{I_{4M}}, \qquad I_{4M} = \mathbf{C} : \mathbf{M_0}, \tag{3.85}$$

where $\mathbf{M_0} = \mathbf{m_0} \otimes \mathbf{m_0}$ with $\mathbf{m_0}$ the unit vector in the circumferential direction (see Section 3.3.4). The functional form and parameters of the stress function are identical to that used in the 1D model and thus the stress response of VSMCs in the circumferential direction is illustrated in Figure 3.9, which is identical to Figure 2.4 in Chapter 2 but reported here for ease of readability.

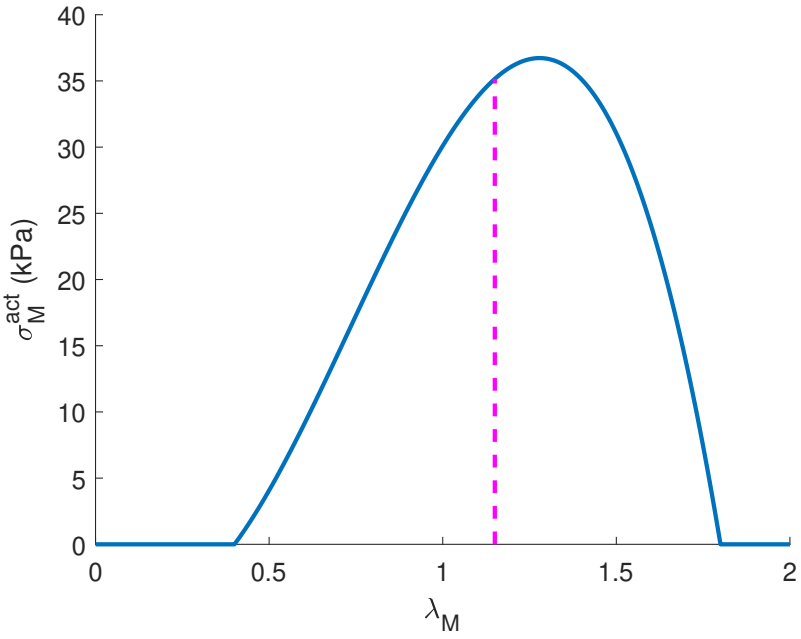

Figure 3.9: Active component of the stress response of vascular smooth muscle cells as a function of their stretch (continuous curve). The dashed line corresponds to the stress response when VSMC stretch equals its attachment value $\lambda_M = \lambda_M^{ATT} = 1.15$.

3.3.3 Remodelling

Similarly to what has been defined for the collagen fibres, VSMCs are assumed to have a recruitment stretch λ_M^R such that

$$\lambda_M^R = \frac{\lambda}{\lambda_M} \tag{3.86}$$

where λ is the current tissue stretch and λ_M the current cell stretch of VSMCs. The value of the recruitment stretch can change in response to a changing mechano-chemical environment. In the models presented in this work remodelling will be used in two cases:

- **towards health**: as explained in Section 3.2.4, the finite element model requires two phases in order for the modelled tissue to represent healthy arterial tissue; the first phase is a loading phase in which internal pressure and axial pre-stretch are applied, while the second phase is needed to allow constituent stretches to attain their attachment values;
- **vasospasm**: it is assumed that a driving mechanism of vasospasm is the remodelling of VSMCs about the new geometry, namely the fact that at the reduced vessel diameter (and therefore circumferential stretch) they remodel their configuration (in the form of the recruitment stretch) in order that their stretch equals the attachment stretch.

It is assumed that the target value (VSMC attachment stretch λ_M^{ATT}) is known and that the remodelling process is linear in the deviation of the current recruitment stretch from the target:

$$\frac{\partial \lambda_M^R}{\partial t} = \alpha_M \frac{\lambda_M - \lambda_M^{ATT}}{\lambda_M^{ATT}}. \tag{3.87}$$

This is the equivalent of the remodelling equations used for the collagen distribution.

3.3.4 Implementation

The passive response of VSMCs is modelled as isotropic neo-Hookean and thus the same material model for elastin is used, with the material parameter modified accordingly. The active response is modelled to only act in the circumferential direction. This choice is motivated by the experimental observation that VSMCs are mostly aligned in this direction in arterial tissue. Similarly to collagen, a unitary direction vector $\mathbf{m_0}$ must be supplied to represent this direction. The corresponding structural tensor for VSMCs is constructed by

$$\mathbf{M_0} = \mathbf{m_0} \otimes \mathbf{m_0}. \tag{3.88}$$

The structure vector $\mathbf{m_0}$ is defined differently according to the numerical model used.

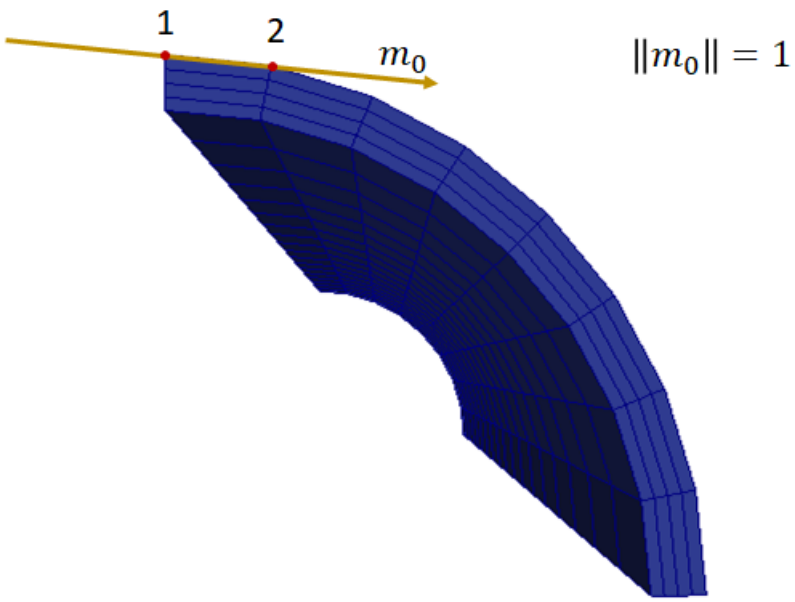

Figure 3.10: Numerical computation of circumferential direction at each element (represented for one element only). The normalised vector difference between nodes 1 and 2 is the unit tangent to the element in the middle point of the outer surface and represents a good approximation of the circumferential direction. The same calculation is performed at each element.

In the case of biaxal stretching of a cubic material sample, which is used for the verification of the material model, the active stress response is assumed to be positive only in the x direction and therefore $\mathbf{m_0} = (1, 0, 0)$. In the case of the cylindrical model, which is used for the verification of remodelling and damage, the active stress response will be assumed to be positive only in the circumferential direction. This is less straight-forward to implement and the chosen process is the following: $\mathbf{m_0}$ is computed for each element as the normalised difference vector between two nodes that share the same radial and axial coordinates (see Figure 3.10). This gives the unit vector tangent to the cylinder at the middle point on the element surface, which represents a good approximation of the circumferential direction in this application.

Similarly to the case of collagen, two subroutines are created: the first computes the first and second derivative of the SEDF in the circumferential direction, while the second takes the two derivatives as input and derives the stress tensor and tangent stiffness matrix, which depend on the direction vector of the material.

As far as remodelling is concerned, the evolution equation (3.87) is again discretised by the explicit Euler method and implemented in the "user macros" subroutine, which is called from the input file via a custom phrase.

The passive and active material parameters as well as the direction vector are supplied by the user via the input file. In the implementation used for this model the remodelling rate parameter α_M has been hard-coded into the program, but it would be straightforward to make it available for user customisation through the input file.

3.3.5 Verification

The correct implementation of the material model is verified through the same model used in Section 3.2.5 for the verification of the material model of collagen: symmetric biaxial stretching of a cube. In this model the active response of VSMCs is assumed to be positive only in the x-direction.

The principal stresses are computed at every time step and compared to the analytical solution, which is available for this simple case and derived in the software MATLAB. The analytical solution is computed by solving Eq. (3.57) via the steps described in Section 3.2.5. The results are plotted in Fig. 3.11.

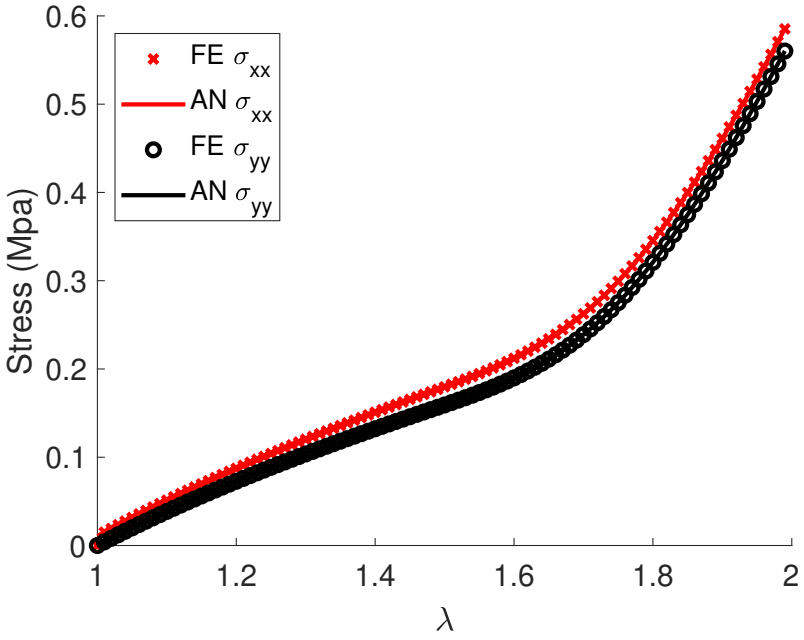

Figure 3.11: Comparison of principal stresses in the x- (σ_{xx}) and y- (σ_{yy}) directions for the analytical (AN) versus the numerical (FE) solution. The active stress only acts in the $x-$ direction and thus the principal stress σ_{xx} is higher than σ_{yy}. The graph shows excellent agreement between the numerical and analytical solution.

From Fig. 3.11 it is immediately visible that there is excellent agreement between the analytical and the numerical solution and thus the model is considered as correctly implemented. It is easily noticeable that the stress response in the x-direction is higher, which is consistent with the VSMC active response only affecting said direction.

3.3.6 Verification of remodelling

In order to verify the correct implementation of the evolution equation for the recruitment stretch of VSMCs the simulation of biaxial stretching of a cube is abandoned and a cylindrical geometry is used instead, which will be useful for the model of cerebral vasospasm discussed in Chapter 4.

The verification model used to test the correct implementation of VSMC remodelling is a cylinder inflation. A mesh for a quarter cylinder is used with 8 elements in the circumferential direction, 4 in the radial and 12 in the axial. The radial layers do not correspond to anatomical layers, but are all composed of the same material that is the composition of the three main constituents. The cylinder is internally pressurised to physiological systolic blood pressure $p = 16kPa$ and axially pre-stretched by a factor $\lambda_z = 1.2$. The boundary conditions are assigned as follows:

- $u_x(x = 0) = 0$,
- $u_y(y = 0) = 0$,
- $u_z(z = 0) = 0$,
- $u_z(z = 0.0125) = 0.0025$,

where the former three conditions fix the boundary surfaces $x = 0$, $y = 0$ and $z = 0$, so that the geometry can be thought of as the symmetric eighth of a $3cm$ cylinder. The latter condition enforces the axial pre-stretch of $\lambda_z = 1.2$. The cylinder has a diameter of $d = 2.9mm$ and thickness $h = 0.29mm$, and thus $h/r = 1/5$.

The cylinder is assumed to be a constrained mixture of elastin, collagen and VSMCs. Thus:

$$\Psi = \Psi_{\text{el}} + \Psi_{\text{col,a}_0} + \Psi_{\text{col,g}_0} + \Psi^{pass}_{VSMC} + \Psi^{act}_{VSMC}. \tag{3.89}$$

Two families of collagen fibres are included with direction vectors $\mathbf{a_0}$ and $\mathbf{g_0}$ of the form $(\sin(\phi), \cos(\phi), 0)$ with $\phi_{\mathbf{a_0}} = \pi/4$ and $\phi_{\mathbf{g_0}} = -\pi/4$. Elastin is modelled as isotropic

neo-Hookean material, while collagen and VSMCs are modelled according to the constitutive equations described in Sections 3.2.5 and 3.3.2 respectively. The material parameters and other relevant parameters for the model are reported in Table 3.2. The material parameters have been chosen so that, similarly to what is hypothesised in Chapter 2, elastin and passive VSMCs would bear about 80% of the pressure load and deactivation of the active response of VSMCs would result in a dilation of about 15% (Latorre et al. (2019)).

Parameter	Value
h	0.29mm
d	2.9mm
h/r	1/5
λ_z	1.2
k_E	$93kPa$
k_C	$5800kPa$
k_M^{pass}	$45.1kPa$
k_M^{act}	$11kPa$
$\phi_{\mathbf{a_0}}$	$\frac{\pi}{4}$
$\phi_{\mathbf{g_0}}$	$-\frac{\pi}{4}$

Table 3.2: Table of relevant model parameters for simulation of VSMC remodelling.

The model is divided into four phases:

- Phase 1 (time steps: $0-50$): **Loading**
  Pressurisation and axial pre-stretching of unloaded cylinder;
- Phase 2 (time steps: $51-500$): **Health**
  Remodelling of collagen and VSMCs towards homeostatic stretch; the end of this phase corresponds to arterial tissue in health;
- Phase 3 (time steps: $501-1000$): **Constriction**
  Increase of VSMC active stress response;
- Phase 4 (time steps: $1001-1500$): **Remodelling**
  Remodelling of VSMCs towards homeostatic stretch.

With regards to the stretch of VSMCs, the following is expected to occur in the four phases:

- Phase 1 (time steps: $0-50$): **Loading**
  Pressurisation and axial pre-stretching of unloaded cylinder: VSMC stretch increases linearly according to the deformation, recruitment stretch is constant;

- Phase 2 (time steps: $51 - 500$): **Health**
  Remodelling of collagen and VSMCs towards homeostatic stretch: recruitment stretch changes in order to return VSMC stretch to attachment value;
- Phase 3 (time steps: $501 - 1000$): **Constriction**
  Increase of VSMC active stress response; VSMC stretch decreases as the geometry shrinks in response to the stress increase, recruitment stretch is constant;
- Phase 4 (time steps: $1001 - 1500$): **Remodelling**
  Remodelling of VSMCs towards homeostatic stretch: recruitment stretch changes in order to return VSMC stretch to attachment value;

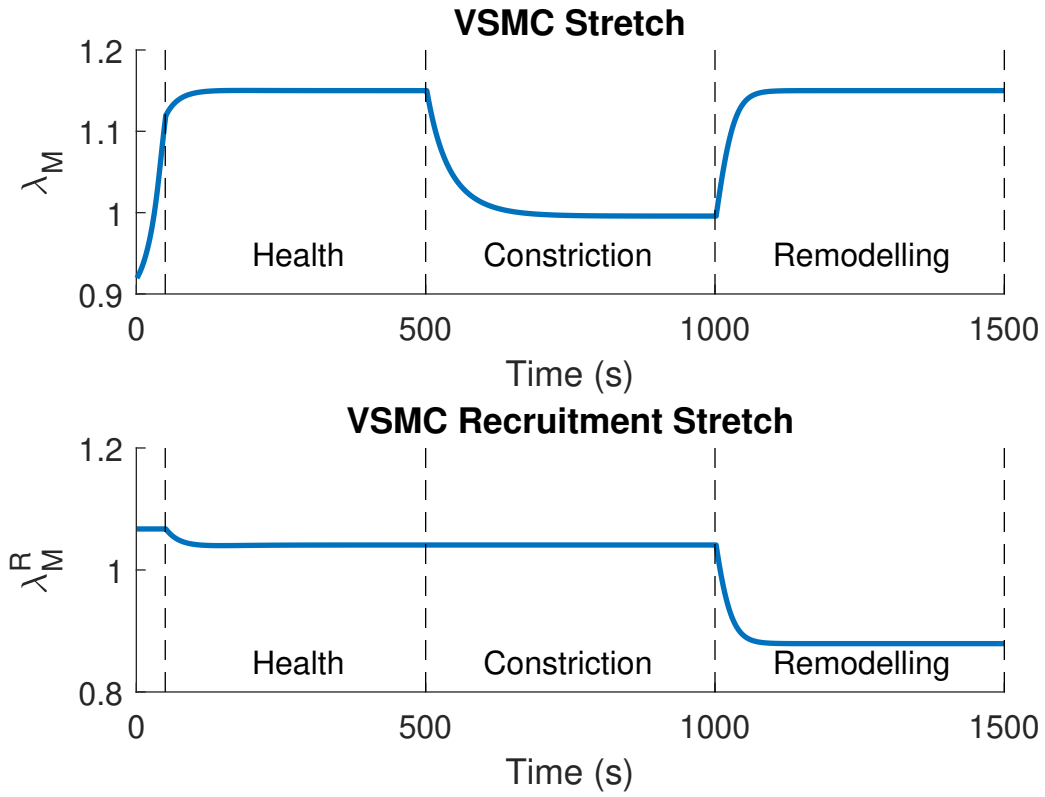

Figure 3.12: Evolution of VSMC cell stretch and recruitment stretch in homeostasis and following constriction. Following the initial pressurisation (time steps 0-50) remodelling of VSMC stretch towards its homeostatic value occurs (time steps 50-500) and the recruitment stretch adapts accordingly. After the arterial geometry is constricted due to an increase in the active response (time steps 500-1000, no remodelling in this phase), VSMC remodelling occurs and the recruitment stretch adapts to the new geometry reaching a value that results in the cell stretch to equal its attachment stretch (steps 1000-1500).

Figure 3.12 shows the evolution of the cell stretch λ_M and recruitment stretch λ_M^R over time, where the two values have been averaged across all elements. The results

are as expected:

1. Phase 1: **Loading**
   VSMC stretch increases linearly as the cubic sample is gradually stretched by a factor of 2; the recruitment stretch remains constant as no remodelling occurs in this phase;

2. Phase 2: **Health**
   Recruitment stretch remodels in order to obtain $\lambda_M = \lambda_M^{ATT} = 1.15$ at current tissue stretch; λ_M indeed evolves towards its target value;

3. Phase 3: **Constriction**
   The increase in active stress response causes the tissue to shrink and thus its circumferential stretch decreases; since no remodelling occurs in this phase, the cell stretch decreases according to the deformation while the recruitment stretch remains constant;

4. Phase 4: **Remodelling**
   Recruitment stretch remodels in order to obtain $\lambda_M = \lambda_M^{ATT} = 1.15$ at current tissue stretch; λ_M is indeed returned to its target value while λ_M^R has attained a different value than in Phase 2 since the new geometry has a different circumferential stretch and thus λ_M^R adapts according to $\lambda_M^R = \lambda/\lambda_M$.

In Figure 3.13 a “time lapse" is presented of the evolution of the cell and recruitment stretch for vascular smooth muscle cells, which allows us to contextualise the results in the geometry. Each row corresponds to the end of the related phase: the first row shows the end of Phase 1 at $t = 50$, the second row end of Phase 2 at $t = 500$, the third end of Phase 3 at $t = 1000$ and finally the fourth end of Phase 4 at $t = 1500$. The results outlined above are uniform in the circumferential and axial directions, but vary in the radial direction: indeed the circumferential stretch presents a gradient across the thickness of the vessel and thus, in order for the cell stretch to be uniform in the radial direction, the recruitment stretch must also present a gradient. The results presented in Figure 3.13 use a scale that covers the range of the entire simulation. In order to better appreciate the radial gradient, Figure 3.14 shows the same variables with the scale localised to a specific time point ($t = 500$ above and $t = 1500$ below). Here it is easier to notice the change in geometry and the range of values the recruitment stretch needs to attain in either configuration.

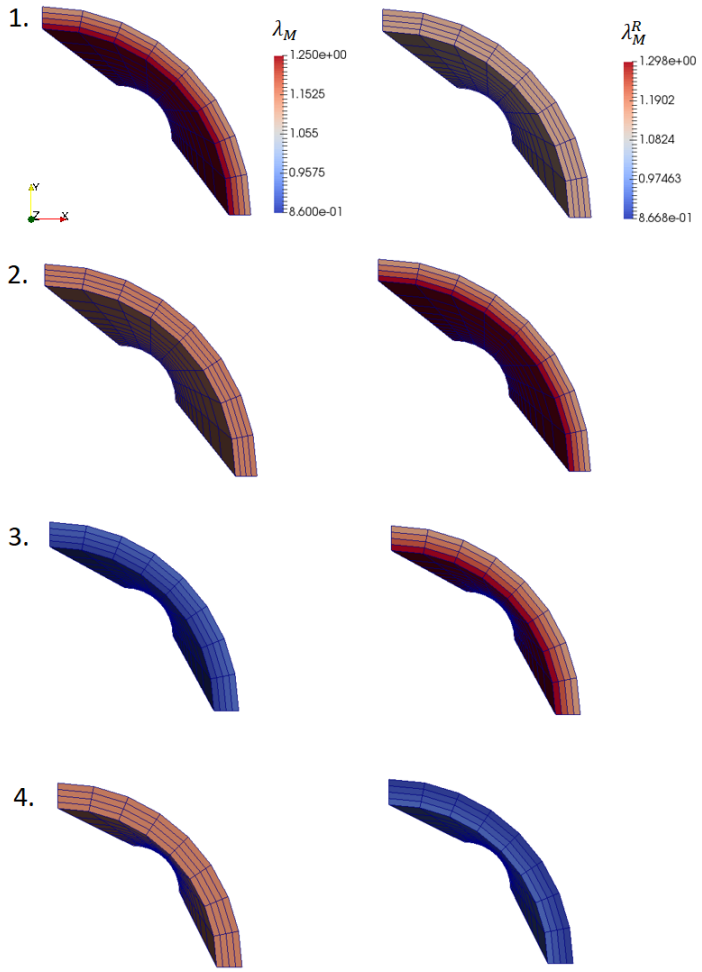

Figure 3.13: Evolution of cell stretch (left) and recruitment stretch (right) over the four phases of the simulation. During Phase 1 (pressurisation) λ_M^R is constant and equal to an initial value set by the user while λ_M changes consistently with the geometry. Following Phase 2 (physiological remodelling) λ_M is equal to its attachment value and λ_M^R has evolved in order to achieve that: notice that λ_M^R changes across the vessel thickness which is necessary since the circumferential stretch is different. Following the constriction of Phase 3, during which no remodelling occurs (therefore λ_M^R is unchanged and λ_M evolves with the geometry), during Phase 4 VSMCs achieve homeostasis again where λ_M^R has attained a new distribution which allows λ_M to return to its attachment value in the new geometry.

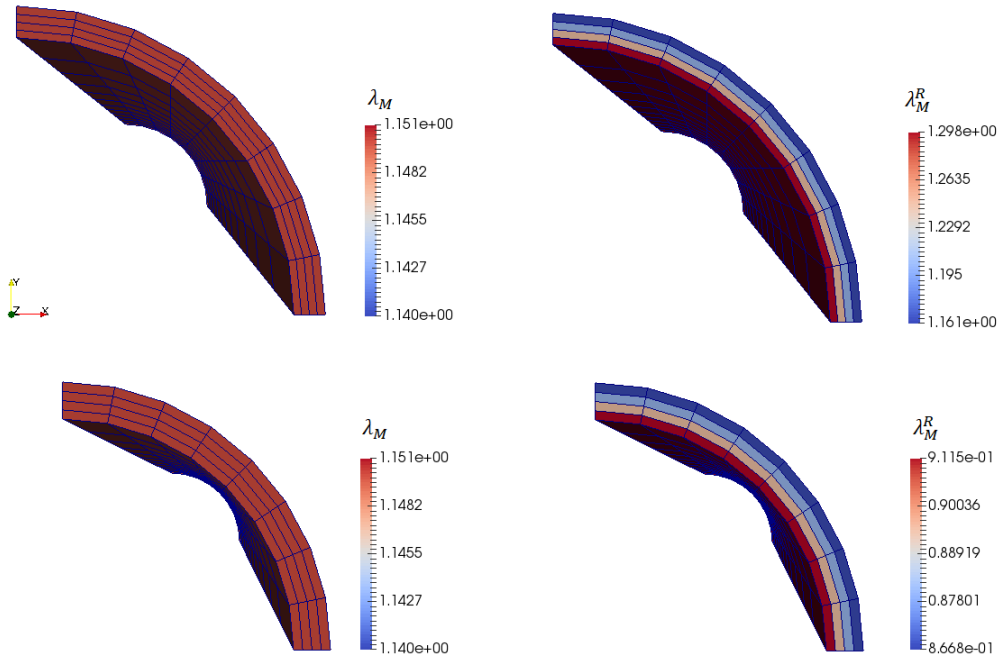

Figure 3.14: VSMC stretch and recruitment stretch at $t = 500$ (end of Phase 2, above) and $t = 1500$ (end of Phase 4, below) with localised value scale. Since the circumferential stretch is non-uniform across the vessel thickness, the recruitment stretch must attain a gradient of values across the radial direction in order for the cell stretch to be uniform in all directions.

3.4 Damage Model

3.4.1 Motivation

The absence of a damage model for constituents is a shortcoming of many existing mathematical and computational models of soft tissue (Ambrosi et al. (2019)). In the case of this model, where the aim is to simulate mechanical treatment of cerebral vasospasm, this is a feature that cannot be missing from the modelling framework. This can be a useful addition to several models of soft tissue diseases and/or treatment.

Following Li et al. (2012) a scalar damage variable is introduced per constituent, varying between a minimum of 0 (no damage) to 1 (complete failure), where damage is represented in a decrease of the constituent's contribution to load bearing, i.e. of its stress response. The continuous nature of the damage variable allows for easier numerical implementation, though in reality damage to a constituent is likely to be of a more discrete nature (detachment or rupture of fibrils within a collagen fibres, detachment of focal adhesions and/or tight junctions, rupture of a stress fibre forming the cytoskeleton of a cell, etc.). However the model of vasospasm treatment presented here does not aim to describe the structure of the tissue down to this small scale and thus this formulation of cell damage is sufficient. The mathematical details and numerical implementation are discussed in Section 3.4.2.

3.4.2 Implementation

Following Li et al. (2012) a scalar damage variable is introduced for each constituent $d_{0,i} \in [0,1]$, with $i \in \{E, C_M, C_A, M^{pass}, M^{act}\}$, which represents the extent of damage to the constituent. The case $d_{0,i} = 0$ corresponds to no damage, while $d_{0,1} = 1$ corresponds to complete failure. Indeed, the strain energy density functions of the individual constituents are pre-multiplied by the quantity $(1 - d_{0,1})$ and thus damage to a constituent corresponds to a decrease in its contribution to load-bearing:

$$\Psi_i \longrightarrow (1 - d_{0,i})\Psi_i, \tag{3.90}$$

for $i \in \{E, C_M, C_A, M^{pass}, M^{act}\}$.

In other words, the total SEDF of the tissue is now given by

$$\Psi = (1 - d_{0,E})\Psi_E + (1 - d_{0,C})\Psi_C + (1 - d_{0,M^{pass}})\Psi_M^{pass} + (1 - d_{0,M^{act}})\Psi_M^{act}. \quad (3.91)$$

For the purposes of the model, it is only necessary to have a damage criterion for VSMCs, but it would be straight-forward to extend the framework to accommodate criteria for all the damage variables.

A strain-based damage criterion is used. In a first implementation, the aim was to parallel the mathematical model presented in Chapter 2 as complete failure when cell stretch $\lambda_M = 1.8$. However, implementing a sudden step increase of $d_{0,M^{act}}$ from 0 to 1 gave numerical problems and convergence was never obtained. The criterion was therefore changed to the following: it is assumed that there is a level of strain $\lambda_{M,d}^{min}$ (with $I_{4M,d}^{min} = (\lambda_{M,d}^{min})^2$), called *minimum damage threshold*, at which damage would begin to occur. The amount of damage added at each time step would be dependent on the deviation of the cell stretch from the minimum damage threshold. If the cell continued to be in overextension, damage would increase at every time step. It is ensured that $d_{0,M}$ never exceeds one.

Algorithmically, this translates to the following:

$$\begin{aligned}
&\text{IF } I_{4M} \geq I_{4M,d}^{min} \text{ THEN} \\
&\quad d_{0,M} = d_{0,M} + \alpha_d(I_{4M} - I_{4M,d}^{min}) \\
&\text{END IF} \\
&\text{IF } d_{0,M} \geq 1 \text{ THEN} \\
&\quad d_{0,M} = 1 \\
&\text{END IF}
\end{aligned} \quad (3.92)$$

where $I_{4M} = (\lambda_M)^2$.

The damage variables are hard-coded into the model and for each constituent they are defined as a $l \times n$ matrix, with l being the number of nodes and n the number of elements. The material parameters used in this simulation are reported in Table 3.3.

The damage criterion is implemented as a user macro in a dedicated "user macros"

Parameter	Value
h	0.29mm
d	2.9mm
h/r	1/5
λ_z	1.2
k_E	$93kPa$
k_C	$5800kPa$
k_M^{pass}	$45.1kPa$
k_M^{act}	$11kPa$
$\phi_{\mathbf{a_0}}$	$\frac{\pi}{4}$
$\phi_{\mathbf{g_0}}$	$-\frac{\pi}{4}$
λ_M^{ATT}	1.15
$\lambda_C^{ATT,min}$	0.85
$\lambda_C^{ATT,mod}$	0.95
$\lambda_C^{ATT,max}$	1.05
$I_{4M,d}^{min}$	1.7
α_d	$\frac{1}{100}$

Table 3.3: Table of relevant model parameters for verification of damage model.

file and is called by the user from the input file through a four-letter code word. The implementation is similar to the remodelling routines described in previous Sections of this Chapter.

3.4.3 Verification

The model is divided into four phases:

- Phase 1 (time steps: $0 - 50$): **Loading**
  Pressurisation and axial pre-stretching of unloaded cylinder;
- Phase 2 (time steps: $51 - 500$): **Health**
  Remodelling of collagen and VSMCs towards homeostatic stretch;
- Phase 3 (time steps: $501 - 1000$): **Constriction**
  Increase of VSMC active response resulting in cylinder diameter reduction;
- Phase 4 (time steps: $1000 - 1500$): **Damage**
  Gradual application of additional internal pressure up to $12kPa$.

Phases 1 and 2 are analogous to what has been implemented in the previous verification cases. Phase 3 is implemented by pre-multiplying the active stress response of VSMC by a factor k_A:

$$\sigma_M^{act} = k_A \; c_v \; k_M^{act} \; \lambda_M \; \left[1 - \left(\frac{\lambda_M^{mean} - \lambda_M}{\lambda_M^{mean} - \lambda_M^{min}}\right)\right]. \tag{3.93}$$

which is initially set to 1, thus $k_A = 1$ at $t = 0$. At the beginning of phase 3, k_A is prescribed to increase by the following law:

$$\frac{\partial k_A}{\partial t} = k_A^{max} - k_A, \tag{3.94}$$

where k_A^{max} is a parameter regulating the maximum increase in active stress and thus the maximum diameter reduction this increase achieves. For this simulation this value has been chosen as $k_A^{max} = 5$.

In phase 4 an additional internal pressure is applied to the luminal layer of the vessel wall. In FEAP this is done through command "NEWForce" which allows the prescription of an increase in internal pressure as a percentage of the initially prescribed value. For this simulation a percentage of 75% was selected as this was the maximum possible value before numerical convergence problems would arise. Given that the initial internal pressure was prescribed as 16kPa, this results in a total additional pressure of 12kPa.

Figure 3.15 shows the evolution of the geometry across Phases 2, 3 and 4. From the physiological configuration (first row, end of Phase 2) the increase in active stress causes a constriction of the artery (second row, end of Phase 3). After the application of additional internal pressure, the arterial geometry is dilated (third row, end of Phase 4).

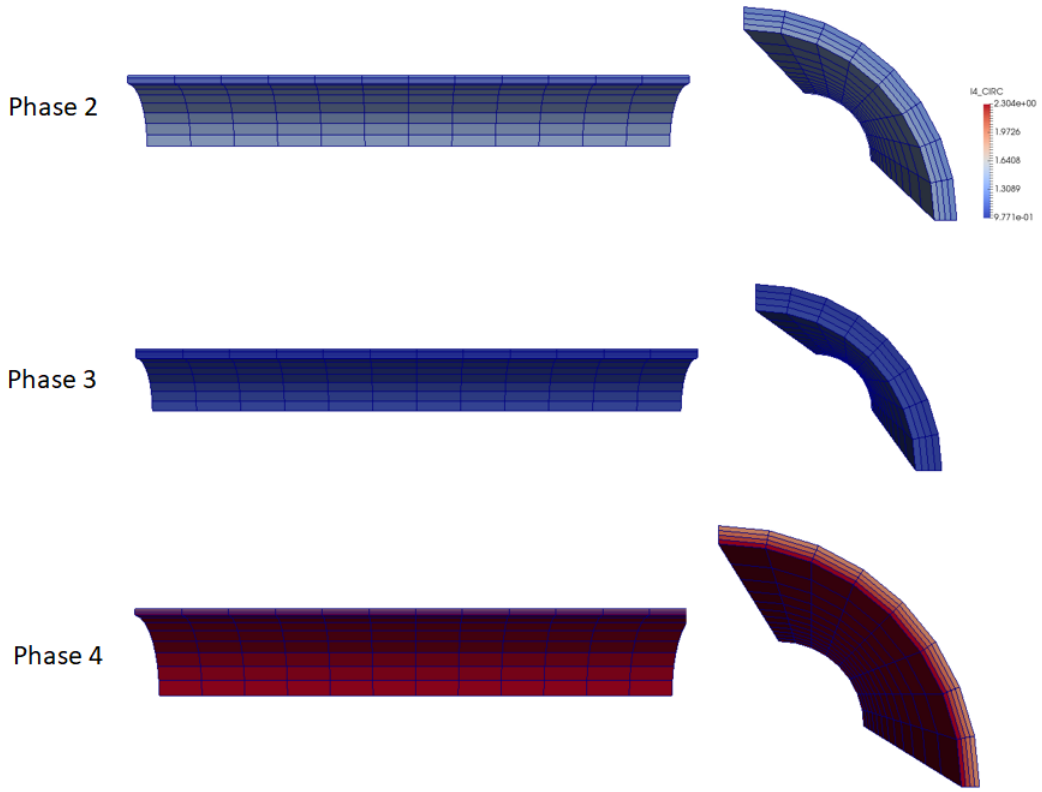

Figure 3.15: Evolution of the arterial geometry across Phases 2, 3 and 4 of the simulation. From the physiological configuration (Phase 2) the increase in active stress causes a constriction of the artery (Phase 3) and finally an additional internal pressure is applied with dilates the geometry (Phase 4).

In Figure 3.16 it is possible to observe the behaviour of λ_M and λ_M^R over the first three phases of the simulation. Similarly to what has been presented in Section 3.3.6, the remodelling mechanism aims at maintaining the cell stretch equal to its attachment value and the recruitment stretch adapts to the evolving geometry accordingly.

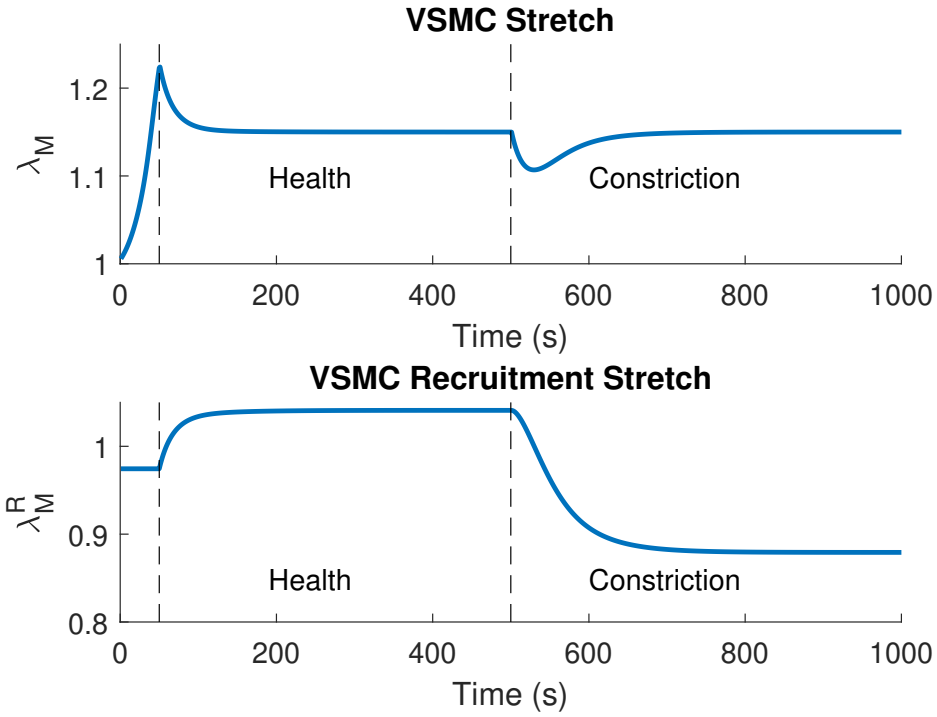

Figure 3.16: Evolution of VSMC cell and attachment stretch during Phases 1, 2 and 3 of the simulation. The remodelling mechanism aims at maintaining the cell stretch equal to its attachment value and the recruitment stretch evolves with the changing geometry in order to attain $\lambda_M = \lambda_M^{ATT}$.

In this simulation it is obtained that damage initiates at $t = 1516$, corresponding to an additional internal pressure of 6.192kPa and all layers are damaged at $t = 1864$, corresponding to an additional internal pressure of 10.368kPa. Figure 3.17 reports four significative time points of the simulation from damage initiation until all layes are completely damaged ($d_{0,M_i=1},\ \forall i = 1, 2, 3, 4$). In the left column the evolution of the damage variable $d_{M,0}$ is reported, while in the right column the VSMC stretch λ_M is considered. The results are symmetric in the circumferential and axial direction and thus the focus is placed on the radial. It is immediate to notice the damage occurs in the luminal, innermost layer first: this is consistent with the intuition that the stress exerted by the internal pressure on the tissue decreases with increasing distance from the lumen and is thus highest on the innermost layer. The damage then propagates across the wall thickness towards the adventitial, outermost layer. Moreover, from a qualitative point of view, the damage appears to increase consistently with increasing VSMC stretch λ_M (right column).

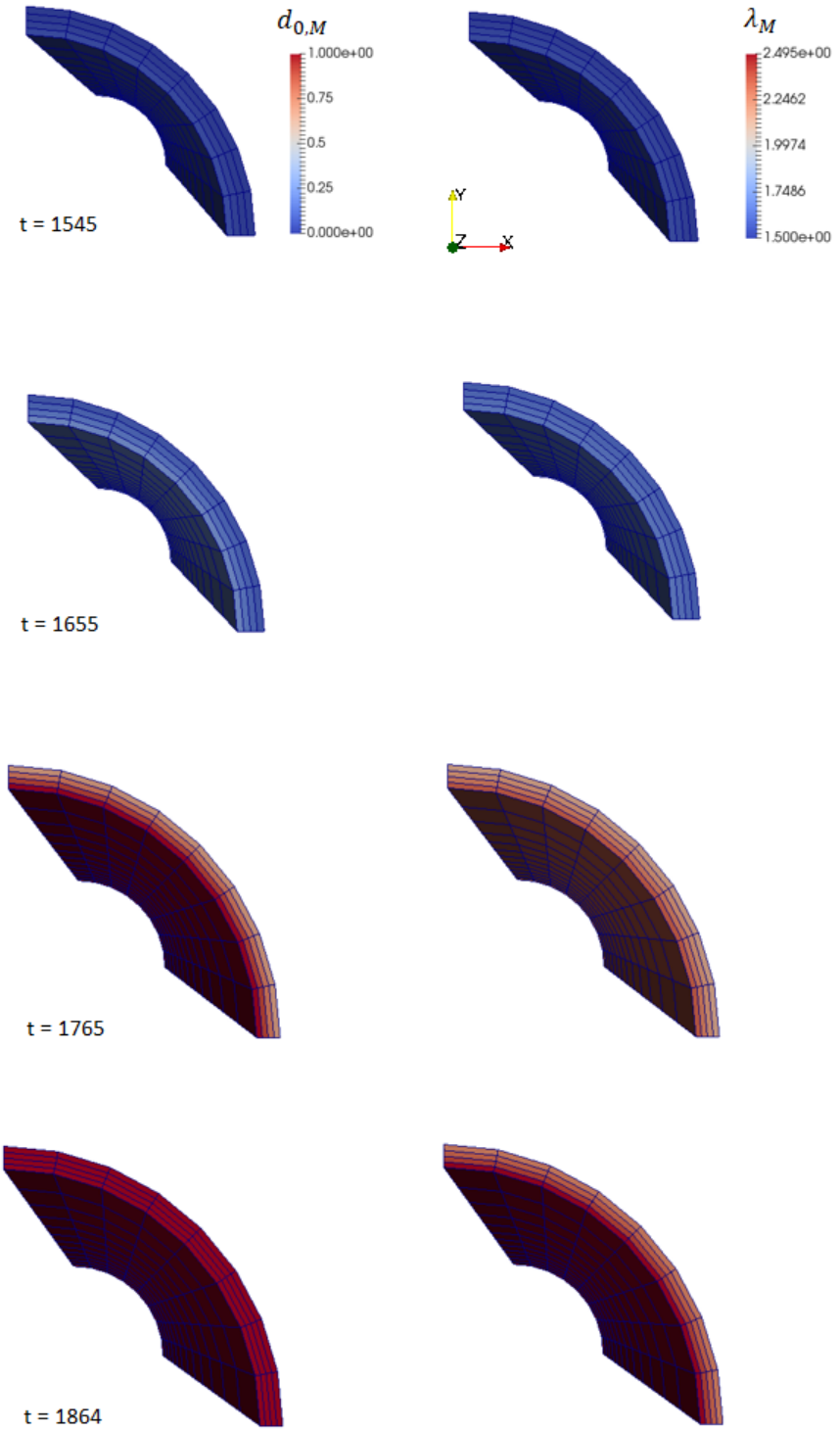

Figure 3.17: Damage variable $d_{M,0}$ and VSMC stretch λ_M at four meaningful time points of the simulation. Time point $t = 1545$ is the minimum time at which the second layer is damaged ($d_{0,M_2} > 0$) while the last time point, $t = 1865$ is the minimum time at which all layers are completely damaged ($d_{0,M_{i=1}}$, $\forall i = 1, 2, 3, 4$). Time points $t = 1655$ and $t = 1765$ are evenly spaced between the first and last to represent intermediate phases of the damage process.

In Table 3.4 the state of damage of the four layers is reported at significant time points: the time points considered are the minimum times at which wither $d_{0,M_i} > 0$ or $d_{0,M_i} = 1$ for some i.

Time	$\mathbf{d_{0,M_1}}$	$\mathbf{d_{0,M_2}}$	$\mathbf{d_{0,M_3}}$	$\mathbf{d_{0,M_4}}$
1516	0.000004	0	0	0
1546	0.003494	0.000005	0	0
1573	0.014726	0.002942	0.000001	0
1598	0.033267	0.012975	0.002627	0.000004
1815	1	0.88064	0.746887	0.633351
1831	1	1	0.884883	0.757252
1847	1	1	1	0.887759
1864	1	1	1	1

Table 3.4: Evolution of damage variables at representative time points for each of the four radial layers.

In Figure 3.18 the evolution of the damage variables for each of the four layers is plotted, where the layers are numbered from innermost ($i = 1$) to outermost ($i = 4$). The same damage variable are then plotted as a function of the tissue stretch in Figure 3.19. The two figures mentioned above report the evolution over the entire dilation phase, while in Figures 3.20 and 3.21 the plot is localised where the four variables range from their minimum value 0 to their maximum 1: the first shows how the damage variable evolves over time, while the latter shows it as a function of tissue stretch.

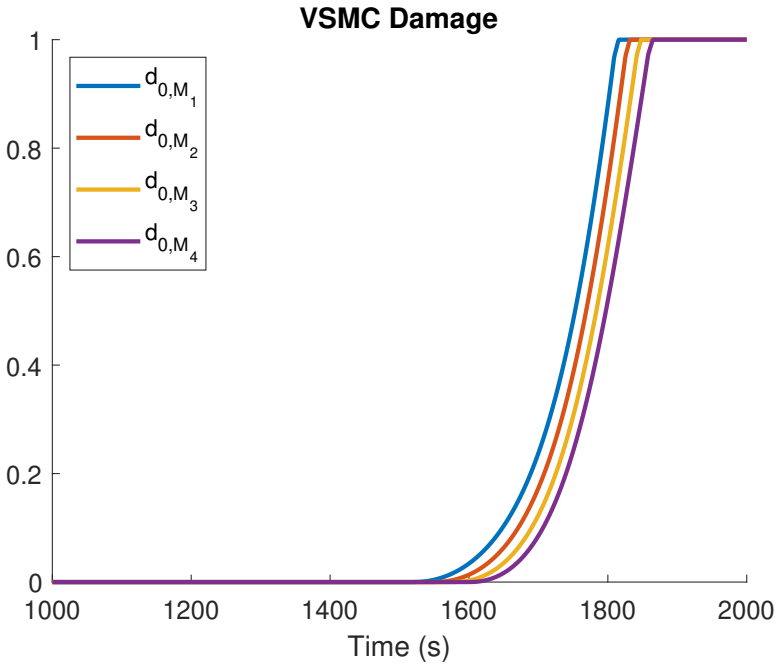

Figure 3.18: Evolution of the damage variables for each of the four cross-thickness layers over the entire dilation phase of the simulation.

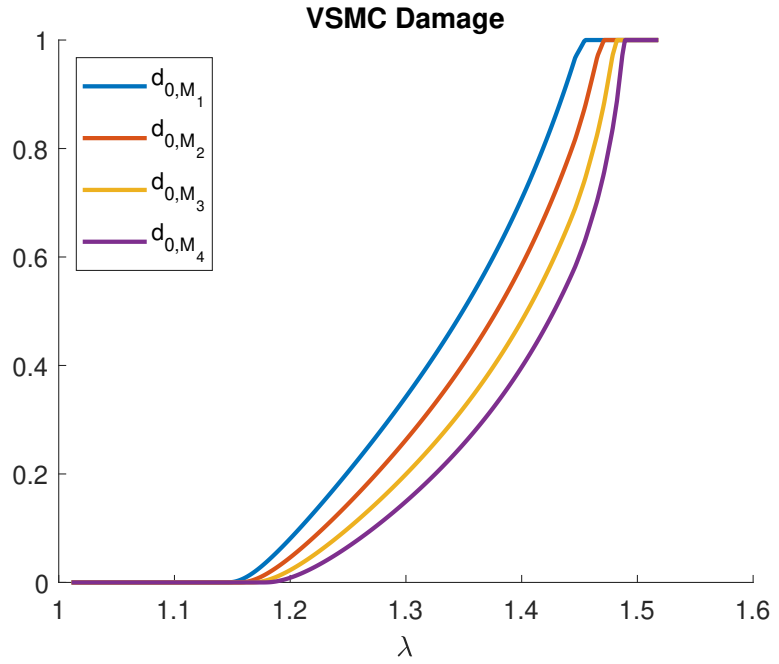

Figure 3.19: Damage variables as a function of tissue stretch for each of the four cross-thickness layers over the entire dilation phase of the simulation.

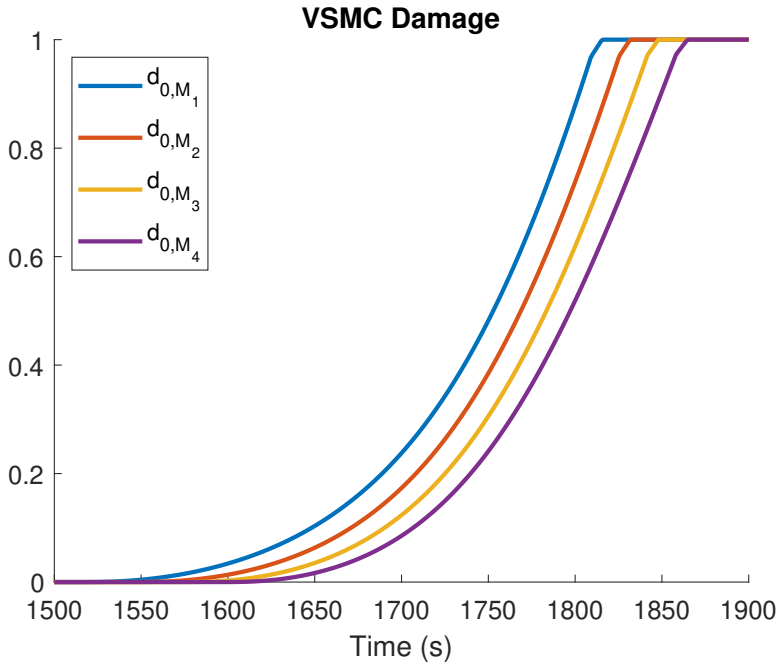

Figure 3.20: Evolution of the damage variables for each of the four cross-thickness layers over the local temporal range within which all variables increase from their minimum value 0 to their maximum 1.

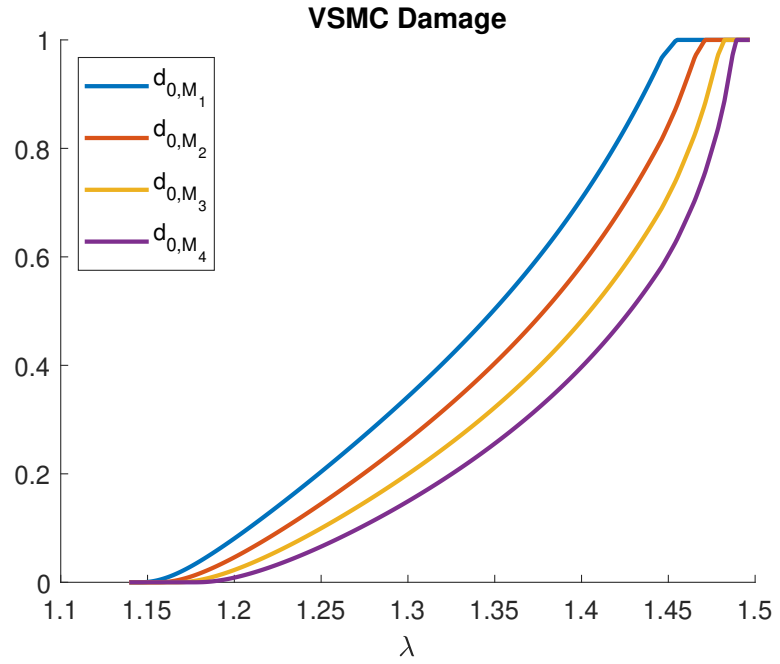

Figure 3.21: Damage variables as a function of tissue stretch for each of the four cross-thickness layers over the local temporal range within which all variables increase from their minimum value 0 to their maximum 1.

It is easy to notice how damage starts in the innermost layer first, then propagates across the other layers towards the outermost layer which is the last to be damaged. Figures 3.19 and 3.19 highlight how damage propagates faster through the outermost layer than in the innermost. This is due to the fact that, during damage of the outermost layer, there is more damage overall in the tissue than during damage of the innermost layer; moreover the overall tissue stretch is higher and therefore so is the VSMC stretch. Therefore the total active stress response of the tissue is lower and the expansion is faster: $I_{4M} - I^{min}_{4M,d}$ is higher and damage propagates faster in the outermost layer compared to the innermost.

Finally the criterion for correct implementation is verified, namely that damage propagation initiates if and only if $I_{4M} \geq I^{min}_{4M,d}$. To this end a plot of $d_{0,M}$ versus $I_{4M} - I^{min}_{4M,d}$ is shown (Figure 3.22): the damage criterion is correctly implemented since $d_{0,M} = 0$ as long as $I_{4M} - I^{min}_{4M,d} \leq 0$, $d_{0,M} > 0$ if and only if $I_{4M} - I^{min}_{4M,d} > 0$, and finally $d_{0,M}$ does not exceed 1.

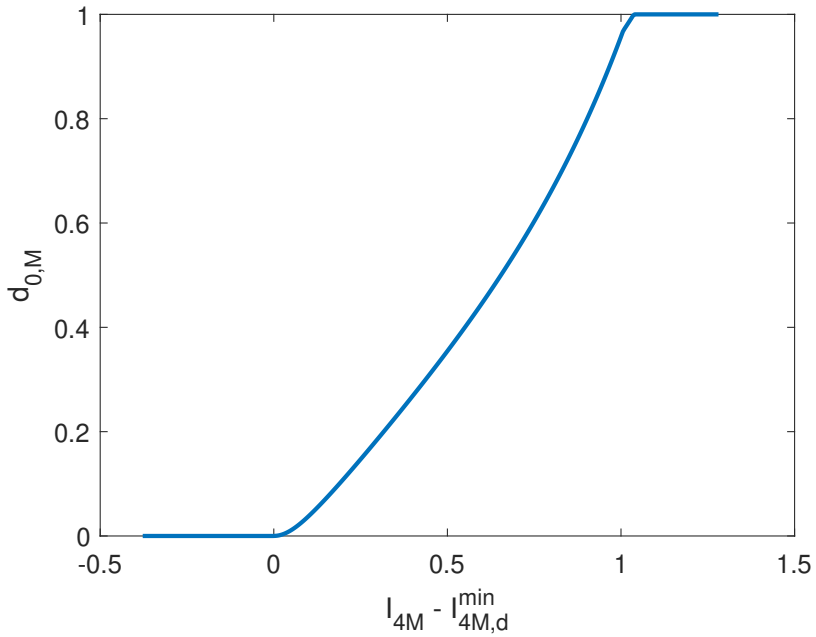

Figure 3.22: Damage variable $d_{0,M}$ vs $I_{4M} - I^{min}_{4M,d}$ for verification of correct implementation of damage criterion. The criterion is verified since $d_{0,M} = 0$ as long as $I_{4M} - I^{min}_{4M,d} \leq 0$, $d_{0,M} > 0$ if and only if $I_{4M} - I^{min}_{4M,d} > 0$, and finally $d_{0,M}$ does not exceed 1.

3.5 Conclusions and Discussion

The framework presented in this Chapter has wide scope of application, being able to model multi-layered, multi-material tissue with complete customisation of material properties and evolution laws. Although the initial framework has been mostly used to model the evolution of aneurysms, both cerebral (Mandaltsi (2016)) and abdominal aortic (Eriksson et al. (2014), Grytsan et al. (2017, 2015), Schmid et al. (2012), Watton et al. (2004), Watton, Ventikos & Holzapfel (2009)), and although the extensions presented here have focused on application to arterial tissue, the framework is easily adapted to model different soft tissues as well as several pathologies of said tissues. Heart, oesophagus, trachea and bladder among others would all be straight-forward applications of the model and examples of related disease that could be studied include oesophagea athresia, asthma and bladder outlet obstruction.

The constrained mixture model easily accommodates the addition or removal of relevant materials, each endowed with suitable material properties and constitutive model. It is possible to implement either isotropic or anisotropic volumetric growth with custom laws describing the volume changes. Growth and remodelling evolution laws are also fully customisable as they are written as finite difference equations in a dedicated macro scripts. The damage model has been implemented with different, independent variables for each material so that custom damage propagation equations can be used for each constitutive material.

The software allows for the integration of fluid dynamics into the model and thus there is potential to further extend the framework to couple the blood flow to the G&R laws thus obtaining a fluid-solid-interaction (FSI) model. The mesh is also read from standard input files and thus easily allows the use of patient-specific meshes.

A recommended refinement would be the inclusion of a bio-chemo-mechanical modelling framework such as that proposed by Aparìcio et al. (2016). The implementation would be straight-forward as it would consist of adding custom coupling equations to the macros master file that describe the feedback cycles between the signalling molecules and relevant model variables. The incorporation of a new molecular scale to the framework has great potential for the study of relationships between the mechanical properties and stimuli of the system and the signalling cascades governing the maintenance of the tissue structure and function. Care should be taken in selecting suitable variables and inter-dependencies however as computational complexity could increase rapidly with the introduction of several variables that interact in complex

ways.

Moreover this refinement would be highly model-specific as no structural change needs to be made to the framework and thus each individual model would implement its own chemo-mechanical feedback coupling model.

3.6 Conclusion

In this Chapter an extension of the finite element framework proposed by Watton, Ventikos & Holzapfel (2009) and extended by Eriksson et al. (2014) and Grytsan et al. (2017) has been described which includes

- a material model for vascular smooth muscle cells with both active and passive stress responses,
- a material model for collagen that includes a distribution of collagen stretches, and
- a model of damage to the individual constituents.

The framework resulting from this extension is a constrained mixture finite element model with microstructurally motivated material models, growth and remodelling, anisotropic volumetric growth, active stress response and damage. To the author's knowledge this is the most complete finite element framework currently available to model biological soft tissue diseases.

It has a wide scope of application and is easily customisable to a model's specific needs. Together with the coupling of the growth and remodelling to the haemodynamics and with the inclusion of complex bio-chemo-mechanical interaction laws, there is vast potential to apply this framework to the study of various soft tissue diseases and further their understanding.

This page has been intentionally left blank.

Chapter 4

Finite Element Model of Vasospasm

This Chapter presents a finite element model of cerebral vasospasm and treatment. The mathematical model developed in Chapter 2 and published in Bhogal et al. (2019) is integrated into the finite element framework developed by Eriksson, T. and Grytsan, A. (Eriksson et al. (2014), Grytsan et al. (2017, 2015)) which was extended in Chapter 3. The artery is modelled as a thick-walled cylinder subject to internal pressure and axial pre-stretch. A constrained mixture approach is adopted where the stress response of the tissue is given by the sum of the stress contributions of its microstructural constituents. The constriction of the healthy geometry is achieved by increase in the vasoactive tone of the vascular smooth muscle cells and their remodelling to maintain a homeostatic stretch. Mechanical treatment via stents is evaluated on the basis of a strain-based damage criterion applied to VSMCs.

4.1 Methods

The artery is modelled as a fibre-reinforced cylinder comprised of a contrained mixture of elastin, vascular smooth muscle cells and two families of collagen fibres. The geometry is internally pressurised to a pressure $p = 16kPa$, corresponding to physiological systolic blood pressure, and subject to an axial pre-stretch λ_z (see Table 4.1).

The strain energy density function of the whole tissue is the sum of the SEDFs of the individual constituents, i.e.

$$\Psi = \Psi_{\text{el}} + \Psi_{\text{col,a}_0} + \Psi_{\text{col,g}_0} + \Psi^{pass}_{VSMC} + \Psi^{act}_{VSMC}. \tag{4.1}$$

Two families of collagen fibres are considered with direction vectors $\mathbf{a_0}$ and $\mathbf{g_0}$ of the form $(\sin(\phi), \cos(\phi), 0)$ with $\phi_{\mathbf{a_0}} = \pi/4$ and $\phi_{\mathbf{g_0}} = -\pi/4$ (Table 4.1).

Regarding constitutive models, the material models previously described in this thesis are selected:

- **Elastin** is modelled as isotropic neo-Hookean material, as is standard from the literature (see eq. (3.56));
- **Collagen** fibre families are modelled with a distribution of recruitment stretches as described in Section 3.2.2;
- **VSMCs** are modelled with both a passive and active response as described in Section 3.3.2.

The following boundary conditions are applied to the cylinder:

- $u_x(x = 0) = 0$,
- $u_y(y = 0) = 0$,
- $u_z(z = 0) = 0$,
- $u_z(z = 0.0125) = 0.0025$,

where the former three conditions fix the boundary surfaces $x = 0$, $y = 0$ and $z = 0$, so that the geometry can be thought of as the symmetric eight of a $3cm$ cylinder. The latter condition enforces the axial pre-stretch of $\lambda_z = 1.2$.

Material parameters and other parameters relevant to the constitutive models of the constituents are reported in Table 4.1.

The development of vasospasm is modelled according to the same dynamics used in Chapter 2:

- the increase in vasoconstrictors and scavengers of vasodilators, result of a signalling cascaded initiated by the extravascular blood clot, causes an increase in the active tone of VSMCs;
- following this chemically-driven constriction, the smooth muscle cells remodel to return their level of stretch to its homeostatic value;
- elastin and collagen do not remodel.

The increase in the active stress response of VSMCs is achieved by pre-multiplication of their stress function by a parameter k_A, which is set equal to 1 in healthy conditions

Parameter	Value
h	0.29mm
d	2.9mm
h/r	1/5
p	$16kPa$
λ_z	1.2
k_E	$93kPa$
k_C	$5800kPa$
k_M^{pass}	$45.1kPa$
k_M^{act}	$11kPa$
$\phi_{\mathbf{a_0}}$	$\frac{\pi}{4}$
$\phi_{\mathbf{g_0}}$	$-\frac{\pi}{4}$
λ_M^{att}	1.15
$\lambda_C^{ATT,min}$	0.85
$\lambda_C^{ATT,mod}$	0.95
$\lambda_C^{ATT,max}$	1.05
k_A^{max}	11

Table 4.1: Table of relevant model parameters for finite element model of cerebral vasospasm.

and increases in vasospasm. It substantially serves the same role as parameter f_a in the model presented in Chapter 2. Parameter k_A is defined as a $(l \times n)$-matrix where l is the number of nodes and n the number of elements. Therefore the equation for the active stress response of VSMCs in the circumferential direction becomes:

$$\sigma_M^{act} = k_A \; c_v \; k_M^{act} \; \lambda_M \; \left[1 - \left(\frac{\lambda_M^{mean} - \lambda_M}{\lambda_M^{mean} - \lambda_M^{min}}\right)\right]. \tag{4.2}$$

In order to model constriction in only part of the artery, the increase in vasoactive tone is prescribed only in the central third of the geometry. Let z_{min} and z_{max} be the coordinates in the axial direction that delimit the central third of the cylinder. The following increase in tone is therefore prescribed for the nodes which satisfy $z_{min} \leq z \leq z_{max}$, where z is the node's axial coordinate:

$$\frac{\partial k_A}{\partial t} = k_A^{max} - k_A, \tag{4.3}$$

where k_A^{max} is the maximum increase in the active stress response. In this model k_A^{max} is set equal to 11 to achieve a peak constriction of 50% in the middle of the geometry.

In parallel to the increase in active stress, the evolution equations for remodelling of

VSMCs are run, which have been described in Section 3.3.3:

$$\frac{\partial \lambda_M^R}{\partial t} = \alpha_M \frac{\lambda_M - \lambda_M^{ATT}}{\lambda_M^{ATT}}, \tag{4.4}$$

with $\alpha_M = 2$.

Finally, in order to simulate treatment, an increase in the internal pressure is prescribed up to a maximum of $12kPa$. The implementation procedure has been described in Section 3.4.3. This additional pressure is applied equally to all elements, so it does not differentiate between the location of the spasm and the areas of physiological geometry.

In order to test whether this additional pressure would be sufficient to bring VSMCs to functional failure, which is the success criterion for an interventional device, the damage model that was implemented as described in Section 3.4 is used.

The model is divided into four phases:

- Phase 1 (time steps: $0 - 50$): **Loading**
  Internal pressurisation and axial pre-stretching of cylinder;
- Phase 2 (time steps: $51 - 500$): **Health**
  Remodelling of collagen and VSMCs towards homeostatic values of stretch;
- Phase 3 (time steps: $501 - 1000$): **Vasospasm**
  Development of vasospasm with vessel constriction;
- Phase 4 (time steps: $1001 - 2000$): **Treatment**
  Simulation of treatment via application of additional internal pressure.

4.2 Results

The model can be considered to consist of three parts: simulation of healthy arterial tissue ($t = 0$ to 500), the development of vasospasm (from $t = 500$ to $t = 1000$) and the modelling of treatment (from $t = 1000$ to $t = 2000$). In Section 4.2.1 the results regarding the development of vasospasm are discussed, while Section 4.2.2 is concerned with the results relating to treatment.

4.2.1 Vasospasm

In the first part of the simulation the arterial geometry is transformed from a healthy, physiological state to a constricted, vasospastic state with a degree of stenosis ranging from 43.95% to 51.01% across the vessel thickness. Figures 4.1 and 4.2 show the evolution of the geometry over time. The reference configuration ($t = 0$) is first pressurised and axially pre-stretched ($t = 50$), then remodelling routines are implemented so that each constituent achieves its attachment configuration thus realising a state of physiological homeostasis at $t = 500$. This is the configuration corresponding to a healthy artery in homeostasis. Finally an increase in the active tone of vascular smooth muscle cells in the central (axial) third of the geometry causes a local stenosis of the vessel until peak constriction is achieved at $t = 1000$.

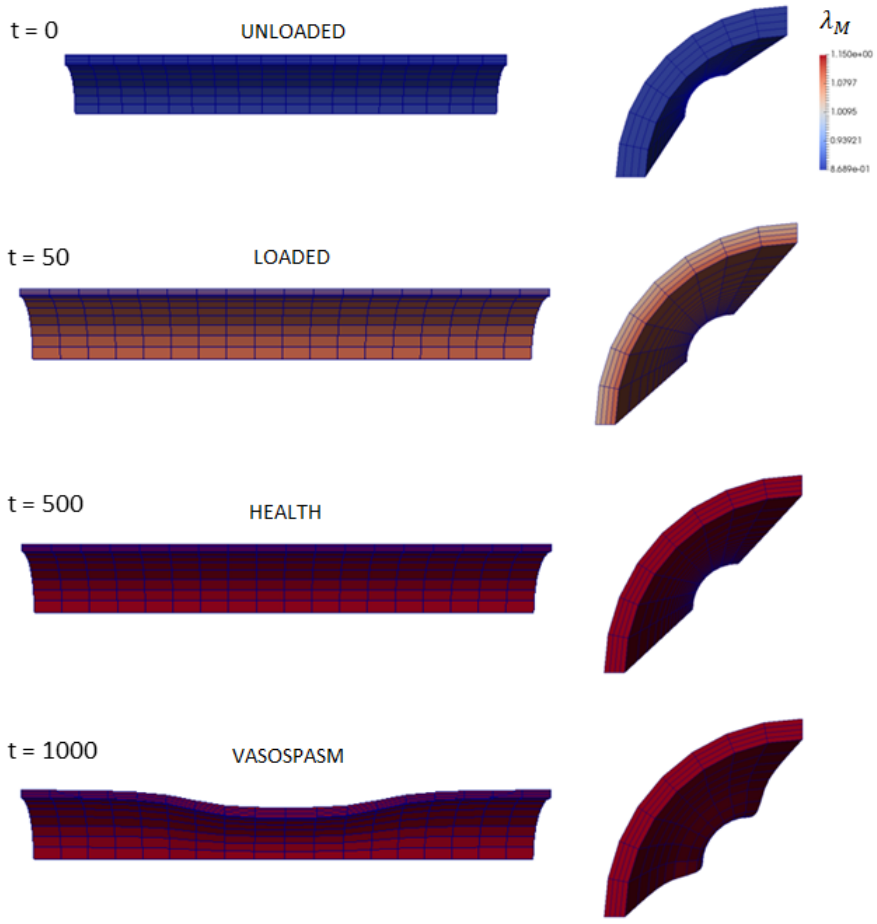

Figure 4.1: Evolution of VSMC stretch λ_M at four representative stages of the development of vasospasm in axial and radial view. At the peak of constriction, $t = 1000$, VSMC stretch equals its attachment value uniformly across the geometry.

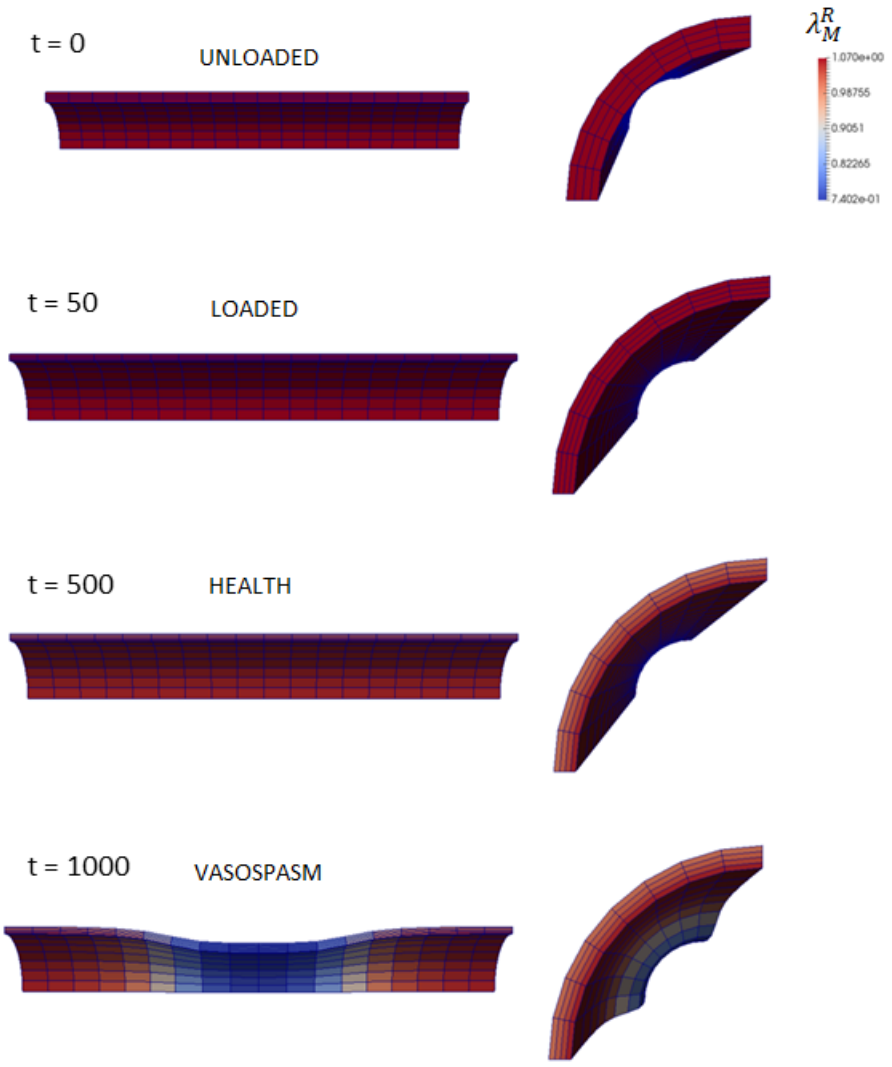

Figure 4.2: Evolution of VSMC recruitment stretch λ_M^R at four representative stages during the development of vasospasm in axial and radial view. In order to attain $\lambda_M = \lambda_M^{ATT}$ in the constricted geometry, the recruitment stretch must assume a distribution value with gradients in both the radial and axial direction.

Figures 4.1 and 4.2 also report the VSMC cell stretch λ_M and recruitment stretch λ_M^R to verify that remodelling is occurring correctly. Both variables are initialised as uniform throughout the entire geometry and thus both are uniform at $t = 0$. Following pressurisation and axial pre-stretch, where no remodelling occurs, VSMC stretch now varies across the wall thickness, since the internal pressure exerts a higher stress on the layers closer to the lumen, while the recruitment stretch has remained unchanged. Following remodelling of the recruitment stretch so that VSMC stretch equals its

attachment value, a uniform transmural strain field is realised at $t = 500$: this is the configuration corresponding to a healthy artery. In the third phase increase in the active stress response of VSMC occurs and remodelling of VSMC recruitment stretch: $t = 1000$ corresponds to the artery in vasospasm at peak constriction where the remodelling process is complete and VSMC stretch equals the attachment value throughout the entire geometry. It is worth noting how wide the range of VSMC recruitment stretch needs to be in order to accommodate homeostatic VSMC stretch through such a significant change in geometry. While in the healthy artery only a gradient in the radial direction was necessary, in vasospasm the recruitment stretch has attained a distribution of values with gradients across both the axial and radial directions. The addition of a gradient in the axial direction is indeed necessary to maintain the cell stretch in homeostasis when the geometry is no longer uniform in the axial direction.

The quantitative evolution of λ_M and λ_M^R is displayed in Figure 4.4 on a continuous-in-time scale. The values of cell and recruitment stretch are reported for four representative elements which are identified in Figure 4.3: one pair of elements is chosen from a section of the artery unaffected by constriction (identified by the letter h), while the other from the section where constriction is maximal (identified by acronym cvs). Each pair consists of an element on the innermost (luminal) layer (inn) and one on the outermost (adventitial) layer (out).

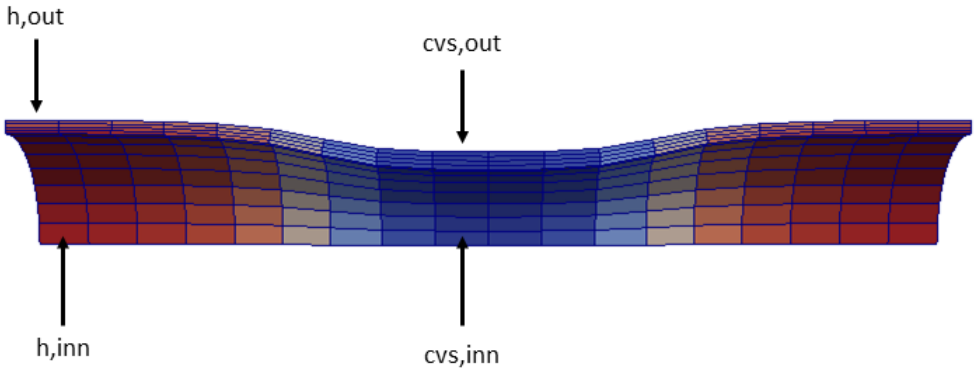

Figure 4.3: Identification of four representative locations on vessel geometry for interpretation of Figure 4.4.

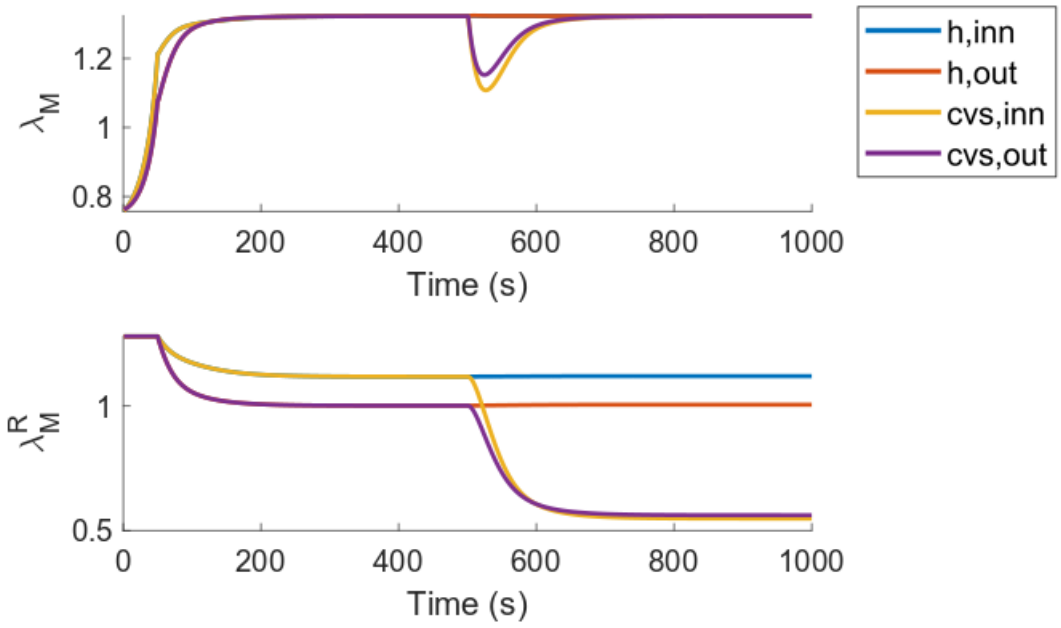

Figure 4.4: Evolution of VSMC cell and recruitment stretch in four representative locations of the artery during the development of vasospasm. Label h indicates a location unaffected by the constriction, while *cvs* indicates an area of maximum constriction. Label *inn* indicates the innermost layer of the artery, while *out* indicates the outermost.

Time steps $0 - 50$ corresponds to loading of the geometry: you can see how the cell stretch increases while the recruitment stretch remains constant, which is consistent with the progressive loading and lack of remodelling in this phase. Time steps $51 - 500$ correspond to remodelling of the VSMCs towards their homeostatic state of stretch: you can see the level of cell stretch is independent of both the axial and radial directions, while the recruitment stretch depends on the radial direction; this is due to the internal pressure requiring a different stress response from the luminal layer compared to the outermost layer. Finally, time steps $501 - 1000$ correspond to development of vasospasm. Looking at the evolution of λ_M, it is easy to see that the increase in vasoactive tone is the dominating factor at the inception of the disease and initially there is a significant deviation of the VSMCs from their attachment stretch. As remodelling "catches up" with the constricting geometry, cell stretches across all elements are gradually returned to their homeostatic value and the process is complete by time step 1000, though quite stable already at time step 700. Looking at the recruitment stretches λ_M^R, one can notice significant differences following vasospasm. There is still a gradient in the radial direction but the range of values it covers is wider

in health rather than in vasospasm, where the curves corresponding to the luminal and adventitial layer are much closer together than those corresponding to a healthy vessel. This is a consequence of the incompressibility of the material. Indeed in this finite element model the ends of the arterial segment are fixed. The constriction causes an increase in the surface of the vessel (if a line was drawn on the vessel surface along the axial direction, its length would increase following vasospasm due to the newly present concavity in the middle) and thus, in order to preserve volume, the thickness must be reduced. Since incompressibility is conserved per element, this results in the elements affected by vasospasm having smaller thickness than those corresponding to healthy tissue. Lower thickness implies smaller gradient in circumferential stretch and this results in a smaller gradient between recruitment stretches in the radial direction in the arterial segment affected by the disease.

The most significant difference is however in the axial direction, i.e. with dependence on the level of vasoconstriction. The recruitment stretch indeed needs to adapt to the new geometry and, the more pronounced the constriction, the wider the deviation is of the recruitment stretch from its physiological value.

Finally in Figure 4.6 the distribution of recruitment stretch λ_M^R is shown in four representative locations across along the longitudinal direction of the artery, between healthy and maximally constricted, at the peak of the disease ($t = 1000$) (see Figure 4.5 to identify locations). In the left column the distribution is shown on a global value scale, while in the right column it is shown on a local scale in order to highlight the magnitude of the gradient across the vessel thickness. In the first row the section of the artery corresponds to the region of maximum constriction and each subsequent row corresponds to a shift of two elements along the axial direction towards the edge of the artery; the fourth row corresponds to the edge layer in the axial direction.

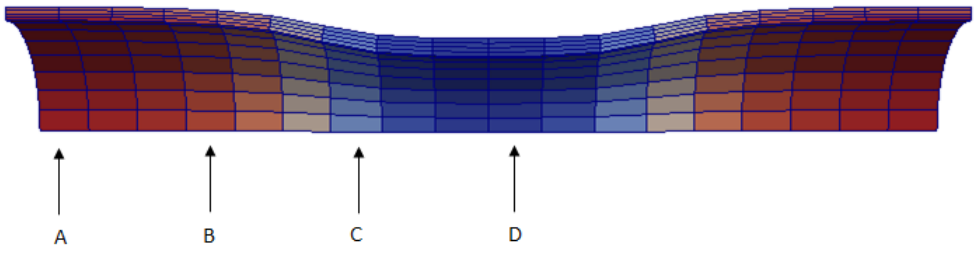

Figure 4.5: Four representative locations for the distribution of recruitment stretch shown in Figure 4.6.

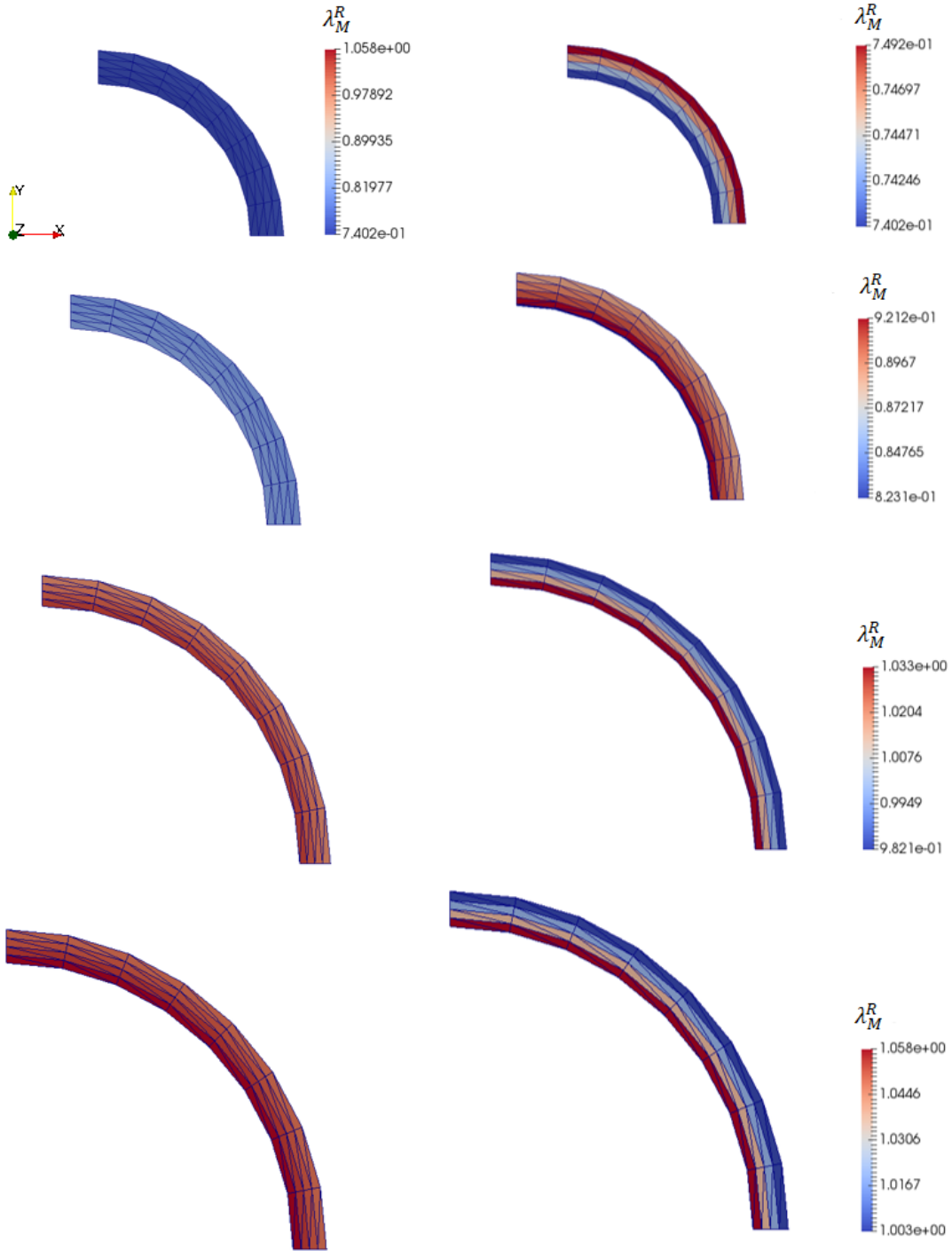

Figure 4.6: Transmural distribution of VSMC recruitment stretch in four representative locations across along the longitudinal direction of the artery, between healthy and maximally constricted, at the peak of the disease ($t = 1000$)

It is worth noting here that in order to obtain the same level of constriction the active

stress response of vascular smooth muscle cells had to be increased by a factor of 11 while in the one-dimensional model it had been increased by at most 1.75. A key difference that partially explains this stark difference is that in the $1D$ model the passive response was increased as well, whereas in this finite element model only the active stress response is increased. A future study is warranted where both models adopt the same mechanisms of increase in active and/or passive response to more precisely study if and how the thick-wall model affects the degree of increase in stress responses necessary to model vasospasm.

4.2.2 Treatment

The second part of the simulation is concerned with modelling treatment of vasospasm via the use of a stent retriever. This is modelled by the application of an additional internal pressure to the luminal layer, which is gradually increased from 0 to $12kPa$.

The evolution of the damage variables $d_{0,M}$ is shown in Figure 4.8 where each subplot corresponds to one of the four radial layers and each line corresponds to a slice in the longitudinal direction as shown in Figure 4.7: z_1 corresponds to the edge of the artery in the axial direction (e.g. $z = 0$) and each subsequent index corresponds to a shift of two elements towards the middle of the artery; z_5 corresponds to the area of peak constriction.

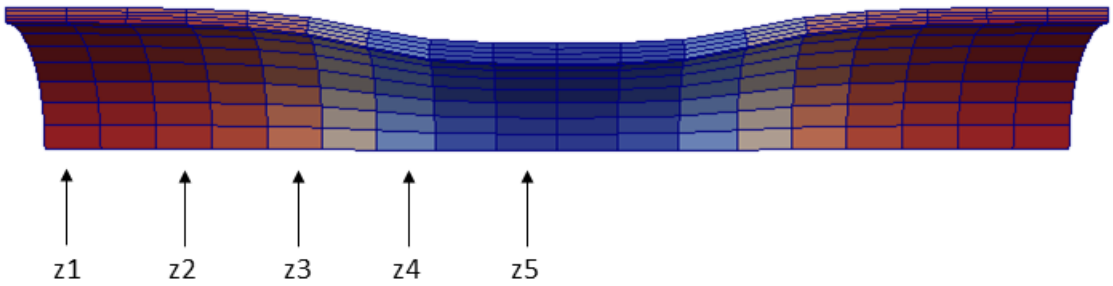

Figure 4.7: Visualisation of the locations of elements $z1, , z5$ in the arterial geometry as used in Figure 4.8

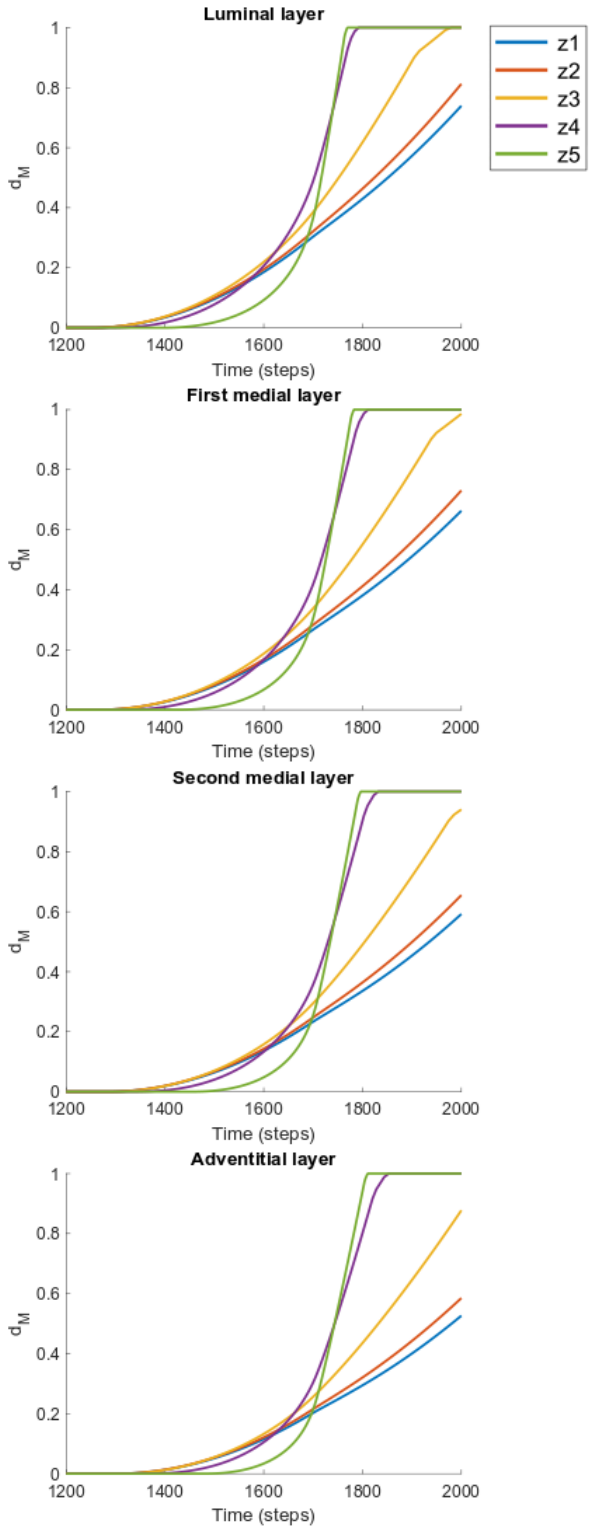

Figure 4.8: Evolution of damage variables during treatment of vasospasm.

It is of interest to focus on the area of peak constriction to study the propagation of damage and its relationship with the corresponding amount of additional internal pressure applied. Moments of interest are either times at which damage is initiated, i.e. $\min_t d_{0,M}(t) > 0$, or times at which complete functional failure is achieved, i.e. $\min_t d_{0,M}(t) = 1$. Table 4.2 reports these values, together with the corresponding levels of additional pressure and values of the damage variables for the section of the artery characterised by maximum constriction. These values are extracted from the data set plotted in Fig. 4.8. In order to identify the four transmural elements of the arterial section the following abbreviations are adopted: lum identifies the luminal layer, $me1$ the first medial layer, $me2$ the second medial layer and adv the adventitial layer; finally p_{add} is used to indicate the amount of additional internal pressure in kPa applied at that moment on the luminal layer.

Time	$\mathbf{p_{add}}$	$\mathbf{d_{0,M_{lum}}}$	$\mathbf{d_{0,M_{me1}}}$	$\mathbf{d_{0,M_{me2}}}$	$\mathbf{d_{0,M_{adv}}}$
1387	4.64	0.000001	0	0	0
1417	5.00	0.000713	0.000001	0	0
1445	5.34	0.003718	0.000582	0.000001	0
1470	5.64	0.008798	0.003006	0.000461	0.000001
1769	9.23	1	0.907848	0.797063	0.703572
1782	9.38	1	1	0.909878	0.805558
1796	9.55	1	1	1	0.916994
1810	9.72	1	1	1	1

Table 4.2: Evolution of damage variables at representative time points for each of the four radial layers.

The results reported in Table 4.2 highlight the relationship between the additional internal pressure and damage propagation. For an artery of physiological diameter $2.9mm$ at about 50% stenosis the prediction is that:

- $4.64kPa$ of additional pressure are necessary to initiate damage in the luminal layer,
- $5.64kPa$ are necessary to initiate damage in all layers,
- $9.23kPa$ to bring VSMCs in the luminal layer to $d_{0,M} = 1$, and
- $9.72kPa$ to bring VSMCs to functional failure across all layers.

Therefore initiating damage in the outermost layer compared to the innermost requires

an additional $1kPa$ of pressure whereas to reach functional failure in the outermost compared to the innermost layer requires an additional $0.49kPa$. With reference to Figure 2.10, which shows the amount of pressure exerted by four stent retrievers as a function of the diameter at which they're extended (or compressed), this difference would not influence the selection of an appropriate device: indeed the finite element model predicts that the only stent potentially capable of exerting the necessary amount of pressure is the Solitaire 6, which is the same prediction resulting from the $1D$ model. In the case of a smaller artery, however, where multiple stents could potentially be suitable, this difference in pressure requirement between the luminal and the adventitial layer might have greater influence in the selection of a suitable device, since even a $0.5kPa$ difference could determine the success or lack thereof of a specific stent retriever. It is therefore recommended that the finite element simulation be run for arteries of different physiological diameter for a more direct comparison with the one-dimensional model.

When considering the magnitude of pressure necessary to reach functional failure of VSMCs, this result is comparable to that obtained in the one-dimensional model presented in Chapter 2: for an artery of $2.9mm$ at about 50% stenosis the $1D$ model predicted that an additional pressure of about $7.5kPa$ was necessary to reach the dilatation threshold, while the finite element model presented here predicts that a pressure between 9 and $10kPa$ is necessary. These results can be considered consistent since a direct comparison of numerical values is not entirely appropriate: indeed the $1D$ model considers the experimental measurements of the outward pressure applied by the stents and the fact that this pressure is higher when the stent is "compressed" just before deployment and gradually decreases as the stent expands; on the contrary the finite element implementation of this model uses an *increasing* internal pressure which is less accurate in representing the behaviour of a stent. As a consequence, the $1D$ model predicts an additional pressure of $7.5kPa$ *at* the dilatation threshold, but the stent must have been able to apply higher pressures before reaching that threshold or it would not have been able to dilate the artery up until that level of stretch.

4.3 Discussion

The objective of the model of cerebral vasospasm presented in this Chapter is to explore whether the membrane assumption adopted in the one-dimensional model presented in Chapter 2 is suitable or whether the non-uniformity of the strain field

across the thickness of the arterial wall leads to a significantly different prediction in the magnitude of pressure necessary to treat the disease. In order to address this question the model presented in Chapter 2 has been integrated into the finite element framework discussed in Chapter 3 to obtain a constrained mixture finite element model of cerebral vasospasm and treatment which, to the author's knowledge, is the only one of its kind.

In the case of a middle cerebral artery of physiological diameter $2.9mm$ at about 50% stenosis we find that the difference in the amount of pressure required to damage the adventitial layer compared to the luminal is about $0.5kPa$. When considering the chronic outward force profiles of four commonly available stent retrievers (Figure 2.10), the same ones used in Chapter 2, this difference would not influence the selection of the most appropriate for the specific case as the differences between them are around 10 or $20kPa$. In particular in this case only one stent is predicted to be potentially successful, i.e. the Solitaire 6. However it is possible that in arteries of smaller physiological diameter, where it becomes increasingly important to not apply excessive pressure, this same difference could indicate a better stent selection among similar choices and a difference of $0.5kPa$ could have a more significant impact on the potential damage incurred by other constituents of the wall. Moreover, as new stents are designed with the specific goal of treating vasospasm (as opposed to the current situation in which the stents used to treat vasospasm had been designed to retrieve blood clots), it may be beneficial to have more accurate predictions on the amount of additional pressure required for treatment. It is therefore recommended that a wider selection of cases is made to apply this model to in order to obtain a broader set of results to be compared with the $1D$ model. In particular, arteries of different physiological diameters should be considered, for which predictions from the one-dimensional model are still available.

It is worth noting that direct numerical comparisons between the two models are not entirely appropriate as two key differences have a significant impact of the numerical results: the mode of application of the additional internal pressure and the damage criterion.

The one-dimensional model presented in Chapter 2 allows for the direct use of the pressure profiles of the stents which are validated by experimental measurements. A key property of these profiles is that, as the stent expands, the amount of pressure they apply decreases with a functional form similar to a negative exponential. On the contrary, in the finite element model the additional internal pressure is gradually

increased from $0kPa$ to a maximum of $12kPa$ in a linear fashion resulting in the pressure increasing as the arterial wall expands, which is the opposite behaviour of the stents.

The damage criterion has also been needed to be adapted to the finite element framework: the damage criterion employed in the $1D$ model is "instantaneous" and the VSMC active response jumps from positive to null in a step-wise fashion. This criterion was initially implemented in the framework for direct comparison with the membrane model but convergence problems arose which could not be fixed by other means (such as use of a finer mesh) and thus the instantaneous damage model was abandoned. A gradually increasing damage model was adopted where it was assumed that there exists a stretch-based threshold at which damage of the VSMCs initiates and further propagates at a rate proportional to the difference between the current cell stretch and the threshold (see (3.92)). This minimum damage threshold is different from the one used in the one-dimensional model. The step-wise criterion was that a vascular smooth muscle cell would be completely damaged when $\lambda_M = 1.8$. In the finite element model it is assumed that damage initiates at $I_{4M} = 1.7$, which corresponds to a cell stretch of about $\lambda_M \sim 1.3$, while the cell stretch at which complete damage occurs varies depending on the distance from the area of peak constriction: where the constriction is maximal complete damage occurs at a cell stretch of $\lambda_M \sim 1.89$ while halfway between the area of peak constriction and the edge of the artery it corresponds to a cell stretch of $\lambda_M \sim 1.45$. This is consistent with the different damage propagation profiles in five different positions along the axial direction shown in Figure 4.8.

A comparative analysis between the two models should therefore take these aspects into account and consider a margin of error in the numerical values obtained by the models. A study on the influence of various model parameters on the final predictions is also warranted. In the next Section recommendations for future work are discussed, including numerical methods that would allow a more consistent alignment of the two models and thus a more thorough analysis of the effect or lack thereof of the transmural strain gradient on the predictions of pressure requirements and thus on the selection of a treatment device.

The model presented in this Chapter still shows that much lower pressures than balloon angioplasty are sufficient for the treatment of vasospasm, at least in selected cases, and thus warrants further study.

4.3.1 Comparison with one-dimensional model

Three key differences between the one-dimensional and the finite element model presented in this dissertation hinder the validity of a direct comparison between the respective predictions:

1. Mechanism for increase of VSMC stress response,
2. Representation of the additional pressure exerted by the stent,
3. Damage criterion.

In the one-dimensional model both the passive and the active stress responses of VSMCs are increased and a parameter study is run on the relationship between the two factors f_a and f_p (Chapter 2, Section 2.3.3). This results by the active response requiring an increase of up to 1.75 and the passive factor up to 1.55. In the finite element model only the active response of VSMCs is increased and the value of the multiplicative factor that achieves a comparable level of stenosis is $k_a = 11$. The implementation in the finite element model corresponds in the $1D$ model to the special case of the parameter study in which $f_p = 1$, which resulted in $f_a = 1.75$: this means that the introduction of a thick-walled representation of the wall compared to a membrane idealisation results in a 6.3-fold increase in the factor that regulates the increase in active VSMC stress. This is an important difference and it is worth exploring whether the introduction of an increase of the passive response in the finite element model alongside the increase of the active response affects these increase factors and, if so, how these differences eventually translate in the stent pressure predictions.

Another limitation of the finite element model is the modality of simulation of the additional pressure exerted by the stent. When cerebral vasospasm is treated via stent retrievers, the stent is inserted in a compressed state inside the lumen and, following deployment, it expands towards its stress-free configuration which is a larger diameter than that at which it is inserted. As shown by the experimental measurements reported in Chapter 2 Section 2.3, the pressure exerted by the stent decreases rapidly as it expands then slowly tapers towards 0 as it nears its stress-free configuration. While this is represented in the one-dimensional model, in the finite element model the additional pressure exerted by the stent is modelled as linearly increasing, which is the opposite behaviour to that presented by the stent. This is less straight-forward to address but a possible solution method could be the use of a custom surface mesh, ideally placed only on the section of the artery affected by vasospasm, to which either

force or displacement conditions can be applied that result in the mesh simulating the pressure profile applied by the stent to the inner wall.

Finally a damage criterion should be selected that can be consistently applied to both models. Since the implementation of the step-wise criterion has been unsuccessful in the finite element framework, it is recommended that the criterion is changed in the one-dimensional model to one that is continuous in the cell stretch. A parameter study should also be carried out in both models on the influence of the stretch-based damage threshold $I_{4M,d}^{min}$ and the damage propagation rate α_d on the final stent pressure predictions. Indeed the choice implemented in this model is that damage is initiated at $\lambda_M \sim 1.3$ which could be argued to be too small since the attachment stretch of VSMCs is assumed to be $\lambda_M^{ATT} = 1.15$. Moreover, while complete damage is assumed to occur at $\lambda_M = 1.8$ in the $1D$ model, in the finite element model it is observed to occur at values as low as $\lambda_M = 1.45$ but also at $\lambda_M = 1.9$ depending on the local level of constriction and on the radial distance from the lumen. In absence of experimental data, it is recommended that a parameter space spanning values for both $I_{4M,d}^{min}$ and α_d is explored and that a study on the level of cell stretch at which complete damage occurs is carried out.

4.3.2 Future Directions

The most immediate recommendation for improving the current model is to implement the three key changes outlined in the previous Section. A great limitation in selecting parameters and evolution laws to address those limitations is the current scarcity of experimental data on the growth and remodelling of vascular smooth muscle cells in vasospasm as well as their mechanical and failure properties. For example the hypothesis that both the active and passive response of VSMCs are increased during vasospasm is that the increase of vasoconstrictors and scavengers of vasodilators causes the cells to contract more (increase in active response); in response to this sustained state of contraction, remodelling of their cytoskeleton and/or focal adhesion occurs affecting their material properties including increasing their stiffness (increase in passive response). This hypothesis is based on observed behaviour of these cells in circumstances other than vasospasm and is therefore reasonable but complex behaviour of these cells has been observed in this disease (see Chapter 1, Section 1.2) and it would be highly desirable to obtain more precise information on their remodelling in this disease.

The damage criterion is another aspect of the model that requires a biologically-

informed foundation. Not only would it be difficult to establish a “reasonable" parameter space for the criterion implemented in this model, but the functional form of the criterion itself can be discussed. Indeed the criterion implemented in this model has been selected according to the hypothesis that functional failure of the smooth muscle cells is due to either their detachment from the extracellular matrix or the breakage of the stress fibers composing their cytoskeleton. However either failure mechanisms could be more suitable: for example it is possible that cell damage occurs by delamination and the damage propagation law should therefore reflect that behaviour. More precise information on the failure mechanics of VSMCs is a key aspect of the model that needs experimental data for proper validation.

It is crucial that in the future the adopted damage criterion is corroborated by experimental measurements. A possible initial experiment could consist of progressively stretching individual cells along their preferred direction (recognisable due to their “spindle" shape) in order to identify both the mode of failure of the cell and the magnitude of deformation required. A more desirable experiment would be to excise an intracranial arterial segment *ex vivo* and, after fixing the two ends, applying an internal pressure with either a balloon or a stent, to study what kind and amount of damage a specified magnitude of pressure causes. The use of stents would more directly provide information on their performance on arterial tissue, while the use of a balloon would have the advantage of greater control on the amount of pressure applied.

Another aspect of VSMC mechanobiology that has a significant effect on the model is the remodelling rate: indeed in this model it is assumed that VSMCs have returned to their homeostatic state of stretch at the time of treatment whereas this might not be the case. The state of stretch of the cell at the moment of treatment would be a key factor in the predicted magnitude of pressure and thus more experimental data is warranted on this topic.

In general it is necessary to have more precisely biologically-informed laws for the sophistication of this model towards one that is suitable for clinical application. As long as experimental data is not available, the most thorough approach would be to select evolution laws that most closely resemble real-world behaviour to the modeller’s knowledge and to run parameter studies on the variables deemed most influential on the model results on suitably selected parameter spaces.

After the limitations of the model discussed so far are addressed, a few sophistications

of the mathematical and computational aspects of the model are recommended.

The third main assumption on the pathophysiology of vasospasm made in both the one-dimensional and the finite element model is that no collagen remodelling occurs during disease progression and thus no damage is necessary to this constituent. As discussed in Chapter 2 it is worth exploring how the stent pressure predictions change if this hypothesis is no longer satisfied. This is addressed in Chapter 5 where a study on the remodelling of the collagen stretch distribution is carried out.

The material model for collagen also warrants a further sophistication, namely the inclusion of a dispersion model, i.e. a distribution of fibre orientations in the wall.

An immediate model extension that could be explored is the inclusion of anisotropic volumetric growth since this is already present in the framework. Indeed Eriksson et al. (2014), Grytsan et al. (2017) have reported significant differences in the evolution of the considered geometries when different modes of volumetric growth, isotropic in Eriksson et al. (2014) and anisotropic in Grytsan et al. (2017), were adopted. This is therefore another sophistication highly worth exploring since it might affect what is required in terms of VSMC remodelling in order to achieve the same level of constriction in presence compared to in absence of volumetric growth.

In order to make the model more realistic and more suitable for clinical use, it is worth improving on the idealisation of the stent treatment as an increase in internal pressure. It would be more realistic if the stent geometry was represented since the mesh density and material properties might affect the application of pressure on the arterial wall and in particular the propagation of cell damage across the wall thickness (Geith et al. (2020)).

Finally it would be ideal to move towards model personalisation and abandon the perfectly cylindrical geometry in favour of a patient-specific mesh. Indeed arteries usually display irregular surfaces and it might be insufficient to consider the degree of stenosis and the physiological diameter of the affected artery as the only inputs for the selection of a treatment device. Instead the patient-specific geometry of the vasospastic section of arterial tissue must be taken into consideration. Indeed an irregular geometry might lead to irregular damage patterns on the vasospastic area and result in ineffective treatment.

4.4 Conclusion

The mathematical model described in Chapter 2 has been integrated into the finite element framework described in Chapter 3 with the objective of studying the effect of the thick-walled assumption on the stent pressure predictions compared to the membrane assumption. To the author's knowledge this is the only finite element model of cerebral vasospasm to date. Consistently with the membrane model, it is based on a constrained mixture formulation with microstructurally motivated material models and based on the key hypotheses that vessel constriction is driven by vascular smooth muscle cell remodelling towards a homeostatic level of stretch and that the condition for successful treatment is functional disruption of VSMCs.

Although direct comparisons with the membrane model are not entirely appropriate due to two key differences in the model formulations and implementations, it is suggested that the use of a thick-walled finite element model would provide more precise predictions for the magnitude of pressure necessary for an interventional device to resolve the disease. In order to achieve clinical application, however, more sophistications are required which are discussed in the previous Section and experimental validation is warranted to inform properties and remodelling processes for both VSMCs and collagen.

Implementation of these sophistications would represent crucial steps in the formulation of a constrained mixture finite element model with patient-specific geometry and parametrisation that could be a useful aid to the clinician in the selection of the most suitable treatment method and device for a patient-specific case.

This page has been intentionally left blank.

Chapter 5

Study on Collagen Remodelling in Vasospasm

The model presented in Chapter 2 is extended to study the role of collagen growth and remodelling in vasospasm and its potential effect on treatment requirements. The fibre population is divided into *mature* and *immature* collagen where the distinction is made according to whether the fibre was produced respectively before or after subarachnoid haemorrhage. The material model of collagen includes a distribution of fibre stretches and it is assumed that remodelling of this constituent consists of changes in the shape and position of this distribution. Two studies are carried out: one in which growth occurs but no remodelling, and other other in which the opposite takes place.

5.1 Motivation

In this Chapter an extension is formulated to the 1D model of cerebral vasospasm developed in Chapter 2 Bhogal et al. (2019) where the hypothesis that no collagen remodelling or growth/atrophy occurs is relaxed. The assumption was made because the halflife of collagen (~ 70 days) is longer than the time a vasospastic vessel takes to reach peak constriction ($\sim 7-10$ days), which is usually also the time neurological symptoms emerge and the disease is treated. However it is possible that even partial remodelling affects the effectiveness of stent-retrievers as a treatment strategy and thus it is important to investigate if and how this may occur.

Moreover, experimental evidence of increased collagen deposition has been reported in animal models of vasospasm (Hughes & Schianchi (1978), Kapp et al. (1985), Kasuya

et al. (1993), Mayberg et al. (1990), Nagasawa et al. (1982), Smith et al. (1985), Yamaguchi-Okada et al. (2005)). Three of these studies are animal models that only report qualitative observations drawn from imaging of the tissue samples (Kapp et al. (1985), Mayberg et al. (1990), Nagasawa et al. (1982)). Only two of these studies are on human samples. Hughes & Schianchi (1978) conducted a retrospective review of 20 autopsies for SAH which revealed an increase in collagen concentration and a marked difference in the morphology of the tissue samples starting about 3 weeks after the time of haeomrrhage. After this time, the increase in collagen content was more evident. Smith et al. (1985) reported a histological study of human tissue where arterial specimens from three patients who had suffered SAH were studied and the morphology compared to angiograms taken only a few days prior. The samples were stained for Type V collagen and a significant increase in the mass of this constituent was observed in two cases out of three. Three studies looked explicitely at the time dependence of the disease. In Kasuya et al. (1993) an increase in procollagen type I and III, as well as in the collagen-promoting molecule TGF-β was observed: the concentration of procollagen type I was highest on day 7 and had diminished by day 14, while the concentration of procollagen type III had increased by day 7 and maintained the same level on day 14; TGF-β, which is known to promote collagen deposition by vascular cells, reached its highest concentration on day 3 and then gradually diminished. In Mayberg et al. (1990) a qualitative increase in collagen was observed in TEM images of a porcine model of MCA vasospasm starting at 14 days after SAH. Yamaguchi-Okada et al. (2005) is to the author's knowledge the only quantitative study on collagen content in cerebral vasospasm. The study is a canine model and the authors reported increases of collagen concentration compared to control of $12 \pm 42\%$ at day 7, $43 \pm 29\%$ at day 14, $-2 \pm 28\%$ at day 21 and $-28 \pm 18\%$ at day 28 after SAH.

However, evidence of increased collagen deposition in models of vasospasm is not consistent. For example, Macdonald et al. (1992) did not observe any increase in collagen at any point during vasospasm, using both semi-quantitative (immunofluorescence microscopy) and quantitative (amino acid analysis) methods. Furthermore, they used different antibodies for collagen type I, III, IV and V and reported no increase in any type, which is in direct contradiction to the findings of Kasuya et al. (1993) and Smith et al. (1985).

In absence of definitive evidence of collagen growth and remodelling in vasospasm and with limited literature on the remodelling processes of collagen fibres in general,

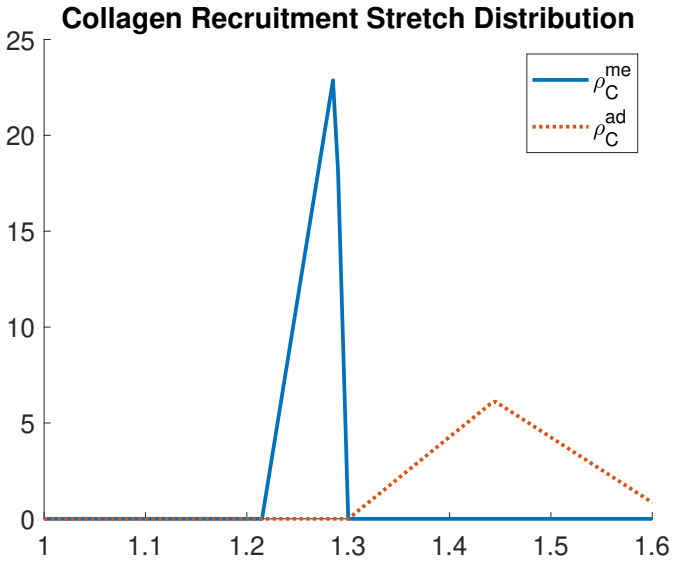

Figure 5.1: Recruitment stretch distributions for medial and adventitial collagen in healthy conditions. Physiological tissue stretch is $\lambda = 1.3$: since the entire distribution of recruitment stretches for medial collagen is to the left of this value, all medial fibres have been recruited to load bearing and thus make a positive contribution to the stress response of the artery; on the contrary, the distribution of recruitment stretches for adventitial collagen is to the right of this value, signifying that fibres have not yet been recruited to load bearing and their contribution to the vessel's stress response is null.

a simple theoretical model is formulated to explore preliminary hypotheses on these mechanisms in the context of cerebral vasospasm.

5.2 Methods: 1D model

In the model developed in Chapter 2 a constitutive model for collagen was adopted that accounts for the observed distribution of levels of waviness (Aparìcio et al. (2016), Cheng et al. (2017)). A distinction was made between medial and adventitial collagen and separate distributions were assigned to each population: $\rho^R_{C,me}$ and $\rho^R_{C,ad}$ for medial and adventitial collagen respectively. In healthy conditions, where the physiological tissue stretch at systole is $\lambda = 1.3$, the former is load-bearing while the latter plays a protective role and is only recruited to bear load at supraphysiological levels of tissue stretch (Fig. 5.1).

In this model extension a distinction is introduced between **mature** and **immature** collagen. The two populations of collagen fibres are then defined as follows:

- **mature** collagen is defined as the fibre population present in the vessel wall at the time of SAH;

- **immature** collagen is the fibre population produced at any time after SAH (where the time of the considered model is 4 weeks and it is assumed that the maturation time for collagen is the same).

Immature collagen is thus produced in pathological conditions, due to the development of vasospasm, and is the fibre population that will have the most relevant effect on the treatment. In the following, it is assumed that SAH occurs at $t = 0$.

As reported in Ryan & Humphrey (1999), the halflife of collagen has been observed to range between 15 and 70 days, where the shorter values correspond to pathological chemo-mechanical conditions. Since vasospasm presents such a pathological environment to the cells, it is assumed that medial collagen degrades exponentially with a halflife of 15 days.

$$m_C^{me}(t) = e^{-\alpha_C^{me} t}, \tag{5.1}$$

with $\alpha_C^{me} = 0.462$, which is obtained by imposing $m_C^{me}(15) = \frac{1}{2} m_C^{me}(0)$, i.e. that the mass density is halved at $t = 15$ days. For simplicity, it is assumed that no mass change occurs in adventitial collagen since this would have no effect on the effectiveness of vasospasm treatment. For the same reason remodelling of mature collagen, both medial and adventitial, is also neglected, while focus is placed on the growth and remodelling of the newly produced immature collagen.

There are two key quantities that greatly affect the stress response of collagen: its mass and its maximum attachment stretch. More broadly, the entire stretch distribution of the fibres should be considered, but for simplicity it will be assumed that the width and skew of the distribution remains constant. Therefore, once the maximum attachment stretch is known, so is the entire distribution. As a preliminary theoretical study, the two variables, mass and maximum attachment stretch, are considered separately and two independent studies are conducted:

- **Study A**: (growth, no remodelling) where immature collagen is attached with a fixed maximum attachment stretch, and thus fixed distribution, while mass increases;

- **Study B**: (remodelling after growth) where immature collagen is deposited instantaneously at $t = 0$, and remodelling gradually occurs afterwards.

5.2.1 Study A: Growth without Remodelling

In this study it is assumed that the distribution of immature collagen stretches is fixed with

$$\lambda_{C,i}^{ATT,max} = 1.05. \tag{5.2}$$

This value is chosen because VSMCs, which become the primary load bearer in vasospasm, are assumed to aim to transfer part of the load to the newly produced collagen without risking overloading the fibres, for which damage is known to occur at $\lambda_C = 1.1$. Assuming that the distribution has the same width and skew as that of mature collagen in healthy conditions, it follows that:

$$\lambda_{C,i}^{ATT,mod} = 0.95, \tag{5.3}$$
$$\lambda_{C,i}^{ATT,min} = 0.85. \tag{5.4}$$

As far as mass growth is concerned, a linear increase will be assumed for this variable, according to equation (5.5):

$$m_C^i(t) = m_{C,i}^{max} \frac{t}{\tau_{gr}}, \tag{5.5}$$

and consider a range of values for the variables $m_{C,i}^{max}$ and τ_{gr}, which signify the maximum mass of immature collagen deposited in the vasospastic vessel and the number of days after which the mass of immature collagen reaches said maximum value.

With reference to the study by Yamaguchi-Okada et al. (2005), the range for $m_{C,i}^{max}$ is assumed to be $0.2 \leq m_{C,i}^{max} \leq 0.7$ and is spanned at an interval of 0.1. With regards to the collagen deposition speed τ_{gr}, a discrete set of values is considered: $3, 7, 10, 14, 21$ and 28 days. In other words,

$$m_{C,i}^{max} \in \{0.2, 0.3, 0.4, 0.5, 0.6, 0.7\}, \tag{5.6}$$
$$\tau_{gr} \in \{3, 7, 10, 14, 21, 28\}. \tag{5.7}$$

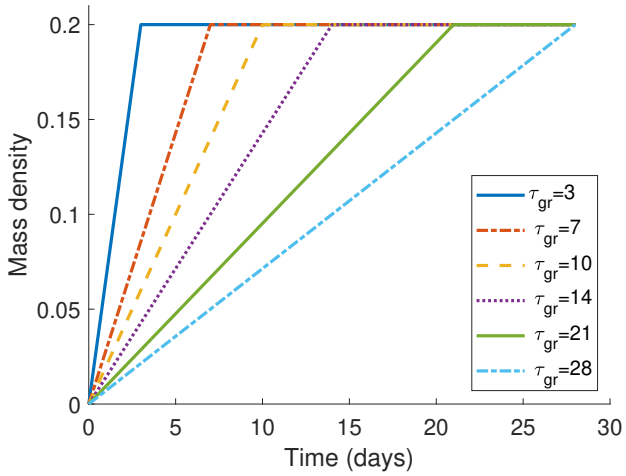

Figure 5.2: Evolution of the mass density of immature collagen in a subset of cases for Study A: $m_{C,i}^{max}$ is held constant and equal to 0.2 while τ_{gr} takes on all values considered in the study.

All possible pairings of the values for the two variables are considered giving a total of 36 cases.

The evolution of the mass density of immature collagen over time is plotted for two subsets of cases: in Fig. 5.2 $m_{C,i}^{max} = 0.2$ is constant and τ_{gr} varies through all its possible values, while in Fig. 5.3 $\tau_{gr} = 14$ is constant and $m_{C,i}^{max}$ varies through all its possible values.

5.2.2 Study B: Remodelling after Growth

In this study it is assumed that all immature collagen fibres are secreted instantaneously at time $t = 0$ (Sang et al. (2020)). Vascular cells then attach the secreted fibres to the matrix in progressively load bearing configurations and thus remodelling occurs.

With regards to mass growth, in this study the mass of immature collagen is assumed to be

$$m_C^i = 0.43, \qquad \forall t > 0, \tag{5.8}$$

where the value is taken from the quantitative estimation reported in Yamaguchi-Okada et al. (2005).

The target maximum attachment stretch for the remodelling process is assumed to be $\lambda_{C,i}^{ATT,max} = 1.05$. For simplicity, the stretch distribution maintains fixed width and skew, thus only shifting (translating) along the $x-$axis. The modal and minimum stretches are therefore obtained by subtracting the half-width and width of the

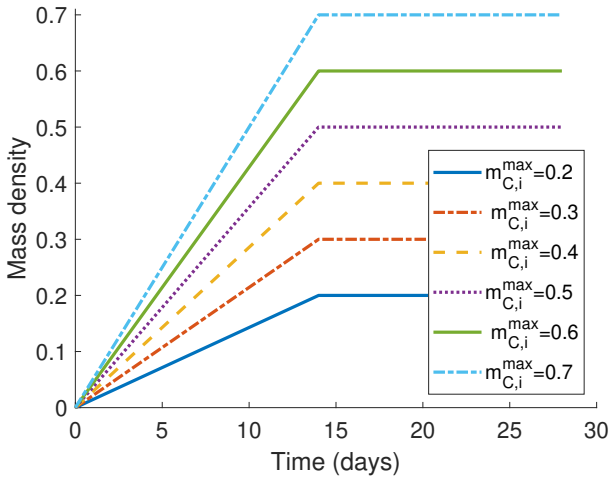

Figure 5.3: Evolution of the mass density of immature collagen in a subset of cases for Study A: τ_{gr} is held constant and equal to 14 while $m_{C,i}^{max}$ takes on all values considered in the study.

distribution respectively from the maximum stretch.

Similarly to study A, a linear increase of the fibre stretches is prescribed over time:

$$\lambda_{C,i}^{max}(t) = \lambda_{C,i}^{max}(0) + \left(\lambda_{C,i}^{ATT,max} - \lambda_{C,i}^{max}(0)\right) \frac{t}{\tau_{rem}}, \tag{5.9}$$

A range of values for the variables $\lambda_{C,i}^{max}(0)$ and τ_{rem} is considered, where the former is the level of stretch at which a new fibre is secreted from the cell and the latter is the number of days at which the maximum attachment stretch of the distribution reaches the value $\lambda_{C,i}^{ATT,max} = 1.05$, thus stabilising the remodelling process. As a lower bound for the variable $\lambda_{C,i}^{max}(0)$, 0.5 is chosen, which is the closest approximation to one decimal place for the maximum stretch of mature medial collagen when the artery is at 50% stenosis, i.e. $\lambda_{C,me}^{max}(0) = 0.525$. As an upper bound 1.0 is selected, since any value higher than that would be very close to a collagen fibre immediately deposited and attached at maximum target stretch, which is the case of Study A. As far as the remodelling speed is concerned, the same range of values for τ_{rem} is used as for τ_{gr} in Study A. Therefore:

$$\lambda_{C,i}^{max}(0) \in \{0.5, 0.6, 0.7, 0.8, 0.9, 1.0\}, \tag{5.10}$$

$$\tau_{rem} \in \{3, 7, 10, 14, 21, 28\}. \tag{5.11}$$

All possible pairings of the values for the two variables are explored and thus a total of 36 cases.

In Figures 5.4 and 5.5 the evolution of the stretch distribution of immature collagen over time is shown: Fig. 5.4 refers to the case where $\lambda_{C,i}^{max}(0) = 0.5$ and $\tau_{rem} = 28$, while Fig. 5.5 refers to the case where $\lambda_{C,i}^{max}(0) - 0.7$ and again $\tau_{rem} = 28$. The distribution is plotted at time points $t = 0, 14$ and 28.

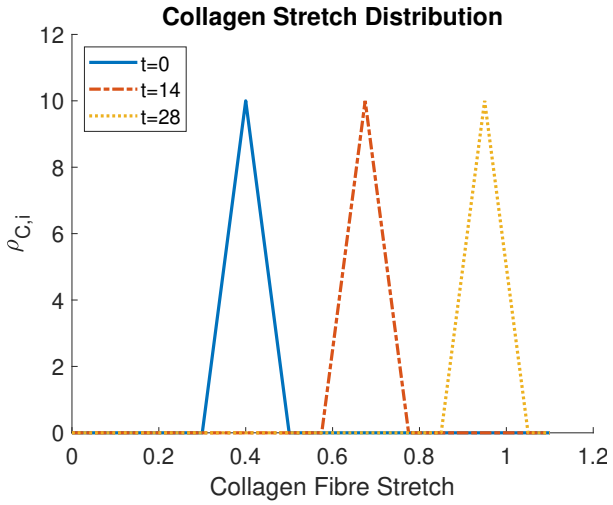

Figure 5.4: Evolution of stretch distribution of immature collagen for case $\lambda_{C,i}^{max}(0) = 0.5$ and $\tau_{rem} = 28$ of Study B. The distribution maintains fixed skew and width but shifts to the right from its initial point $\lambda_{C,i}^{max}(0) = 0.5$ to the final $\lambda_{C,i}^{max}(\tau_{rem}) = 1.05$.

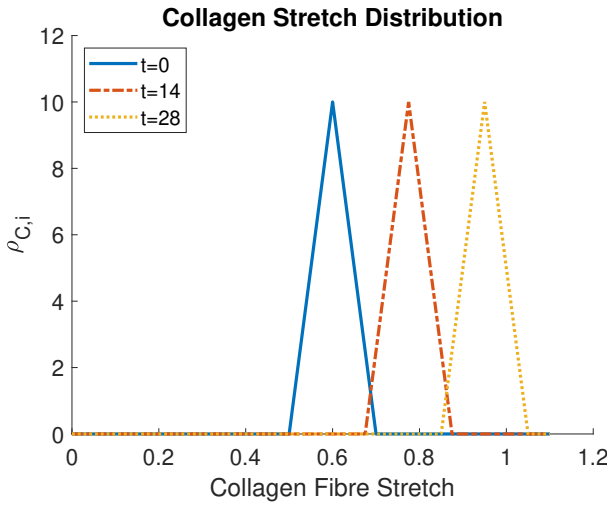

Figure 5.5: Evolution of stretch distribution of immature collagen for case $\lambda_{C,i}^{max}(0) = 0.7$ and $\tau_{rem} = 28$ of Study B. The distribution maintains fixed skew and width but shifts to the right from its initial point $\lambda_{C,i}^{max}(0) = 0.7$ to the final $\lambda_{C,i}^{max}(\tau_{rem}) = 1.05$.

Similarly to Study A, the evolution of the maximum attachment stretch is shown for two subsets of cases: in Fig. 5.6 $\lambda_{C,i}^{max}(0) = 0.5$ is fixed while τ_{rem} varies over all its possible values, while in Fig. 5.7 $\tau_{rem} = 14$ is constant while $\lambda_{C,i}^{max}(0)$ varies over all its possible values.

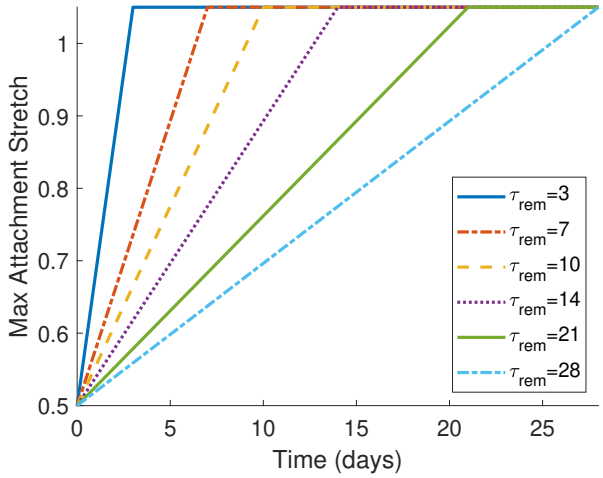

Figure 5.6: Evolution of the maximum attachment stretch of immature collagen for a fixed initial value of $\lambda_{C,i}^{max}(0) = 0.5$ and all possible values of τ_{rem}.

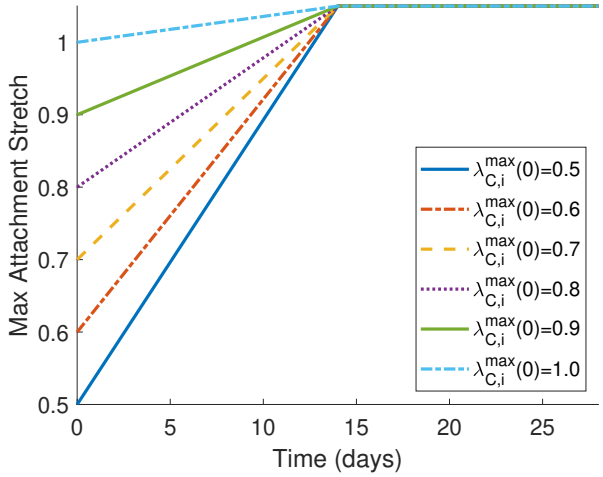

Figure 5.7: Evolution of the maximum attachment stretch of immature collagen for a fixed remodelling time of $\tau_{rem} = 14$ and all possible values of the initial stretch $\lambda_{C,i}^{max}(0)$.

5.3 Results

The results are reported for an artery of physiological diameter $2mm$ at a 50% level of stenosis. This level of stenosis was chosen for consistency with the model described in Chapter 2 and the specific arterial diameter since it provides the most interesting

results: with reference to the results from Chapter 2 it is obtained that at a larger diameter only one, if any, stent is successful and thus incorporation of collagen G&R would likely result in stents being unsuccessful in most if not all cases; conversely in smaller vessels the stents had a wider margin of success and collagen G&R would have likely not affected the results.

Similarly to what has been done in Chapter 2, it is possible to look at how the pressure-diameter curve changes from health to vasospasm. In Fig. 5.8 the curve for a healthy artery is shown.

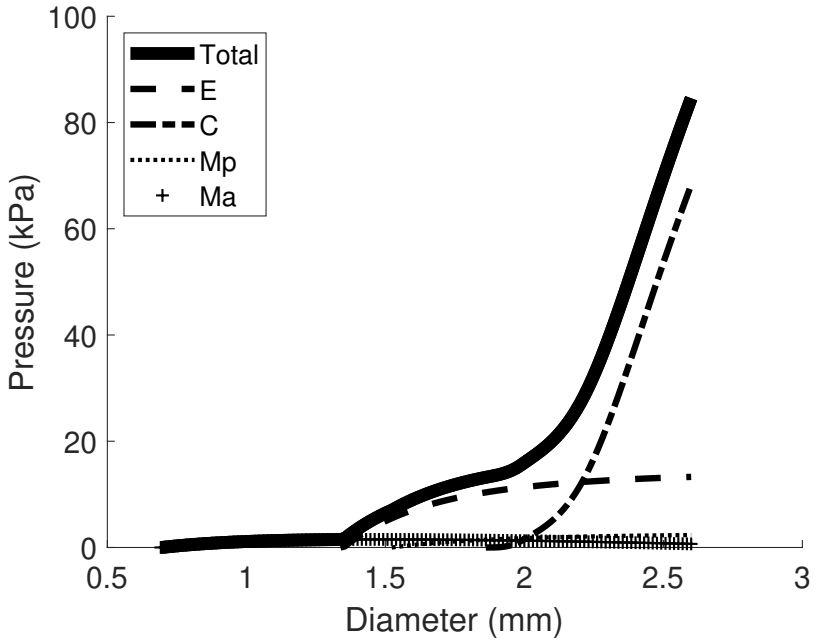

Figure 5.8: Pressure diameter curve for a healthy cerebral artery of physiological diameter $2mm$. The solid line represents the response of the whole tissue, while the non-solid curves illustrate the contribution of the individual constituents within the wall: E for elastin, C for collagen, Mp and Ma for the passive and active response of vascular smooth muscle cells respectively.

Recall the results for the case in which no collagen remodelling was hypothesised, i.e. in the model presented in Chapter 2. Figure 5.9 shows the pressure-diameter curve for the artery in vasospasm and the pressure curves that the stents exert while expanding within the vessel. One can see that both Solitaire 6 and Capture 3 are successful, with a generous margin of error, as well as Solitaire 4.

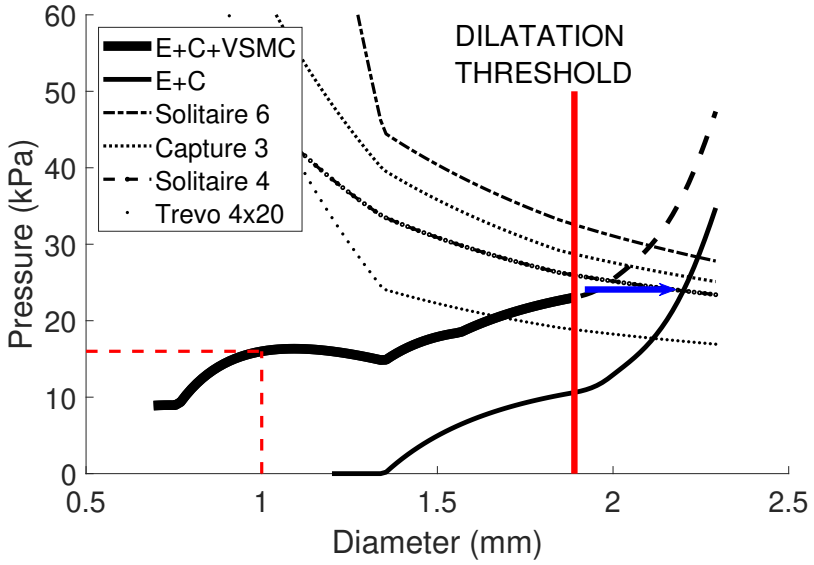

Figure 5.9: Effectiveness of four commonly available stent retrievers in treating a vasospastic artery of original physiological diameter $2mm$ and current 50% level of stenosis. A stent is successful if its related pressure curve remains above the thick solid curve up until the dilatation threshold. Stents Solitaire 6, Capture 3 and Solitaire 4 would be effective in treating the disease, while Trevo 4x20 would be unsuccessful.

5.3.1 Study A

For Study A, the pressure-diameter curve for a case of vasospasm with 50% stenosis is obtained for each possible pair of values $(m_{C,i}^{max}, \tau_{gr})$ and the effectiveness of commonly available stents is tested for treatment of the constriction. The two strongest stents out of the four considered in Chapter 3 are selected, i.e. Solitaire 6 and Capture 3mm, and last day at which the stent would be successful in damaging the VSMCs and thus resolving the spasm is recorded. The results are reported in Table 5.1 for the Solitaire 6 stent and in Table 5.2 for the Capture 3mm.

	$\tau_{gr} = 3$	$\tau_{gr} = 7$	$\tau_{gr} = 10$	$\tau_{gr} = 14$	$\tau_{gr} = 21$	$\tau_{gr} = 28$
$m_{C,i}^{max} = 0.2$	2	4	6	9	14	18
$m_{C,i}^{max} = 0.3$	1	3	4	6	9	12
$m_{C,i}^{max} = 0.4$	1	2	3	4	7	9
$m_{C,i}^{max} = 0.5$	0	1	2	3	5	7
$m_{C,i}^{max} = 0.6$	0	1	2	3	4	6
$m_{C,i}^{max} = 0.7$	0	0	1	2	4	5

Table 5.1: Clinical window in days after SAH for treating vasospasm in a $2mm$ artery at 50% stenosis using a Solitaire 6 stent.

	$\tau_{gr} = 3$	$\tau_{gr} = 7$	$\tau_{gr} = 10$	$\tau_{gr} = 14$	$\tau_{gr} = 21$	$\tau_{gr} = 28$
$m_{C,i}^{max} = 0.2$	1	3	4	6	9	12
$m_{C,i}^{max} = 0.3$	0	1	2	4	6	8
$m_{C,i}^{max} = 0.4$	0	1	2	3	4	6
$m_{C,i}^{max} = 0.5$	0	1	1	2	3	4
$m_{C,i}^{max} = 0.6$	0	0	1	2	3	4
$m_{C,i}^{max} = 0.7$	0	0	0	1	2	3

Table 5.2: Clinical window in days after SAH for treating vasospasm in a $2mm$ artery at 50% stenosis using a Capture 3 stent.

The pressure-diameter curves and stent pressure curves for four representative cases from this study are also presented in Figure 5.10

- A1: $m_{C,i}^{max} = 0.3,\ \tau_{gr} = 7,$
- A2: $m_{C,i}^{max} = 0.3,\ \tau_{gr} = 21,$
- A3: $m_{C,i}^{max} = 0.6,\ \tau_{gr} = 7,$
- A4: $m_{C,i}^{max} = 0.6,\ \tau_{gr} = 21.$

5.3.2 Study B

Similarly to study A, for each possible pair of values the pressure-diameter curve is obtained for the vessel at 50% stenosis and the effectiveness of two stents in resolving the constriction is compared. The clinical window for treatment in each case is reported, i.e. the last day after SAH at which the stent would be successful in resolving the disease: the results for the Solitaire 6 stent are reported in Table 5.3 and those for the Capture 3 stents in Table 5.4.

	$\tau_{gr} = 3$	$\tau_{gr} = 7$	$\tau_{gr} = 10$	$\tau_{gr} = 14$	$\tau_{gr} = 21$	$\tau_{gr} = 28$
$\lambda_{C,i}^{max}(0) = 0.5$	1	4	5	8	12	16
$\lambda_{C,i}^{max}(0) = 0.6$	1	3	4	6	10	13
$\lambda_{C,i}^{max}(0) = 0.7$	1	2	3	4	7	9
$\lambda_{C,i}^{max}(0) = 0.8$	0	0	0	1	1	2
$\lambda_{C,i}^{max}(0) = 0.9$	0	0	0	0	0	0
$\lambda_{C,i}^{max}(0) = 1.0$	0	0	0	0	0	0

Table 5.3: Clinical window in days after SAH for treating vasospasm in a $2mm$ artery at 50% stenosis using a Solitaire 6 stent.

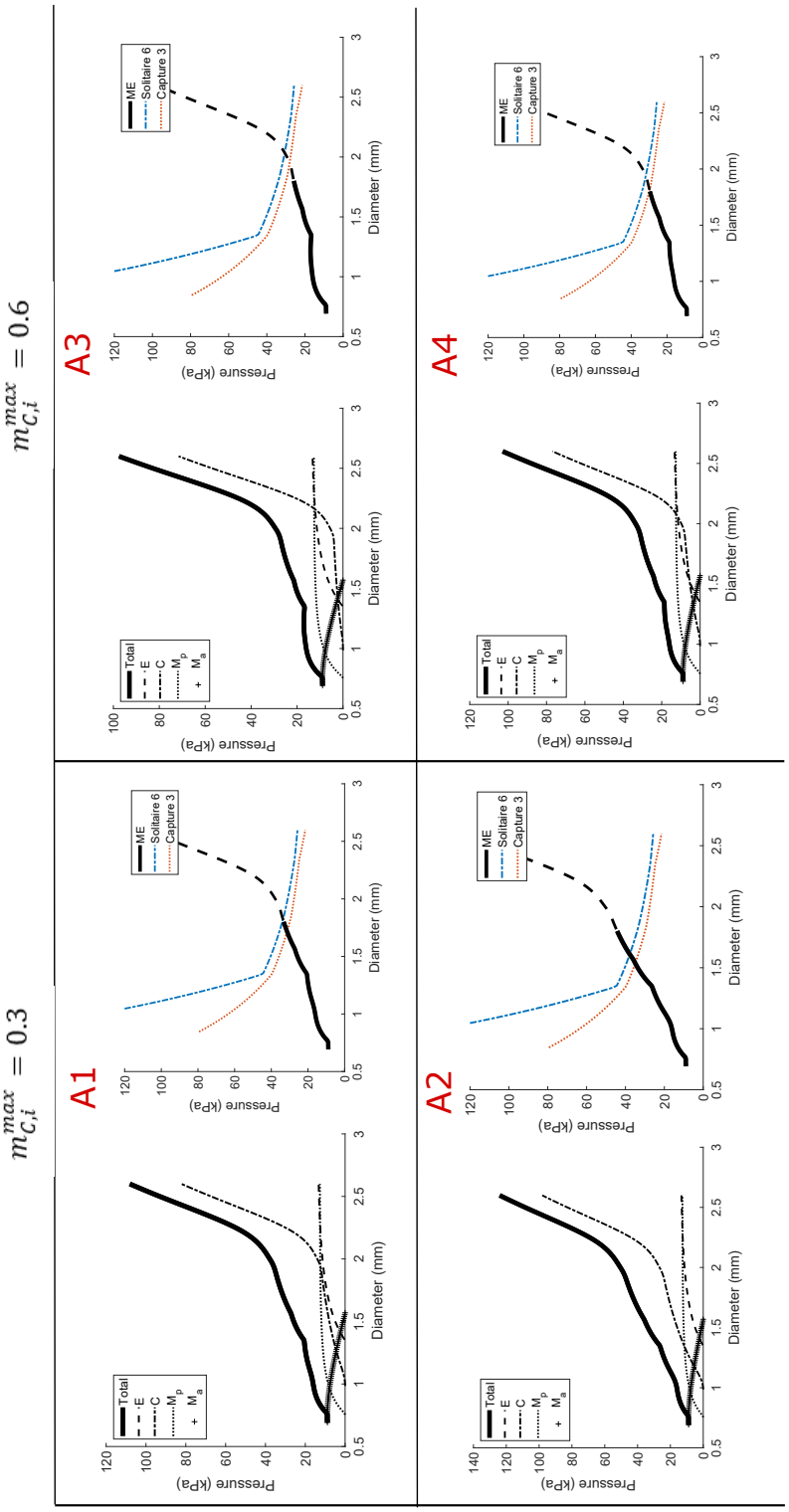

Figure 5.10: For each case of study A: on the left pressure-diameter curve for artery in vasospasm at 50% stenosis 3 days after SAH; on the right test of effectiveness of two commonly available stent retrievers in resolving vasospasm: a stent is successful if its pressure curve remains above the solid part of the mechanical equilibrium (ME) curve.

	$\tau_{gr} = 3$	$\tau_{gr} = 7$	$\tau_{gr} = 10$	$\tau_{gr} = 14$	$\tau_{gr} = 21$	$\tau_{gr} = 28$
$\lambda_{C,i}^{max}(0) = 0.5$	1	3	4	6	10	13
$\lambda_{C,i}^{max}(0) = 0.6$	1	2	3	5	8	10
$\lambda_{C,i}^{max}(0) = 0.7$	0	1	2	3	4	5
$\lambda_{C,i}^{max}(0) = 0.8$	0	0	0	0	0	0
$\lambda_{C,i}^{max}(0) = 0.9$	0	0	0	0	0	0
$\lambda_{C,i}^{max}(0) = 1.0$	0	0	0	0	0	0

Table 5.4: Clinical window in days after SAH for treating vasospasm in a $2mm$ artery at 50% stenosis using a Capture 3 stent.

The pressure-diameter curves and stent pressure curves are also reported in Figure 5.11 for four representative cases from this study:

- B1; $\lambda_{C,i}^{max} = 0.5, \tau_{rem} = 7$,
- B2; $\lambda_{C,i}^{max} = 0.5, \tau_{rem} = 21$,
- B3; $\lambda_{C,i}^{max} = 0.8, \tau_{rem} = 7$,
- B4; $\lambda_{C,i}^{max} = 0.8, \tau_{rem} = 21$.

5.4 Discussion

A theoretical model of collagen growth and remodelling has been incorporated into the cerebral vasospasm model presented in Chapter 2 in order to evaluate its effect on both the pathophysiology of the disease and the model predictions regarding the amount of pressure required for treatment. It represents a first step in the research of accurate evolution laws that can capture the complex changes that the extracellular matrix undergoes in various soft tissue diseases. The model has shown that collagen growth and remodelling, even if partial, can greatly affect the predictions on the effectiveness or lack thereof of treatment via stent retrievers and thus further study is warranted on the subject. It is first recommended that various limitations of the model are addressed which are discussed in Section 5.4.1.

5.4.1 Limitations of the Model

The model that has been presented in this Chapter is an extension of the model presented in Chapter 2 and thus all limitations of that model still apply here.

The membrane assumption is reasonable when the stress field across the thickness is

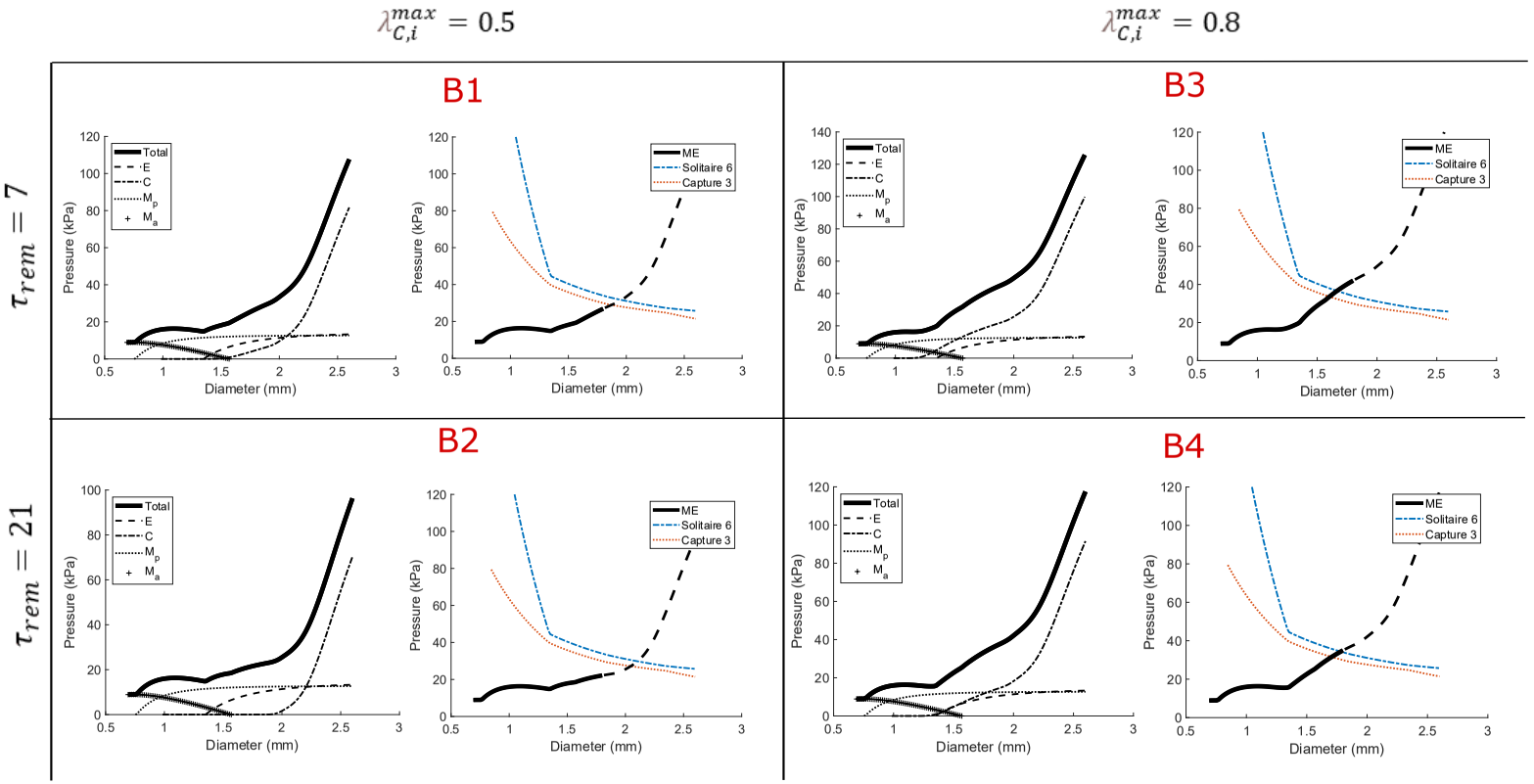

Figure 5.11: For each case of study B: on the left pressure-diameter curve for artery in vasospasm at 50% stenosis 3 days after SAH; on the right test of effectiveness of two commonly available stent retrievers in resolving vasospasm: a stent is successful if its pressure curve remains above the solid part of the mechanical equilibrium (ME) curve.

likely to remain uniform. In the case of vasospasm, however, the significant change of geometry caused by the constriction is likely to make this hypothesis no longer valid. It is therefore recommended to integrate this model into a finite element framework to obtain more realistic results.

The time-course of vasospasm is also not modelled directly, but rather a 50% level of stenosis is imposed and it is assumed that VSMCs have returned to their homeostatic state of stretch. In reality this is likely to be a continuous process and it is possible that, when a patient becomes symptomatic and treatment is considered, the VSMCs have not returned to their homeostatic state of stretch yet.

In this idealised geometry it is also assumed that collagen is aligned circumferentially. However, experimental observations have shown that the dispersion of collagen fibres is different for different tissues and, in the case of arterial tissue, even from layer to layer. It is recommended that the orientation of the fibres is therefore considered. The simplest extension to include this could assume collagen fibres aligned at $\pm\pi/4$ radians from the circumferential direction. A more sophisticated extension could include a continuous distribution of fibre directions (Gasser et al. (2006)).

Another limitation of the model is how treatment is simulated. Indeed an interventional device is idealised as an increase in pressure, uniform across the inner surface of the vessel, irrespective of the device's geometry. A recommended improvement would be the consideration of the geometry of the stent, since this might affect the distribution of the additional pressure on the inner surface, especially depending on the mesh density.

This model does not consider the endothelial layer. Endothelial cells play a negligible role in the mechanics of the vessel but a crucial one in mechanotransduction, i.e. the translation of mechanical signals, such as pressure and shear stress, to the other layers in the tissue. The constriction causes the internal elastic lamina to become corrugated (Findlay et al. (1989), Hughes & Schianchi (1978), Kapp et al. (1985), Macdonald et al. (1992), Mayberg et al. (1990), Mizukami et al. (1976), Nakagomi et al. (1990), Sacher & Tenner (1978), Zubkov et al. (2002)), which can damage the attached endothelial cells, and some studies have also observed endothelial desquamation. This can impair the translation of mechanical stimuli to chemo-biological ones and thus impair cell function in VSMCs and fibroblasts.

Aside from smooth muscle cells, which are assumed to be functionally disrupted and brought to failure when a mechanical treatment is effective, damage to the other

constituents of the wall was not considered. Although VSMCs are likely to be the first constituent to reach failure in the context of vasospasm treatment, it would be important to consider even just partial damage to the other components, since it is for example possible that damage to some collagen fibres occurs during treatment of CVS although that might not be the main criterion of success or lack thereof of a specific strategy.

Finally, a significant limitation is that in this model the evolution of either the mass density or the stretch distribution is prescribed and given as a function of time. In reality, collagen is maintained by vascular cells residing in the vessel wall, most notably vascular smooth muscle cells and fibroblasts. The current biological knowledge is that pro-collagen molecules are formed within the cell wall, then secreted into the extracellular space where they self-assemble into fibrils and then into fibres, and finally are attached to the existing matrix by a crawling-like movement of the cell (Alberts et al. (2015), Robertson & Watton (2013)).It would therefore be more realistic to have the collagen growth and remodelling processes coupled to the state of their neighboring cells. Suggestions for possible coupling mechanisms are discussed in the next Section.

5.4.2 Recommendations for Future Directions

Despite the limitations mentioned in the previous section, the main obstacle to modelling growth and remodelling of collagen is a lack of experimental observations upon which to base choices for parameter values, variables of interest and evolution laws. It would therefore be highly desirable that more experimental studies were carried out on growth and remodelling processes, in both health and disease.

Although some knowledge exists on how collagen fibres are synthesised and deposited by the vascular cells, the process by which they attach the fibres to the matrix and how they determine what stretch and orientation would be optimal for the tissue function is still an open question. This is a complex process which could involve several variables of interest: rate of synthesis of new collagen, rate of production of matrix metalloproteinases (collagen-degrading molecules) and their inhibitors TIMPs, and stretch distribution, stiffness and orientation of new collagen. Ultimately it would be ideal to be able to describe the behaviour of these variables in terms of the state of the cell that regulates them, which would in turn depend on the chemo-mechanical environment of the cell. To this end the approach of Aparìcio et al. (2016) could be adopted, who developed a bio-chemo-mechanical framework in which a feedback loop is established between molecular-level processes, the mechanical structure and properties

of the wall and the blood flow with its resulting metrics such as radial pressure and wall shear stress. It would be mathematically straight-forward to integrate a similar model into the framework presented here while the challenge would lie in the selection of variables of interest among the countless involved in molecular processes within the cell and choice of laws of mutual interaction between them.

Limited information is also available regarding collagen growth and remodelling in the specific case of vasospasm. There are indeed conflicting results in the experimental literature: while some studies observed an increase in collagen mass, others found no increase or decrease; different studies that stained for specific collagen types reported contradicting results (see Section 1.2, Hughes & Schianchi (1978), Kapp et al. (1985), Macdonald et al. (1992), Mayberg et al. (1990), Sacher & Tenner (1978), Smith et al. (1985), Yamaguchi-Okada et al. (2005)). One study showed that, despite noticing a statistically significant increase in collagen mass at day 14, the collagen content had returned to base value by day 28 (Yamaguchi-Okada et al. (2005)). Due to this lack of definitive results of increased collagen content, a few studies even suggested that the molecule reacting to the stain in models that do report increases in collagen mass is actually not collagen, but a different type of ECM molecule, perhaps fibronectin or something unspecified (Macdonald et al. (1992), Yamaguchi-Okada et al. (2005)). It would therefore be important that more experimental studies were carried out to identify this protein, or perhaps family of proteins, and determine its mechanical properties as well as what factors in the development of vasospasm have determined its production.

A possible experimental design to address some of these questions is to replicate vasospasm *ex vivo*. If the current technology allows it, one could apply arterial blood to a segment of a cerebral artery and observe whether changes have occurred in the collagen fabric and, if so, quantify them. The main challenge of such an experiment would be to maintain the tissue sample in *in vivo*-like conditions, such as by maintaining flow through the tissue and providing nutrients to the cells, but it would provide the most direct answer to the research questions involved in this work and thus accelerate the development of a clinical tool.

From the perspective of computational modelling, there are four research directions it would be most valuable to explore in future studies.

The first one addresses the limitation of modelling the artery as a membrane. It is likely that the property of having a uniform strain field through the wall thickness

is lost in vasospasm due to the high level of constriction and thus it is important to integrate this model into a finite element framework and compare the results, since the prediction of the magnitude of pressure necessary for mechanical treatment might be significantly different. This would also move in the direction of being able to apply this model to patient-specific geometries in the future, which is highly desirable for clinical applications.

From a theoretical point of view, the prescribed temporal evolution of the variables of interest should be abandoned in favour of one that depends directly on the state of the cell. In order to do this, it would be necessary to formulate an explicitly time-dependent model, which would be straight-forward to do. It would be ideal to have some experimental evidence upon which to base hypotheses on how collagen growth and remodelling depends on the cell mechanobiology but, until these are available, theoretical models can be tested. A initial simple scenario that could be explored involves using a similar approach to Chen (2014) and use a modified Richards' growth function (Richards (1959)) to evolve one of the three stretches that define the distribution, for example $\lambda_C^{ATT,max}$. Two cases could be explored: one in which the evolution depends on the deviation of the VSMC *stretch* from its attachment value, i.e.

$$\lambda_C^{ATT,max} = \lambda_C^{ATT,max}{}_{|t=0} + \frac{\lambda_C^{fail} - \lambda_C^{ATT,max}{}_{|t=0}}{1 + \exp(-B\,(\lambda_M - \lambda_M^{ATT}))}, \tag{5.12}$$

and one where it depends on the deviation of the cell *stress* from its homeostatic value, i.e.

$$\lambda_C^{ATT,max} = \lambda_C^{ATT,max}{}_{|t=0} + \frac{\lambda_C^{fail} - \lambda_C^{ATT,max}{}_{|t=0}}{1 + \exp(-B\,(\frac{\sigma_M - \sigma_M^h}{10^5}))}, \tag{5.13}$$

where λ_C^{fail} is the maximum assumed collagen stretch before damage occurs, σ_M^h is the homeostatic level of VSMC stress and 10^5 is chosen as normalising value that could be adapted if necessary. The implementation of laws of this kind would be a first step in the study of the effect of remodeling mechanisms that depend on the state of the tissue.

In regards to specific variables, the assumption that remodelling of the collagen network is achieved by a "shifting-only" change in the stretch distribution is rather limiting.

Other studies have shown that including skewing and narrowing/expanding of the distribution can yield more realistic results Chen (2014). Therefore hypotheses where the width and skew of the distribution can also change should be tested.

Finally, a dispersion model, i.e. a distribution of the orientations of the collagen fibres, should be included in the model (Gasser et al. (2006)). Beside including it in the material model of collagen, it is worth considering the possibility that the dispersion might change in pathological conditions and thus include it in the remodelling process.

5.5 Conclusion

In this Chapter a simple theoretical model has been presented to study the effect of collagen growth and remodelling on the effectiveness of stent retrievers as a treatment strategy to mechanically resolve cases of cerebral vasospasm. It includes a novel distinction between mature and immature collagen, where the former is the population present at the time of subarachnoid haemorrhage and the latter the population newly synthesized after SAH. Two distinct studies were carried out: Study A focused on the growth aspect and assumed a fixed stretch distribution (no remodelling), while Study B focused on the remodelling aspect and assumed that all the mass of immature fibres would be secreted at the time of SAH and remained constant afterwards (no growth).

Across all cases it is evident that collagen growth and remodelling can play a decisive role in the stiffening of the vessel wall in vasospasm to the point where stents would no longer be effective. It is therefore crucial to include this aspect of the disease in any computational model that wishes to make predictions on the time-course of vasospasm so as to guide clinicians in the selection of an optimal treatment strategy for a specific patient . The presented formulation is but a simple theoretical framework that was used as a preliminary exploration. It is the author's hope that this work motivates further exploration of the subject through both computational and experimental efforts. The study of collagen growth and remodelling can be decisive not only for the study of cerebral vasospasm, but also other diseases, such as aneurysms (Hill et al. (2012), Phillippi et al. (2014), Watton, Ventikos & Holzapfel (2009)), asthma (Hill et al. (2018)), myocardial infarction and others. A stronger collaboration between the modelling and experimental community is therefore necessary to develop accurate models of disease progressions that would be able to achieve clinical application.

Chapter 6

Discussion and Future Research

A novel hypothesis on the pathophysiology of vasospasm is formulated and used to develop a mathematical membrane model of the disease (Ch. 2) and a thick-walled finite element model (Ch. 3,4). The membrane model is extended to study the potential impact of collagen growth and remodelling in the evolution and treatment of the disease (Ch. 5).

In this Chapter the main findings produced by the work described in this Dissertation are summarised and a discussion is presented on the recommended directions for future work.

6.1 Summary and Main Findings

The normal functioning of blood vessels is highly dependent on their structure and most cardiovascular diseases can be explained as maladaptive changes in the structure of the vessel walls. Vascular cells play a fundamental role in this as they continuously maintain the extracellular matrix and regulate their biological activity according to their surrounding chemo-mechanical environment. The processes of wall structure maintenance are very complex, multifactorial and multiscalar, ranging from gene transcription to the diffusion or transport of molecules that constitute chemical signalling to the mechanical interplay between the properties of the blood flow in the vessel lumen and the stress responses of the wall constituents. Therefore it is crucial for modelling frameworks of soft tissues to not limit themselves to the biomechanical description of their behaviour, but to consider the mechanobiology of vascular cells, i.e. the processes by which the mechanical environment of the cells affects their biological

activity thus altering the microstructure of the vessel.

In this work existing frameworks for modelling the growth and remodelling of arterial tissue have been adapted and extended to formulate a mathematical model of cerebral vasospasm with the objective of estimating the amount of pressure necessary for its mechanical treatment. Consistently with experimental observations on the morphology of the spastic vessel as well as on the time-dependent effectiveness of pharmacological treatment, it is hypothesised that the main driver of vasospasm is the remodelling of vascular smooth muscle cells which attempt to maintain their homeostatic level of stretch. This follows an initial change in vessel geometry caused by a chemically-driven increase in VSMC active contraction. Contrary to a commonly held belief among clinicians, it is assumed that successful mechanical treatment does not require damage to the extracellular matrix, but only to the VSMCs. The predictions of the magnitude of pressure necessary to treat vasospasm are consistent with reported clinical observations of success or lack thereof of stent-retrievers as a treatment strategy. More importantly they highlight that, even in case of stent failure, the pressure required would only be slightly higher than what the stent could provide and thus there is potential to specialise stent design for the purpose of treating vasospasm (the currently used ones are designed for blood clot removal) with significant clinical benefits: the far lower pressures exerted by the stents dramatically decrease if not nullify the risk of tissue rupture and, compared to balloon cathethers, they have better maneuverability and thus can reach branches of the distal vasculature that would otherwise not be treatable.

As a first stage, a conceptual mathematical model was developed where the artery is modelled as a cylindrical membrane (Chapter 2). Following the conceptual framework of Watton et al. (2004), Watton, Ventikos & Holzapfel (2009), a constrained mixture model is adopted where the constitutive elements of the vessel wall have independent reference configurations so as to capture their different mechanical roles and properties. Each constituent has a preferred state of stretch, called homeostatic or attachment stretch, which optimizes its mechanical function in some sense. While elastin is the main contributor to the elasticity of the blood vessel and bears the majority of the pressure load, VSMCs play a dynamic role by actively contracting or relaxing in response to a changing mechanical environment. It is therefore assumes that, after a prolonged period of chemically-driven contraction, estimated to be about $2-3$ days, a remodelling process is initiated by which the cells attempt to return to their homeostatic state of stretch and level of active contraction. On a molecular level, it is

imagined that this may correspond to rearrangement of their internal cytoskeleton and/or attachment to the ECM and other neighbouring cells, but more experimental data is warranted on this hypothesis. The remodelling causes a leftward shift in the pressure-diameter curve of the VSMC response and thus of the whole arterial wall as well as an increase in the proportion of pressure load borne by these cells: due to lack of remodelling of elastin and collagen, VSMCs become the only load bearing constituent in moderate to severe levels of stenosis. The model thus predicts how the pressure-diameter curve adapts in vasospasm and can predict the magnitude of pressure necessary to resolve the disease. It is assumed that the necessary pressure is such that it would overstretch the VSMCs beyond a *dilatation threshold* at which the cells would sustain such damage as to no longer be able to bear any pressure load or contract. Experimental measurements of the force exerted by four commonly available stent-retrievers are used to test their effectiveness or lack thereof in treating vasospasm in vessels of different original diameter (and thus different arteries or branches of arteries in the cerebral circulation). The model predictions are consistent with clinical observations and seem to identify a "cut off" point at a diameter of about 3mm such that stents are likely to be successful in arteries smaller than that value but usually fail in larger vessels. The consistency with clinical data suggests validity of the central hypothesis and provides motivation to address some model limitations and further sophisticate it.

The mathematical model presented in Chapter 2 models the artery as a membrane, which assumes a uniform transmural strain field across the vessel wall. Although this is reasonable for a healthy vessel, it is likely to no longer hold true when the artery is constricted as a consequence of vasospasm. This is likely to affect the results since, following stent deployment, the VSMCs closer to the lumen would be subject to a higher stress compared to those farther away and thus the damage provided by the stents may not be uniform across the wall thickness. In order to address this the model developed in Chapter 2 is integrated into a suitable finite element framework. The framework developed by Eriksson et al. (2014), Grytsan et al. (2015) and Grytsan et al. (2017) is adopted, which has successfully been applied to the modelling of abdominal aortic and intracranial aneurysms. Before it is applied directly to model cerebral vasospasm, the framework required a few extensions and sophistications, which are described in Chapter 3. The material model of collagen is sophisticated in order to include the experimentally observed distribution of fibre waviness and evolution equations that allow it to remodel are implemented. A material model for vascular smooth muscle cells is added which includes both a passive and active response, as

well as remodelling of their mechanical stretch. Finally, a damage model is introduced via the inclusion of a damage variable for each constituent and a damage criterion for VSMCs for the purpose of modelling vasospasm. Although these aspects are not used in this model, the framework includes the possibility of modelling anisotropic volumetric growth as well as growth/atrophy of the constituents, alongside their remodelling. The framework is implemented in the software FEAP, an open source academic software with a high level of customisation from the modeller. To the author's knowledge, this is an internationally leading framework for modelling growth and remodelling of arterial tissue due to its inclusion of anisotropic volumetric growth, VSMC active contraction, microstructurally motivated collagen material model and constituent-specific damage criteria. The framework can also easily accommodate an extension to describe the interaction between the wall structure and the dynamics of blood flow (fluid-solid growth model) as well as patient-specific geometries.

In Chapter 4 the model developed in Chapter 2 is integrated into the finite element framework developed in Chapter 3. The model is structured so as to be as close a comparison as possible to the 1D model in order to obtain consistent predictions. A small deviation from the model had to be accommodated for with regards to the damage model due to numerical reasons. While in the 1D model there was no need to quantify the damage and simply assume null stress response in the VSMC whenever their stretch was equal to or exceeded the dilatation threshold, in the finite element framework the approach by Li et al. (2012) is followed and a damage variable $d_0 \in [0, 1]$ is introduced such that $d = 0$ corresponds to no damage and $d = 1$ to complete damage and null stress response. The implementation of a sudden step-change in the damage parameter from 0 to 1 in correspondence of the VSMC stretch being equal to the dilatation threshold, which would be the closest translation of the 1D criterion in the FE framework, would prevent numerical convergence. In order to resolve this, the existence of a "damage threshold" is postulated, mathematically equivalent to a level of stretch smaller than the dilatation threshold, at which damage to the cell begins to occur. Whenever the cell stretch exceeded the damage threshold, the damage variable would increase proportionally to the deviation of the cell stretch from the damage threshold. If the dilatation threshold was exceeded or the damage variable became larger than one, the equality $d_0 = 1$ is prescribed.

When comparing the predictions from the FE models to those yielded by the 1D model, we find, as expected, that the non-uniformity of the transmural strain and stress fields in the vasospastic vessel has the potential to affect the results. Indeed

simulations suggest that the cells experience decreasing pressure from the stents and thus are less damaged with increasing distance from the vessel lumen. Since the blood clot is also localised in the axial direction, the model predicts that there would be a "tapering" transition region between the region of maximal constriction and the region of physiological geometry and thus the effects of mechanical treatment would be non-homogeneous in the longitudinal direction as well. It is therefore recommended that any model that in the future would like to serve as guidance for clinicians in treatment selection be a three-dimensional finite element model. To the author's knowledge this model is the only three-dimensional finite element model of cerebral vasospasm. The model predictions corroborate the results of the one-dimensional model: the order of magnitude necessary to treat vasospasm is far lower than that exerted by balloon angioplasty and closer to that of currently available stents. However, the threshold between success and failure of a specific stent in a specific case is small and thus small parameter changes would yield opposing predictions. It is highly desirable that more experimental work is carried out in order to increase understanding of the time course of vasospasm and identify which factors play a more prominent role in its evolution in order to be able to determine the most suitable treatment course for a specific patient.

The one-dimensional model developed in Chapter 2 assumes that the role of collagen growth and remodelling is negligible with regards to vasospasm treatment, since its halflife is much longer than the time course of the disease. However it has been shown that collagen degradation and deposition processes can accelerate in pathological conditions and halflives as low as 15 days have been reported. In Chapter 5 we therefore investigated if and how collagen growth and remodelling affects the model predictions on the magnitude of pressure necessary for treatment. Experimental data on collagen remodelling in vasospasm is lacking and only one study was found that reported quantitative information on collagen mass changes. Moreover there are conflicting reports among studies on whether there indeed are changes in collagen mass at all and, if so, in which types of collagen fibres. In absence of definitive observations, a conceptual model is developed where foundational concepts of collagen growth and remodelling are established and competing hypotheses on how these processes occur can be tested.

The process of collagen deposition can be roughly divided into three phases: intracellular production of pro-collagen molecules, secretion of pro-collagen into the extracellular space where the molecules self-assemble into fibres and finally attachment of the fibres to the ECM (Robertson & Watton (2013)). The time course of this process is not yet

clear but there likely is a transition phase between fibre secretion and achievement of a "mature" fibre with a homeostatic level of stretch. The model presented in Chapter 5 aims at capturing this delayed "maturation" of collagen and distinguishes between two fibre populations: "mature" and "immature" (Sang et al. (2020)). The former is defined as the population present at the time of SAH, while the latter is comprised of all fibres secreted after that time. The maturation process is not explicitly followed for each individual fibre but aim to capture the global behaviour of the two populations over time.

Two independent studies are formulated: the first focuses on growth/atrophy of the collagenous matrix and assumes a fixed stretch distribution, while the second emphasizes the remodelling process and assumes instantaneous deposition of immature collagen at the time of SAH. A large parameter space is considered for the deposition and the remodelling rates and for each case a clinical window of treatment is provided, i.e. the maximum number of days from SAH at which the strongest stent would be successful in treating vasospasm. The results suggest that collagen G&R can indeed affect the effectiveness of stents as a treatment strategy and thus should be included in models of the disease. There is however a pressing need to obtain experimental data on how collagen GR is regulated by resident vascular cells and what chemo-mechanical factors affect these processes. An increased understanding of these mechanisms has a wide scope of application and can be applied not only in modelling cerebral vasospasm and treatment, but also other soft tissue diseases such as aneurysms, bladder obstruction, myocardial infarction or oesophageal athresia. In general it is fundamental to gain a deeper understanding of the mechanobiology of vascular cells in order to provide realistic and biologically informed models that can achieve real clinical impact.

6.2 Limitations and Recommendations

6.2.1 Cell Mechanobiology

The most remarkable feature of biological tissues is engrained in their name: "bio", meaning "living", underlines that these tissues are constantly evolving and it would thus be reductive to model them only as elastic geometries. In order to fully understand and thus model biological tissues so as to achieve clinical impact and real world applications it is therefore fundamental to consider the microstructure of these materials and its evolution across time in response to chemical and mechanical signals. Since it is

resident cells which regulate the growth and remodelling of the tissue structure, it is towards them and their interplay with the surrounding chemo-mechanical environment that the modelling and experimental community are invited to turn their attention (Ambrosi et al. (2019), Irons & Humphrey (2020)).

In the case of cerebral vasospasm, it has been hypothesised that the disease is driven by VSMC remodelling aimed at maintaining a homeostatic level of stretch. This hypothesis is based on the concept of mechanical homeostasis and the assumption that this is of crucial importance to VSMCs since they play a fundamental role in vessel diameter regulation. There is no direct evidence of this process occurring in vasospasm (albeit probably because no one has thought to look for this before), but some studies report shortening and "rounding" of the smooth muscle cells (Findlay et al. (1989), Yamaguchi-Okada et al. (2005), Zubkov et al. (2002)), which may be a consequence of cytoskeleton reconfiguration. A relevant role of VSMC remodelling has been hypothesised for other diseases as well, such as arterial stiffness (Sehgel, Vatner & Meininger (2015)) and hypertension in aging (Sehgel, Sun, Hong, Hunter, Hill, Vatner, Vatner & Meininger (2015)). However, there is a significant lack of experimental data on many aspects of this process: what it entails at a (macro)molecular level, what is its time scale and how does it depend on the chemo-mechanical environment of the cell.

Furthermore it has been assumed that there exists a "dilatation threshold" at which VSMCs become damaged to the point of not being able to bear the pressure load. Although the damage criterion adopted in these models is based on experimental measurements of VSMC damage (Fischell et al. (1990)), there is a lack of information on how damage occurs in VSMCs, how does it affect the cell at the (macro)molecular level and what is the time scale of recovery, if and when that is possible. Indeed a deeper knowledge of how damage occurs in VSMC would help clarify the mechanisms by which mechanical intervention resolves vasospasm, thus guiding the choice of treatment or the design of specific stents, and aid the prevention of restenosis, i.e. the return of the vessel to a contracted state after mechanical treatment. The latter is a problem that occurs not only in the treatment of vasospasm, but in other modes of endovascular treatment of various cardiovascular diseases. Thus the availability of more experimental data on this topic would be relevant not only for the purpose of modelling vasospasm, but would have wide implications in a clinical setting whenever there is a risk of post-operatorial vessel narrowing following corrective surgery of some cardiovascular pathology (i.e. atherosclerosis, aneurysms, etc.)

Growth and remodelling of collagen fibres is another aspect of the pathophysiology of vasospasm which the modelling presented in this thesis suggests has the potential to affect the effectiveness of different treatment strategies. The proposition of a new microstructurally motivated material model for collagen that would include the distribution of fibre waviness as experimentally observed (Hill et al. (2012), Schrauwen et al. (2012)) is only recent (Aparìcio et al. (2016), Chen (2014)) and to the author's knowledge there is no experimental data on how this distribution evolves in evolving chemo-mechanical environments. The adaptation of the stretch distribution of the collagen fabric is likely to play a role not only in vasospasm, but other cardiovascular diseases such as aneurysms or myocardial infarction.

The process of collagen maintenance consists of two parallel activities: degradation of existing fibres and deposition of new ones. These processes are continuously regulated by resident vascular cells and their harmonious interplay plays a key role in the maintenance of a physiologically functioning tissue. Degradation of collagen fibres is carried out by specific enzymes called collagenases (a type of matrix metalloproteinase) which are inhibited by other enzymes called TIMPs (tissue inhibitors of metalloproteinases). Both these types of enzymes are secreted by the cells. Collagen deposition is roughly tri-phasic: pro-collagen molecules are created intracellularly, then secreted by the cells into the extracellular space where they appear to self-assemble in fibrils and then into fibres, and finally they are attached to the existing ECM by the secreting cell via a "crawling"-like movement of the cell (Robertson & Watton (2013)). Beside this, little is known about this process and there are several questions that biological experiments could address: how do the production rates of matrix metalloproteinases and TIMPs depend on the mechanical environment? What is the time scale of the collagen deposition, from pro-collagen formation to attachment to the ECM, and how does it depend on the chemo-mechanical environment? What factors does the stretch at which the cell configures the fibre depend on and in what way? What factors influence the orientation of the fibrel when it is attached to the ECM? Do different cell types maintain the collagen fabric differently (e.g. fibroblasts compared to VSMCs)? Furthermore "collagen" does not refer to a single protein, but to a family of them and at least 29 distinct types are known. It would therefore be interesting to also investigate whether the proportions of different collagen types change in changing chemo-mechanical conditions. The process of collagen maintenance regulated by vascular cells is highly complex and there is a plethora of research questions worth investigating on the subject. The most important aspect that focus should be placed on is the adaptation of the stretch distribution of the collagen fabric to a changing

chemo-mechanical environment. Further understanding of this adaptation has wide application in modelling soft tissue diseases and is a good compromise between microstructural level of detail to inform the constituent's potentially evolving stress response and numerical complexity for the purposes of computational implementation.

Finally it would be highly desirable to obtain more experimental data on the pathophysiology of cerebral vasospasm and its time course. The experimental studies identified by the author are for the vast majority animal models: for obvious reasons the possibility of conducting experiments directly in humans is severely limited. The limitation of animal models is that there may be significant differences among animal species (most models were rabbit, canine or porcine) as well as between animals and humans: for example the process of clearing out the blood clot in the subarachnoid space is significantly faster than in humans and, since the progression of the disease is highly time dependent, this somewhat invalidates results on the temporal scale of the three phases of vasospasm. However there are interesting aspects to be explored in animal models and technological improvements now make *ex vivo* studies on human cerebral vessels possible.

In either case it is recommended that the temporal evolution of the cystoskeletal structure of VSMCs as well as their attachment to surrounding ECM and other cells is observed. Indeed the hypothesis that VSMC remodelling drives the second phase of vasospasm (where the first covers the first $2-3$ days and is characterised by a principally chemically-driven contraction) is reasonably based on the concept of mechanical homeostasis, there is so far no direct evidence in support of this hypothesis. It is therefore crucial to first and foremost corroborate this main hypothesis. If validation for this assumption was provided, it would then be recommended that the process of damage to the VSMCs be studied: since VSMCs appear tightly arranged in the medial layer of arteries and are therefore likely to be connected to one another, damage should be investigated not only in isolated cells but if possible in whole vessels, ideally following vasospasm. Finally, a further key component worth examining is collagen growth and remodelling, as addressed in previous paragraphs.

Further exploration of the morphology of vasospastic vessels in the third phase of vasospasm (at $2-3$ weeks from SAH) is also warranted. Indeed there are conflicting reports in the literature on whether there is an increase in collagen mass of any kind, what type of collagen is secreted or even if it is collagen at all: some authors speculate that it may be a different ECM protein that is secreted at this stage (Mayberg et al. (1990)) with one group suggesting fibronectin (Yamaguchi-Okada et al. (2005)). It

would therefore be important to investigate how the morphology of the spastic vessel changes in the chronic phase of vasospasm since, if increased production of a different ECM protein is initiated at an earlier stage, this process might affect the treatment predictions.

6.2.2 1D Model of Vasospasm

The model presented in Chapter 2 and published in Bhogal et al. (2019) is a fundamental first step for testing the novel hypotheses on the mechanisms of vasospasm development and its treatment formulated in this thesis. In order to improve the biological realism of the model and move closer to clinical translation, a number of extensions are recommended.

The fundamental shortcoming of this model is the lack of explicit representation of the cell. Although assumptions are made on the mechanobiological processes that mediate the changes in wall structure in vasospasm, these are not represented explicitly and only the macroscopic mechanical variables relevant for the model (e.g. constituent stretch) are considered. However, as suggested by other world-leading researchers in the field (Ambrosi et al. (2019), Humphrey & Latorre (2020)) as well as encouraged by the relevance of models that do incorporate this mechanobiological aspect (Aparìcio et al. (2016), Hill et al. (2018)), the most relevant model extension to be made is the inclusion of an explicit representation of the vascular cell and a more detailed description of the complex interplay between chemical signals, mechanical behaviour and biological cell function that drive the growth and remodelling of the vessel wall Ambrosi et al. (2019). The highly multifactorial nature of vasospasm is such that the pathophysiology of the disease may be different in different patients and a more detailed biologically informed framework, without excessively impinging on computational complexity, may allow for personalised parametrisation of the model according to patient specific data and thus become an invaluable tool in the clinical setting. Moreover such a framework would allow for the testing of competing hypothesis on mechanobiological processes which would apply not only to vasospasm but to other soft tissue diseases as well.

The constitutive model of collagen that has been selected incorporates the microstructural description of a distribution of collagen fibre stretches. However it has been assumed that collagen is circumferentially aligned which is usually not the case in healthy arteries (Finlay et al. (1995), Hill et al. (2012), Holzapfel et al. (2002)). It is therefore recommended to include a fibre dispersion model as proposed by Gasser et al. (2006) and ideally of its potential remodelling in the case of a changing mechanical

environment.

In the model extension described in Chapter 5 a first theoretical implementation of remodelling of the stretch distribution of the collagen fabric has been implemented. With ideally more data from experimental measurements, it is recommended that a study on how this stretch distribution adapts to the changing chemo-mechanical environment is carried out. It is often assumed in G&R models that there exists a homeostatic level of stretch at which a given constituent tries to maintain its actual stretch. This can be reasonable in many cases but it is possible that the definition of homeostatic stretch/distribution may be dependent on the chemical and mechanical environment of the cells: in other words, while in conditions that are only a small deviation from the physiological state vascular cells may degrade and secrete collagen so as to maintain a fixed stretch distribution, it is possible that the definition of this "target" distribution are not fixed and conditions-independent but instead depend on the mechanical environment of the cell. Investigations on this problem may be useful not only in vasospasm, but also for models of aneurysms and myocardial infarction, among others.

There are other aspects of the pathophysiology of vasospasm which have been assumed negligible thus not included in the one-dimensional model. However these have the potential to affect the model predictions and should therefore be considered in future model extensions.

Inflammation is thought to play a significant role in vasospasm (Hughes & Schianchi (1978), Mayberg et al. (1990)) and the complex signalling pathways that characterise it are likely to guide the growth and remodelling processes occurring in the arterial wall. Further experimental studies on the role and form of inflammatory pathways are therefore warranted which can inform a modelling framework that would include this important aspect of the disease. As for other investigations recommended in this Chapter, the study of inflammation is another ubiquitous research area which would find application in other soft tissue diseases, such as aneurysms (Tulamo et al. (2018)), atherosclerosis (Libby et al. (2002)) or asthma (Hill et al. (2018)).

A few studies also reported evidence of VSMC differentiation into a synthetic phenotype, migration towards the endothelial layer and/or partial apoptosis. These changes in the wall morphology have the potential to affect the treatment predictions and it is worth investigating whether these effects would be negligible or should instead be integrated into the model for improved accuracy. Apoptosis of part of the smooth

muscle population would result in the remaining living cells taking on an even larger proportion of the pressure load and thus their remodelling process might be different from what has been hypothesised in this work; differentiation of part of the population would have the same effect as apoptosis but also suggest there may indeed be an increase in ECM proteins deposition since the synthetic phenotype of VSMCs has less of a contractile role but is capable of secreting higher amounts of ECM; finally migration towards the endothelium suggests VSMC differentiation, since the synthetic phenotype is more migratory than the contractile, and is also likely to affect the load bearing proportion of the constituent as well as probably involve a change in cell orientation. It is therefore recommended that this aspect of the evolution of the wall morphology be investigated through *in vitro* or *ex vivo* experiments and hypotheses be tested in mathematical or computational models with regards to the potential impact on the effectiveness of a given treatment strategy.

The endothelial layer has not been considered in this model since its load bearing contribution is considered negligible. However it plays a fundamental role in mechanotransduction, i.e. the “translation" of mechanical signals that the blood flow directly applies to the endothelial cells into molecular signalling pathways that regulate cell activity within the vessel wall. In vasospasm it is thought that, although the disease is initiated by the extravascular blood clot, the released Oxyhaemoglobin travels (or communicates via further signalling) to the endothelial layer where it signals the endothelial cells to increase production of vasoconstrictors and of scavengers of vasodilators (Pluta (2005), Weir & BK (1991)). Together with the incorporation of chemical signalling pathways and their interactions with resident cells it would therefore be of interest to study the role of the endothelial layer in vasospasm. This would be necessary if in the future the model aimed to include the potential of the disease to self-resolve as a constant interplay between the wall structure and the haemodynamics is required to explain this. Furthermore, the study of mechanotransduction and the role of the endothelial layer is relevant not only for vasospasm but other soft tissue diseases as this cell type is the universal fluid-solid mediator in all soft tissues. For example it is thought to play a significant role in the development and evolution of aneurysms (Robertson & Watton (2013), Vamsi Krishna et al. (2020)) and thus the study of this crucial process could be useful for predicting the evolution of this disease, in particular its stabilisation or risk of rupture.

Although the mechanical response of several soft tissues, including cardiovascular and arterial tissues, has been shown to be viscoelastic (Golob & Chesler (2018)), the

majority of biomechanical model of soft tissue growth and remodelling use a hyperelastic formulation. This is in part due to the increase complexity of implementation for viscoelastic constitutive modes compared to hyperelastic. Holzapfel et al. (2002) proposed a two-layer constitutive formulation aimed at simulating the passive mechanical behaviour of healthy arteries in the large viscoelastic strain regime. The local stress in each layer was decomposed into a volumetric componenet, an elastic isochoric component and finally a viscoelastic component. Zhang et al. (2019) introduced *fractional* viscoelasticity which brings the benefit a low number of parameters and effectiveness at simulating materials with power-law behaviour at the cost of the high computational requirements needed for the approximation of the fractiona derivative. A numerical implementation is proposed in which fractional viscoelasticity is evaluated via a recursive approximation, resulting in computational costs comparable to those of hyperelastic models. The adoption of a viscoelastic model allows a more realistic representation of the behaviour of various soft tissues, however at the cost of increase complexity of implementation. It is therefore worth analysing in which cases it is warranted to make use of a viscoelastic framework and in which it is a sufficiently good approximation to use the simpler and less computationally expensive hyperelastic formulation.

Finally it would be of interest to explore a further sophistication of the constitutive model of the collagen network to include the sub-components of an individual fibre thus explaining the macroscale behaviour of the material by means of its nanoscale properties. Indeed a collagen fibre can present multiple levels of "assembly" of molecules: collagen polypeptide α chains secreted by the cells are assembled into triple-stranded ropelike superhelical structures which define the collagen molecule; these molecules can then be assembled into microfibrils, fibrils, filaments and network-like structures (Alberts et al. (2015), Robertson & Watton (2013)). A collagen *fibre* is defined as an aggregate of collagen *fibrils* but the degree and mode of assembly varies between collagen types. An important factor in the determination of the material stiffness is the density of cross-linking between the sub-structures of the fibres. Marino & Vairo (2013) and Maceri et al. (2010) have proposed a novel constitutive model for collagen that captures this nano- to macro-scale structure of the constituent and grounds its highly nonlinear behaviour in its molecular structure. The model uses a few parameters which are biologically informed but need to be correctly evaluated as small changes at the nanoscale result in large variations at the macroscale. The inclusion of cross-linking would be a useful sophistication to adopt for the model of cerebral vasospasm as it is possible that the observed increased tissue stiffness is due

not only to medial fibrosis but to increased cross-linking of the connective tissue as well. Testing this hypothesis would be useful in addressing the apparently contradictory observations in the experimental literature regarding the increased presence or lack thereof of collagen in the medial layer in vasospasm.

6.2.3 Finite Element Model of Vasospasm

The structure of a blood vessel wall is highly dependent on its function. This can vary across different vessel types, such as coronary compared to cerebral arteries, but in general consists in maintaining a level of elasticity which balances vessel compliance, which is needed to accommodate significant changes in blood flow (e.g. in exercise), with vessel resistance, which is necessary to allow the blood to continue flowing through the circulatory system. Therefore the haemodynamics of blood flow play a crucial role in the determination of the growth and remodelling processes occurring in the vessel wall, in both physiological and pathological conditions. The modelling frameworks presented in this work do not incorporate this aspect and this is a significant limitation of the work. The framework proposed by Watton, Raberger, Holzapfel & Ventikos (2009), Watton et al. (2011) and extended by Aparício et al. (2014) and Grytsan et al. (2015) is a natural candidate for adapting the models presented in this dissertation since it builds on the same modelling assumptions used in the model presented in Chapter 2, such as modelling soft tissues as constrained mixtures of suitable constituents, postulating the existence of (potentially environment-dependent) homeostatic configurations for such constituents and incorporation of evolution laws that regulate the growth and remodelling of the tissue. The framework has been applied to model abdominal aortic aneurysms and the adaptation to modelling cerebral vasospasm would be straight-forward.

The two-dimensional model of vasospasm proposed by Baek et al. (2007), Humphrey et al. (2007 September*a*) includes equations that couple the wall structure to the haemodynamics with the vessel lumen. Incorporation of this relationship allows the modelling of a self-resolving case of vasospasm, which is the interesting evolution of this disease in the case it does not manifest in neurological symptoms and thus does not require treatment. Indeed, although the model proposed in does not include VSMC remodelling, it considers the effect of a decreasing chemically-driven active contraction of VSMCs due to the progressive removal of the extravascular blood clot, which is responsible for the initiation of the spasm. It would therefore be of great interest to study how the progressive relaxation of VSMCs, which has not been considered in

the models here presented, interacts with their remodelling and with the blood flow dynamics.

The finite element framework presented in Chapter 3 accommodates the possibility of modelling anisotropic volumetric growth (AVG). The question of how mass changes of different constituents are accommodated in the finite space occupied by a soft tissue is still an open question, but it has been shown by Schmid et al. (2012) that assuming isotropic volumetric growth for all constituents can lead to unrealistic results, such as the shrinking of arterial tissue in response to elastin degradation as opposed to the experimental observation that this would cause an enlargement. Initial steps for modelling volumetric growth were taken by Schmid et al. (2012) and Valentín et al. (2013) who verified the initial concepts in ideal cubic and cylindrical geometries. Eriksson et al. (2014) applied the framework to modelling abdominal aortic aneurysms and tested competing hypotheses of constant density compared to constant volume laws for volumetric growth. In 2017 Grytsan et al. (2017) extended the framework to incorporate *anisotropic* volumetric growth and compared four modes of anisotropic growth in their predictions of aneurysm growth. They found that different types of anisotropy lead to significantly different results, some of which are unrealistic. However there is still a significant lack of experimental data to inform the growth models: thus care must be taken in prescribing specific AVG laws and further experimental investigations on this subject are warranted.

Moving towards clinical applications it is highly desirable to move away from idealised geometries, such as cylinders for arteries or sphere for the heart, and adapt the modelling frameworks to patient-specific geometries. The finite element framework used in this work already accommodates for this and it is recommended that the model be applied to a variety of patient-specific data so that treatment predictions can be compared. This can be highly valuable tool since it allows the identification of the patient-specific factors that are more likely to influence the model predictions and can therefore guide the study and acquisition of patient data to parametrise the model accordingly thus moving ever closer to the desirable world of personalised medicine.

The predictions made by the models presented in this dissertation are based on the idealisation of stent retrievers as additional pressures acting on the vessel lumen, which are therefore uniform in the axial and circumferential direction. This does not capture the influence of the stent geometry and properties (e.g. material, mesh

density) and may affect the treatment predictions. There already exist finite element meshes describing specific stents which capture their geometry, design and mechanical properties. It would therefore be straight-forward to incorporate this into the model presented in Chapter 4 and test whether the stent design has an influence on its effectiveness in the treatment of vasospasm or whether the idealisation as a uniform additional pressure is sufficiently accurate.

6.3 Conclusion

The work presented in this dissertation is a striking example of how mathematical and computational modelling can become valuable tools not only in testing hypotheses on the physiology and pathophysiology of soft tissue but also as a clinical tool to aid the selection of the most appropriate course of treatment for various diseases. A novel hypothesis on the pathophysiology of vasospasm is tested which potentially reconciles apparently conflicting experimental observations on the disease and supports the use of stent retrievers as a treatment strategy with essential benefits such as increased safety for the patient. Modelling frameworks are extended and sophisticated into world-leading standards with high customisation potential, microstructurally-informed material models and evolution laws, anistropic volumetric growth and the possibility to model constituent damage with custom criteria. The model of vasospasm presented here is at an early stage of development but there appears to be potential to eventually design a model that balances biological detail with computational tractability and allows personalised tailoring to patient-specific cases.

This work highlights the importance of considering not only the mechanical behaviour of arterial tissue but also its mechanobiology, which plays a fundamental role in the morphological evolution of the wall structure in development, aging and disease. The pursuit of experimental studies on this topic would benefit from a wide scope of application and greatly aid the sophistication of computational models towards increased biological realism. There is indeed a need for stronger collaboration between the modelling and the experimental community: experimental data informs and validates the mathematical formulations of tissue properties and behaviour while computational modelling can highlight which aspects of a research question should take higher priority for further study. The synergistic collaboration between the two fields is therefore of the utmost value and helps maximise translational impact in the field of *in silico* medicine.

References

Alberts, B., Johnson, A., Lewis, J. ., Morgan, D. ., Raff, M., Roberts, K. . & Walter, P. (2015), *Molecular biology of the cell*, Vol. 21, 6th edn, GARLAND SCIENCE, TAYLOR & FRANCIS, 270 MADISON AVENUE, NEW YORK, NY 10016 USA.

Ambrosi, D., Ben Amar, M., Cyron, C. J., DeSimone, A., Goriely, A., Humphrey, J. D. & Kuhl, E. (2019), 'Growth and remodelling of living tissues: perspectives, challenges and opportunities', *Journal of The Royal Society Interface* **16**(157), 20190233.

Aparìcio, P., Thompson, M. & Watton, P. (2016), 'A novel chemo-mechano-biological model of arterial tissue growth and remodelling', *Journal of Biomechanics* **49(12)**, 2321–2330.

Aparício, P., Mandaltsi, A., Boamah, J., Chen, H., Selimovic, A., Bratby, M., Uberoi, R., Ventikos, Y. & Watton, P. (2014), 'Modelling the influence of endothelial heterogeneity on the progression of arterial disease: application to abdominal aortic aneurysm evolution', *Numerical Methods in Biomedical Engineering* **30(5)**, 563–586.

Ateshian, G. A. & Humphrey, J. D. (2012), 'Continuum Mixture Models of Biological Growth and Remodeling: Past Successes and Future Opportunities'.
URL: *www.annualreviews.org*

Baek, S., Rajagopal, K. R. & Humphrey, J. D. (2005), 'Competition Between Radial Expansion and Thickening in the Enlargement of an Intracranial Saccular Aneurysm'.

Baek, S., Valentín, A. & Humphrey, J. D. (2007), 'Biochemomechanics of cerebral vasospasm and its resolution: II. Constitutive relations and model simulations', *Annals of Biomedical Engineering* **35**(9), 1498–1509.

Beningo, K. A., Dembo, M., Kaverina, I., Small, J. V. & Wang, Y. L. (2001), 'Nascent focal adhesions are responsible for the generation of strong propulsive forces in migrating fibroblasts', *Journal of Cell Biology* **153**(4), 881–887.
URL: *http://www.jcb.org/cgi/content/full/153/4/881*

Bevan, J. A., Bevan, R. D. & Frazee, J. G. (1987), 'Functional arterial changes in chronic cerebrovasospasm in monkeys: an in vitro assessment of the contribution to arterial narrowing.', *Stroke* **18**(2), 472–81.
URL: *http://www.ncbi.nlm.nih.gov/pubmed/3564106*

Bhogal, P., Loh, V., Brouwer, P., Andersson, T. & Söderman, M. (2016), 'Treatment of cerebral vasospasm with self-expandable retrievable stents: proof of concept', *Journal of Neurointerventional Surgery* . doi:10.1136/neurintsurg-2016-012546.

Bhogal, P., Paraskevopoulos, D. & Makalanda, H. (2017), 'The use of a stent-retriever to cause mechanical dilatation of a vasospasm secondary to iatrogenic subarachnoid haemorrhage', *Interventional NeuroRadiology* **0(00)**, 1–6. doi:10.1177/1591019917694838.

Bhogal, P., Pederzani, G., Grytsan, A., Loh, Y., Brouwer, P. A., Andersson, T., Gundiah, N., Robertson, A. M., Watton, P. N. & Söderman, M. (2019), 'The unexplained success of stentplasty vasospasm treatment', *Clinical Neuroradiology* pp. 1–12.
URL: *http://link.springer.com/10.1007/s00062-019-00776-2*

Cabrera, M., Oomens, C. & Baaijens, F. (2017), 'Understanding the requirements of self-expandable stents for heart valve replacement: Radial force, hoop force and equilibrium', *Journal of the Mechanical Behavior of Biomedical Materials* **68**, 252–264.

Chen, D., Chen, J.-J., Yin, Q., Guan, J.-H. & Liu, Y.-H. (2009), 'Role of ERK1/2 and vascular cell proliferation in cerebral vasospasm after experimental subarachnoid hemorrhage', *Acta Neurochirurgica* **151**(9), 1127–1134.
URL: *http://link.springer.com/10.1007/s00701-009-0385-3*

Chen, H. (2014), 'Intracranial aneurysm disease; novel modelling of inception and microstructural adaption of collagen fabric', *Ph.D. Thesis, Department of Engineering Science, University of Oxford* .

Cheng, F., Robertson, A., Birder, L., Kullmann, F., Hornsby, J., Watton, P. & Watkins, S. (2017), 'Layer dependent role of collagen recruitment during loading of the rat bladder wall'.

Cyron, R. C. A. C. J. (2019), 'Anisotropic stiffness and tensional homeostasis induce a natural anisotropy of volumetric growth and remodeling in soft biological tissues',

Biomechanics and Modeling in Mechanobiology **18**(2), 327–345.
URL: *https://doi.org/10.1007/s10237-018-1084-x*

Eriksson, T., Watton, P., Luo, X. & Ventikos, Y. (2014), 'Modelling volumetric growth in a thick walled fibre reinforced artery', *Journal of the Mechanics and Physics of Solids* **73**, 134–150. doi:10.1016/j.jmps.2014.09.003.

Findlay, J. M., Weir, B. K., Kanamaru, K. & Espinosa, F. (1989), 'Arterial wall changes in cerebral vasospasm.'.
URL: *http://www.ncbi.nlm.nih.gov/pubmed/2586727*

Finlay, H. M., McCullough, L. & Canham, P. B. (1995), 'Three-Dimensional Collagen Organization of Human Brain Arteries at Different Transmural Pressures', *Journal of Vascular Research* **32**(5), 301–312.
URL: *https://www.karger.com/Article/FullText/159104*

Fischell, T. A., Grant, G. & Johnson, D. E. (1990), 'Determinants of smooth muscle injury during balloon angioplasty', *Circulation* **82**(6), 2170–2184.

Gasser, T. C., Ogden, R. W. & Holzapfel, G. A. (2006), 'Hyperelastic modelling of arterial layers with distributed collagen fibre orientations'.

Geith, M. A., Nothdurfter, L., Heiml, M., Agrafiotis, E., Gruber, M., Sommer, G., Schratzenstaller, T. G. & Holzapfel, G. A. (2020), 'Quantifying vascular damage by investigating stent-induced mechanical and morphological alterations in coronary arteries', *Acta Biomaterialia* p. In press.
URL: *https://linkinghub.elsevier.com/retrieve/pii/S1742706120304761*

Golob, M. J. & Chesler, N. (2018), 'Chapter 7 Viscoelastic Properties of Cardiovascular Tissues'.

Grytsan, A., Eriksson, T., Watton, P. & Gasser, T. (2017), 'Growth description for vessel wall adaptation: A thick-walled mixture model of abdominal aortic aneurysm evolution', *Materials* **10(9)**. doi:10.3390/ma10090994.

Grytsan, A., Watton, P. & Holzapfel, G. (2015), 'A thick-walled fluid–solid-growth model of abdominal aortic aneurysm evolution: Application to a patient-specific geometry', *Journal of Biomechanical Engineering* **137(3)**. doi: 10.1115/1.4029279.

Gundiah, N., B Ratcliffe, M. & A Pruitt, L. (2007), 'Determination of strain energy function for arterial elastin: Experiments using histology and mechanical tests', *Journal of Biomechanics* **40**(3), 586–594.

Hill, M. R., Duan, X., Gibson, G. A., Watkins, S. & Robertson, A. M. (2012), 'A theoretical and non-destructive experimental approach for direct inclusion of measured collagen orientation and recruitment into mechanical models of the artery wall', *Journal of Biomechanics* **45**(5), 762–771.
URL: *https://www.sciencedirect.com/science/article/pii/S0021929011006981*

Hill, M. R., Philp, C. J., Billington, C. K., Tatler, A. L., Johnson, S. R., O'Dea, R. D. & Brook, B. S. (2018), 'A theoretical model of inflammation- and mechanotransduction-driven asthmatic airway remodelling', *Biomechanics and Modeling in Mechanobiology* **17**(5), 1451–1470.

Holzapfel, G. (2000), *Nonlinear Solid Mechanics*, Wiley.

Holzapfel, G. A., Gasser, T. C. & Stadler, M. (2002), A structural model for the viscoelastic behavior of arterial walls: Continuum formulation and finite element analysis, Technical report.
URL: *http://www.cis.tu-graz.ac.at/biomech.*

Holzapfel, G., Gasser, T. & Ogden, R. (2000), 'A new constitutive framework for arterial wall mechanics and a comparative study of material models', *Journal of elasticity and the physical science of solids* **61**, 1–48.

Hughes, J. T. & Schianchi, P. M. (1978), 'Cerebral artery spasm', *Journal of Neurosurgery* **48**(4), 515–525.

Humphrey, J., Baek, S. & L.E., N. (2007 September*a*), 'Biochemomechanics of cerebral vasospasm and its resolution', *Annals of Biomedical Engineering* **35(9)**, 1485—-1497. doi:10.1007/s10439-007-9321-y.

Humphrey, J., Baek, S. & L.E., N. (2007 September*b*), 'Biochemomechanics of cerebral vasospasm and its resolution', *Annals of Biomedical Engineering* **35(9)**, 1485—-1497. doi:10.1007/s10439-007-9321-y.

Humphrey, J. D. (2008), 'Vascular adaptation and mechanical homeostasis at tissue, cellular, and sub-cellular levels'.
URL: *https://link.springer.com/article/10.1007/s12013-007-9002-3*

Humphrey, J. D. & Holzapfel, G. A. (2012), 'Mechanics, mechanobiology, and modeling of human abdominal aorta and aneurysms'.

Humphrey, J. D. & Latorre, M. (2020), Biomechanics and Mechanobiology of Extracellular Matrix Remodeling, pp. 1–20.

Humphrey, J. D. & Rajagopal, K. R. (2002), A CONSTRAINED MIXTURE MODEL FOR GROWTH AND REMODELING OF SOFT TISSUES, Technical Report 3.
URL: *www.worldscientific.com*

Irons, L. & Humphrey, J. D. (2020), 'Cell signaling model for arterial mechanobiology', *PLOS Computational Biology* **16**(8), e1008161.
URL: *https://journals.plos.org/ploscompbiol/article?id=10.1371%2Fjournal.pcbi.1008161&utm_s*

Kapp, J., Neill, W., Neill, C., Hodges, L. & Smith, R. (1982), 'The three phases of vasospasm', *Surgical Neurology* **18**, 40–45.

Kapp, J. P., Clower, B. R., Azar, F. M., Yabuno, N. & Smith, R. R. (1985), 'Heparin reduces proliferative angiopathy following subarachnoid hemorrhage in cats', *Journal of Neurosurgery* **62**(4), 570–575.
URL: *http://www.ncbi.nlm.nih.gov/pubmed/3973727*
http://thejns.org/doi/10.3171/jns.1985.62.4.0570

Kassell, N., Sasaki, T., Colohan, A. & Nazar, G. (1985), 'Cerebral vasospasm following aneurysmal subarachnoid hemorrhage', *Stroke* **16(4)**.

Kasuya, H., Weir, B., Shen, Y., Hariton, G., Vollrath, B. & Ghahary, A. (1993), 'Procollagen Types I and III and Transforming Growth Factor-Beta Gene Expression in the Arterial Wall after Exposure to Periarterial Blood', *Neurosurgery* **33**(4), 716–722.
URL: *https://doi.org/10.1097/00006123-199310000-00023*

Latorre, M., Bersi, M. R. & Humphrey, J. D. (2019), 'Computational modeling predicts immuno-mechanical mechanisms of maladaptive aortic remodeling in hypertension', *International Journal of Engineering Science* .

Li, D., Robertson, A. M., Lin, G. & Lovell, M. (2012), 'Finite element modeling of cerebral angioplasty using a structural multi-mechanism anisotropic damage model', *International Journal for Numerical Methods in Engineering* **92**(5), 457–474.
URL: *http://doi.wiley.com/10.1002/nme.4342*

Li, K., Barras, C. D., Chandra, R. V., Kok, H. K., Maingard, J. T., Carter, N. S., Russell, J. H., Lai, L., Brooks, M. & Asadi, H. (2019), 'A Review of the Management of Cerebral Vasospasm After Aneurysmal Subarachnoid Hemorrhage', *World Neurosurgery* **126**, 513–527.
URL: *https://www.sciencedirect.com/science/article/pii/S187887501930751X?via%3Dihub*

Libby, P., Ridker, P. M. & Maseri, A. (2002), 'Inflammation and atherosclerosis', *Circulation* **105**(9), 1135–1143.

Macdonald, R. L. (2006), 'Management of cerebral vasospasm', *Neurosurgical Review* **29**(3), 179–193.

Macdonald, R. L., Weir, B. K. A., Young, J. D. & Grace, M. G. A. (1992), 'Cytoskeletal and extracellular matrix proteins in cerebral arteries following subarachnoid hemorrhage in monkeys', *Journal of Neurosurgery* **76**(1), 81–90.
URL: *http://thejns.org/doi/10.3171/jns.1992.76.1.0081*

Macdonald, R. L., Zhang, J., Sima, B. & Johns, L. (1995), 'Papaverine-sensitive Vasospasm and Arterial Contractility and Compliance after Subarachnoid Hemorrhage in Dogs', *Neurosurgery* **37**(5), 962–968.
URL: *http://dx.doi.org/10.1227/00006123-199511000-00016*

Macdonald, R. & Weir, B. (1991), 'A review of hemoglobin and the pathogenesis of cerebral vasospasm', *Stroke* **22**(8), 971–982. issn:0039-2499, doi:10.1161/01.STR.22.8.971.

Maceri, F., Marino, M. & Vairo, G. (2010), 'A unified multiscale mechanical model for soft collagenous tissues with regular fiber arrangement', *Journal of Biomechanics* **43**(2), 355–363.

Mandaltsi, A. (2016), 'Modelling the mechanobiological evolution of aneurysms: An integrative in vivo, in vitro and in silico approach', *Ph.D. Thesis* .

Marino, M. & Vairo, G. (2013), Multiscale Elastic Models of Collagen Bio-structures: From Cross-Linked Molecules to Soft Tissues, pp. 73–102.

Matsui, T., Kaizu, H., Iron, S. & Asano, T. (1994), 'The role of active smooth-muscle contraction in the occurrence of chronic vasospasm in the canine two-hemorrhage model', *Journal of Neurosurgery* **80**(2), 276–282.
URL: *http://thejns.org/doi/10.3171/jns.1994.80.2.0276*

Mayberg, M., Batjer, H., Dacey, R., Diringer, M., Haley, E., Heros, R., Sternau, L., Torner, J., Adams, H. & Feinberg, W. e. a. (1994), 'Guidelines for the management of aneurysmal subarachnoid hemorrhage', *Circulation* **90(5)**, 2592–2605.

Mayberg, M. R., Okada, T. & Bark, D. H. (1990), 'The significance of morphological changes in cerebral arteries after subarachnoid hemorrhage', *J Neurosurg* **72**, 626–633.

Mizukami, M., Kin, H., Araki, G., Mihara, H. & Yoshida, Y. (1976), 'Is angiographic spasm real spasm?', *Acta Neurochirurgica* **34**(1-4), 247–259.

Nagasawa, S., Handa, H., Naruo, Y., Moritake, K. & Hayashi, K. (1982), 'Experimental cerebral vasospasm arterial wall mechanics and connective tissue composition.', *Stroke* **13**(5), 595–600.
URL: *http://www.ncbi.nlm.nih.gov/pubmed/7123591*

Nakagomi, T., Kassell, N. F., Hongo, K. & Sasaki, T. (1990), 'Pharmacological reversibility of experimental cerebral vasospasm.', *Neurosurgery* **27**(4), 582–6.
URL: *http://www.ncbi.nlm.nih.gov/pubmed/2234362*

Phillippi, J. A., Green, B. R., Eskay, M. A., Kotlarczyk, M. P., Hill, M. R., Robertson, A. M., Watkins, S. C., Vorp, D. A. & Gleason, T. G. (2014), 'Mechanism of aortic medial matrix remodeling is distinct in patients with bicuspid aortic valve', *Journal of Thoracic and Cardiovascular Surgery* **147**(3), 1056–1064.

Pluta, R. M. (2005), 'Delayed cerebral vasospasm and nitric oxide: Review, new hypothesis, and proposed treatment', *Pharmacology and Therapeutics* **105**(1), 23–56.

Provencio, J. & Vora, N. (2005), 'Subarachnoid hemorrhage and inflammation: Bench to bedside and back', *Seminars in Neurology* **25(4)**, 435–444. doi:10.1055/s-2005-923537.

Rachev, A. & Hayashi, K. (1999), Theoretical Study of the Effects of Vascular Smooth Muscle Contraction on Strain and Stress Distributions in Arteries, Technical report.

Reilly, C., Amidei, C., Tolentino, J., Jahromi, B. S. & Macdonald, R. L. (2004), 'Clot volume and clearance rate as independent predictors of vasospasm after aneurysmal subarachnoid hemorrhage', *Journal of Neurosurgery* **101**(2), 255–261.
URL: *https://thejns-org.sheffield.idm.oclc.org/view/journals/j-neurosurg/101/2/article-p255.xml*

Richards, F. J. (1959), 'A flexible growth function for empirical use', *Journal of Experimental Botany* .

Robertson, A. M. & Watton, P. N. (2013), 'Chapter 8 - Mechanobiology of the Arterial Wall', *Transport in Biological Media* pp. 275–347.
URL: *http://www.sciencedirect.com/science/article/pii/B9780124158245000084*

Rothermel, T. M., Win, Z. & Alford, P. W. (2020), 'Large-deformation strain en-

ergy density function for vascular smooth muscle cells', *Journal of Biomechanics* **111**, 110005.

Ryan, J. M. & Humphrey, J. D. (1999), 'Finite Element Based Predictions of Preferred Material Symmetries in Saccular Aneurysms', *Annals of Biomedical Engineering* **27**(5), 641–647.
URL: *http://link.springer.com/10.1114/1.208*

Sacher, M. & Tenner, M. (1978), 'Structural changes of the intradural arteries following subarachnoid haemorrhage', *British Journal of Radiology* **51**(609), 736–738.

Sang, C., Kallmes, D. F., Kadirvel, R., Durka, M. J., Ding, Y. H., Dai, D., Watkins, S. C. & Robertson, A. M. (2020), 'Adaptive Remodeling in the Elastase-Induced Rabbit Aneurysms', *Experimental Mechanics* pp. 1–21.
URL: *https://doi.org/10.1007/s11340-020-00671-9*

Schmid, H., Pauli, L., Paulus, A., Kuhl, E. & Itskov, M. (2012), 'Consistent formulation of the growth process at the kinematic and constitutive level for soft tissues composed of multiple constituents', *Computer Methods in Biomechanics and Biomedical Engineering* **15**(5), 547–561.

Schrauwen, J., Vilanova, A., Rezakhaniha, R., Stergiopulos, N., van de Vosse, F. & Bovendeerd, P. (2012), 'A method for the quantification of the pressure dependent 3d collagen configuration in the arterial adventitia', *Journal of Structural Biology* **180**, 335–342.

Sehgel, N., Sun, Z., Hong, Z., Hunter, W., Hill, M., Vatner, D., Vatner, S. & Meininger, G. (2015), 'Augmented vascular smooth muscle cell stiffness and adhesion when hypertension is superimposed on aging', *Hypertension* **65(2)**, 370–377. doi:10.1161/hypertensionaha.114.04456.

Sehgel, N., Vatner, S. & Meininger, G. (2015), '"smooth muscle cell stiffness syndrome" — revisiting the structural basis of arterial stiffness', *Frontiers in Physiology* **6:335**. doi: 10.3389/fphys.2015.00335.

Smith, R. R., Clower, B. R., Grotendorst, G. M., Yabuno, N. & Cruse, J. M. (1985), 'Arterial wall changes in early human vasospasm'.

Steucke, K. E., Tracy, P. V., Hald, E. S., Hall, J. L. & Alford, P. W. (2015), 'Vascular smooth muscle cell functional contractility depends on extracellular mechanical

properties', *Journal of Biomechanics* **48**(12), 3044–3051.
URL: *https://pubmed.ncbi.nlm.nih.gov/26283412/*

Tulamo, R., Frösen, J., Hernesniemi, J. & Niemelä, M. (2018), 'Inflammatory changes in the aneurysm wall: A review'.

Ushiwata, I. & Ushiki, T. (1990), 'Cytoarchitecture of the smooth muscles and pericytes of rat cerebral blood vessels. A scanning electron microscopic study', *Journal of Neurosurgery* **73**(1), 82–90.
URL: *https://thejns.org/view/journals/j-neurosurg/73/1/article-p82.xml*

Valentín, A., Humphrey, J. & Holzapfel, G. (2013), 'A finite element-based constrained mixture implementation for arterial growth, remodeling, and adaptation: Theory and numerical verification', *International Journal for Numerical Methods in Biomedical Engineering* **29**(8), 822–849.
URL: *http://doi.wiley.com/10.1002/cnm.2555*

Vamsi Krishna, C., Chandran Suja, V., Watton, P. N., Arakeri, J. H. & Gundiah, N. (2020), 'Shear stress rosettes capture the complex flow physics in diseased arteries', *Journal of Biomechanics* **104**, 109721.

Vorkapic, P., Bevan, J. A. & Bevan, R. D. (1991*a*), 'Clentiazem protects against chronic cerebral vasospasm in rabbit basilar artery.', *Stroke* **22**(11), 1409–13.
URL: *http://www.ncbi.nlm.nih.gov/pubmed/1750049*

Vorkapic, P., Bevan, R. & Bevan, J. (1990), 'Pharmacologic irreversible narrowing in chronic cerebrovasospasm in rabbits is associated with functional damage', *Stroke* **21**, 1478–1484.

Vorkapic, P., Bevan, R. D. & Bevan, J. A. (1991*b*), 'Longitudinal time course of reversible and irreversible components of chronic cerebrovasospasm of the rabbit basilar artery.', *Journal of neurosurgery* **74**(6), 951–955.

Watton, P. N., Hill, N. A. & Heil, M. (2004), 'A mathematical model for the growth of the abdominal aortic aneurysm', *Biomechanics and Modeling in Mechanobiology* **3**(2), 98–113.

Watton, P. N., Raberger, N. B., Holzapfel, G. A. & Ventikos, Y. (2009), 'Coupling the Hemodynamic Environment to the Evolution of Cerebral Aneurysms: Computational Framework and Numerical Examples', *Journal of Biomechanical Engineering*

131(10), 101003.
URL: *http://biomechanical.asmedigitalcollection.asme.org/article.aspx?articleid=1475778*

Watton, P. N., Selimovic, A., Raberger, N. B., Huang, P., Holzapfel, G. A. & Ventikos, Y. (2011), 'Modelling evolution and the evolving mechanical environment of saccular cerebral aneurysms', *Biomechanics and Modeling in Mechanobiology* **10**(1), 109–132.

Watton, P., Ventikos, Y. & Holzapfel, G. (2009), 'Modelling the growth and stabilization of cerebral aneurysms', *Mathematical Medicine and Biology* **26(2)**, 133–164.

Webster, K. D., Ng, W. P. & Fletcher, D. A. (2014), 'Tensional homeostasis in single fibroblasts', *Biophysical Journal* **107**(1), 146–155.
URL: */pmc/articles/PMC4119263/ /pmc/articles/PMC4119263/?report=abstract https://www.ncbi.nlm.nih.gov/pmc/articles/PMC4119263/*

Weir, R. M. & BK (1991), 'A review of hemoglobin and the pathogenesis of cerebral vasospasm', *Stroke* (22), 971–982.

Wicker, B. K., Hutchens, H. P., Wu, Q., Yeh, A. T. & Humphrey, J. D. (2008), 'Computer Methods in Biomechanics and Biomedical Engineering Normal basilar artery structure and biaxial mechanical behaviour Normal basilar artery structure and biaxial mechanical behaviour', *Computer Methods in Biomechanics and Biomedical Engineering* **11**(5), 539–551.
URL: *https://www.tandfonline.com/action/journalInformation?journalCode=gcmb20*

Yamaguchi-Okada, M., Nishizawa, S., Koide, M. & Nonaka, Y. (2005), 'Biomechanical and phenotypic changes in the vasospastic canine basilar artery after subarachnoid hemorrhage', *Journal of Applied Physiology* **99**(5), 2045–2052.
URL: *http://www.physiology.org/doi/10.1152/japplphysiol.01138.2004*

Zhang, W., Capilnasiu, A., Sommer, G., Holzapfel, G. A. & Nordsletten, D. A. (2019), An Efficient and Accurate Method for Modeling Nonlinear Fractional Viscoelastic Biomaterials, Technical report.

Zubkov, A. Y., Tibbs, R. E., Clower, B., Ogihara, K., Aoki, K. & Zhang, J. H. (2002), 'Morphological changes of cerebral arteries in a canine double hemorrhage model', *Neuroscience Letters* **326**(2), 137–141.
URL: *https://www-sciencedirect-com.sheffield.idm.oclc.org/science/article/pii/S030439400200188X*

Appendix A

The following code has been used for the implementation of the model presented in Chapter 2.

```
% ---------- WORKSPACE CLEANUP ----------

clear; clc; close all

% ---------- Parameters ---------- #

c_diam_tzero_mm = 2.9;     % physiological diameter at t=0 in mm

c_radius_tzero          = c_diam_tzero_mm * 10^(-3) / (2 * 1.3);
                                % unloaded radius at=0 in m
c_thickness_tzero     = c_radius_tzero/5;       % thickness at t=0
c_pressure_sys        = 16000;    % systolic blood pressure in Pa

% ---------- Initial Stretch Considerations ---------- #

c_lambda_z       = 1.3;
c_lambda_elastin          = 1.3;

c_collagen_ratio_ad_me = 8;

% Collagen distribution in media

c_att_min_me = 1.00001;
c_att_mod_me =  1.01;
c_att_max_me = 1.07;

c_rec_max_me = c_lambda_elastin / c_att_min_me;
c_rec_min_me = c_lambda_elastin / c_att_max_me;
```

```
c_rec_mod_me = c_lambda_elastin / c_att_mod_me;

v_a_me = c_rec_min_me;
v_c_me = c_rec_mod_me;
v_b_me = c_rec_max_me;

% Collagen distribution in adventitia

c_att_min_ad = 0.8;
c_att_mod_ad =  0.9;
c_att_max_ad = 0.99999;

c_rec_max_ad = c_lambda_elastin / c_att_min_ad;
c_rec_min_ad = c_lambda_elastin / c_att_max_ad;
c_rec_mod_ad = c_lambda_elastin / c_att_mod_ad;

v_a_ad = c_rec_min_ad;
v_c_ad = c_rec_mod_ad;
v_b_ad = c_rec_max_ad;

% Muscle stretches: attachment stretch + mean and min
%               for active response

c_lambda_muscle      = 1.15;
c_rec_muscle             = c_lambda_elastin / c_lambda_muscle;

c_musc_mean = 1.1;
c_musc_min = 0.4;
c_vasodil_conc = 0.68;   % Concentration of vasodilators to
                         % vasoconstrictors at homeostasis

c_ge_muscle          = (c_lambda_muscle^2 - 1.0) / 2.0;
                         % from stretch to green strain



% ---------------------- Material Parameters ------------------------- #

% Assign load bearing proportions to each constituent
% then solve force-balance equation for k_(.)
% using systolic blood pressure for P
% and attachment stretches for lambda's
%
```

```
% for example for muscle passive
% c_load_borne_muscle_p * P =
% (H/R) * ( 1 / (lambda * lambda_z) )*sigma_M^pass (lambda_M)
% k_M is inside sigma_M



c_load_borne_elastin    = 0.50;
c_load_borne_muscle_p      = 0.20;
c_load_borne_muscle_a      = 0.20;
c_load_borne_collagen          = 1 - c_load_borne_elastin - ...
                      c_load_borne_muscle_p - c_load_borne_muscle_a;

c_common_factor = ( c_pressure_sys * c_radius_tzero * ...
    c_lambda_elastin^2 * c_lambda_z ) / c_thickness_tzero;

c_k_elastin     = ( c_load_borne_elastin * c_common_factor ) / ...
   ( c_lambda_elastin^2 * ...
( 1 - (1 / ( c_lambda_z^2 * c_lambda_elastin^4)) ) );

c_k_collagen  =( c_load_borne_collagen * c_common_factor ) / ...
( ( 2 * c_lambda_elastin / ( (v_b_me-v_a_me)*(v_c_me-v_a_me) ) )...
*( (v_a_me+c_lambda_elastin)*log(c_lambda_elastin/v_a_me)...
+ 2*(v_a_me-c_lambda_elastin) ) ) ;

c_k_muscle_p = (c_load_borne_muscle_p * c_common_factor ) / ...
  ( c_lambda_muscle^2 * ...
  ( 1 - (1/  ( c_lambda_z^2 * c_lambda_muscle^4) ) )    );

c_k_muscle_a = (c_load_borne_muscle_a * c_common_factor ) / ...
     ( c_vasodil_conc * ( c_lambda_muscle * ( 1 - ...
    ( (c_musc_mean - c_lambda_muscle) ...
    /(c_musc_mean - c_musc_min) )^2 ) )   );



%% ---------- HEALTHY ARTERY ----------

% ----------STRESS FUNCTIONS LOOP -----

 n=235;

 % Storage arrays
```

```
sv_stretch_var = zeros(1,n);
sv_stress_var_elastin = zeros(1,n);
sv_stress_var_collagen = zeros(1,n);
sv_stress_var_muscle_a = zeros(1,n);
sv_stress_var_muscle_p = zeros(1,n);
sv_stress_var_muscle_t = zeros(1,n);
sv_stress_var_total = zeros(1,n);
sv_pressure_var = zeros(1,n);
sv_pressure_var_elastin = zeros(1,n);
sv_pressure_var_collagen = zeros(1,n);
sv_pressure_var_muscle = zeros(1,n);
sv_pressure_var_muscle_a = zeros(1,n);
sv_pressure_var_muscle_p = zeros(1,n);
sv_pressure_var_collagen_me = zeros(1,n);
sv_pressure_var_collagen_ad = zeros(1,n);
% Loop

for i=1:n

    % Initialize stretch
    sv_stretch_var(i) = 0.55 + (i-1)*0.01;

    % Define stress functions
   v_lambda_collagen    = @(x) x / c_rec_collagen;
   v_lambda_muscle      = @(x) x / c_rec_muscle;
   v_m = @(x) (x / c_rec_muscle);

   v_ge_collagen    = @(x) (v_lambda_collagen(x)^2 - 1.0) / 2.0;
   v_ge_muscle          = @(x) (v_lambda_muscle(x)^2 - 1.0) / 2.0;
   v_ge                     = @(x) ( x^2 - 1 ) / 2;

   v_sigma_elastin          = @(x) x^2 * c_k_elastin * ...
       ( 1 - (1 /  ( c_lambda_z^2 * x^4 ) ) );
   v_sigma_muscle_p     = @(x) v_lambda_muscle(x)^2 *...
       c_k_muscle_p * ...
       ( 1 - (1 / (c_lambda_z^2 * v_lambda_muscle(x)^4)) );
   v_sigma_muscle_a     = @(x)    c_vasodil_conc * c_k_muscle_a * ...
       v_m(x)  * ( 1 - ( (c_musc_mean - v_m(x)) ...
       / (c_musc_mean - c_musc_min) )^2 );
   v_sigma_muscle_t     = @(x) v_sigma_muscle_a(x) ...
       + v_sigma_muscle_p(x) ;
```

```
% Collagen Cauchy stresses in media

v_gamma_me  = c_k_collagen / ...
    ( (v_b_me - v_a_me) * (v_c_me - v_a_me)  );
v_delta_me  = c_k_collagen / ...
    ( (v_b_me - v_a_me) * (v_b_me - v_c_me) );

v_sigma_collagen_me_0       = @(x) x * 0;
v_sigma_collagen_me_ac      = @(x) x * v_gamma_me * 2 * ...
    ( (x + v_a_me) * log(x/v_a_me) + 2*(v_a_me - x) ) ;
v_sigma_collagen_me_cb      = @(x) x * v_gamma_me * 2 * ...
    ( (x + v_a_me)*log(v_c_me/v_a_me) + v_a_me - v_c_me + ...
    ( (v_a_me - v_c_me) / v_c_me ) * x) ...
    - x * v_delta_me * 2 * ( (x + v_b_me)*log(x/v_c_me) + ...
    v_b_me + v_c_me - ( (v_b_me + v_c_me) / v_c_me ) * x );
v_sigma_collagen_me_b       = @(x) x * v_gamma_me * 2 * ...
    ( (x + v_a_me)*log(v_c_me/v_a_me) + v_a_me - v_c_me + ...
    ( (v_a_me - v_c_me) / v_c_me ) * x) ...
    - x * v_delta_me * 2 * ( (x + v_b_me)*log(v_b_me/v_c_me) ...
    - v_b_me + v_c_me - ( (v_b_me - v_c_me) / v_c_me ) * x );

v_sigma_collagen_me   =@(x) ...
    v_sigma_collagen_me_0(x).*(x<v_a_me)...
    + v_sigma_collagen_me_ac(x).*( x>=v_a_me & x<v_c_me)...
    + v_sigma_collagen_me_cb(x).*(x>=v_c_me & x<=v_b_me)...
    + v_sigma_collagen_me_b(x).*(x>v_b_me);

% Collagen Cauchy stresses in adventitia

v_gamma_ad                  =  c_collagen_ratio_ad_me * ...
    c_k_collagen / ( (v_b_ad - v_a_ad) * (v_c_ad - v_a_ad)  );
v_delta_ad                  =  c_collagen_ratio_ad_me *...
    c_k_collagen / ( (v_b_ad - v_a_ad) * (v_b_ad - v_c_ad) );

v_sigma_collagen_ad_0       = @(x) x * 0;
v_sigma_collagen_ad_ac      = @(x) x * v_gamma_ad * 2 * ...
    ( (x + v_a_ad) * log(x/v_a_ad) + 2*(v_a_ad - x) ) ;
v_sigma_collagen_ad_cb      = @(x) x * v_gamma_ad * 2 * ...
    ( (x + v_a_ad)*log(v_c_ad/v_a_ad) + v_a_ad - v_c_ad + ...
    ( (v_a_ad - v_c_ad) / v_c_ad ) * x) ...
    - x * v_delta_ad * 2 * ( (x + v_b_ad)*log(x/v_c_ad) + ...
    v_b_ad + v_c_ad - ( (v_b_ad + v_c_ad) / v_c_ad ) * x );
v_sigma_collagen_ad_b       = @(x) x * v_gamma_ad * 2 * ...
```

```
    ( (x + v_a_ad)*log(v_c_ad/v_a_ad) + v_a_ad - v_c_ad + ...
    ( (v_a_ad - v_c_ad) / v_c_ad ) * x) ...
    - x * v_delta_ad * 2 * ( (x + v_b_ad)*log(v_b_ad/v_c_ad) - ...
    v_b_ad + v_c_ad - ( (v_b_ad - v_c_ad) / v_c_ad ) * x );

v_sigma_collagen_ad          =@(x) v_sigma_collagen_ad_0(x).*...
    (x<v_a_ad)...
    + v_sigma_collagen_ad_ac(x).*( x>=v_a_ad & x<v_c_ad)...
    + v_sigma_collagen_ad_cb(x).*(x>=v_c_ad & x<=v_b_ad)...
    + v_sigma_collagen_ad_b(x).*(x>v_b_ad);

v_sigma_collagen    =@(x) v_sigma_collagen_me(x) +...
                      v_sigma_collagen_ad(x);


v_pres_prefactor     = @(x) c_thickness_tzero / ...
    ( c_radius_tzero * c_lambda_z * x^2 );

v_pressure_ECM = @(x) v_pres_prefactor(x) * ...
    ( v_sigma_elastin(x) + v_sigma_collagen(x) + v_sigma_muscle_t(x) );
v_pressure_EC = @(x) v_pres_prefactor(x) * ...
    ( v_sigma_elastin(x) + v_sigma_collagen(x) );
v_pressure_EM = @(x) v_pres_prefactor(x) * ...
    ( v_sigma_elastin(x) + v_sigma_muscle_t(x) );
v_pressure_E = @(x) v_pres_prefactor(x) * ( v_sigma_elastin(x) );

v_pressure_elastin       = @(x) v_pres_prefactor(x) *...
                         v_sigma_elastin(x);
v_pressure_collagen      = @(x) v_pres_prefactor(x) * ....
                         v_sigma_collagen(x);
v_pressure_muscle        = @(x) v_pres_prefactor(x) * ...
                         v_sigma_muscle_t(x);
v_pressure_muscle_a        = @(x) v_pres_prefactor(x) * ...
                         v_sigma_muscle_a(x);
v_pressure_muscle_p        = @(x) v_pres_prefactor(x) * ...
                         v_sigma_muscle_p(x);
v_pressure_collagen_me      = @(x) v_pres_prefactor(x) * ...
                         v_sigma_collagen_me(x);
v_pressure_collagen_ad      = @(x) v_pres_prefactor(x) * ...
                         v_sigma_collagen_ad(x);


% Store results
```

```
    sv_stress_var_elastin(i) = v_sigma_elastin(sv_stretch_var(i));
    sv_stress_var_collagen(i) = v_sigma_collagen(sv_stretch_var(i));
    sv_stress_var_muscle_a(i) = v_sigma_muscle_a(sv_stretch_var(i));
    sv_stress_var_muscle_p(i) = v_sigma_muscle_p(sv_stretch_var(i));
    sv_stress_var_muscle_t(i) = v_sigma_muscle_t(sv_stretch_var(i));
    sv_stress_var_total(i) = sv_stress_var_elastin(i) + ...
        sv_stress_var_collagen(i) + sv_stress_var_muscle_t(i);

    sv_pressure_var_elastin(i) = v_pressure_elastin(sv_stretch_var(i));


    sv_pressure_var_elastin(i)       = max( v_pressure_elastin( ...
        sv_stretch_var(i)) , 0 );
    sv_pressure_var_collagen(i)      =v_pressure_collagen(...
        sv_stretch_var(i));
    sv_pressure_var_collagen_me(i)   =v_pressure_collagen_me(...
        sv_stretch_var(i));
    sv_pressure_var_collagen_ad(i)  =v_pressure_collagen_ad(...
        sv_stretch_var(i));
    sv_pressure_var_muscle_p(i)  = max( v_pressure_muscle_p(...
        sv_stretch_var(i)) , 0 );
    sv_pressure_var_muscle_a(i) = max( v_pressure_muscle_a(...
        sv_stretch_var(i)) , 0 );
    sv_pressure_var_muscle(i)   = sv_pressure_var_muscle_a(i) + ...
        sv_pressure_var_muscle_p(i); ...
    sv_pressure_var(i)     = sv_pressure_var_elastin(i) +...
    sv_pressure_var_collagen_me(i) +...
         sv_pressure_var_collagen_ad(i) + sv_pressure_var_muscle(i);


end


%% ---------------- PLOTS PRESSURE VS STRETCH

n_zoom = 120;

figure

hold on
plot(sv_stretch_var(1:n_zoom), ...
    sv_pressure_var(1:n_zoom)./(10^3),'LineWidth',2)
```

```
plot(sv_stretch_var(33:n_zoom),...
    sv_pressure_var_elastin(33:n_zoom)./(10^3), '--','LineWidth',2)
plot(sv_stretch_var(65:n_zoom),...
    sv_pressure_var_collagen_me(65:n_zoom)./(10^3), '--','LineWidth',2)
plot(sv_stretch_var(65:n_zoom),...
    sv_pressure_var_collagen_ad(65:n_zoom)./(10^3), '--','LineWidth',2)
plot(sv_stretch_var(45:n_zoom),...
    sv_pressure_var_muscle_p(45:n_zoom)./(10^3),'--', 'LineWidth',2)
plot(sv_stretch_var(1:n_zoom),...
    sv_pressure_var_muscle_a(1:n_zoom)./(10^3), '--', 'LineWidth',2)
plot(sv_stretch_var(1:n_zoom),...
    sv_pressure_var(1:n_zoom)./(10^3),'LineWidth',2)
hold off
legend('Total','Elastin','Collagen media', 'Collagen adve',...
    'Muscle Passive', 'Muscle Active','Location','northwest')

xlabel('Stretch')
ylabel('Pressure (kPa)')
set(gca, 'fontsize', 16)



%% ---------- PAPER - PRESSURE VS DIAMETER - CONSTITUENTS


n_zoom = 125;

sv_diam_var = 2 * c_radius_tzero * 10^3 * sv_stretch_var;

sv_pressure_var_smc = sv_pressure_var_muscle_a + ...
    sv_pressure_var_muscle_p;
sv_pressure_var_coll = sv_pressure_var_collagen_me + ...
    sv_pressure_var_collagen_ad;
sv_pressure_var2 = sv_pressure_var_elastin + ...
    sv_pressure_var_coll + sv_pressure_var_smc;

figure

hold on
plot(sv_diam_var(1:n_zoom),...
    sv_pressure_var2(1:n_zoom)./(10^3),'k','LineWidth',6)
plot(sv_diam_var(33:n_zoom),...
```

```
    sv_pressure_var_elastin(33:n_zoom)./(10^3), 'k—','LineWidth',3)
plot(sv_diam_var(67:n_zoom),...
    sv_pressure_var_coll(67:n_zoom)./(10^3), 'k-.','LineWidth',3)
plot(sv_diam_var(45:n_zoom),...
    sv_pressure_var_muscle_p(45:n_zoom)./(10^3),'k+', 'LineWidth',2)
plot(sv_diam_var(1:n_zoom),...
    sv_pressure_var_muscle_a(1:n_zoom)./(10^3), 'k.', 'LineWidth',2)
plot(sv_diam_var(1:n_zoom),...
    sv_pressure_var2(1:n_zoom)./(10^3),'k','LineWidth',6)
line([2.9 2.9],[0 16],'color','red','LineStyle','—','LineWidth',2)
line([1 2.9],[16 16],'color','red','LineStyle','—','LineWidth',2)
plot(2.9, 16, 'ro', 'LineWidth',3)
hold off
legend('Total','E','C','VSMCp', 'VSMCa', 'Location','northwest')

xlabel('Diameter (mm)')
ylabel('Pressure (kPa)')
set(gca, 'fontsize', 24)
ylim([0 60])
```

```
%% ———————— VASOSPASM ————————


c_stiffness_factor  = 1.1;
c_k_muscle_p        = c_stiffness_factor * c_k_muscle_p;
c_k_muscle_a        = c_stiffness_factor * c_k_muscle_a;

%v_rec_collagen      =  c_rec_collagen;
v_rec_muscle        = 0.72;         % New recruitment stretch for SMC


% ——————————————————————STRESS FUNCTIONS LOOP ———
```

```
n=215;

sv_stretch_var = zeros(1,n);
sv_stress_var_elastin = zeros(1,n);
sv_stress_var_collagen = zeros(1,n);
sv_stress_var_muscle_a = zeros(1,n);
sv_stress_var_muscle_p = zeros(1,n);
sv_stress_var_muscle_t = zeros(1,n);
sv_stress_var_total = zeros(1,n);
sv_pressure_var = zeros(1,n);
sv_pressure_var_elastin = zeros(1,n);
sv_pressure_var_collagen = zeros(1,n);
sv_pressure_var_muscle = zeros(1,n);
sv_pressure_var_muscle_a = zeros(1,n);
sv_pressure_var_muscle_p = zeros(1,n);



for i=1:n

    % Initialize stretch

    sv_stretch_var(i) = 0.55 + (i-1)*0.01;

    % Define stress functions

    v_lambda_collagen    = @(x) x / v_rec_collagen;
    v_lambda_muscle      = @(x) x / v_rec_muscle;

    v_ge_collagen    = @(x) (v_lambda_collagen(x)^2 - 1.0) / 2.0;
    v_ge_muscle      = @(x) (v_lambda_muscle(x)^2 - 1.0) / 2.0;
    v_ge         = @(x) ( x^2 - 1 ) / 2;

    v_sigma_elastin          = @(x) x^2 * c_k_elastin * ...
        ( 1 - (1 / ( c_lambda_z^2 * x^4 ) ) );
    v_sigma_muscle_p     = @(x) v_lambda_muscle(x)^2 *...
        c_k_muscle_p * ...
        ( 1 - (1 / (c_lambda_z^2 *v_lambda_muscle(x)^4 )) );
    v_sigma_muscle_a     = @(x) 0.952 * v_lambda_muscle(x) *....
        c_k_muscle_a * ( 1 - ...
        ( (c_musc_mean - v_lambda_muscle(x)) / ...
        (c_musc_mean - c_musc_min) )^2);
    v_sigma_muscle_t     = @(x) v_sigma_muscle_a(x) +...
```

```
    v_sigma_muscle_p(x) ;

 % Collagen Cauchy stresses in media

v_gamma_me                  = c_k_collagen / ...
    ( (v_b_me - v_a_me) * (v_c_me - v_a_me)  );
v_delta_me                      = c_k_collagen / ...
    ( (v_b_me - v_a_me) * (v_b_me - v_c_me) );

v_sigma_collagen_me_0       = @(x) x * 0;
v_sigma_collagen_me_ac      = @(x) x * v_gamma_me *...
    2 * ( (x + v_a_me) * log(x/v_a_me) + 2*(v_a_me - x) ) ;
v_sigma_collagen_me_cb      = @(x) x * v_gamma_me * ...
    2 * ( (x + v_a_me)*log(v_c_me/v_a_me) + v_a_me - ...
    v_c_me + ( (v_a_me - v_c_me) / v_c_me ) * x) ...
    - x * v_delta_me * 2 * ( (x + v_b_me)*log(x/v_c_me) +...
    v_b_me + v_c_me - ( (v_b_me + v_c_me) / v_c_me ) * x );
v_sigma_collagen_me_b       = @(x) x * v_gamma_me * 2 *...
    ( (x + v_a_me)*log(v_c_me/v_a_me) + v_a_me - v_c_me + ...
    ( (v_a_me - v_c_me) / v_c_me ) * x) ...
    - x * v_delta_me * 2 * ( (x + v_b_me)*log(v_b_me/v_c_me) ...
    - v_b_me + v_c_me - ( (v_b_me - v_c_me) / v_c_me ) * x );

v_sigma_collagen_me =@(x) v_sigma_collagen_me_0(x).*...
    (x<v_a_me)...
    + v_sigma_collagen_me_ac(x).*( x>=v_a_me & x<v_c_me)...
    + v_sigma_collagen_me_cb(x).*(x>=v_c_me & x<=v_b_me)...
    + v_sigma_collagen_me_b(x).*(x>v_b_me);

% Collagen Cauchy stresses in adventitia

v_gamma_ad                  =  c_collagen_ratio_ad_me *...
    c_k_collagen / ( (v_b_ad - v_a_ad) * (v_c_ad - v_a_ad)  );
v_delta_ad                      =  c_collagen_ratio_ad_me * ...
    c_k_collagen / ( (v_b_ad - v_a_ad) * (v_b_ad - v_c_ad) );

v_sigma_collagen_ad_0       = @(x) x * 0;
v_sigma_collagen_ad_ac      = @(x) x * v_gamma_ad * 2 * ...
    ( (x + v_a_ad) * log(x/v_a_ad) + 2*(v_a_ad - x) ) ;
v_sigma_collagen_ad_cb      = @(x) x * v_gamma_ad * 2 * ...
    ( (x + v_a_ad)*log(v_c_ad/v_a_ad) + v_a_ad - v_c_ad + ...
    ( (v_a_ad - v_c_ad) / v_c_ad ) * x) ...
    - x * v_delta_ad * 2 * ( (x + v_b_ad)*log(x/v_c_ad) + ...
```

```
    v_b_ad + v_c_ad - ( (v_b_ad + v_c_ad) / v_c_ad ) * x );
v_sigma_collagen_ad_b       = @(x) x * v_gamma_ad * 2 *...
    ( (x + v_a_ad)*log(v_c_ad/v_a_ad) + v_a_ad - v_c_ad + ...
    ( (v_a_ad - v_c_ad) / v_c_ad ) * x) ...
    - x * v_delta_ad * 2 * ( (x + v_b_ad)*log(v_b_ad/v_c_ad) -...
    v_b_ad + v_c_ad - ( (v_b_ad - v_c_ad) / v_c_ad ) * x );

v_sigma_collagen_ad          =@(x) v_sigma_collagen_ad_0(x).*...
    (x<v_a_ad)...
    + v_sigma_collagen_ad_ac(x).*( x>=v_a_ad & x<v_c_ad)...
    + v_sigma_collagen_ad_cb(x).*(x>=v_c_ad & x<=v_b_ad)...
    + v_sigma_collagen_ad_b(x).*(x>v_b_ad);

v_sigma_collagen             =@(x) v_sigma_collagen_me(x) +...
    v_sigma_collagen_ad(x);



v_pres_prefactor    = @(x) c_thickness_tzero / ...
    ( c_radius_tzero * c_lambda_z * x^2 );


v_pressure_ECM = @(x) v_pres_prefactor(x) * ...
    ( v_sigma_elastin(x) + v_sigma_collagen(x) +...
    v_sigma_muscle_t(x) );
v_pressure_EC = @(x) v_pres_prefactor(x) * ...
    ( v_sigma_elastin(x) + v_sigma_collagen(x) );
v_pressure_EM = @(x) v_pres_prefactor(x) * ...
    ( v_sigma_elastin(x) + v_sigma_muscle_t(x) );
v_pressure_CM = @(x) v_pres_prefactor(x) *...
    ( v_sigma_collagen(x) + v_sigma_muscle_t(x) );
v_pressure_E = @(x) v_pres_prefactor(x) *...
    ( v_sigma_elastin(x) );
v_pressure_C = @(x) v_pres_prefactor(x) *...
    ( v_sigma_collagen(x) );
v_pressure_M = @(x) v_pres_prefactor(x) *...
    (  v_sigma_muscle_t(x) );


v_pressure_elastin      = @(x) v_pres_prefactor(x) *...
    v_sigma_elastin(x);
v_pressure_collagen     = @(x) v_pres_prefactor(x) * ...
    v_sigma_collagen(x);
```

```
v_pressure_muscle_p        = @(x) v_pres_prefactor(x) * ...
    v_sigma_muscle_p(x);
v_pressure_muscle_a        = @(x) v_pres_prefactor(x) *...
    v_sigma_muscle_a(x);
v_pressure_muscle          = @(x) v_pres_prefactor(x) * ...
    v_sigma_muscle_t(x);
v_pressure_collagen_me     = @(x) v_pres_prefactor(x) * ...
    v_sigma_collagen_me(x);
v_pressure_collagen_ad     = @(x) v_pres_prefactor(x) * ...
    v_sigma_collagen_ad(x);


% Store results

sv_stress_var_elastin(i) = v_sigma_elastin(sv_stretch_var(i));
sv_stress_var_collagen(i) = v_sigma_collagen(sv_stretch_var(i));
sv_stress_var_muscle_a(i) = v_sigma_muscle_a(sv_stretch_var(i));
sv_stress_var_muscle_p(i) = v_sigma_muscle_p(sv_stretch_var(i));
sv_stress_var_muscle_t(i) = v_sigma_muscle_t(sv_stretch_var(i));
sv_stress_var_total(i) = sv_stress_var_elastin(i) +...
    sv_stress_var_collagen(i) + sv_stress_var_muscle_t(i);


sv_pressure_var_elastin(i)      = max( ...
    v_pressure_elastin(sv_stretch_var(i)) , 0 );
sv_pressure_var_collagen(i)     = max( ...
    v_pressure_collagen(sv_stretch_var(i)) , 0 );
sv_pressure_var_muscle_p(i)     = max( ...
    v_pressure_muscle_p(sv_stretch_var(i)) , 0 );
sv_pressure_var_muscle_a(i)     = max( ...
    v_pressure_muscle_a(sv_stretch_var(i)) , 0 );
sv_pressure_var_muscle(i)       = sv_pressure_var_muscle_a(i) +...
    sv_pressure_var_muscle_p(i); ...
sv_pressure_var(i)    = sv_pressure_var_elastin(i) + ...
sv_pressure_var_collagen(i) +...
sv_pressure_var_muscle_p(i) + sv_pressure_var_muscle_a(i);
sv_pressure_var_collagen_me(i)     = max(...
    v_pressure_collagen_me(sv_stretch_var(i)), 0 );
sv_pressure_var_collagen_ad(i)     = max( ...
    v_pressure_collagen_ad(sv_stretch_var(i)), 0 );


end
```

```
diameters = [1, 1.5, 2, 2.5, 3, 3.5, 4, 4.5];
forces_sol6 = [0.0897, 0.0215, 0.0172, 0.0141, 0.0127, 0.0109, ...
    0.0080, 0];
forces_sol4 = [0.0202, 0.0132, 0.0103, 0.0089, 0.0074, 0.0066, 0, 0];
forces_capt3 = [0.0317, 0.0178, 0.0132, 0.0109, 0.0042, 0, 0, 0];
forces_trevo420 = [0.0257, 0.0061, 0.0031, 0.0009, 0, 0, 0, 0];


query_stretches = 0.55:0.01:3;
query_radii = c_radius_tzero * 10^3 * query_stretches;
query_diam = 2 * query_radii;

interpolate_forces = @(x)  interp1(diameters,x,query_diam,'linear');
    interp_forces_sol6       = interpolate_forces(forces_sol6);
    interp_forces_sol4        = interpolate_forces(forces_sol4);
    interp_forces_capt3      = interpolate_forces(forces_capt3);
    interp_forces_trevo420   = interpolate_forces(forces_trevo420);

force_to_pressure = @(x) 10^3 * x ./ query_radii;
    interp_pressure_sol6   = force_to_pressure(interp_forces_sol6);
    interp_pressure_sol4   = force_to_pressure(interp_forces_sol4);
    interp_pressure_capt3 = force_to_pressure(interp_forces_capt3);
    interp_pressure_trevo420 = force_to_pressure(...
        interp_forces_trevo420);



%% ---------- PAPER - PRESSURE VS DIAMETER - CONSTITUENTS

figure

n_zoom = 115;

sv_diam_var = 2 * c_radius_tzero * 10^3 * sv_stretch_var;

sv_pressure_var_coll = sv_pressure_var_collagen_me + ...
    sv_pressure_var_collagen_ad;

hold on
plot(sv_diam_var(1:n_zoom),...
sv_pressure_var(1:n_zoom)./(10^3), 'k', 'LineWidth', 6)
plot(sv_diam_var(34:n_zoom),...
```

```
    sv_pressure_var_elastin(34:n_zoom)./(10^3), 'k—', 'LineWidth', 3)
plot(sv_diam_var(67:n_zoom),...
    sv_pressure_var_coll(67:n_zoom)./(10^3), 'k-.','LineWidth', 3)
plot(sv_diam_var(9:n_zoom),...
    sv_pressure_var_muscle_p(9:n_zoom)./(10^3), 'k+','LineWidth', 2)
plot(sv_diam_var(1:76),...
    sv_pressure_var_muscle_a(1:76)./(10^3), 'k.','LineWidth', 3)
plot(sv_diam_var(1:n_zoom),...
    sv_pressure_var(1:n_zoom)./(10^3), 'k', 'LineWidth', 6)
line([1.46 1.46],[0 16],'color','red','LineStyle','—','LineWidth',2)
line([1 1.46],[16 16],'color','red','LineStyle','—','LineWidth',2)
plot(1.46, 16, 'ro', 'LineWidth',3)
hold off
legend('Total','E','C','VSMCp', 'VSMCa','Location','northwest')
xlabel('Diameter (mm)')
ylabel('Pressure (kPa)')
ylim([0, 60])
set(gca, 'fontsize', 24)



%% ———— COLLAGEN REMODELLING ————————————————

c_tissue_stretch_cvs = c_lambda_muscle * v_rec_muscle;

c_rec_min_vs_me = c_tissue_stretch_cvs / c_att_max_me;
c_rec_mod_vs_me = c_tissue_stretch_cvs / c_att_mod_me;
c_rec_max_vs_me = c_tissue_stretch_cvs / c_att_min_me;
    v_a_vs_me = c_rec_min_vs_me;
    v_c_vs_me = c_rec_mod_vs_me;
    v_b_vs_me = c_rec_max_vs_me;

c_rec_min_vs_ad = c_tissue_stretch_cvs / c_att_max_ad;
c_rec_mod_vs_ad = c_tissue_stretch_cvs / c_att_mod_ad;
c_rec_max_vs_ad = c_tissue_stretch_cvs / c_att_min_ad;
    v_a_vs_ad = c_rec_min_vs_ad;
    v_c_vs_ad = c_rec_mod_vs_ad;
    v_b_vs_ad = c_rec_max_vs_ad;

t_start = 0;
t_end = 30;
t_step = 0.01;
t = t_start : t_step : t_end;
```

```
halflife = 72;
alpha = 1 / halflife;

f =@(t) exp(-alpha.*t);

    % Collagen Cauchy stresses in media - VASOSPASM

v_gamma_vs_me                    = c_k_collagen /...
    ( (v_b_vs_me - v_a_vs_me) * (v_c_vs_me - v_a_vs_me)  );
v_delta_vs_me                      = c_k_collagen / ...
    ( (v_b_vs_me - v_a_vs_me) * (v_b_vs_me - v_c_vs_me) );

v_sigma_collagen_vs_me_0         = @(x) x * 0;
v_sigma_collagen_vs_me_ac        = @(x) x * v_gamma_vs_me * 2 *...
    ( (x + v_a_vs_me) * log(x/v_a_vs_me) + 2*(v_a_vs_me - x) ) ;
v_sigma_collagen_vs_me_cb        = @(x) x * v_gamma_vs_me * 2 *...
    ( (x + v_a_vs_me)*log(v_c_vs_me/v_a_vs_me) + v_a_vs_me -...
    v_c_vs_me + ( (v_a_vs_me - v_c_vs_me) / v_c_vs_me ) * x) ...
    - x * v_delta_vs_me * 2 * ( (x + v_b_vs_me)*log(x/v_c_vs_me) + ...
    v_b_vs_me + v_c_vs_me - ( (v_b_vs_me + v_c_vs_me) /...
    v_c_vs_me ) * x );
v_sigma_collagen_vs_me_b         = @(x) x * v_gamma_vs_me * 2 *...
    ( (x + v_a_vs_me)*log(v_c_vs_me/v_a_vs_me) + v_a_vs_me -...
    v_c_vs_me + ( (v_a_vs_me - v_c_vs_me) / v_c_vs_me ) * x) ...
    - x * v_delta_vs_me * 2 * ( (x + v_b_vs_me)*log(v_b_vs_me/...
    v_c_vs_me) - v_b_vs_me + v_c_vs_me - ((v_b_vs_me - v_c_vs_me)...
    / v_c_vs_me ) * x );

v_sigma_collagen_vs_me  =@(x) v_sigma_collagen_vs_me_0(x).*...
    (x<v_a_vs_me)...
    + v_sigma_collagen_vs_me_ac(x).*...
    ( x>=v_a_vs_me & x<v_c_vs_me)...
    + v_sigma_collagen_vs_me_cb(x).*...
    (x>=v_c_vs_me & x<=v_b_vs_me)...
    + v_sigma_collagen_vs_me_b(x).*(x>v_b_vs_me);

% Collagen Cauchy stresses in adventitia - VASOSPASM

v_gamma_vs_ad  =  c_collagen_ratio_ad_me * c_k_collagen / ...
    ( (v_b_vs_ad - v_a_vs_ad) * (v_c_vs_ad - v_a_vs_ad)  );
v_delta_vs_ad =  c_collagen_ratio_ad_me * c_k_collagen / ...
    ( (v_b_vs_ad - v_a_vs_ad) * (v_b_vs_ad - v_c_vs_ad) );
```

```
v_sigma_collagen_vs_ad_0       = @(x) x * 0;
v_sigma_collagen_vs_ad_ac      = @(x) x * v_gamma_vs_ad * 2 * ...
    ( (x + v_a_vs_ad) * log(x/v_a_vs_ad) + 2*(v_a_vs_ad - x) ) ;
v_sigma_collagen_vs_ad_cb      = @(x) x * v_gamma_vs_ad * 2 *...
    ( (x + v_a_vs_ad)*log(v_c_vs_ad/v_a_vs_ad) + v_a_vs_ad - ...
    v_c_vs_ad + ( (v_a_vs_ad - v_c_vs_ad) / v_c_vs_ad ) * x) ...
    - x * v_delta_vs_ad * 2 * ( (x + v_b_vs_ad)*log(x/v_c_vs_ad) +...
    v_b_vs_ad + v_c_vs_ad - ( (v_b_vs_ad + v_c_vs_ad) / v_c_vs_ad )...
    * x );
v_sigma_collagen_vs_ad_b       = @(x) x * v_gamma_vs_ad * 2 *...
    ( (x + v_a_vs_ad)*log(v_c_vs_ad/v_a_vs_ad) + v_a_vs_ad - ...
    v_c_vs_ad + ( (v_a_vs_ad - v_c_vs_ad) / v_c_vs_ad ) * x) ...
    - x * v_delta_vs_ad * 2 * ( (x + v_b_vs_ad)*...
    log(v_b_vs_ad/v_c_vs_ad) - v_b_vs_ad + v_c_vs_ad - ...
    ( (v_b_vs_ad - v_c_vs_ad) / v_c_vs_ad ) * x );

v_sigma_collagen_vs_ad =@(x) v_sigma_collagen_vs_ad_0(x).*...
    (x<v_a_vs_ad)...
    + v_sigma_collagen_vs_ad_ac(x).*...
    ( x>=v_a_vs_ad & x<v_c_vs_ad)...
    + v_sigma_collagen_vs_ad_cb(x).*...
    (x>=v_c_vs_ad & x<=v_b_vs_ad)...
    + v_sigma_collagen_vs_ad_b(x).*(x>v_b_vs_ad);

v_sigma_collagen_healthy       =@(x) v_sigma_collagen_me(x) + ...
    v_sigma_collagen_ad(x);
v_sigma_collagen_vs             =@(x) v_sigma_collagen_vs_me(x) +...
    v_sigma_collagen_vs_ad(x);

v_pressure_collagen_vs_me      = @(x) v_pres_prefactor(x) * ...
    v_sigma_collagen_vs_me(x);
v_pressure_collagen_vs_ad      = @(x) v_pres_prefactor(x) * ...
    v_sigma_collagen_vs_ad(x);

sv_pressure_var_collagen_vs_me = zeros(1,n);
sv_pressure_var_collagen_vs_ad = zeros(1,n);
sv_pressure_var_coll_vs = zeros(1,n);
sv_pressure_coll_0 = zeros(1,n);
sv_pressure_coll_5 = zeros(1,n);
sv_pressure_coll_10 = zeros(1,n);
sv_pressure_coll_15 = zeros(1,n);
sv_pressure_coll_20 = zeros(1,n);
```

```
sv_pressure_coll_25 = zeros(1,n);
sv_pressure_coll_30 = zeros(1,n);

for i=1:n

    sv_stretch_var(i) = 0.55 + (i-1)*0.01;

    sv_pressure_var_collagen_vs_me(i)      = max( ...
        v_pressure_collagen_vs_me(sv_stretch_var(i)), 0 );
    sv_pressure_var_collagen_vs_ad(i)      = max( ...
        v_pressure_collagen_vs_ad(sv_stretch_var(i)), 0 );
    sv_pressure_var_coll_vs(i)= sv_pressure_var_collagen_vs_me(i) ...
                          + sv_pressure_var_collagen_vs_ad(i);

    sv_pressure_coll_0(i) = f(0) * sv_pressure_var_coll(i) +...
        (1-f(0)) * sv_pressure_var_coll_vs(i);
    sv_pressure_coll_5(i) = f(5) * sv_pressure_var_coll(i) +...
        (1-f(5)) * sv_pressure_var_coll_vs(i);
    sv_pressure_coll_10(i) = f(10) * sv_pressure_var_coll(i) +...
        (1-f(10)) * sv_pressure_var_coll_vs(i);
    sv_pressure_coll_15(i) = f(15) * sv_pressure_var_coll(i) +...
        (1-f(15)) * sv_pressure_var_coll_vs(i);
    sv_pressure_coll_20(i) = f(20) * sv_pressure_var_coll(i) +...
        (1-f(20)) * sv_pressure_var_coll_vs(i);
    sv_pressure_coll_25(i) = f(25) * sv_pressure_var_coll(i) +...
        (1-f(25)) * sv_pressure_var_coll_vs(i);
    sv_pressure_coll_30(i) = f(30) * sv_pressure_var_coll(i) +...
        (1-f(30)) * sv_pressure_var_coll_vs(i);

end


%% ------ REMODELLING VS TIME ---------------- MASS VS TIME ----------------

n_zoom=125;
n_start=20;


figure
hold on
plot(sv_diam_var(n_start:n_zoom),...
    sv_pressure_coll_5(n_start:n_zoom)./(10^3), 'k', 'LineWidth', 2)
plot(sv_diam_var(n_start:n_zoom),...
```

```
    sv_pressure_coll_10(n_start:n_zoom)./(10^3), 'r', 'LineWidth', 2)
plot(sv_diam_var(n_start:n_zoom),...
    sv_pressure_coll_15(n_start:n_zoom)./(10^3), 'r-.', 'LineWidth', 2)
plot(sv_diam_var(n_start:n_zoom),...
    sv_pressure_coll_20(n_start:n_zoom)./(10^3), 'k--', 'LineWidth', 2)
plot(sv_diam_var(n_start:n_zoom),...
    sv_pressure_coll_25(n_start:n_zoom)./(10^3), 'm', 'LineWidth', 2)
plot(sv_diam_var(n_start:n_zoom),...
    sv_pressure_coll_30(n_start:n_zoom)./(10^3), 'k-.', 'LineWidth', 2)
hold off
ylim([ 0 60 ])
xlabel('Diameter')
ylabel('Collagen pressure contribution')
legend('t=5','t=10','t=15','t=20','t=25','t=30','Location','northwest')
set(gca, 'fontsize', 24)


figure
hold on
plot(t,f(t), 'k', 'LineWidth', 2)
plot(t,1-f(t), 'k--', 'LineWidth',2)
hold off
xlabel('Time (days)')
ylabel('Mass proportion')
legend('Old collagen', 'New collagen')
set(gca, 'fontsize', 24)

saveas(gcf,'1dmodel_colremod_massvstime.png');


%% --- DAY 7 REMODELLING FOR DIFFERENT HALFLIVES -----

fhl =@(x) exp(-7/x);

sv_pressure_var_collagen_vs_me = zeros(1,n);
sv_pressure_var_collagen_vs_ad = zeros(1,n);
sv_pressure_var_coll_vs = zeros(1,n);
sv_pressure_coll_hl5 = zeros(1,n);
sv_pressure_coll_hl10 = zeros(1,n);
sv_pressure_coll_hl15 = zeros(1,n);
sv_pressure_coll_hl30 = zeros(1,n);
sv_pressure_coll_hl45 = zeros(1,n);
sv_pressure_coll_hl60 = zeros(1,n);
```

```
sv_pressure_coll_hl72 = zeros(1,n);

sv_pressure_var_tot_hl5 = zeros(1,n);
sv_pressure_var_tot_hl10 = zeros(1,n);
sv_pressure_var_tot_hl15 = zeros(1,n);
sv_pressure_var_tot_hl30 = zeros(1,n);
sv_pressure_var_tot_hl45 = zeros(1,n);
sv_pressure_var_tot_hl60 = zeros(1,n);
sv_pressure_var_tot_hl72 = zeros(1,n);

sv_pressure_var_part = sv_pressure_var_elastin +...
    sv_pressure_var_muscle_a + sv_pressure_var_muscle_p;

for i=1:n

    sv_stretch_var(i) = 0.55 + (i-1)*0.01;

    sv_pressure_var_collagen_vs_me(i)     = max( ...
        v_pressure_collagen_vs_me(sv_stretch_var(i)), 0 );
    sv_pressure_var_collagen_vs_ad(i)     = max( ...
        v_pressure_collagen_vs_ad(sv_stretch_var(i)), 0 );
    sv_pressure_var_coll_vs(i)  = sv_pressure_var_collagen_vs_me(i) ...
                                    + sv_pressure_var_collagen_vs_ad(i);

    sv_pressure_coll_hl5(i) = fhl(5) * sv_pressure_var_coll(i) +...
        (1-fhl(5)) * sv_pressure_var_coll_vs(i);
    sv_pressure_coll_hl10(i) = fhl(10) * sv_pressure_var_coll(i) +...
        (1-fhl(10)) * sv_pressure_var_coll_vs(i);
    sv_pressure_coll_hl15(i) = fhl(15) * sv_pressure_var_coll(i) +...
        (1-fhl(15)) * sv_pressure_var_coll_vs(i);
    sv_pressure_coll_hl30(i) = fhl(30) * sv_pressure_var_coll(i) +...
        (1-fhl(30)) * sv_pressure_var_coll_vs(i);
    sv_pressure_coll_hl45(i) = fhl(45) * sv_pressure_var_coll(i) +...
        (1-fhl(45)) * sv_pressure_var_coll_vs(i);
    sv_pressure_coll_hl60(i) = fhl(60) * sv_pressure_var_coll(i) +...
        (1-fhl(60)) * sv_pressure_var_coll_vs(i);
    sv_pressure_coll_hl72(i) = fhl(72) * sv_pressure_var_coll(i) +...
        (1-fhl(72)) * sv_pressure_var_coll_vs(i);

    sv_pressure_var_tot_hl5(i) = sv_pressure_var_part(i) +...
        sv_pressure_coll_hl5(i);
    sv_pressure_var_tot_hl10(i) = sv_pressure_var_part(i) + ...
        sv_pressure_coll_hl10(i);
```

```
    sv_pressure_var_tot_hl15(i) = sv_pressure_var_part(i) + ...
        sv_pressure_coll_hl15(i);
    sv_pressure_var_tot_hl30(i) = sv_pressure_var_part(i) +...
        sv_pressure_coll_hl30(i);
    sv_pressure_var_tot_hl45(i) = sv_pressure_var_part(i) +...
        sv_pressure_coll_hl45(i);
    sv_pressure_var_tot_hl60(i) = sv_pressure_var_part(i) +...
        sv_pressure_coll_hl60(i);
    sv_pressure_var_tot_hl72(i) = sv_pressure_var_part(i) + ...
        s.v_pressure_coll_hl72(i);

end


figure

n_zoom = 115;
sv_diam_var = 2 * c_radius_tzero * 10^3 * sv_stretch_var;
sv_pressure_var_coll = sv_pressure_var_collagen_me + ...
    sv_pressure_var_collagen_ad;

hold on

plot(sv_diam_var(1:n_zoom),...
    sv_pressure_var_tot_hl5(1:n_zoom)./(10^3), 'k—', 'LineWidth', 2)
plot(sv_diam_var(1:n_zoom),...
    sv_pressure_var_tot_hl10(1:n_zoom)./(10^3), 'k-.', 'LineWidth', 2)
plot(sv_diam_var(1:n_zoom),...
    sv_pressure_var_tot_hl15(1:n_zoom)./(10^3), 'k.', 'LineWidth', 2)
plot(sv_diam_var(1:n_zoom),...
    sv_pressure_var_tot_hl30(1:n_zoom)./(10^3), 'b', 'LineWidth', 2)
plot(sv_diam_var(1:n_zoom),...
    sv_pressure_var_tot_hl45(1:n_zoom)./(10^3), 'b—', 'LineWidth', 2)
plot(sv_diam_var(1:n_zoom),...
    sv_pressure_var_tot_hl60(1:n_zoom)./(10^3), 'b-.', 'LineWidth', 2)
plot(sv_diam_var(1:n_zoom),...
    sv_pressure_var_tot_hl72(1:n_zoom)./(10^3), 'b.', 'LineWidth', 2)
plot(sv_diam_var(1:n_zoom),...
    sv_pressure_var(1:n_zoom)./(10^3), 'k', 'LineWidth', 2)

plot(sv_diam_var(1:n_zoom),16+ interp_pressure_sol6(1:n_zoom),...
    'm','LineWidth', 4)
```

```
line([1.46 1.46],[0 16],'color','red','LineStyle','--','LineWidth',2)
line([1 1.46],[16 16],'color','red','LineStyle','--','LineWidth',2)
plot(1.46, 16, 'ro', 'LineWidth',3)

line([2.96 2.96], [0 60], 'color', 'red', 'LineWidth', 6)

hold off
legend('HL = 5 days','HL = 10 days','HL = 15 days', 'HL = 30 days', ...
    'HL = 45 days', 'HL = 60 days', 'HL = 72 days', 'no remodelling',...
    'Solitaire 6', 'Location','northwest')
xlabel('Diameter (mm)')
ylabel('Pressure (kPa)')
ylim([0, 60])
set(gca, 'fontsize', 16)

saveas(gcf,'1dmodel_colremod_stenteval.png');
```

Appendix B

The following are subroutines that constitute key command sequences in the finite element framework presented in Chapter3 and applied to cerebral vasospasm in Chapter 4. The following subroutines are reported:

- **cacgmodel.f** is the main subroutine that calls the material models for each constituents and computes the stresses;
- **umacr6.f** contains several subroutines governing the evolution of the tissue, such as collagen and VSMC remodelling, increase in active stress response and damage. Subroutines in this file are called from the input file by command *gmac* followed by the four-lettered label of the desired subroutine;
- **activestressd.f**, **activecircumfdam.f**, **fiberremdistdam.f** and **fibdistdam.f** relate to the material models of VSMCs and collagen and compute the first and second derivative of the SEDF in the appropriate material directions.

The following is the code contained in **cacgmodel.f**

```
c       Editor: Thomas S.E. Eriksson

        subroutine cacgmodel(F,finv,jacc,ud,l,h1,nh,sig,dd,isw)

c       * * F E A P * * A Finite Element Analysis Program

c.... Copyright (c) 1984-2010: Regents of the University of California
c                              All rights reserved
c-----[--.----+----.----+----.-----------------------------------------]
c       Modification log                                 Date (dd/mm/year)
c         Original version                                   19/04/2013
c-----[--.----+----.----+----.-----------------------------------------]
c       Purpose: User Constitutive Model (AFCG)
c                Arterial Fiber Composite Growth model
```

```
c     Input:
c          F(*)    -  Current strains at point      (small deformation)
c                  -  Deformation gradient at point (finite deformation)
c          finv(*) -  Inverse of deformation gradient(finite deformation)
c          jacc     -  Trace of strain at point
c                  -  Determinant of deformation gradient
c          ud(*)   -  User material parameters (nud)
c          l       -  Current quadrature point number

c     Output:
c          sig(*)  -  Stresses at point.
c                     N.B. 1-d models use only sig(1)
c          dd(6,*) -  Current material tangent moduli
c                     N.B. 1-d models use only dd(1,1) and dd(2,1)
c-----[--.----+----.----+----.-----------------------------------------]
      implicit none

      integer  l,isw,nh
      real*8   F(3,3),finv(3,3),jacc,ud(*),sig(10),dd(6,6)

c     Model parameters
      real*8   h1(nh)
      real*8   jm13, jm12          ! J^{-1/3} modified jacobian
      real*8   invdet          ! J^{-1} inverse jacobian
      real*8   pdgr(3)         ! growth in principal directions
c      real*8   Ft(3,3)         ! Modified deformation gradient F*J^{-1/3}
      real*8   Ft(3,3)         ! Transpose of deformation gradient
      real*8   Fmod(3,3)       ! Modified (isochoric) deformation gradient
      real*8   Fmodt(3,3)      ! transpose of modified (isochoric) deformation gradient
      real*8   detfg,detll        ! determinant of growth deformation gradient
      real*8   Fg(3,3)
c      real*8   invFg(3,3)
      real*8   rCG(3,3)        ! right Cauchy-Green tensor
      real*8   lCG(3,3)        ! left Cauchy-Green tensor
      real*8   tau_f(6)        ! Kirchoff stress, fiber
      real*8   tau_ff          ! Kirchoff stress, in fiber
      real*8   tau_e(6)        ! Kirchoff stress, elastin
      real*8   tau_gm(6)       ! Kirchoff stress, ground matrix
      real*8   taucir
      real*8   dd_ma(6,6)
      real*8   dd_mp(6,6)
      real*8   tau_ma(6)
```

```
      real*8   tau_mp(6)
      real*8   l1,l2,l3
      real*8   kt, kmp, dmd
      real*8   dd_f(6,6)       ! Tangent moduli, fiber
      real*8   dd_e(6,6)       ! Tangent moduli, elastin
      real*8   dd_gm(6,6)      ! Tangent moduli, ground matrix
      real*8   be(6)           ! Left Cauchy-Green tensor
      real*8   anl(3)          ! Fiber vector, Lagrangian
      real*8   ni(3),nii(3),nni(3)          ! Normal vector, intermediate
      real*8   nn(3,3)          ! Normal tensor product, intermediate
      real*8   ani(3,2)       ! Fiber vector, intermediate
      real*8   ane(3)          ! Fiber vector, Eulerian
      real*8   FDTN(nel),FDTG
      real*8   vhat
      real*8   am(3)
      real*8   bm(3)
      real*8   I4mh
      real*8   I4m_r0
      real*8   I4t
      real*8   norm, xdiff, ydiff, zdiff
      real*8 test_colmod
      integer  i,j,k,ff,ndirv    ! Counters
      integer  cnp             ! Closest element node to quadrature point
      integer  clnode          ! Closest node number to quadrature point
      integer  neld            ! Number of elements with direction vectors
      integer nnum(nel)
      integer eln
      integer isoan, eliso     ! flag: 0 - no growth; 1 - isotropic growth; 2 - trans
      logical isogr            ! flag: true - isotropic growth; false - anisotropic g

c     Include header file, general in FEAP
      include  'eldata.h'
      include  'iofile.h'
      include  'pconstant.h'
      include  'pointer.h'
      include  'comblk.h'
      include  'sdata.h'
      include  'cdata.h'
      include  'fluco.h'
      include  'teln.h'
      include  'tdata.h'
      include  'pfeapb.h'
      include  'elcoor.h'
```

```
c      include  'defgrd.h'
c     Include header files, problem specific
c      include  'grow.h'
      include  'grup.h'
      include  'gpcoord.h'
      include  'umac1.h'
      include  'upar.h'
      include  'volg.h'
      include  'afcgparam.h'
      include 'qudshp.h'
      include  'fibstr.h'
      include 'vsmc.h'
      include 'damage.h'

C      if (hr(up(5)).eq.0) then
C        call asspoint(hr(up(5)),nhex*3*8)
C        call asspoint(hr(up(6)),nhex*3*8)
C      endif

      if (nvolu(l,n).EQ.0.0d0) then
        nvolu(l,n) = 1.0d0
      endif
      vhat = nvolu(l,n)
      if (jacc.EQ.0.0d0) then
         WRITE(*,*) 'oops!'
      endif
      invdet = nvolu(l,n)/jacc   ! inverse of modified J^e
      jm13 = invdet**(one3)      !

c     Retrieve and store the gauss point coordinates
      do i = 1,3
        gpcl(i,l,n) = xref(i)
C        call asspoint(hr(up(5)+(n-1)*8*3+(l-1)*3+i),xref(i))
        gpce(i,l,n) = xcur(i)
C        call asspoint(hr(up(6)+(n-1)*8*3+(l-1)*3+i),xcur(i))
      enddo

      if (fsgtrue) then
C        INTERPOLATE FD TO GPs
c        Retrieve the element node numbers
         do i = 1,nel
           nnum(i) = mr(np(33) + i-1 + nen1*(n-1))
         enddo
```

```
c         Use global node number if paralell run
          if (pfeap_on) then
            do i = 1,nel
              nnum(i) = mr(np(244) + nnum(i) - 1 )
            enddo
          endif
c         Retrieve FD for each node
          do i = 1,nel
c             FDTN(i) = hr(up(7)+nnum(i))
             FDTN(i) = FDND(nnum(i))
          enddo
c         Retreive FD interpolation at quadrature point
          FDTG = 0.0d0
          do i = 1,nel
             FDTG = FDTG+shp3(4,i,l)*FDTN(i)
          enddo
c         call asspoint(hr(up(8)+(n-1)*8+l),FDTN)
          fdgp(l,n) = FDTG
        endif ! fsgtrue

c       Compute Fg
c       Compute right and left Cauchy-Green tensor

c       Initialize arrays
        call pzero(tau_e,6)         ! Stress Elastin
        call pzero(tau_gm,6)        ! Stress Ground matrix
        call pzero(tau_ma,6)        ! Stress Muscle Active
        call pzero(tau_mp,6)        ! Stress Muscle Passive
        call pzero(dd_e,36)         ! Tangent stiffness matrix Elastin
        call pzero(dd_gm,36)        ! Tangent stiffness matrix Ground matrix
        call pzero(dd_ma,36)        ! Tangent stiffness matrix Muscle Active
        call pzero(dd_mp,36)        ! Tangent stiffness matrix Muscle Passive
        call pzero(Fg,9)            ! Growth tensor

c       Convert quadrature point to closest node in element
        call gp2np( l, cnp )

c       Find closest node to quadrature point
        clnode =  mr(np(33) + cnp-1 + nen1*(n-1))

c       Use global node number if paralell run
        if (pfeap_on) then
```

```
        clnode = mr(np(244) + clnode - 1 )
      endif

c     Retrieve number of fiber families
      ndirv = nint( hr(up(2)) )

c     Loop over number of fiber families
      do ff = 1,ndirv
c       Retrieve fiber angles
        if (direl) then
c       If dirv is used (direction vectors on element centers)
          do j = 1,3
            anl(j) = hr(up(2)+(n-1)*3*ndirv+ (ff-1)*3 + j)
          enddo
        endif
        if (dirno) then
c       If ndir is used (direction vectors on nodes)
          call prvec(1,ndirv,ff,anl)  !Can't be used with user,21 element
c           do j = 1,3
c             anl(j) = hr(up(2)+(clnode-1)*3*ndirv+(ff-1)*3 + j)
c           enddo
         endif
c       Store direction vectors in 2 columns
        do i = 1,3
          ani(i,ff) = anl(i)
        enddo
      enddo
      isoan = volg(1)
      eliso = volg(2)
      if ((isoan .eq. 2) .or. (isoan .eq. 3)) then
c      Cross product to find normal
      if (ndirv .eq. 1) then
         ni(1) = 0.0d0
         ni(2) = 0.0d0
         ni(3) = 1.0d0
      else
         ni(1) = ani(2,1)*ani(3,2)-ani(3,1)*ani(2,2)
         ni(2) = -(ani(1,1)*ani(3,2)-ani(3,1)*ani(1,2))
         ni(3) = ani(1,1)*ani(2,2)-ani(2,1)*ani(1,2)
      endif
      call normalizevector(ni,nni)

      do i = 1,3
```

```
            do j = 1,3
               nn(i,j) = nni(i)*nni(j)
            enddo
          enddo
          endif !calculate normal
            do i=1,3
              Fg(i,i) = 1.0d0
            enddo
          if ((isoan .EQ. 1) .OR. (eliso .EQ. 1)) then
            ! isotropic growth
            vhat = vhat**(-one3)
            do i=1,3
              Fg(i,i) = vhat
            enddo
          else if ((isoan .EQ. 2) .OR. (eliso .EQ. 2)) then
            ! transversely isotropic (in-plane)
            vhat = vhat**one2
            do i = 1,3
              Fg(i,i) = vhat
            enddo
            do i = 1,3
             do j = 1,3
               Fg(i,j) = Fg(i,j) + nn(i,j)*(1.0d0-vhat)
             enddo
           enddo
           call invert3(Fg,detfg)
          else if ((isoan .EQ. 3) .OR. (eliso .EQ. 3)) then
            ! transversely isotropic (in-thickness)
c            do i = 1,3
c              Fg(i,i) = Fg(i,i) + 1.0d0
c            enddo
            do i = 1,3
             do j = 1,3
             Fg(i,j) = Fg(i,j) - nn(i,j)*(1.0d0-vhat)
             enddo
           enddo
           call invert3(Fg,detfg)
c         else
c            WRITE(*,*) 'Volumetric growth model not supported!'
          else if ((isoan .EQ. 4) .OR. (eliso .EQ. 4)) then
              ! transversely isotropic (cross-section)
            vhat = vhat**one2
            Fg(1,1) = vhat
```

```
          Fg(2,2) = vhat
          call invert3(Fg,detfg)
        else if ((isoan .EQ. 5) .OR. (eliso .EQ. 5)) then
          ! transversely isotropic (axial growth)
          Fg(3,3) = vhat
          call invert3(Fg,detfg)
        end if

c       call invert3(Fg,detfg)
        call pzero(Fmod,9)

c       call matrixmult(F,Fg,Fmod)
        do i=1,3
          do j=1,3
            do k=1,3
              Fmod(i,j) = Fmod(i,j) + F(i,k)*Fg(k,j)
            enddo
            Fmod(i,j) = Fmod(i,j)*jm13
          enddo
        enddo
c       write (*,*) Fmod
c       lCG is now modified (isochoric) lCg!
        call matrixtranspose(Fmod,Fmodt)
        call matrixmult(Fmod,Fmodt,lCG)
c       Get left Cauchy tensor in Voigt notation
        call voigt(lCG,be)



c       Loop over number of fiber families
        do ff = 1,ndirv
c         Initialize fiber contributions
          call pzero(tau_f,6)
          call pzero(dd_f,36)

c         Compute direction vectors in eulerian description
          do i = 1,3
            ane(i) = 0.0d0
          enddo

          do i= 1,3
            do j= 1,3
              ane(i) = ane(i) + Fmod(i,j)*ani(j,ff)
```

```
            enddo
          enddo

c         Number of ELement with Direction vectors
          neld = nint(hr(up(4)))

c          Store Eulerian fiber angles
          do j = 1,3
          if (direl) then
c            If dirv is used (dirv on element)
            hr(up(3)+(n-1)*3*ndirv+(ff-1)*3+j) = ane(j)
          endif
          if (dirno) then
c            If ndir is used (dirv on nodes)
            hr(up(3)+(clnode-1)*3*ndirv+(ff-1)*3 + j) = ane(j)
          endif
          enddo

c          Calculate Kirchoff stresses and tangent
          call fiberremdistdam(ff,l,ud(4),ane,dam_f, tau_f,tau_ff,dd_f)

          sigff(ff,l,n)=tau_ff
c         Sum up fiber contributions
          do i = 1,6
            sig(i) = sig(i) + ndensc(ff,l,n)*tau_f(i)
            do j = 1,6
              dd(i,j) = dd(i,j) + ndensc(ff,l,n)*dd_f(i,j)
            enddo
          enddo
        enddo



c       Compute contribution to stresses and elasticity due to elastin
c       Only do this for material 1 (media). [ma stored in eldata.h]
c       AG 07.12.2015: no need to pass jacc! be is already modified
        if (ma.eq.1) then
          call neohookdam(ud(3),be,dam_el, tau_e,dd_e)
c            call fungmodel(ud(3),ud(3)/10,be,tau_e,dd_e)
c       Elastin degradation
          do i = 1,6
            tau_e(i) = ndense(l,n)*tau_e(i)
            do j = 1,6
```

```
            dd_e(i,j) = ndense(l,n)*dd_e(i,j)
          enddo
        enddo
      endif

c     Comp. contr. to stresses and elasticity due to ground matrix
c     AG 07.12.2015: no need to pass jacc! be is already modified
      call neohookdam(ud(2),be,dam_gm, tau_gm,dd_gm)
c      call fungmodel(ud(2),ud(3)/10,be,tau_gm,dd_gm)

c     Ground matrix response to elastin degradation
      do i = 1,6
        tau_gm(i) = ndensg(l,n)*tau_gm(i)
          do j = 1,6
c           dd_e(i,j) = fe(l,n)*dd_e(i,j)
            dd_gm(i,j) = ndensg(l,n)*dd_gm(i,j)
          enddo
      enddo



c     Comp. contr. to stresses and elasticity due to passive muscle
c     AG 07.12.2015: no need to pass jacc! be is already modified
      kmp=kp(l,n)
      call neohookdam(ud(6),be,dam_mp, tau_mp,dd_mp)


c    Sum up elastin and ground matrix contribution
      do i = 1,6
        sig(i) = sig(i) + tau_e(i) + tau_gm(i) + tau_mp(i)
        do j = 1,6
          dd(i,j) = dd(i,j) + dd_e(i,j) + dd_gm(i,j) + dd_mp(i,j)
        enddo
      enddo

c     Compute contribution to active muscle stress
c     am = structure tensor
c     bm = F*am
      xdiff = (gpcl(1,1,n) - gpcl(1,2,n))
      ydiff = (gpcl(2,1,n) - gpcl(2,2,n))
      norm = SQRT(xdiff*xdiff + ydiff*ydiff)
      am(1) = xdiff / norm
      am(2) = ydiff / norm
      am(3) = 0.0d0
```

```
c       am(1) = ani(1,1)/SQRT(ani(1,1)*ani(1,1)+ani(2,1)*ani(2,1))
c       am(2) = ani(2,1)/SQRT(ani(1,1)*ani(1,1)+ani(2,1)*ani(2,1))
c       am(3) = 0.0d0
c       am = (/ 1.0d0,0.0d0,0.0d0 /)
        do i = 1,3
          bm(i) = 0.0d0
        enddo
        do i= 1,3
          do j= 1,3
            bm(i) = bm(i) + Fmod(i,j)*am(j)
          enddo
        enddo


        l1 = 0.4d0
        l2 = 1.1d0
        l3 = 1.8d0
        I4t = I4m(l,n)
        kt = ka(l,n)
        dmd = dMa(l,n)
        call activestressd(l,ud(5),l1,l2,l3,bm,dmd,kt,tau_ma,taucir,dd_Ma)
        sigvsmc(l,n) = taucir



c     Add active contribution to previous ones
        do i = 1,6
          sig(i) = sig(i) + tau_Ma(i)
          do j = 1,6
            dd(i,j) = dd(i,j) + dd_Ma(i,j)
          enddo
        enddo



c       Turn Kirchhoff stress into Cauchy stress
c        invdet = 1.0/jacc
!        invdet = nvolu(l,n)/jacc
        do i = 1,6
          sig(i) = sig(i)*invdet
          do j = 1,6
            dd(j,i) = dd(j,i)*invdet
          end do
```

```
      end do


c     Add volumetric component
      call afcgvolumetric(ud,l,jacc,sig,dd)

      end
```

The following is the code contained in **umacr6.f**

```
      subroutine umacr6(lct,ctl)

c     * * F E A P * * A Finite Element Analysis Program

c.... Copyright (c) 1984-2010: Regents of the University of California
c                              All rights reserved

c-----[--.----+----.----+----.-----------------------------------------]
c     Modification log                                 Date (dd/mm/year)
c       Original version                                   01/11/2006
c       1. Remove 'prt' from argument list                 09/07/2009
c-----[--.----+----.----+----.-----------------------------------------]
c     Purpose:  User interface for adding solution command language
c               instructions.

c     Inputs:
c        lct       - Command character parameters
c        ctl(3)    - Command numerical parameters
c     Outputs:
c        N.B.  Users are responsible for command actions.  See
c              programmers manual for example.
c-----[--.----+----.----+----.-----------------------------------------]
      implicit  none



      include  'iofile.h'
      include  'cdata.h'
      include  'eldata.h'
      include  'sdata.h'
      include  'tdata.h'
      include  'comblk.h'
      include  'pointer.h'
      include  'umac1.h'
      include  'grup.h'
      include  'gpcoord.h'
      include  'fluco.h'
      include  'afcgparam.h'
      include  'teln.h'
      include  'epar.h'
```

```
      include  'upar.h'
      include  'volg.h'
      include  'fibstr.h'
      include  'pconstant.h'
      include  'vsmc.h'
      include  'damage.h'

      logical   pcomp
      character lct*15
      real*8    ctl(3)
      integer   ff,fff,l,eln,ndirv
      integer   varinit
      integer   uprecr
      integer   uprecc
      integer   uprecd
      integer   uprecs
      integer   upcoll, upelas, upesog, upgrma
      integer   upcolc
      integer   upcolls
      integer   eldeg_hom
      integer   eldeg_half
      integer   eldeg_halfc
      integer   eldeg_spot
      integer   eldeg_exp
      integer   eldeg_test
      integer   eldeg_fluid
      integer   eldeg_flumod
      logical   smc_rem_cvs
      logical   smc_rem_hom
      logical   dmg_vsmc
      logical   ks_remod
      logical   ks_increase
      logical   ks_decrease
      integer   matnum
      integer   pnv,deb
      real*8    F(3,3)
      real*8    lini  ! length at which remodell. begins
      real*8    lend  ! length at which it ends
      real*8    alpha
      real*8    I4at
      real*8    I4et
      real*8    I4ea(2)
      real*8    I4r
```

```
      real*8     I4mrh, I4m_r0
      real*8     I4mh
      real*8     I4m_r_cvs
      real*8     dI4m_r
      real*8     dI4m
      real*8     dmgmax
      real*8     lam_dmg_min, lam_dmg_max, diff
      real*8     fe0
      real*8     cmin
      real*8     Tend
      real*8     muv
      real*8     DMAX
      real*8     lamz
      real*8     Lv
      real*8     z
      real*8     Lve
      real*8     beta
      real*8     beta0
      real*8     phi
      real*8     volfrg(2)
      real*8     volfre(2)
      real*8     volfrgp(2)
      real*8     volfrep(2)
      real*8     volfrc(4)
      real*8 test_colmod
      real*8     sigh, dsig, sigat, k1
      real*8     maxI4c,minI4c,meanI4c, dlamr, dmass
      real*8     dks
      real*8     atmin, atmod, atmax
      logical    eldeg_step,wri,homeost
      logical    CID_c,CID_e,CID_g
      logical    collsig,recrsig
      logical    volchange
      save

c     Set command word

      if(pcomp(uct,'mac6',4)) then        ! Usual     form
       uct = 'GMAC'                      ! Specify 'name'
      elseif(urest.eq.1) then             ! Read  restart data

      open(unit=98,file='teln.restart',status='old')
       read(98,'(4(i6))') nhex,nqua,ntet,ntri
```

```
      close(98)

      open(unit=98,file='growth1.restart',status='old')
       read(98,'(E14.6)') I4at
       read(98,'(E14.6)') alpha
       read(98,'(E14.6)') beta0
       read(98,'(E14.6)') fe0
       read(98,'(E14.6)') cmin
       read(98,'(E14.6)') Tend
       read(98,'(E14.6)') muv
       read(98,'(E14.6)') DMAX
       read(98,'(E14.6)') Lv
       read(98,'(E14.6)') Lve
       read(98,'(E14.6)') volfrg(1)
       read(98,'(E14.6)') volfrg(2)
       read(98,'(E14.6)') volfre(1)
       read(98,'(E14.6)') volfre(2)
       read(98,'(E14.6)') volfrc(1)
       read(98,'(E14.6)') volfrc(2)
       read(98,'(E14.6)') volfrc(3)
       read(98,'(E14.6)') volfrc(4)
       read(98,'(E14.6)') volfrgp(1)
       read(98,'(E14.6)') volfrgp(2)
      close(98)


      open(unit=98,file='growth2.restart',status='unknown')

c       Recruitment variable and normalized density variable
        do eln = 1,nhex !numel
          do l = 1,8
            read(98,'(E14.6)') fe(l,eln)
            read(98,'(E14.6)') nmasse(l,eln)
            read(98,'(E14.6)') ndense(l,eln)
            read(98,'(E14.6)') nmassg(l,eln)
            read(98,'(E14.6)') ndensg(l,eln)
            read(98,'(E14.6)') nvolu(l,eln)
            do ff = 1,nint( hr(up(2)) )
              read(98,'(E14.6)') lamr(ff,l,eln)
              read(98,'(E14.6)') fco(ff,l,eln)
              read(98,'(E14.6)') nmassc(ff,l,eln)
              read(98,'(E14.6)') ndensc(ff,l,eln)
            enddo
```

```
      enddo
    enddo
  close(98)

  elseif(urest.eq.2) then              ! Write restart data

  open(unit=98,file='growth1.restart',status='unknown')
   write(98,'(E14.6)') I4at
   write(98,'(E14.6)') alpha
   write(98,'(E14.6)') beta0
   write(98,'(E14.6)') fe0
   write(98,'(E14.6)') cmin
   write(98,'(E14.6)') Tend
   write(98,'(E14.6)') muv
   write(98,'(E14.6)') DMAX
   write(98,'(E14.6)') Lv
   write(98,'(E14.6)') Lve
   write(98,'(E14.6)') volfrg(1)
   write(98,'(E14.6)') volfrg(2)
   write(98,'(E14.6)') volfre(1)
   write(98,'(E14.6)') volfre(2)
   write(98,'(E14.6)') volfrc(1)
   write(98,'(E14.6)') volfrc(2)
   write(98,'(E14.6)') volfrc(3)
   write(98,'(E14.6)') volfrc(4)
   write(98,'(E14.6)') volfrgp(1)
   write(98,'(E14.6)') volfrgp(2)
  close(98)


  open(unit=98,file='growth2.restart',status='unknown')

c       Recruitment variable and normalized density variable
        do eln = 1,nhex !numel
          do l = 1,8
            write(98,'(E14.6)') fe(l,eln)
            write(98,'(E14.6)') nmasse(l,eln)
            write(98,'(E14.6)') ndense(l,eln)
            write(98,'(E14.6)') nmassg(l,eln)
            write(98,'(E14.6)') ndensg(l,eln)
            write(98,'(E14.6)') nvolu(l,eln)
            do ff = 1,nint( hr(up(2)) )
              write(98,'(E14.6)') lamr(ff,l,eln)
```

```
            write(98,'(E14.6)') fco(ff,l,eln)
            write(98,'(E14.6)') nmassc(ff,l,eln)
            write(98,'(E14.6)') ndensc(ff,l,eln)
          enddo
        enddo
      enddo
      close(98)

      else                                  ! Perform user operation

c     Initialize input
      varinit = 0
      uprecr = 0
      uprecc = 0
      uprecs = 0
      upcoll = 0
      upcolc = 0
      upcolls = 0
      upelas = 0
      upgrma = 0
      upesog = 0
      uprecd = 0
      eldeg_hom = 0
      eldeg_exp = 0
      eldeg_half = 0
      eldeg_halfc = 0
      eldeg_spot = 0
      eldeg_test = 0
      eldeg_fluid = 0
      eldeg_flumod = 0
      eldeg_step = .false.
      wri = .false.
      homeost = .false.
      CID_c = .false.
      CID_g = .false.
      CID_e = .false.
      volchange = .false.
      collsig = .false.
      recrsig = .false.
      smc_rem_hom = .false.
      dmg_vsmc = .false.
      ks_remod = .false.
      ks_increase = .false.
```

```
      ks_decrease = .false.

c     Which type CID (true) or CIV (false) for the consitutents
      if (volg(1).ge.1.0d0) CID_c = .true.
      if (volg(2).ge.1.0d0) CID_e = .true.
      if (CID_e) CID_g = .true.

c     Check input
      if (pcomp(lct,'init',4)) then
        varinit = 1 ! Initialize variables
      elseif (pcomp(lct,'recr',4)) then
        uprecr = 1 ! update recruitment variable
      elseif (pcomp(lct,'recc',4)) then
        uprecc = 1 ! update recruitment variable (constant over element)
      elseif (pcomp(lct,'recs',4)) then
        uprecs = 1 ! update recruitment variable - stabilization fase
      elseif (pcomp(lct,'coll',4)) then
        upcoll = 1 ! update mass of collagen (stretch based)
      elseif (pcomp(lct,'colc',4)) then
        upcolc = 1 ! update mass of collagen (stretch based) (constant over element)
      elseif (pcomp(lct,'recd',4)) then
        uprecd = 1 ! update mass of collagen (distribution stretch based)
      elseif (pcomp(lct,'cols',4)) then
        upcolls = 1 ! update mass of collagen (stretch based) - stabilization fase
      elseif (pcomp(lct,'edho',4)) then
        eldeg_hom = 1 ! Elastin degradation (exponential function)
      elseif (pcomp(lct,'edex',4)) then
        eldeg_exp = 1 ! Elastin degradation (exponential function)
      elseif (pcomp(lct,'edha',4)) then
        eldeg_half = 1 ! Elastin degradation (half length)
      elseif (pcomp(lct,'edhc',4)) then
        eldeg_halfc = 1 ! Elastin degradation (half length)
      elseif (pcomp(lct,'edsp',4)) then
        eldeg_spot = 1 ! Elastin degradation (half length)
c      elseif (pcomp(lct,'edte',4)) then
c        eldeg_test = 1 ! Elastin degradation test
      elseif (pcomp(lct,'edfc',4)) then
        eldeg_fluid = 1 ! Elastin degradation - fluid coupling
      elseif (pcomp(lct,'edfm',4)) then
        eldeg_flumod = 1 ! Elastin degradation - fluid coupling
      elseif (pcomp(lct,'edst',4)) then
        eldeg_step = .true. ! Elastin degradation (step wise)
      elseif (pcomp(lct,'elas',4)) then
```

```
        upelas = 1 ! update mass of elastin (stretch based)
      elseif (pcomp(lct,'esog',4)) then
        upesog = 1 ! update mass of elastin (stretch based)
      elseif (pcomp(lct,'grma',4)) then
        upgrma = 1 ! update mass of elastin (stretch based)
      elseif (pcomp(lct,'home',4)) then
        homeost = .true. ! Set homeostatic state
      elseif (pcomp(lct,'nvol',4)) then
        volchange = .true. ! Set normalized volume and densities
      elseif (pcomp(lct,'writ',4)) then
        wri = .true. ! Write output
      elseif (pcomp(lct,'csig',4)) then
        collsig = .true. ! Update mass of collagen (stress based)
      elseif (pcomp(lct,'rsig',4)) then
        recrsig = .true. ! Update recruitment variable (stress based)
      elseif (pcomp(lct,'vsmh',4)) then
        smc_rem_hom = .true. ! Smooth muscle remodelling in health
      elseif (pcomp(lct,'dmgm',4)) then
        dmg_vsmc = .true.     ! Active VSMC damage
      elseif (pcomp(lct,'ksrm',4)) then
        ks_remod = .true.
      elseif (pcomp(lct,'ksup',4)) then
        ks_increase = .true.
      elseif (pcomp(lct,'ksdw',4)) then
        ks_decrease = .true.
      else
        write(*,*) 'Invalid gmac specification'
      endif
      ndirv = nint( hr(up(2)) )

c     Initialize paramters ------------------------------------------------------------------
      if (varinit.eq.1) then
c       Attachment stretch
c        I4at =  1.196d0 !1.146d0 !1.19d0 !W2009 1.196, Schmid 2010 1.146
        I4at = upar(1)**2.0d0
c       Remodelling parameter (recruitment variable)
c        alpha =  0.6d0 !cube 0.80d0 !W2009 2.0, Schmid 2010 0.6
        alpha = upar(2)
c       Remodelling parameter (collagen growth)
c        beta0 = 2.0d0!2.0d0 !25.0d0  !     2009      25, Schmid 2010 2.0
        beta0 = upar(3)

c       Elastin degradation parameters
```

```
      fe0 = epar(1)        ! Initial amount of elastin
      cmin = epar(2)      ! Target amount of elastin
      Tend = epar(3)     ! Time of maximum degradation
      muv = epar(4)      ! Zone of degradation (0 means entire domain)
      DMAX = 0.75d0        ! Maximum degradation per year (fluid coupling)
      Lv = epar(5)/2.0d0  ! Length of undeformed artery (quarter symm)
      lamz = epar(6) ! Extension in z dir
      Lve = Lv*lamz ! Length of deformed artery (quarter symm)
c     Volume fractions
        volfre(1) = volg(3) ! ! Elastin
        volfrc(1) = volg(4)  ! Collagen fiber family 1
        volfrc(2) = volg(4)  ! Collagen fiber family 2
        volfrg(1) = 1.0d0-volg(3)-volg(4)*ndirv  ! Ground matrix

        volfre(2) = volg(5) ! ! Elastin
        volfrc(3) = volg(6)  ! Collagen fiber family 1
        volfrc(4) = volg(6)  ! Collagen fiber family 2
        volfrg(2) = 1.0d0-volg(5)-volg(6)*ndirv  ! Ground matrix
c        WRITE(*,*) volfrg(1) , volfrg(2)

      volfrgp(1) = volfrg(1)/(volfrg(1)+volfre(1))  ! Gr mat. Volume frac. of CIV
      volfrep(1) = volfre(1)/(volfrg(1)+volfre(1))  ! El mat. Volume frac. of CIV
      volfrgp(2) = volfrg(2)/(volfrg(2)+volfre(2))  ! Gr mat. Volume frac. of CIV
      volfrep(2) = volfre(2)/(volfrg(2)+volfre(2))  ! El mat. Volume frac. of CIV

c     Damage variables
      dam_el = 0.0000d0
      dam_gm = 0.0000d0
      dam_mp = 0.0000d0
      dam_f = 0.0000d0


c     Recruitment variable and normalized density variable
      if (colmod.eq.2.0d0) then
       I4mh = upar(10)
       I4m_r0 = upar(11)
      endif
       do eln = 1,nhex !numel
        do l = 1,8
          fe(l,eln) = 1.0d0
          nmasse(l,eln) = 1.0d0
          ndense(l,eln) = 1.0d0
          nmassg(l,eln) = 1.0d0
```

```
            ndensg(l,eln) = 1.0d0
            nvolu(l,eln) = 1.0d0
            if (colmod.eq.2.0d0) then
             I4m(l,eln) = I4mh
             I4m_r(l,eln) = I4m_r0
             I4_circ(l,eln) = 1.00001d0
             ka(l,eln) = 1.000d0
             kp(l,eln) = 1.000d0
             dMa(l,eln) = 0.0000d0
            endif
            do ff = 1,ndirv
c              lamr(ff,l,eln) = 1.13d0 ! Watt2009 1.13, Schmid 2010 1.07
              lamr(ff,l,eln) = upar(4) ! Watt2009 1.13, Schmid 2010 1.07
              if (colmod.eq.2.0d0) then
                  lamrmin(ff,l,eln) = upar(5)
                  lamrmax(ff,l,eln) = upar(6)
                  lamatmod(ff,l,eln) = upar(7)
                  lamatmin(ff,l,eln) = upar(8)
                  lamatmax(ff,l,eln) = upar(9)
              endif
              nmassc(ff,l,eln) = 1.0d0
              ndensc(ff,l,eln) = 1.0d0
            enddo
          enddo
        enddo



c       Reset output file
       open(unit=99,file='nvol.out',status='unknown')
       write(99,'(a)') '# Written from umacr6.f'
       close(99)

        write(iow,*) 'T.SE.E MESSAGE: Initiation of variables'
      endif

c     Set homeostatic state ------------------------------------------------------------
      if (homeost) then
c       I4at = I4c(1,1,1)
        do eln = 1,nhex
         do l = 1,8
          sigfh(l,eln) = sigf(l,eln)
         enddo
```

```
        enddo
      endif

c     Update recruitment variable
      if (uprecr.eq.1) then
c      write(*,*) 'sigff(1,1,1)=',sigff(1,1,1)
       do eln = 1,nhex !numel
         do l = 1,8
           do ff = 1,ndirv
             I4r = lamr(ff,l,eln)*lamr(ff,l,eln)
               lamr(ff,l,eln) = alpha*dt*( I4e(ff,l,eln) / I4r
     1                          - I4at ) / ( I4at - 1.0d0 )
     2                          + lamr(ff,l,eln)
c             endif
           enddo
         enddo
       enddo
       write(iow,*) 'T.SE.E MESSAGE: Updated recruitment variable'
      endif


c     Update recruitment variable - constant over element
      if (uprecc.eq.1) then
       do eln = 1,nhex !numel
         call averagefun(I4e(1,1:8,eln),8,I4et)
         I4ea(1) = I4et
         call averagefun(I4e(2,1:8,eln),8,I4et)
         I4ea(2) = I4et
         do l = 1,8
           do ff = 1,ndirv
             I4r = lamr(ff,l,eln)*lamr(ff,l,eln)
             dlamr = alpha*dt*(I4ea(ff)/I4r - I4at) / (I4at-1.d0)
             lamr(ff,l,eln) = dlamr + lamr(ff,l,eln)
           enddo
         enddo
       enddo
       write(iow,*) 'A.G. MESSAGE: Updated recruitment variable'
      endif


c     Update recruitment variable - stabilization
      if (uprecs.eq.1) then
       do eln = 1,nhex !numel
```

```
          do l = 1,8
            do ff = 1,ndirv
              I4r = lamr(ff,l,eln)**2
                lamr(ff,l,eln) = 3.0d0*alpha*dt*( I4e(ff,l,eln) / I4r
     1                          - I4at ) / ( I4at - 1.0d0 )
     2                          + lamr(ff,l,eln)
c               endif
            enddo
          enddo
        enddo
        write(iow,*) 'T.SE.E_MESSAGE:_Updated_recruitment_variable'
      endif

c     Update normalized collagen mass change
      if (upcoll.eq.1) then


        do eln = 1,nhex !numel
          do l = 1,8
            do ff = 1,ndirv
              dmass = beta*dt*( I4c(ff,l,eln) - I4at ) / (I4at - 1.0d0)
              nmassc(ff,l,eln) = nmassc(ff,l,eln) * ( dmass + 1.0d0 )
            enddo
          enddo
        enddo
        write(iow,*) 'T.SE.E_MESSAGE:_Updated_normalized_collagen_mass'
      endif

c     Update normalized collagen mass change (stabilization)
      if (upcolls.eq.1) then

          beta = beta0*5.0d0

        do eln = 1,nhex !numel
          do l = 1,8
            do ff = 1,ndirv
c               nmassc(ff,l,eln) = ( beta * dt *
c     1                         ( I4c(ff,l,eln) - I4at ) / ( I4at - 1.0d0 )
c     2                         + nmassc(ff,l,eln) )
              nmassc(ff,l,eln) = nmassc(ff,l,eln) * ( beta * dt *
     1                         ( I4c(ff,l,eln) - I4at ) / ( I4at - 1.0d0 )
     2                         + 1.0d0 )
c             if (nmassc(ff,l,eln).lt.1.0d0) nmassc(ff,l,eln) = 1.0d0
```

```
c               fco(ff,l,eln) = nmassc(ff,l,eln)
              enddo
            enddo
          enddo
          write(iow,*) 'T.SE.E MESSAGE: Updated normalized collagen mass'
        endif

c       Update normalized collagen mass change (stabilization)
        if (upcolc.eq.1) then
          do eln = 1,nhex !numel
            call averagefun(I4e(1,1:8,eln),8,I4et)
            I4ea(1) = I4et
            call averagefun(I4e(2,1:8,eln),8,I4et)
            I4ea(2) = I4et
            do l = 1,8
              do ff = 1,ndirv
                I4r = lamr(ff,l,eln)*lamr(ff,l,eln)
                nmassc(ff,l,eln) = nmassc(ff,l,eln) * ( beta * dt *
     1                     ( I4ea(ff) / I4r - I4at ) / (I4at - 1.0d0)
     2                     + 1.0d0 )
              enddo
            enddo
          enddo
          write(iow,*) 'A.G. MESSAGE: Updated normalized collagen mass'
        endif


c       Update mass according to stress based evolution law
        if (collsig) then

        beta = beta0

        do eln = 1,nhex
        if (eln.le.(2*nhex/3)) then
            k1 = 0.00352d0
            sigat = 0.0047d0
         else
            k1 = 0.00088d0
            sigat = 0.00127d0
         endif
         do l = 1,8
          do ff = 1,ndirv
          dsig = 2.0d0*k1*(I4c(ff,l,eln) - I4at)*
```

```
     1          exp(40d0*(I4c(ff,l,eln) - I4at)**2.0d0)
c          sigat = 2.0d0*k1*(I4at - 1.0d0)*
c     1          exp(40d0*(I4at - 1.0d0)**2)/lamr(ff,l,eln)**2
           nmassc(ff,l,eln) = nmassc(ff,l,eln) * ( beta * dt *
     1                        dsig/sigat + 1.0d0 )
c          nmassc(ff,l,eln) = nmassc(ff,l,eln) * ( beta * dt *
c     1                       (sigff(ff,l,eln)-sigh)/sigh
c     2                          + 1.0d0 )

            enddo
           enddo
          enddo
            write(iow,*) 'T.SE.E MESSAGE: Updated normalized collagen mass'
          endif

c         Update recruitment stretch according to stress based evolution law
          if (recrsig) then
          do eln = 1,nhex
          if (eln.le.(2*nhex/3)) then
              k1 = 0.00352d0
              sigat = 0.0047d0
           else
              k1 = 0.00088d0
              sigat = 0.00127d0
           endif
           do l = 1,8
            do ff = 1,ndirv

           dsig = 2.0d0*k1*(I4c(ff,l,eln) - I4at)*
     1          exp(40d0*(I4c(ff,l,eln) - I4at)**2.0d0)
c          sigat = 2.0d0*k1*(I4at - 1.0d0)*
c     1          exp(40d0*(I4at - 1.0d0)**2)/lamr(ff,l,eln)**2
           lamr(ff,l,eln) = alpha*dt*dsig/sigat + lamr(ff,l,eln)
c           lamr(ff,l,eln) = alpha*dt*( sigff(ff,l,eln) - sigh )/
c           lamr(ff,l,eln) = alpha*dt*( sigff(ff,l,eln) - 0.192d0 )/
c     1                              sigh + lamr(ff,l,eln)

            enddo
           enddo
          enddo
            write(iow,*) 'T.SE.E MESSAGE: Updated normalized collagen mass'
          endif
```

```
c      Update recruitment variable
       if (uprecd.eq.1) then
c       write(*,*) 'sigff(1,1,1)=',sigff(1,1,1)
        do eln = 1,nhex !numel
          do l = 1,8
            do ff = 1,ndirv
              dlamr =alpha*dt*(lmcmax(ff,l,eln)-lamatmax(ff,l,eln))
     1                 /lamatmax(ff,l,eln)
              lamrmin(ff,l,eln) = dlamr + lamrmin(ff,l,eln)

              dlamr =alpha*dt*(lmcmod(ff,l,eln)-lamatmod(ff,l,eln))
     1                 /lamatmod(ff,l,eln)
              lamr(ff,l,eln) = dlamr + lamr(ff,l,eln)

              dlamr =alpha*dt*(lmcmin(ff,l,eln)-lamatmin(ff,l,eln))
     1                 /lamatmin(ff,l,eln)
              lamrmax(ff,l,eln) = dlamr + lamrmax(ff,l,eln)
            enddo
          enddo
        enddo
        write(iow,*) 'A.G. MESSAGE: Updated min recruitment stretch'
       endif

c      Update normalized collagen mass change
       if (upesog.eq.1) then

          beta = beta0

        do eln = 1,nhex !numel
          do l = 1,8
            dmass = beta*dt*( I4c(1,l,eln) - I4at ) / (I4at - 1.0d0)
            nmassg(l,eln) = nmassg(l,eln) * ( dmass + 1.0d0 )
            nmasse(l,eln) = nmasse(l,eln) * ( dmass + 1.0d0 )
            nmassc(1,l,eln) = nmassc(1,l,eln) * ( dmass + 1.0d0 )
          enddo
        enddo
        write(iow,*) 'A.G. MESSAGE: Updated normalized esophagus mass'
       endif

       if (upgrma.eq.1) then

          beta = beta0
```

```
          do eln = 1,nhex !numel
            do l = 1,8
              dmass = beta*dt*( I4c(1,l,eln) - I4at ) / (I4at - 1.0d0)
              nmassg(l,eln) = nmassg(l,eln) * ( dmass + 1.0d0 )
            enddo
          enddo
          write(iow,*) 'A.G. MESSAGE: Updated normalized gr matrix mass'
        endif


c       Update normalized volume and density change
        if (volchange) then
c         if (ttim.le.Tend) then
c           Calculate total volume
            do eln = 1,nhex !numel
             do l = 1,8
               nvolu(l,eln) = 0.0d0
             enddo
            enddo


          do eln = 1,nhex !numel
c           Get material element number
            call getelmat(mr(np(33)),nen1,eln,matnum)
            do l = 1,8
             do ff = 1,ndirv
              fff = ff+2*(matnum-1)
              if (CID_c) then
               nvolu(l,eln) = nvolu(l,eln) + nmassc(ff,l,eln)*volfrc(fff)
              else
               nvolu(l,eln) = nvolu(l,eln) + volfrc(fff)
              endif
             enddo
             if (CID_e) then
              nvolu(l,eln) = nvolu(l,eln) + nmasse(l,eln)*volfre(matnum)
             else
              nvolu(l,eln) = nvolu(l,eln) + volfre(matnum)
             endif
             if (CID_g) then
               nvolu(l,eln) = nvolu(l,eln) + nmassg(l,eln)*volfrg(matnum)
             else
               nvolu(l,eln) = nvolu(l,eln) + volfrg(matnum)
             endif
```

```
          enddo
         enddo
c       endif
         write(iow,*) 'T.SE.E MESSAGE: Updated normalized volume change'
c         write(iow,*) 'CID_c value (vol) at time',ttim,' is ',CID_c

c       Calculate normalized density
        do eln = 1,nhex !numel
c        Get material element number
         call getelmat(mr(np(33)),nen1,eln,matnum)
         do l = 1,8
          do ff = 1,ndirv
           if (CID_c) then
             ndensc(ff,l,eln) = nmassc(ff,l,eln)/nvolu(l,eln)
           else
c             ndensc(ff,l,eln) = nmassc(ff,l,eln)
             ndensc(ff,l,eln) = nmassc(ff,l,eln)/nvolu(l,eln)
           endif
          enddo
          if (CID_e) then
            ndense(l,eln) = nmasse(l,eln)/nvolu(l,eln)
            ndensg(l,eln) = nmassg(l,eln)/nvolu(l,eln)
          else
c            ndense(l,eln) = nmasse(l,eln)
            ndense(l,eln) = nmasse(l,eln)/nvolu(l,eln)
c           Mass change of ground matrix in response to elastin change
c           Only calculate for media (material num 1)
            if ((matnum.eq.1).and.(volfrgp(matnum).ne.0.0d0)) then
              nmassg(l,eln) = (1.0d0 - nmasse(l,eln)*volfrep(matnum))/
     1                         volfrgp(matnum)
            endif
            ndensg(l,eln) = nmassg(l,eln)/nvolu(l,eln)
c            ndensg(l,eln) = 1.0d0
c            ndensg(l,eln) = 2.0d0 - ndense(l,eln)
          endif
         enddo
        enddo
         write(iow,*) 'T.SE.E MESSAGE: Updated normalized density'

c       close(99)

       endif
```

```
      if (eldeg_hom.eq.1) then
        do eln = 1,nhex !numel
c         Get material element number
          call getelmat(mr(np(33)),nen1,eln,matnum)
c         Only calculate for media (material num 1)
c          if (matnum.eq.1) then
           do l = 1,8
c            Keep elastin constant if time is larger than Tend
c             if (ttim.gt.Tend) then
c               nmasse(l,eln) = fe0 * cmin
c             else
c               fe(l,eln) = fe0 * cmin**( ttim / Tend )
              nmasse(l,eln) = fe0 * cmin**( ttim / Tend )
c             endif
           enddo
c          else
c           do l = 1,8
cc             fe(l,eln) = 1.0d0
c             nmasse(l,eln) = 1.0d0
c           enddo
c          endif
        enddo
       write(iow,*) 'T.SE.E MESSAGE: edho-Elastin degradation performed'
      endif

      if (eldeg_exp.eq.1) then
        do eln = 1,nhex !numel
c         Get material element number
          call getelmat(mr(np(33)),nen1,eln,matnum)
c         Only calculate for media (material num 1)
          if (matnum.eq.1) then
            do l = 1,8
c             Calculate elastin degradation
c             fe(l,eln) = 1 - ( 1 - cmin**( ttim / Tend ) )
c     1                     * exp( -muv * ( gpcl(3,l,eln) / Lv )**2.0d0 )
              nmasse(l,eln) = 1.0d0 - ( 1.0d0 - cmin**( ttim / Tend ) )
     1                      * exp(-muv*(1.0d0-gpcl(3,l,eln) / Lv )**2.d0)
C             nmasse(l,eln) = 1 - ( 1 - cmin**(ttim / Tend))*exp(-muv
C     1                   * exp(-muv * (1-gpce(3,l,eln) / Lve )**2.0d0)
C     1           *(1-hr(up(6)+(eln-1)*24+(l-1)*3+3)/ Lve )**2.0d0)
            enddo
          else
            do l = 1,8
```

```
c               fe(l,eln) = 1.0d0
                nmasse(l,eln) = 1.0d0
              enddo
            endif
          enddo
        endif

        if (eldeg_half.eq.1) then
          do eln = 1,nhex !numel
c           Get material element number
            call getelmat(mr(np(33)),nen1,eln,matnum)
c           Only calculate for media (material num 1)
            if (matnum.eq.1) then
              do l = 1,8
c               Calculate elastin degradation
                nmasse(l,eln) = 1.0d0 - ( 1.0d0 - cmin**( ttim / Tend ) )
     1                    *exp(-muv*(1.0d0-gpcl(3,l,eln)/Lv/2.0d0)**2.d0)
c               nmasse(l,eln) = 1 - ( 1 - cmin**( ttim / Tend ) )
c     1                       * exp(-muv*(1-gpce(3,l,eln) / Lve )**2.0d0)
C               nmasse(l,eln) = 1 - ( 1 - cmin**(ttim / Tend))*exp(-muv
C     1                       * exp(-muv * (1-gpce(3,l,eln) / Lve )**2.0d0)
C     1             *(1-hr(up(6)+(eln-1)*24+(l-1)*3+3)/ Lve )**2.0d0)
              enddo
            else
              do l = 1,8
c               fe(l,eln) = 1.0d0
                nmasse(l,eln) = 1.0d0
              enddo
            endif
          enddo
        endif

        if (eldeg_halfc.eq.1) then
          do eln = 1,nhex !numel
c           Get material element number
            call getelmat(mr(np(33)),nen1,eln,matnum)
c           Only calculate for media (material num 1)
            if (matnum.eq.1) then
              call averagefun(gpcl(3,1:8,eln),8,z)
              do l = 1,8
c               Calculate elastin degradation
                nmasse(l,eln) = 1.0d0 - ( 1.0d0 - cmin**( ttim / Tend ) )
     1                    *exp(-muv*(1.0d0-z/Lv/2.0d0)**2.d0)
```

```
c               nmasse(l,eln) = 1 - ( 1 - cmin**( ttim / Tend ) )
c     1                       * exp(-muv*(1-gpce(3,l,eln) / Lve )**2.0d0)
C               nmasse(l,eln) = 1 - ( 1 - cmin**(ttim / Tend))*exp(-muv
C     1                   * exp(-muv * (1-gpce(3,l,eln) / Lve )**2.0d0)
C     1           *(1-hr(up(6)+(eln-1)*24+(l-1)*3+3)/ Lve )**2.0d0)
            enddo
          else
            do l = 1,8
c               fe(l,eln) = 1.0d0
              nmasse(l,eln) = 1.0d0
            enddo
          endif
        enddo
      endif


      if (eldeg_spot.eq.1) then
        do eln = 1,nhex !numel
c         Get material element number
          call getelmat(mr(np(33)),nen1,eln,matnum)
c         Only calculate for media (material num 1)
          if (matnum.eq.1) then
            do l = 1,8
c             Calculate elastin degradation
c             atan provides answers in a range [-pi/2 pi/2]
              phi = atan(gpcl(2,l,eln)/gpcl(1,l,eln))
c             TODO: add case for 3rd quadrant!!!
              if (gpcl(1,l,eln).le.0.0d0) then
c                 2nd quadrant
                phi = phi + pi
              endif
              if (phi.le.1.5d0) then
              nmasse(l,eln) = 1.0d0 - ( 1.0d0 - cmin**( ttim / Tend ) )
     1                   *exp(-muv*(phi*0.5d0/pi)**2.d0)
     2                   *exp(-muv*(1.0d0-gpcl(3,l,eln)/Lv/2.0d0)**2.d0)
              endif
c              nmasse(l,eln) = 1 - ( 1 - cmin**( ttim / Tend ) )
c     1                       * exp(-muv*(1-gpce(3,l,eln) / Lve )**2.0d0)
C              nmasse(l,eln) = 1 - ( 1 - cmin**(ttim / Tend))*exp(-muv
C     1                   * exp(-muv * (1-gpce(3,l,eln) / Lve )**2.0d0)
C     1           *(1-hr(up(6)+(eln-1)*24+(l-1)*3+3)/ Lve )**2.0d0)
            enddo
          else
```

```
            do l = 1,8
c               fe(l,eln) = 1.0d0
                nmasse(l,eln) = 1.0d0
            enddo
          endif
        enddo
      endif

      if (eldeg_fluid.eq.1) then
        do eln = 1,nhex !numel
c         Get material element number
          call getelmat(mr(np(33)),nen1,eln,matnum)
c         Only calculate for media (material num 1)
          if (matnum.eq.1) then
            do l = 1,8
c             Calculate elastin degradation
c               nmasse(l,eln) = nmasse(l,eln) * (1-hr(up(8)+(eln-1)*8+l)
                nmasse(l,eln) = nmasse(l,eln) * (1.0d0-fdgp(l,eln)
     1             * (1.0d0 - DMAX ** dt))
            enddo
          else
            do l = 1,8
c               fe(l,eln) = 1.0d0
                nmasse(l,eln) = 1.0d0
            enddo
          endif
        enddo
        deb=0
        if (deb.eq.1) then
        write(*,*) 'FD on nodes, El 1'
        write(*,*) hr(up(7)+1),hr(up(7)+2),hr(up(7)+26),hr(up(7)+25)
      write(*,*) hr(up(7)+265),hr(up(7)+266),hr(up(7)+290),hr(up(7)+289)
        write(*,*) 'FD on GPs, El 1'
        write(*,*) hr(up(8)+1),hr(up(8)+2),hr(up(8)+3),hr(up(8)+4)
        write(*,*) hr(up(8)+5),hr(up(8)+6),hr(up(8)+7),hr(up(8)+8)
        write(*,*) 'GP1coor',hr(up(5)+1),hr(up(5)+2),hr(up(5)+3)
        write(*,*) 'GP2coor',hr(up(5)+4),hr(up(5)+5),hr(up(5)+6)
        write(*,*) 'GP3coor',hr(up(5)+7),hr(up(5)+8),hr(up(5)+9)
        write(*,*) 'GP4coor',hr(up(5)+10),hr(up(5)+11),hr(up(5)+12)
        write(*,*)'GP1coor',gpcl(1,1,1),gpcl(2,1,1),gpcl(3,1,1)
        write(*,*)'GP2coor',gpcl(1,2,1),gpcl(2,2,1),gpcl(3,2,1)
        write(*,*)'GP3coor',gpcl(1,3,1),gpcl(2,3,1),gpcl(3,3,1)
        write(*,*)'GP4coor',gpcl(1,4,1),gpcl(2,4,1),gpcl(3,4,1)
```

```
        write(*,*) nmasse(1,1),' ',nmasse(1,2),' ',nmasse(1,3)
        endif
       write(iow,*) 'A.G. MESSAGE: edfc-Elastin degradation performed'
      endif

        if (eldeg_flumod.eq.1) then
        DMAX = 0.5d0
        do eln = 1,nhex !numel
c         Get material element number
          call getelmat(mr(np(33)),nen1,eln,matnum)
c         Only calculate for media (material num 1)
          if (matnum.eq.1) then
            do l = 1,8
c             Calculate elastin degradation
C              nmasse(l,eln) = nmasse(l,eln) * (1-hr(up(8)+(eln-1)*8+l)
              nmasse(l,eln) = nmasse(l,eln) * (1.5d0-fdgp(l,eln)
     1            * (1.5d0 - DMAX ** dt))
            enddo
          else
            do l = 1,8
c             fe(l,eln) = 1.0d0
              nmasse(l,eln) = 1.0d0
            enddo
          endif
        enddo
        deb=0
        if (deb.eq.1) then
        write(*,*) 'FD on nodes, El 1'
        write(*,*) hr(up(7)+1),hr(up(7)+2),hr(up(7)+26),hr(up(7)+25)
       write(*,*) hr(up(7)+265),hr(up(7)+266),hr(up(7)+290),hr(up(7)+289)
        write(*,*) 'FD on GPs, El 1'
        write(*,*) hr(up(8)+1),hr(up(8)+2),hr(up(8)+3),hr(up(8)+4)
        write(*,*) hr(up(8)+5),hr(up(8)+6),hr(up(8)+7),hr(up(8)+8)
        write(*,*) 'GP1coor',hr(up(5)+1),hr(up(5)+2),hr(up(5)+3)
        write(*,*) 'GP2coor',hr(up(5)+4),hr(up(5)+5),hr(up(5)+6)
        write(*,*) 'GP3coor',hr(up(5)+7),hr(up(5)+8),hr(up(5)+9)
        write(*,*) 'GP4coor',hr(up(5)+10),hr(up(5)+11),hr(up(5)+12)
        write(*,*)'GP1coor',gpcl(1,1,1),gpcl(2,1,1),gpcl(3,1,1)
        write(*,*)'GP2coor',gpcl(1,2,1),gpcl(2,2,1),gpcl(3,2,1)
        write(*,*)'GP3coor',gpcl(1,3,1),gpcl(2,3,1),gpcl(3,3,1)
        write(*,*)'GP4coor',gpcl(1,4,1),gpcl(2,4,1),gpcl(3,4,1)
        write(*,*) nmasse(1,1),' ',nmasse(1,2),' ',nmasse(1,3)
        endif
```

```
        write(iow,*) 'A.G. MESSAGE: edfc-Elastin degradation performed'
      endif

      if (eldeg_step) then
        do eln = 1,nhex !numel
         do l = 1,8
c          Calculate elastin degradation
           nmasse(l,eln) = nmasse(l,eln)*0.8d0
         enddo
        enddo
      endif

c     Update normalized elastin mass change
      if (upelas.eq.1) then
          beta = beta0

        do eln = 1,nhex !numel
          do l = 1,8
              dmass = beta*dt*( I4c(1,l,eln) - I4at ) / (I4at - 1.0d0)
              nmasse(l,eln) = nmasse(l,eln) * ( dmass + 1.0d0 )
          enddo
        enddo
        write(iow,*) 'A.G. MESSAGE: Updated normalized elastin mass'
      endif

c     Model remodelling of vascular smooth muscle cells towards
c       homeostatic stretch
      if (smc_rem_hom) then
       do eln = 1,nhex !numel
        do l = 1,8 ! number of nodes
          I4m_r(l,eln) = I4m_r(l,eln) + 2.0d0*(I4m(l,eln) - I4mh)*dt
        enddo
       enddo
c       write (*,*) I4m(1,1)
      endif


      if (dmg_vsmc) then
       lam_dmg_min = 1.7d0 !1.50d0
       lam_dmg_max = 100.24d0 !1.80d0
       diff = lam_dmg_max - lam_dmg_min
       dmgmax = 1.00d0
       do eln = 1,nhex
```

```
          do l = 1,8
           if (I4m(l,eln).ge.lam_dmg_min) then
             dMa(l,eln) = dMa(l,eln) + 0.01*(I4m(l,eln) - lam_dmg_min)
           endif
           if (dMa(l,eln).ge.dmgmax) then
             dMa(l,eln) = dmgmax
           endif
c           if (l.eq.1) then
c            write (*,*) 'dMa = ', dMa(l,eln), l, eln
c           endif
          enddo
         enddo
        endif


        if (ks_remod) then
          lini = 0.0042d0
          lend = 0.0083d0
          do eln = 1,nhex
           do l = 1,8
            if ((gpcl(3,l,eln).ge.lini).AND.(gpcl(3,l,eln).le.lend)) then
             ka(l,eln) = ka(l,eln) + ( 11.0d0 - ka(l,eln) ) * dt
            endif
           enddo
          enddo
c          write (*,*) 'running KSRM'
          write (*,*) 'ka at cvs', ka(1,156)
        endif


        if (ks_increase) then
          do eln = 1,nhex
           do l = 1,8
             ka(l,eln) = ka(l,eln) + ( 5.0d0 - ka(l,eln) ) * dt
           enddo
          enddo
          write (*,*) 'ks = ', ka(1,4)
        endif

        if (ks_decrease) then
          do eln = 1,nhex
           do l = 1,8
             ka(l,eln) = ka(l,eln) + ( 0.2d0 - ka(l,eln) ) * dt
```

```
      enddo
     enddo
     write (*,*) 'ks = ', ka(1,156)
   endif

   if (wri) then

   open(unit=99,file='nvol.out',status='unknown',access='append')
   write(99,'(14(E18.10))') ttim,nvolu(1,1),nvolu(1,1),
  & nmassc(1,1,1),nmasse(1,1),ndensc(1,1,1),ndense(1,1),
  & lamr(1,1,1)**2,I4e(1,1,1),I4c(1,1,1),I4at,
  & tr_S_c(1,1),tr_E_c(1,1),ndensg(1,1)



   endif
   end
```

The following is the code contained in **fiberremdistdam.f**

```
c       Editor: Thomas S.E. Eriksson

c        subroutine grcollfibersml(ff,l,k1,k2,ae,tau,dd)
        subroutine fiberremdistdam(ff,l,kC,ae,dam, tau,tauff,dd)

c       Purpose:
c         Compute kirchhoff stress and eulerian tangent moduli
c         of a transversally isotropic material

c       Input:
c          k1.........First fiber parameter
c          k2.........Second fiber parameter
c          ae.........Eulerian fibre-vector ae_i=F_ij*al_j
c                     (not identity norm!)
c
c       Output:
c          tau........Kirchhoff stress
c          tauff......Kirchhoff stress in collagen fiber
c          dd.........Eulerian tangent
c
c       Used:
c          I4.........Fourth invariant I4 = ae_i*ae_i
c          w4.........First derivative of the stored energy function
c                      with respect to I4
c          w44........Second derivative of the stored energy function
c                      with respect to I4
c          axa........(ae x ae)
c          dev_axa....dev (ae x ae)
c          tempi......parts of the material tangent
c
c       ----------------------------------------------------------------

        implicit none

        real*8  tau(6), ae(3), dd(6,6), I4, I4at, tauff, w4, w44
        real*8 temp1(6,6), temp2(6,6), temp3(6,6), temp4(6,6),temp5(6,6)
        real*8 dev_axa(6), axa(6), kC, lam, lmr, lmrmin, lmrmax
        integer i,j

        integer ff ! Current fiber family
        integer l  ! Current quadrature point
```

```
      integer ndirv

      real*8  I4r,I4rmin,I4rmax
      real*8  dam

c     Include header file, general in FEAP
      include  'comblk.h'
      include 'iofile.h'
      include 'eldata.h'
      include 'pconstant.h'
      include  'pointer.h'
c     Include header file, problem specific
      include 'grup.h'

c     Initialize I4
      I4=0.0d0

c     Compute 4th invariant
      do i= 1,3
        I4 = I4 + ae(i)*ae(i)
      enddo
      lam = sqrt(I4)

c     Retrieve number of fiber families
      ndirv = nint( hr(up(2)) )

c     Store forth invariant for update of recruitment variable
      I4e(ff,l,n) = I4

c     Compute recruitment parameter I4r
c      I4r = lamr(ff,l,n)**2
c      I4rmin = lamrmin(ff,l,n)**2
c      I4rmax = lamrmax(ff,l,n)**2

c     In iniatilzation I4r is undefined
c      if (I4r.eq.0.0d0)  I4r = 1.01d0
c      if (I4rmin.eq.0.0d0)  I4rmin = 1.01d0
c      if (I4rmax.eq.0.0d0)  I4rmax = 1.01d0

      lmr = lamr(ff,l,n)
      lmrmin = lamrmin(ff,l,n)
      lmrmax = lamrmax(ff,l,n)
```

```
      lmcmin(ff,l,n) = lam / lamrmax(ff,l,n)
      lmcmod(ff,l,n) = lam / lamr(ff,l,n)
      lmcmax(ff,l,n) = lam / lamrmin(ff,l,n)

c       Collect I4c values for updating collagen growth parameter
      I4c(ff,l,n) = lmcmax(ff,l,n)
      I4c(ndirv+ff,l,n) = lmcmod(ff,l,n)
      I4c(2*ndirv+ff,l,n) = lmcmin(ff,l,n)

c     Get W_4 and W_44
      call fibdistdam(kC,lam,lmr,lmrmin,lmrmax,dam, w4,w44)

c     Derive Kirchhoff stress
      call vectorproduct(ae,axa)

      do i = 1,6
        dev_axa(i) = axa(i)
      enddo

      call deviator(dev_axa)
      tauff = w4
      do i = 1,6
        tau(i) = tauff*dev_axa(i)
      enddo

c     Compute elasticity tensor

c     Derive spatial tangent
      do i = 1,6
        do j = 1,6
          temp1(i,j) = 0.0d0
        enddo
      enddo

      do i= 1,6
        do j= i,6
          temp5(i,j) = dev_axa(i)*dev_axa(j)
        enddo
        do j= i,3
          temp1(i,j) = dev_axa(i)
        enddo
      enddo
```

```
      do i = 1,6
        do j = 1,6
          temp2(i,j) = 0.0d0
          temp3(i,j) = 0.0d0
         enddo
      enddo

      do i= 1,3
        do j= i,6
          temp2(i,j) = dev_axa(j)
        enddo
        do j= i,3
          temp3(i,j) = 1.0d0
        enddo
      enddo

      do i = 1,6
        do j = 1,6
          temp4(i,j) = 0.0d0
        enddo
      enddo

      temp4(1,1)=1.0d0
      temp4(2,2)=1.0d0
      temp4(3,3)=1.0d0
      temp4(4,4)=0.5d0
      temp4(5,5)=0.5d0
      temp4(6,6)=0.5d0

      do i = 1,6
        do j = 1,6
          dd(i,j) = 0.0d0
        enddo
      enddo


      do i = 1,6
        do j = 1,6
          dd(i,j) = -(2.0d0*w4/3.0d0) * ( temp1(i,j) + temp2(i,j)
     &                -I4e(ff,l,n) * ( temp4(i,j) - one3*temp3(i,j) ) )
          dd(i,j) = dd(i,j) + (2.0d0*w44)*temp5(i,j)
        enddo
      enddo
```

```
c       Symmetrize tangent
        do i = 1,6
          do j= i+1,6
            dd(j,i) = dd(i,j)
          enddo
        enddo

1000    return

        end
```

The following is the code contained in **fibdistdam.f**

```
      subroutine fibdistdam(kC,lam,me,mu,ma,dam, g,h)

c     Purpose:
c       Derivatives with respect to the fourth invariant
c


c
c  Input:
c         kC.....Collagen material parameter
c         me.....Mean recruitment invariant in the triangle distribution (I4_R^mean
c         mu.....Minimum recruitment invariant in the triangle distribution (I4_R^m
c         ma.....Maximum recruitment invariant in the triangle distribution (I4_R^m
c         I4.....Fourth invariant
c
c  Output:
c         g.....First derivative of the stored-energy function
c                 with respect to the fourt invariant
c         h.....Second derivative of the stored-energy function
c                 with respect to the fourt invariant
c
c  Used:
c         gamm
c         delt
c
c=======================================================================
      implicit none

      real*8 g, h, lam, kC, mu, me, ma, gamm, delt, dam

      gamm = 2.d0 * kC / ( (ma-mu)*(me-mu) )
      delt = 2.d0 * kC / ( (ma-mu)*(ma-me) )

      if (lam.le.mu) then
        g = 0.d0
        h = 0.d0
      elseif (lam.le.me) then
        g = gamm * ( (mu+lam)*log(lam/mu) + 2.d0 * (mu-lam) )
        h = gamm * ( log(lam/mu) + mu/lam - 1.d0 )
      elseif (lam.le.ma) then
        g = gamm * ( (mu+lam)*log(me/mu) +mu-me + (mu/me -1.d0)*lam)
```

```
1       - delt * ( (ma+lam)*log(lam/me) +ma+me - (ma/me +1.d0)*lam)
   h = gamm * (log(me/mu)+mu/me-1.d0)
1                              -delt*(log(lam/me)+ma/lam-ma/me)
 else
   g = gamm * ( (mu+lam)*log(me/mu) + mu-me + (mu/me -1.d0)*lam )
1       - delt * ( (ma+lam)*log(ma/me) -ma+me - (ma/me-1.d0)*lam )
   h = gamm*(log(me/mu)+mu/me-1.d0)-delt*(log(ma/me)-ma/me+1.d0)
 endif

 g = (1-dam)*g/(2*lam)
 h = (1-dam)*h/(2*lam)



 end
```

The following is the code contained in **activestressd.f**

```
c       Editor: Thomas S.E. Eriksson

c        subroutine grcollfibersml(ff,l,k1,k2,ae,tau,dd)
        subroutine activestressd(l,kMa,lmi,lmo,lma,bb,dam,kt, tau,taum,dd)

c       Purpose:
c         Compute kirchhoff stress and eulerian tangent moduli
c         of a transversally isotropic material

c       Input:
c          kMa.............Material parameter for active response
c          lmo/mi/ma.......Lambda_mod/min/max in active stress equation
c          bb..............Left Cauchy-Green tensor
c
c
c       Output:
c          tau........Kirchhoff stress
c          tauff......Kirchhoff stress in collagen fiber
c          dd.........Eulerian tangent
c
c       Used:
c          I4.........Fourth invariant I4 = ae_i*ae_i
c          w4.........First derivative of the stored energy function
c                     with respect to I4
c          w44........Second derivative of the stored energy function
c                     with respect to I4
c          axa........(ae x ae)
c          dev_axa....dev (ae x ae)
c          tempi......parts of the material tangent
c
c       ----------------------------------------------------------------

        implicit none

        real*8   tau(6), bb(6), ae(3), dd(6,6), I4at, taum, w4, w44
        real*8   I4mt, I4circ, I4mh
        real*8   I4M_min, I4M_mod, I4M_max
        real*8   temp1(6,6), temp2(6,6), temp3(6,6), temp4(6,6),temp5(6,6)
        real*8   dev_axa(6), axa(6), kMa, lmo, lmi, lma
        real*8   dam, kt
        integer  i,j,l,eln
```

```
c       Include header file, general in FEAP
        include  'comblk.h'
        include 'iofile.h'
        include 'eldata.h'
        include 'pconstant.h'
        include  'pointer.h'
c       Include header file, problem specific
        include 'grup.h'
        include 'vsmc.h'


c        I4mh = 1.1025d0

        I4circ = 0.0d0                          ! circumferential tissue stretch
        do i= 1,3
          I4circ = I4circ + bb(i)*bb(i)
        enddo
        I4_circ(l,n) = I4circ


        if (I4m_r(l,n).eq.0.0d0) then
         I4m_r(l,n) = 1.00d0
        endif


        I4m(l,n) = I4_circ(l,n) / I4m_r(l,n)
        I4mt = I4m(l,n)


c       Get W_4 and W_44
        call activecircumfdam(kMa,lmi,lmo,lma,I4mt,dam,kt,  w4,w44)
        taum = w4



c       Derive Kirchhoff stress
        call vectorproduct(bb,axa)

        do i = 1,6
          dev_axa(i) = axa(i)
        enddo
```

```
      call deviator(dev_axa)
      do i = 1,6
        tau(i) = taum*dev_axa(i)
      enddo

c     Compute elasticity tensor

c     Derive spatial tangent
      do i = 1,6
        do j = 1,6
          temp1(i,j) = 0.0d0
        enddo
      enddo

      do i= 1,6
        do j= i,6
          temp5(i,j) = dev_axa(i)*dev_axa(j)
        enddo
        do j= i,3
          temp1(i,j) = dev_axa(i)
        enddo
      enddo

      do i = 1,6
        do j = 1,6
          temp2(i,j) = 0.0d0
          temp3(i,j) = 0.0d0
         enddo
      enddo

      do i= 1,3
        do j= i,6
          temp2(i,j) = dev_axa(j)
        enddo
        do j= i,3
          temp3(i,j) = 1.0d0
        enddo
      enddo

      do i = 1,6
        do j = 1,6
          temp4(i,j) = 0.0d0
```

```
        enddo
      enddo

      temp4(1,1)=1.0d0
      temp4(2,2)=1.0d0
      temp4(3,3)=1.0d0
      temp4(4,4)=0.5d0
      temp4(5,5)=0.5d0
      temp4(6,6)=0.5d0

      do i = 1,6
        do j = 1,6
          dd(i,j) = 0.0d0
        enddo
      enddo



      do i = 1,6
        do j = 1,6
          dd(i,j) = -(2.0d0*w4/3.0d0) * ( temp1(i,j) + temp2(i,j)
     &                -I4mt* ( temp4(i,j) - one3*temp3(i,j) ) )
          dd(i,j) = dd(i,j) + (2.0d0*w44)*temp5(i,j)
        enddo
      enddo

c     Symmetrize tangent
      do i = 1,6
        do j= i+1,6
          dd(j,i) = dd(i,j)
        enddo
      enddo

1000  return

      end
```

The following is the code contained in **activecircumfd.f**

```
      subroutine activecircumfdam(kMa,lmin,lmod,lmax,I4m,dam,kt, g,h)

c     Purpose:
c       Derivatives with respect to the fourth invariant
c


c
c  Input:
c         kC.....Collagen material parameter
c         me.....Mean recruitment invariant in the triangle distribution (I4_R^mean
c         mu.....Minimum recruitment invariant in the triangle distribution (I4_R^m
c         ma.....Maximum recruitment invariant in the triangle distribution (I4_R^m
c         I4.....Fourth invariant
c
c  Output:
c         g.....First derivative of the stored-energy function
c                 with respect to the fourt invariant
c         h.....Second derivative of the stored-energy function
c                 with respect to the fourt invariant
c
c  Used:
c         gamm
c         delt
c
c=======================================================================
      implicit none

      real*8 g, h, lmin, lmod, lmax, I4m, kMa, tmp, lam, dam, kt


      lam = sqrt(I4m)

      if ((lam.ge.lmin).AND.(lam.le.lmax)) then
          g = kMa * kt * lam * ( 1 - ((lam - lmod)/(lmod - lmin))**2 )

          tmp = (lmod - lmin)**(-2)
          h = kMa*kt*( 1 - tmp*((lam - lmod)**2)
     1          - 2*tmp*lam*(lam - lmod) ) / (2 * lam)
      else
          g = 0.0d0
```

```
        h = 0.0d0
      endif


      g = (1-dam)*g
      h = (1-dam)*h



      end
```

Appendix C

The following are input files to the main program that have been used for the verification of the implementations described in Chapter 3 and for the finite element model of cerebral vasospasm described in Chapter 4.

The following is the input file for the verification of the correct implementation of the material model for collagen:

```
feap ** Biaxial test - Andrii Grytsan
  0    0       3       3       3       8

material 1 !Media
solid
finite
mixed
ucons cacg  1.000e+06  0.000e-02  9.300e-02  5.800e+00 0.000e+01
! ud vector


rpar ! I4a alpha beta recrmean recrmin recrmax atmod atmin atmax
2
1.195  0.6  1.0  1.3684 1.2381 1.5294 0.95 0.85 1.05

volg ! volgr(0 3) elvg(0 3) volfrac:(elastinM,collagenM,elastinA,collagenA)
3 0 0.18 0.075 0.0 0.075


epar ! fe0 cmin Tend muv Lvf lambda_z
1.0 0.2 10.0 20.0 0.0737 1.2
```

```
BLOCK
    CARTESIAN 4 4 1
    BRICK 8
    1   0.0   0.0  0.0
    2   1.0   0.0  0.0
    3   1.0   1.0  0.0
    4   0.0   1.0  0.0
    5   0.0   0.0  1.0
    6   1.0   0.0  1.0
    7   1.0   1.0  1.0
    8   0.0   1.0  1.0

EBOUN
    1 0.0 1.0 0.0 0.0              ! 1st column: which coordinate is fixed
    1 1.0 1.0 0.0 0.0              ! 2nd column: value of fixed coordinate
    2 0.0 0.0 1.0 0.0              ! 3,4,5th column: which of the three displacements is
    2 1.0 0.0 1.0 0.0
    3 0.0 0.0 0.0 1.0

EDISP
    1 0.0 0.0 0.0 0.0              ! at x1=0 you have u1=0 (u=displacement)
    1 1.0 0.5 0.0 0.0
    2 0.0 0.0 0.0 0.0
    2 1.0 0.0 0.5 0.0
    3 0.0 0.0 0.0 0.0

NDIR
  1 50 2 0
1         0.7071067812    0.7071067812    0       -0.7071067812   0.7071067812    0
2         0.7071067812    0.7071067812    0       -0.7071067812   0.7071067812    0
3         0.7071067812    0.7071067812    0       -0.7071067812   0.7071067812    0
4         0.7071067812    0.7071067812    0       -0.7071067812   0.7071067812    0
5         0.7071067812    0.7071067812    0       -0.7071067812   0.7071067812    0
6         0.7071067812    0.7071067812    0       -0.7071067812   0.7071067812    0
7         0.7071067812    0.7071067812    0       -0.7071067812   0.7071067812    0
8         0.7071067812    0.7071067812    0       -0.7071067812   0.7071067812    0
9         0.7071067812    0.7071067812    0       -0.7071067812   0.7071067812    0
10        0.7071067812    0.7071067812    0       -0.7071067812   0.7071067812    0
11        0.7071067812    0.7071067812    0       -0.7071067812   0.7071067812    0
12        0.7071067812    0.7071067812    0       -0.7071067812   0.7071067812    0
13        0.7071067812    0.7071067812    0       -0.7071067812   0.7071067812    0
14        0.7071067812    0.7071067812    0       -0.7071067812   0.7071067812    0
15        0.7071067812    0.7071067812    0       -0.7071067812   0.7071067812    0
```

16	0.7071067812	0.7071067812	0	−0.7071067812	0.7071067812	0
17	0.7071067812	0.7071067812	0	−0.7071067812	0.7071067812	0
18	0.7071067812	0.7071067812	0	−0.7071067812	0.7071067812	0
19	0.7071067812	0.7071067812	0	−0.7071067812	0.7071067812	0
20	0.7071067812	0.7071067812	0	−0.7071067812	0.7071067812	0
21	0.7071067812	0.7071067812	0	−0.7071067812	0.7071067812	0
22	0.7071067812	0.7071067812	0	−0.7071067812	0.7071067812	0
23	0.7071067812	0.7071067812	0	−0.7071067812	0.7071067812	0
24	0.7071067812	0.7071067812	0	−0.7071067812	0.7071067812	0
25	0.7071067812	0.7071067812	0	−0.7071067812	0.7071067812	0
26	0.7071067812	0.7071067812	0	−0.7071067812	0.7071067812	0
27	0.7071067812	0.7071067812	0	−0.7071067812	0.7071067812	0
28	0.7071067812	0.7071067812	0	−0.7071067812	0.7071067812	0
29	0.7071067812	0.7071067812	0	−0.7071067812	0.7071067812	0
30	0.7071067812	0.7071067812	0	−0.7071067812	0.7071067812	0
31	0.7071067812	0.7071067812	0	−0.7071067812	0.7071067812	0
32	0.7071067812	0.7071067812	0	−0.7071067812	0.7071067812	0
33	0.7071067812	0.7071067812	0	−0.7071067812	0.7071067812	0
34	0.7071067812	0.7071067812	0	−0.7071067812	0.7071067812	0
35	0.7071067812	0.7071067812	0	−0.7071067812	0.7071067812	0
36	0.7071067812	0.7071067812	0	−0.7071067812	0.7071067812	0
37	0.7071067812	0.7071067812	0	−0.7071067812	0.7071067812	0
38	0.7071067812	0.7071067812	0	−0.7071067812	0.7071067812	0
39	0.7071067812	0.7071067812	0	−0.7071067812	0.7071067812	0
40	0.7071067812	0.7071067812	0	−0.7071067812	0.7071067812	0
41	0.7071067812	0.7071067812	0	−0.7071067812	0.7071067812	0
42	0.7071067812	0.7071067812	0	−0.7071067812	0.7071067812	0
43	0.7071067812	0.7071067812	0	−0.7071067812	0.7071067812	0
44	0.7071067812	0.7071067812	0	−0.7071067812	0.7071067812	0
45	0.7071067812	0.7071067812	0	−0.7071067812	0.7071067812	0
46	0.7071067812	0.7071067812	0	−0.7071067812	0.7071067812	0
47	0.7071067812	0.7071067812	0	−0.7071067812	0.7071067812	0
48	0.7071067812	0.7071067812	0	−0.7071067812	0.7071067812	0
49	0.7071067812	0.7071067812	0	−0.7071067812	0.7071067812	0
50	0.7071067812	0.7071067812	0	−0.7071067812	0.7071067812	0

fdno
INCLude input/FD.dat

end

```
!inter

BATCH
teln
gmac,init
opti
check
time,set,-1.00E+00
tol,,1.0e-10
prop,,1                                          ! proportional load step 1
dt,,0.0200
stre node
tvtk,grow
!tvtk,writ
! Loading - stretch, pressure
LOOP time 50
        time
        LOOP newton 10
                tang,,1
        NEXT newton
        stre node 5
        tvtk,grow
NEXT time

! ---- Second load step ----
!dt,,0.02
!prop,,1
!LOOP time 450
!       time
!       LOOP newton 30
!               tang,,1
!       NEXT newton
!       stre node
!       gmac,recd
!       tvtk,grow
!NEXT time


END
1 1  -1.0   0.001   0.00   1.00   0.00   0.00   0.00   1.00
1 2   0.001  20.001  1.00   0.00   0.00   0.00   0.00   1.00

SAVE
```

STOP

The following is the input file for the verification of the correct implementation of collagen remodelling:

```
feap ** Biaxial test - Andrii Grytsan
  0    0       3       3       3       8


material 1 !Media
solid
finite
mixed
ucons cacg  1.000e+04  0.000e-02  9.300e-02  5.800e+00 1.100e-02 4.510e-02
! ud vector


rpar ! I4a alpha beta recrmean recrmin recrmax I4mod I4min I4max
2
1.195  2.0  1.0  1.25 1.11 1.67 0.95 0.85 1.05     !0.9025 0.7225 1.1025

volg ! volgr(0 3) elvg(0 3) volfrac:(elastinM,collagenM,elastinA,collagenA)
3 0 0.18 0.075 0.0 0.075


epar ! fe0 cmin Tend muv Lvf lambda_z
1.0 0.2 10.0 20.0 0.0737 1.2


BLOCK
   CARTESIAN 4 4 1
   BRICK 8
   1  0.0  0.0 0.0
   2  1.0  0.0 0.0
   3  1.0  1.0 0.0
   4  0.0  1.0 0.0
   5  0.0  0.0 1.0
   6  1.0  0.0 1.0
   7  1.0  1.0 1.0
   8  0.0  1.0 1.0

EBOUN
   1 0.0 1.0 0.0 0.0              ! 1st column: which coordinate is fixed
   1 1.0 1.0 0.0 0.0              ! 2nd column: value of fixed coordinate
   2 0.0 0.0 1.0 0.0              ! 3,4,5th column: which of the three displacements is
```

```
    2  1.0  0.0  1.0  0.0
    3  0.0  0.0  0.0  1.0

EDISP
    1  0.0  0.0  0.0  0.0                    ! at x1=0 you have u1=0 (u=displacement)
    1  1.0  0.5  0.0  0.0
    2  0.0  0.0  0.0  0.0
    2  1.0  0.0  0.5  0.0
    3  0.0  0.0  0.0  0.0

NDIR
  1  50  2  0
1          0.7071067812     0.7071067812     0          −0.7071067812    0.7071067812     0
2          0.7071067812     0.7071067812     0          −0.7071067812    0.7071067812     0
3          0.7071067812     0.7071067812     0          −0.7071067812    0.7071067812     0
4          0.7071067812     0.7071067812     0          −0.7071067812    0.7071067812     0
5          0.7071067812     0.7071067812     0          −0.7071067812    0.7071067812     0
6          0.7071067812     0.7071067812     0          −0.7071067812    0.7071067812     0
7          0.7071067812     0.7071067812     0          −0.7071067812    0.7071067812     0
8          0.7071067812     0.7071067812     0          −0.7071067812    0.7071067812     0
9          0.7071067812     0.7071067812     0          −0.7071067812    0.7071067812     0
10         0.7071067812     0.7071067812     0          −0.7071067812    0.7071067812     0
11         0.7071067812     0.7071067812     0          −0.7071067812    0.7071067812     0
12         0.7071067812     0.7071067812     0          −0.7071067812    0.7071067812     0
13         0.7071067812     0.7071067812     0          −0.7071067812    0.7071067812     0
14         0.7071067812     0.7071067812     0          −0.7071067812    0.7071067812     0
15         0.7071067812     0.7071067812     0          −0.7071067812    0.7071067812     0
16         0.7071067812     0.7071067812     0          −0.7071067812    0.7071067812     0
17         0.7071067812     0.7071067812     0          −0.7071067812    0.7071067812     0
18         0.7071067812     0.7071067812     0          −0.7071067812    0.7071067812     0
19         0.7071067812     0.7071067812     0          −0.7071067812    0.7071067812     0
20         0.7071067812     0.7071067812     0          −0.7071067812    0.7071067812     0
21         0.7071067812     0.7071067812     0          −0.7071067812    0.7071067812     0
22         0.7071067812     0.7071067812     0          −0.7071067812    0.7071067812     0
23         0.7071067812     0.7071067812     0          −0.7071067812    0.7071067812     0
24         0.7071067812     0.7071067812     0          −0.7071067812    0.7071067812     0
25         0.7071067812     0.7071067812     0          −0.7071067812    0.7071067812     0
26         0.7071067812     0.7071067812     0          −0.7071067812    0.7071067812     0
27         0.7071067812     0.7071067812     0          −0.7071067812    0.7071067812     0
28         0.7071067812     0.7071067812     0          −0.7071067812    0.7071067812     0
29         0.7071067812     0.7071067812     0          −0.7071067812    0.7071067812     0
30         0.7071067812     0.7071067812     0          −0.7071067812    0.7071067812     0
31         0.7071067812     0.7071067812     0          −0.7071067812    0.7071067812     0
```

32	0.7071067812	0.7071067812	0	−0.7071067812	0.7071067812	0
33	0.7071067812	0.7071067812	0	−0.7071067812	0.7071067812	0
34	0.7071067812	0.7071067812	0	−0.7071067812	0.7071067812	0
35	0.7071067812	0.7071067812	0	−0.7071067812	0.7071067812	0
36	0.7071067812	0.7071067812	0	−0.7071067812	0.7071067812	0
37	0.7071067812	0.7071067812	0	−0.7071067812	0.7071067812	0
38	0.7071067812	0.7071067812	0	−0.7071067812	0.7071067812	0
39	0.7071067812	0.7071067812	0	−0.7071067812	0.7071067812	0
40	0.7071067812	0.7071067812	0	−0.7071067812	0.7071067812	0
41	0.7071067812	0.7071067812	0	−0.7071067812	0.7071067812	0
42	0.7071067812	0.7071067812	0	−0.7071067812	0.7071067812	0
43	0.7071067812	0.7071067812	0	−0.7071067812	0.7071067812	0
44	0.7071067812	0.7071067812	0	−0.7071067812	0.7071067812	0
45	0.7071067812	0.7071067812	0	−0.7071067812	0.7071067812	0
46	0.7071067812	0.7071067812	0	−0.7071067812	0.7071067812	0
47	0.7071067812	0.7071067812	0	−0.7071067812	0.7071067812	0
48	0.7071067812	0.7071067812	0	−0.7071067812	0.7071067812	0
49	0.7071067812	0.7071067812	0	−0.7071067812	0.7071067812	0
50	0.7071067812	0.7071067812	0	−0.7071067812	0.7071067812	0

```
fdno
INCLude input/FD.dat

end

!inter

BATCH
teln
gmac,init
opti
check
time,set,-1.00E+00
tol,,1.0e-10
prop,,1                                    ! proportional load step 1
dt,,0.0200
stre node
tvtk,grow
!tvtk,writ
! Loading - stretch, pressure
LOOP time 50
```

```
        time
        LOOP newton 10
                tang,,1
        NEXT newton
        stre node 5
        tvtk,grow
NEXT time

! ---- Second load step ----
dt,,0.02
prop,,1
LOOP time 450
        time
        LOOP newton 30
                tang,,1
        NEXT newton
        stre node
        gmac,recd
        tvtk,grow
NEXT time


END
1 1  -1.0  0.001  0.00  1.00  0.00  0.00  0.00  1.00
1 2  0.001  20.001  1.00  0.00  0.00  0.00  0.00  1.00

SAVE

STOP
```

The following is the input file for the verification of the correct implementation of the material model for VSMCs with active stress response:

```
feap ** Biaxial test - Andrii Grytsan
  0    0       3       3       3       8


material 1 !Media
solid
finite
mixed
ucons cacg  1.000e+04  0.000e-02  9.300e-02 5.800e+00 1.100e-02 4.510e-02
! ud vector


rpar ! I4a alpha beta recrmean recrmin recrmax
2
1.195  0.6  1.0  1.3684 1.2381 1.5294

volg ! volgr(0 3) elvg(0 3) volfrac:(elastinM,collagenM,elastinA,collagenA)
3 0 0.18 0.075 0.0 0.075


epar ! fe0 cmin Tend muv Lvf lambda_z
1.0 0.2 10.0 20.0 0.0737 1.2


BLOCK
   CARTESIAN 4 4 1
   BRICK 8
   1  0.0  0.0 0.0
   2  1.0  0.0 0.0
   3  1.0  1.0 0.0
   4  0.0  1.0 0.0
   5  0.0  0.0 1.0
   6  1.0  0.0 1.0
   7  1.0  1.0 1.0
   8  0.0  1.0 1.0

EBOUN
   1 0.0 1.0 0.0 0.0              ! 1st column: which coordinate is fixed
   1 1.0 1.0 0.0 0.0              ! 2nd column: value of fixed coordinate
   2 0.0 0.0 1.0 0.0              ! 3,4,5th column: which of the three displacements is
```

```
    2  1.0  0.0  1.0  0.0
    3  0.0  0.0  0.0  1.0

EDISP
    1  0.0  0.0  0.0  0.0                    ! at x1=0 you have u1=0 (u=displacement)
    1  1.0  0.5  0.0  0.0
    2  0.0  0.0  0.0  0.0
    2  1.0  0.0  0.5  0.0
    3  0.0  0.0  0.0  0.0

NDIR
  1  50  2  0
1          0.7071067812     0.7071067812     0          −0.7071067812    0.7071067812     0
2          0.7071067812     0.7071067812     0          −0.7071067812    0.7071067812     0
3          0.7071067812     0.7071067812     0          −0.7071067812    0.7071067812     0
4          0.7071067812     0.7071067812     0          −0.7071067812    0.7071067812     0
5          0.7071067812     0.7071067812     0          −0.7071067812    0.7071067812     0
6          0.7071067812     0.7071067812     0          −0.7071067812    0.7071067812     0
7          0.7071067812     0.7071067812     0          −0.7071067812    0.7071067812     0
8          0.7071067812     0.7071067812     0          −0.7071067812    0.7071067812     0
9          0.7071067812     0.7071067812     0          −0.7071067812    0.7071067812     0
10         0.7071067812     0.7071067812     0          −0.7071067812    0.7071067812     0
11         0.7071067812     0.7071067812     0          −0.7071067812    0.7071067812     0
12         0.7071067812     0.7071067812     0          −0.7071067812    0.7071067812     0
13         0.7071067812     0.7071067812     0          −0.7071067812    0.7071067812     0
14         0.7071067812     0.7071067812     0          −0.7071067812    0.7071067812     0
15         0.7071067812     0.7071067812     0          −0.7071067812    0.7071067812     0
16         0.7071067812     0.7071067812     0          −0.7071067812    0.7071067812     0
17         0.7071067812     0.7071067812     0          −0.7071067812    0.7071067812     0
18         0.7071067812     0.7071067812     0          −0.7071067812    0.7071067812     0
19         0.7071067812     0.7071067812     0          −0.7071067812    0.7071067812     0
20         0.7071067812     0.7071067812     0          −0.7071067812    0.7071067812     0
21         0.7071067812     0.7071067812     0          −0.7071067812    0.7071067812     0
22         0.7071067812     0.7071067812     0          −0.7071067812    0.7071067812     0
23         0.7071067812     0.7071067812     0          −0.7071067812    0.7071067812     0
24         0.7071067812     0.7071067812     0          −0.7071067812    0.7071067812     0
25         0.7071067812     0.7071067812     0          −0.7071067812    0.7071067812     0
26         0.7071067812     0.7071067812     0          −0.7071067812    0.7071067812     0
27         0.7071067812     0.7071067812     0          −0.7071067812    0.7071067812     0
28         0.7071067812     0.7071067812     0          −0.7071067812    0.7071067812     0
29         0.7071067812     0.7071067812     0          −0.7071067812    0.7071067812     0
30         0.7071067812     0.7071067812     0          −0.7071067812    0.7071067812     0
31         0.7071067812     0.7071067812     0          −0.7071067812    0.7071067812     0
```

32	0.7071067812	0.7071067812	0	−0.7071067812	0.7071067812	0
33	0.7071067812	0.7071067812	0	−0.7071067812	0.7071067812	0
34	0.7071067812	0.7071067812	0	−0.7071067812	0.7071067812	0
35	0.7071067812	0.7071067812	0	−0.7071067812	0.7071067812	0
36	0.7071067812	0.7071067812	0	−0.7071067812	0.7071067812	0
37	0.7071067812	0.7071067812	0	−0.7071067812	0.7071067812	0
38	0.7071067812	0.7071067812	0	−0.7071067812	0.7071067812	0
39	0.7071067812	0.7071067812	0	−0.7071067812	0.7071067812	0
40	0.7071067812	0.7071067812	0	−0.7071067812	0.7071067812	0
41	0.7071067812	0.7071067812	0	−0.7071067812	0.7071067812	0
42	0.7071067812	0.7071067812	0	−0.7071067812	0.7071067812	0
43	0.7071067812	0.7071067812	0	−0.7071067812	0.7071067812	0
44	0.7071067812	0.7071067812	0	−0.7071067812	0.7071067812	0
45	0.7071067812	0.7071067812	0	−0.7071067812	0.7071067812	0
46	0.7071067812	0.7071067812	0	−0.7071067812	0.7071067812	0
47	0.7071067812	0.7071067812	0	−0.7071067812	0.7071067812	0
48	0.7071067812	0.7071067812	0	−0.7071067812	0.7071067812	0
49	0.7071067812	0.7071067812	0	−0.7071067812	0.7071067812	0
50	0.7071067812	0.7071067812	0	−0.7071067812	0.7071067812	0

```
fdno
INCLude input/FD.dat

end

!inter

BATCH
teln
gmac,init
opti
check
tol,,1.0e-10
prop,,1 ! proportional load step 1
dt,,0.01000
stre node
tvtk,grow
!tvtk,writ
! Loading - stretch, pressure
LOOP time 100
        time
```

```
        LOOP newton 30
                tang,,1
        NEXT newton
        stre node 5
        tvtk,grow
NEXT time

!tvtk,grow

SAVE

END
1 1 0   1.0001   0.00   1.00   0.00   0.00   0.00   1.00


STOP
```

The following is the input file for the verification of the correct implementation of VSMC remodelling:

```
feap ** Biaxial test - Andrii Grytsan
  0    0       3       3       3       8


material 1 !Media
solid
finite
mixed
ucons cacg  1.000e+04  0.000e-02  9.300e-02  5.800e+00 1.100e-02 4.510e-02
! ud vector

material 2
pressure
load 1.600e-02  ! units should be consistent with material parameters
follower ! load follows the surface, i.e. is applied in current config


rpar ! I4a alpha beta recrmean_t0 recrmin_t0 recrmax_t0 I4mod_at I4min_at I4max_at I4mh I4r
2
1  2.0  1.0  1.25 1.10 1.45 0.95 0.85 1.05 1.15 1.139

volg ! volgr(0 3) elvg(0 3) volfrac:(elastinM,collagenM,elastinA,collagenA)
3 0 0.18 0.075 0.0 0.075


epar ! fe0 cmin Tend muv Lvf lambda_z
1.0 0.2 10.0 20.0 0.0737 2


COORdinates
INCLude input/cyl.node


ELEMents
INCLude input/cyl.elem

EBOUNdary
1  0.0  1 0 0
2  0.0  0 1 0
3  0.0  0 0 1
```

```
3   0.0125  0  0  1

EDISPlacements
1   0.0    0  0  0
2   0.0    0  0  0
3   0.0    0  0  0
3   0.0125   0  0  0.0025


INCLude input/cyl.dirv


fdno
INCLude input/FD.dat

end

!INTEractive



BATCH
teln
gmac,init
opti
check
time,set,-1.00E+00
tol,,1.0e-10
prop,,1                                          ! proportional load step 1
dt,,0.02
! SOLVE FOR EQUILIBRIUM TO ACCOMMODATE ACTIVE STRESS!
LOOP newton 10
        utan,,1
NEXT newton
! END SOLVE
stre node
tvtk,grow

! Loading - stretch, pressure
LOOP time 50
        time
        LOOP newton 10
                utan,,1
```

```
        NEXT newton
        stre node
        tvtk,grow
NEXT time

! ---- Second load step ----
dt,,0.02
prop,,1
LOOP time 450
        time
        LOOP newton 30
                utan,,1
        NEXT newton
        stre node
        gmac,recd
        gmac,vsmh
        tvtk,grow
NEXT time

!tvtk,grow

! ---- Third load step ----
dt,,0.02
prop,,1
LOOP time 500
        time
        LOOP newton 30
                utan,,1
        NEXT newton
        stre node
        gmac,ksup
        tvtk,grow
NEXT time

! ---- Fourth load step ----
dt,,0.02
prop,,1
LOOP time 500
        time
        LOOP newton 30
                utan,,1
        NEXT newton
        stre node
```

```
        tvtk , grow
        gmac , vsmh
NEXT  time
```

END

```
1  1   -1.000   00.001   0.00   1.00   0.00   0.00   0.00   1.00
1  2   00.000   09.001   1.00   0.00   0.00   0.00   0.00   1.00
1  3   09.000   19.001   1.00   0.00   0.00   0.00   0.00   1.00
1  4   19.000   29.001   1.00   0.00   0.00   0.00   0.00   1.00
```

SAVE

STOP

The following is the input file for the verification of the correct implementation of damage:

```
feap ** Biaxial test - Andrii Grytsan
  0    0       3       3       3       8


material 1 !Media
solid
finite
mixed
ucons cacg  1.000e+04  0.000e-02  9.300e-02  5.800e+00 1.100e-02 4.510e-02
! ud vector

material 2
pressure
load 1.600e-02  ! units should be consistent with material parameters
follower ! load follows the surface, i.e. is applied in current config


rpar ! I4a alpha beta recrmean_t0 recrmin_t0 recrmax_t0 I4mod_at I4min_at I4max_at I4mh I4r
2
1  2.0  1.0  1.25 1.10 1.45 0.9025 0.7225 1.1025 1.3225 0.9495

volg ! volgr(0 3) elvg(0 3) volfrac:(elastinM,collagenM,elastinA,collagenA)
3 0 0.18 0.075 0.0 0.075


epar ! fe0 cmin Tend muv Lvf lambda_z
1.0 0.2 10.0 20.0 0.0737 2


COORdinates
INCLude input/cyl.node


ELEMents
INCLude input/cyl.elem

EBOUNdary
1  0.0  1 0 0
2  0.0  0 1 0
3  0.0  0 0 1
```

```
3   0.0125  0  0  1

EDISPlacements
1   0.0    0  0  0
2   0.0    0  0  0
3   0.0    0  0  0
3   0.0125   0  0  0.0025


INCLude input/cyl.dirv


fdno
INCLude input/FD.dat

end

!INTEractive



BATCH
teln
gmac,init
opti
check
time,set,-1.00E+00
tol,,1.0e-10
prop,,1                                          ! proportional load step 1
dt,,0.0200
! SOLVE FOR EQUILIBRIUM TO ACCOMMODATE ACTIVE STRESS!
LOOP newton 10
        utan,,1
NEXT newton
! END SOLVE
stre node
tvtk,grow
!tvtk,writ
! Loading - stretch, pressure
LOOP time 50
        time
        LOOP newton 10
                utan,,1
```

```
        NEXT newton
        stre node
        tvtk,grow
NEXT time

! ---- Second load step ----
dt,,0.02
prop,,1
LOOP time 450
        time
        LOOP newton 30
                utan,,1
        NEXT newton
        stre node
          gmac,recd
        gmac,vsmh
        tvtk,grow
NEXT time

!tvtk,grow

! ---- Third load step ----
dt,,0.02
prop,,1
LOOP time 500
        time
        LOOP newton 30
                utan,,1
        NEXT newton
        stre node
        gmac,ksup
        gmac,vsmh
        tvtk,grow
NEXT time

! --- Fourth load step ----
NEWForce
dt,,0.001
prop,,1
LOOP time 1000
        time
        LOOP newton 30
                utan,,1
```

```
          NEXT newton
           stre node
           tvtk ,grow
           gmac ,dmgm
NEXT time


END
1 1   -1.000   00.001   0.00   1.00   0.00   0.00   0.00   1.00
1 2   00.000   09.001   1.00   0.00   0.00   0.00   0.00   1.00
1 3   09.000   19.001   1.00   0.00   0.00   0.00   0.00   1.00
1 4   19.000   20.001   1.00   0.75   0.00   0.00   0.00   1.00

SAVE

STOP
```

The following is the input file for the finite element model of cerebral vasospasm and treatment:

```
feap ** Biaxial test - Andrii Grytsan
  0    0       3       3       3       8


material 1 !Media
solid
finite
mixed
ucons cacg  1.000e+04  0.000e-02  9.300e-02  5.800e+00 1.100e-02 4.510e-02
! ud vector

material 2
pressure
load 1.600e-02  ! units should be consistent with material parameters
follower ! load follows the surface, i.e. is applied in current config


rpar ! I4a alpha beta recrmean_t0 recrmin_t0 recrmax_t0 I4mod_at I4min_at I4max_at I4mh I4r
2
1  2.0  1.0  1.37 1.24 1.53 0.95 0.85 1.05 1.3225 1.28

volg ! volgr(0 3) elvg(0 3) volfrac:(elastinM,collagenM,elastinA,collagenA)
3 0 0.18 0.075 0.0 0.075


epar ! fe0 cmin Tend muv Lvf lambda_z
1.0 0.2 10.0 20.0 0.0737 2


COORdinates
INCLude input/cyl.node


ELEMents
INCLude input/cyl.elem

EBOUNdary
1  0.0  1 0 0
2  0.0  0 1 0
3  0.0  0 0 1
```

```
3   0.0125  0  0  1

EDISPlacements
1   0.0    0  0  0
2   0.0    0  0  0
3   0.0    0  0  0
3   0.0125   0  0  0.0025


INCLude input/cyl.dirv


fdno
INCLude input/FD.dat

end

!INTEractive



BATCH
teln
gmac,init
opti
check
time,set,-1.00E+00
tol,,1.0e-10
prop,,1                                          ! proportional load step 1
dt,,0.0200
! SOLVE FOR EQUILIBRIUM TO ACCOMMODATE ACTIVE STRESS!
LOOP newton 10
        utan,,1
NEXT newton
! END SOLVE
stre node
tvtk,grow
!tvtk,writ
! Loading - stretch, pressure
LOOP time 50
        time
        LOOP newton 10
                utan,,1
```

```
        NEXT newton
        stre node
        tvtk,grow
NEXT time

! ---- Second load step ----
dt,,0.02
prop,,1
LOOP time 450
        time
        LOOP newton 30
                utan,,1
        NEXT newton
        stre node
          gmac,recd
        gmac,vsmh
        tvtk,grow
NEXT time

!tvtk,grow

! ---- Third load step ----
dt,,0.02
prop,,1
LOOP time 500
        time
        LOOP newton 30
                utan,,1
        NEXT newton
        stre node
        gmac,ksrm
        gmac,vsmh
        tvtk,grow
NEXT time

! --- Fourth load step ----
NEWForce
dt,,0.001
prop,,1
LOOP time 1000
        time
        LOOP newton 30
                utan,,1
```

```
          NEXT newton
           stre node
           tvtk,grow
        gmac,dmgm
NEXT time


END
1 1  −1.000  00.001  0.00  1.00  0.00  0.00  0.00  1.00
1 2  00.000  09.001  1.00  0.00  0.00  0.00  0.00  1.00
1 3  09.000  19.001  1.00  0.00  0.00  0.00  0.00  1.00
1 4  19.000  20.001  1.00  0.75  0.00  0.00  0.00  1.00

SAVE

STOP
```